![University of Glasgow logo]

Jarangdej, Nuttaporn (2023) *Microtopography and stretch activated mechanotransduction in dermal fibroblasts and epithelia.* PhD thesis.

http://theses.gla.ac.uk/83961/

Microtopography and stretch activated mechanotransduction in dermal fibroblasts and epithelia

Nuttaporn Jarangdej

B.S., M.Sc.

Submitted in fulfilment of the requirements of the Degree of Doctor of Philosophy (PhD)

Centre for the Cellular Microenvironment
School of Molecular Biosciences
College of Medical, Veterinary and Life Sciences
University of Glasgow

November 2023

ABSTRACT

Mechanical forces are key contributors to regulating cell function, development, homeostatic turnover, and repair of tissues. To date, the dynamic interactions between cell mechanics and their microenvironment. This study aims to reproduce a biomaterial scaffold that can carry dermal fibroblast and/or epithelia, combined with applied tissue engineering approaches to manipulate the mechanosensitive elements of cells to function for skin regeneration and wound healing. The major focus of this study provide insight into the mechanisms underlying the deformation of cell nuclei which have an impact on transcription factor control, cell memory, and behaviours.

In an attempt to offer an effective biocompatible scaffold, one particular challenge lies in the delivery of functional mechanical stimuli to potential translational outcomes and promote regenerative characteristics of skin grafting and wound healing. This research project highlights how mechanical and biochemical microenvironments link the nuclear reorganization which reflects to functional consequences under mechanical regulation, imposed on nuclear overall shape and transcriptional activities.

Two ways of delivering mechanical signals have been used to convey force to nuclear regulation which connect to the cytoskeleton and/or nucleoskeleton including;

I)   Externally applied force applications to activate cell growth or motility, with active stretch via microtopographic patterns and loading passive stretch by pulling on the cells.

II) Adjusting nuclear force internally via the expression and activity of nuclear membrane proteins (i.e. emerin and binding partners; lamin A/C and BAF).

The read-out of measuring at the end of dynamic changes in actin polymerisation direct to the nuclear entry of mechanosensitive transcription factor (TF), myocardin-related factor A (MRTF-A) have been addressed. As a result of the response of dermal fibroblasts to mechanical stimuli, immunofluorescent staining of n/c ratio showed that have significant enhanced nuclear import of MRTF-A by

~2.0-fold and ~1.3-fold increased subjected to 4.2% unidirectional stretch and 5% cyclic stretch (0.05Hz, 90° grooves), respectively. However, the cells under lower mechanical force promoted the nuclear export of MRTF-A. Immunoblot results revealed that nuclear accumulation of MRTF-A in cell-lacking emerin to the range between 0.3-fold to 0.5-fold decreased confirmed by two knockout clones.

The impact of reduced mechanical tension contributes to the nuclear mechanical properties and histone modification. Assessing the alteration of acetylation status of histones via HDAC3 gene expression was examined using real-time qPCR, with a significant decrease of half expression in knockout models of emerin both in BJ1 and HEK293 cells. With the stated results, the analysis of cell-induced environment deformations can imply chromatin remodelling and thus regulate cell behaviours. Increased mechanical properties lead to chromatin condensation and influence on cell contractility or even differentiation while, low mechanical forces link to chromatin unfold or decondensation with hyperproliferation.

To conclude, this study represents the cell-based tissue-engineered platform which improved delivery via a biocompatible scaffold to offer an alternative artificial tissue layer for enhancing translational qualities in skin regeneration and wound healing. The results suggest condition favours with dynamic microenvironment to regulate cell behaviour specified to mechanical properties for cell contraction or proliferation. In addition to this, the work illustrates how mechanotransduction of cells sense and convert mechanical signals into changes in intracellular biochemistry and nuclear regulation including transcription factor translocation, TF activity, and chromatin reorganisation.
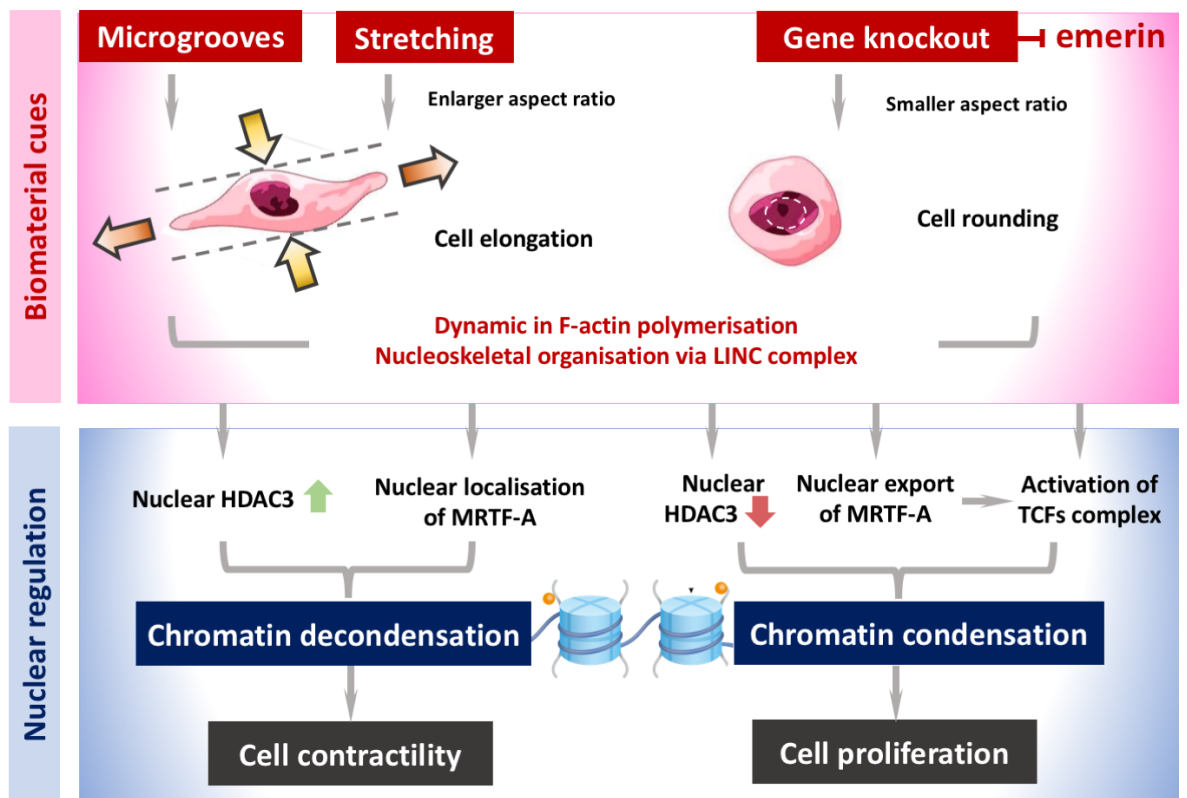
Graphic abstract figure. Biomaterial cues regulate nuclear-cellular deformation and mechanotransduction activated epigenetic mechanisms inside the nucleus, chromatin and transcription factors. Biomaterial approaches applied to guide the cell alignment by shaping cell elongation with increased aspect ratio used microgroove topography and/or mechanical stretching. By direct cell rounding through knockout expression of gene at the nuclear envelope, influence to decreased cell aspect ratio. Dash line and arrows represent force action to the cells. During cell deformation, force transmission from cytoskeleton to nucleus occurs which lead to changes in increased HDAC3 activities and translocation of nuclear MRTF-A, subsequently lead to chromatin decondensation and cell contractility. However, reduced the strength of nuclear membrane with lower deformability affects less HDAC3 production, nuclear export of MRTF-A which switch to transcription factor activator of TCFs complex competitive binding to SRF. In cell rounding, it is likely that controls programming chromatin condensation and link to cell proliferation.

Abbreviation; HDAC3, histone deacetylase 3; MRTF-A, myocardin-related transcription factor A; TCFs, ternary complex factors.

TABLE OF CONTENTS

LIST OF TABLES

LIST OF FIGURES

PRESENTATIONS

Presentations made by the candidate relating to research in this thesis

(2021) Flash poster presentation at RSC Biomaterials Chemistry Group Annual Meeting, Nottingham UK: Mechanical stretching and dynamic surface to influence fibroblast behaviour.

(2019) Poster presentation at 30th Annual Conference of the European Society for Biomaterials (ESB) together with the 26th annual conference of the German society for biomaterials (DGBM), Dresden Germany: Developing a novel system to aid tissue expansion via tensile strain for skin regeneration.

(2018) Poster presentation at Tissue & Cell Engineering Society (TCES) 2018 Conference, Keele UK: Developing a novel system to aid tissue expansion via tensile strain for skin regeneration.

ACKNOWLEDGEMENT

It would not have been possible without the support of all wonderful people who are willingly to accompany my PhD journey from a warm welcome to the end.

Firstly, I would like to sincerely thank you to my long-suffering supervisor Dr Mathis Riehle for the opportunity to carry out the research project under your greatest supervisions. Massive thank you for being my dad supervisor who is not only push the work forward but also take an excellent care of my student life with meaningful guidance. I would also like to thank to member of MR group; Gillian Higgins, Martino Guiotto, Mary Dysko, Bial Taib and Robert Docherty for powerful helps, precious times and all the laughs.

Next, I would definitely have to thank my enthusiastic supervisor Dr Andrew Hamilton who bring me to the CRISPR work and giving sustain DNA/RNA delivery much more inspired and running work smoothly.

I am very grateful to my beloved brother; Wich Orapiriyakul, sisters; Monica Tsimbouri and Carol-Anne Smith for invaluable support, teaching me lots of life lessons and goodwill. I offer my eternal gratitude to the people I have met and the friends I have gained. Particularly, I would like to thank PhD friends who sharing good and hard times together. Sofia Perea Ruiz, Morta Antanaviciute, Yinbo Xiao and Xiang Li, that made my times during PhD roadway worth. I could never forget about any of you; thanks for every moment we made, and for chit-chat, understanding and for more smiley faces it's been awesome.

Of course, I would like to give heartfelt thank you to my family for their love and enduring encouragement throughout all stages in my life. My greatest thanks also go to my BFF; Duanghatai, Damita, Pornsuda, Tanakorn, Tachinee, Pattaranit, Pusacha, Natnicha and Pareena. They are absolutely giant source of energetic kicks, motivated and giving me comfort to keep going, reminding me how far I have come, staying beside me and rewritten my sad mood to become a much more colourful day.

Finally, I would give a credit to myself for the buckets of sweat, blood and tears I would proudly say that I've put any effort into this research project and really looking forward to (still) being a passionate researcher. The (actual last) but really important, I am glad that Siu Hin Lau. You were there to care for me when I was most confused, vulnerable and hopeless. At times were dark, you were my one who is trying to understand and holding my hands to warm my heart that I will never ever be alone.

Love you all
Nuttaporn x

Author's declaration

I declare that, except where explicit reference is made to the contribution of others, that this dissertation is the result of my own work and has not been submitted for any other degree at the University of Glasgow or any other institution.

Nuttaporn Jarangdej

November 2023

LIST OF ABBREVIATIONS

Abbreviation	Full form	Chapter
AAVS1	Adeno-associated virus integration site 1	4
BAF	Barrier-to-autointegration factor	1,5,6
bp	Base pair	4,5
BSA	Bovine serum albumin	2,3
B2M	ß2-microglobulin	4
cDNA	Complementary DNA	2,5
ChIP	Chromatin immunoprecipitation	4,5
CRCs	chromatin remodelling complexes	5
CRISPR	Clustered regularly interspaced short palindromic	1,4,6
CRISPRa	CRISPR activation	1
CRISPRi	CRISPR interference	1,4
CRISPRko	CRISPR knockout	4,5
crRNAs	CRISPR RNA	1
DAMPs	Damage-associated molecular patterns	1
dCas9	Nuclease-dead Cas9	1,4
DMEM	Dulbecco's modified eagle medium	2,4
Dox	Doxycycline	4
DSB	Double-stranded break	1,4
ECL	Enhanced chemiluminescence	2
ECM	Extracellular matrix	1,5,6
EDMD	X-link Emery-Dreifuss muscular dystrophy	1
EGF	Epidermal growth factor	1
ER	Endoplasmic reticulum	1
ERKs	extracellular signal-regulated kinases	1,2,4,5
F-actin	Actin filament	1,3,4,6
FACS	Fluorescence activated cell sorting	4
FBS	Fetal bovine serum	2
FGF	Fibroblast growth factor	1
FITC	Fluorescein isothyiocyanate	2,5
Fn	Fibronectin	3,5,6

Abbreviation	Full form	Chapter
G-actin	Globular actin	1,3,4,6
GDP	Guanosine diphosphate	1
GEFs	Guanine nucleotide exchange factors	1
GFP	Green fluorescent protein	1,4,5
GFR	Growth factor receptor	1
GPCR	G protein-coupled receptors	1
GTP	Guanosine triphosphate	1
HCl	Hydrochloric acid	2
HDAC3	Histone deacetylase 3	4,5,6
HDR	Homology-directed repair	1
H_2O_2	Hydrogen peroxide	1
HP1	Heterochromatin protein 1	1
HRP	Horseradish peroxidase	2
hTERT	human Telomerase reverse transcriptase	2,3,4,5
ICE	Interference of CRISPR Edits	4
INDELs	Insertions and deletions	1,4,5
IEGs	Immediate-early genes	1
IF	Immunofluorescence	4
INM	Inner nuclear membrane	1,5
KO	Knockout	4,5
KRAB	Krüppel-associated box	4
LADs	Lamina-associated domains	1
LATS	Large tumour suppressor kinase	1
LBR	Lamin B receptor	1
LIMK	LIM kinase	1
LINC	Linker of nucleoskeleton and cytoskeleton	1,5
MAPKs	Mitogen-activated protein kinases	1,2,4,5,6
MMPs	Matrix metalloproteinases	1
MRTF-A	Myocardin-related transcription factor A	1,2,3,4,5,6
MST	Mammalian Ste20-like kinase	1
nCas9	nickase Cas9	1
NCoR	Nuclear co-repressor	5
NE	Nuclear envelope	1,5

Abbreviation	Full form	Chapter
NHEJ	Nonhomologous end-joining	1
NPCs	Nuclear pore complexes	1,5
nt	Nucleotide	4
NUPs	Nucleoporins	1
ONM	Outer nuclear membrane	1
PAM	Protospacer adjacent motif	4
PBS	Phosphate-buffered saline	2,3
PCL	Polycaprolactone	2,3
PDGF	Platelet derived growth factor	1
PDMS	Polydimethylsiloxane	2,3,5,6
PI3K	Phosphoinositide 3-kinase	1
Pre-crRNAs	precursor crRNA	1
qRT-PCR	real-time quantitative reverse transcription	2,4,5
RhoA	Ras homolog family member A	1,5
RNPs	Ribonucleoprotein	4
ROCK	Rho-associated protein kinase	1
RTK	Receptor tyrosine kinase	1
SDS	Sodium dodecyl sulphate	2
sgRNAs	single-guided RNA	4
SRF	Serum response factor	1,5
TALENs	Transcription activator-like effector nucleases	4
TAZ	Transcriptional co-activator with PDZ-binding motif	1
TBS	Tris-buffered saline	2
TBST	Tris-buffered saline with Tween®20	2
TCFs	Ternary complex factors	1,5,6
TCP	Tissue culture plate	2,4,5,6
Tet	Tetracycline	4
TF	Transcription factor	4
TIMPs	Tissue inhibitor of metalloproteinases	1
TLRs	Toll-like receptors	
TM	Transmembrane	5
tracrRNA	trans-activating CRISPR RNA	1

Abbreviation	Full form	Chapter
TSS	Transcription start site	4
VEGF	Vascular endothelial growth factor	1
WB	Westernblot	2,4
WT	Wild-type	4,5
YAP	Yes-associated protein	1
ZFNs	Zinc-finger nucleases	4

CHAPTER 1 GENERAL INTRODUCTION

Delayed healing has led to an increase in chronic disability and skin dysfunction in people worldwide. In the field of tissue engineering, utilizing a biocompatible material, applied as an alternative scaffold, combined with varied support cells to optimise conditions for wound contraction and enhancing its regenerative characteristics (Murray et al., 2019). This strategy does not only overcome the limited availablity of donor tissue, it can also avoid unnecessary second surgery at the donor sites. However, the knowledge gap in yielding therapeutically applicable scaffolds and cells deserve further studies for effective medical outcomes (Buganza Tepole and Kuhl, 2013). The underlying mechanisms of the molecular and cellular response of supportive cells in conjunction with biomaterials approaches are the main focused of this study. A variety of mechanical stimulations had been applied, with the aim to optimise regeneration with appropriate cell guidance such as topographic patterns, applied cyclic and unidirectional tensile strain and genetic modification to investigate the relevance of emerin in this context.

1.1 Skin injuries

1.1.1 Incidence and prevalence

Injuries to the skin often cause tissue loss and dysfunction (Zhu et al., 2019). Approximately 2.2 million cases reported in the United Kingdom during 2012-2013 (Guest et al., 2015, Guest et al., 2017a). From 2013 onwards, the incidence of acute, chronic and unspecified skin wounds grew at the annual rate of 11% (Guest et al., 2017b). A study by Lindley et al. (2016), reported over 6.5 million patients with chronic wounds in the United States. The prevalence of chronically open wounds of around 3% escalate in elderly with the incidence of diseases continue to be an increasingly persistent case around 2% by 2020 (Sen and Roy, 2019).

1.1.2 The negative impact of delayed wound care and clinical challenges

Traumatic breaches of skin integrity can lead to substantial physiological imbalance and disabilities, leading to a lower quality of life (Maver et al., 2015).

The spatial and temporal stages of repair depend on the depth of wounds (Tiwari, 2012). Epidermis has the capacity of regeneration and responds to injury by restoring minor defects (Vig et al., 2017). Whereas, deep injuries including 3rd degree burn wounds may require autologous epidermal keratinocytes or dermal-epidermal autografts in order to stimulate a wound closure (Singer and Boyce, 2017). Split thickness autograft is a gold standard technique that is widely used in skin surgery, there is a limited availability of autologous donor tissue (Kanapathy et al., 2016). It also requires healing of donor site, replacement of deep or chronic injuries often takes 9-12 months until it has fully recovered (Edwards, 2013). However, any full-thickness damage to the skin still remains a challenge (Albanna et al., 2019). Poor restoration may trigger a persistent wound particularly in people with chronic disease such as diabetes and may result in pressure ulcers (Albanna et al., 2019). Skin grafting is indicated if the surface area affected is larger than 6-10% of total body surface, but these require a long period to recover in the range of 4 weeks up to more than 3 months (Edwards, 2013).

1.2 Cellular response during wound healing

1.2.1 The cell-cell interaction in the distinct layer of skin

Skin repair occurs under the intricate synchronization of different cell types in skin resident cells and their surroundings such as endothelial and nerve cells. The cellular structure in each layers of the skin is illustrated in Figure 1-1. The epidermis is the outermost layer of skin, mainly comprised of keratinocytes that provide the permeability barrier of the skin (Bazzoni and

Figure 1-1 in this thesis contains material whose copyright belongs to a third party.

See figure 1 available on:

Gurtner, G. C., Werner, S., Barrandon, Y. and Longaker, M. T. (2008) 'Wound repair and regeneration', *Nature,* 453(7193), pp. 314-21.

Figure 1-1. Architecture of skin classified by 3 adjacent layers. Epidermis underlies on the outer surface of the skin, mainly consisting of epithelial cells known as keratinocytes. The inner, thick layer of skin, assembled by fibroblast and consists of collagen in the extracellular matrix of the dermis. Next, the subcutaneous layer of the skin contains vasculature, carrying nutrients and growth factors, nerves and glands (Gurtner et a., 2008).

Dejena, 2002). Next, the core layer of skin in the dermis that locates between epidermis and subcutaneous layers (Brown and Krishnamurthy, 2020). Fibroblasts are the most abundant mesenchymal cells which contain highly mechanoresponsive interface in this skin compartment (Driskell et al., 2013) and provide its strength by production of elastin and collagen (de Araujo et al., 2019). The layer that underlies the dermis called subcutaneous layer, includes vasculature and adipose tissue which serves as the essential sources of nutrients and growth factors (Zaytsev et al., 2022).

1.2.2 The interaction of cells with the surrounding extracellular matrix

Extracellular matrix (ECM) is one of critical factors regulating the functioning of cells (Bissell et al., 1982; Maruthamuthu et al., 2011). The ECM is composed of a large family of matrix proteins and macromolecules that participate to tissue strength by forming a structural scaffold (Eckes et al., 2010). The ECM functions as carrier and modulator of biological activity of several growth factors and cytokines (Aszodi et al., 2006; Myllyharju and Kivirikko, 2004). The composition and characterised function of the ECM are summarised in the table 1-1. The ECM also acts as ligands for specific cell surface receptors such as integrins, dystroglycans and toll-like receptors (TLRs) (Bhattacharjee et al., 2019).

An example of growth factors binding to the ECM in wound healing is heparan sulfate proteoglycan, which contains recognition sites for collagen as well as the sites that interact with basic fibroblast growth factor (FGF), vascular endothelial growth factor (VEGF) and platelet derived growth factor (PDGF) that can trigger cell proliferation (Schlessinger et al., 2000; Robinson and Stringer, 2001). After injury, the cell-ECM interaction recruits the damaged tissue during wound repair. The synthesis of ECM and deposition in connective tissues control in the early phases of healing, follow by remodeling of ECM at the later stages (Watt and Fujiwara, 2011).

Table 1-1. Composition of the ECM and their roles in the skin

Composition	ECM member	Characteristics and functional properties	References
Structural proteins	Collagen	• They represent a diverse protein subfamilies, some of which aggregate into fibrils e.g. collagens (type I-III), transmembrane collagens (XIII, XVII) which can be included at the site of the cell-ECM interactions such as focal adhesions and hemidesmosomes.	Heino, 2007; Woodall et al., 2008
	Elastin	• The fundamental component of the elastic tissue, exist in connective tissue and the dermis. • This can link to a recent differentiation phase of fibroblasts.	Kielty et al., 2002; Zheng et al., 2006
Adhesive glycoproteins	Fibronectin	• It is such one of the best-characterised glycoproteins of the ECM that produced by dermal fibroblasts. • They are initially deposited from blood plasma in response to injury, associated with the release of growth factors and cytokines.	Muro et al., 2003; Clark, 1990
	Laminin	• Laminin chain self-polymerise, generate trimeric structure and interact with other membrane proteins such as collagen IV and perlecan. • They participate in repair as a key regulator of re-epithelialisation and vascularization.	Aumailley et al, 2005; Kyriakydes and Bornstein, 2003
Protein mediating cell communication	Matricellular protein	• These classified group of proteins involve cytokine production, are interacted by forming interaction to other ECM molecules and cell surface receptors. • The subfamilies iSPARC/BM-40/osteonectin, thrombospondins and tenascins.	Agah et al., 2002; Bradshaw et al., 2002

1.2.3 The multi-complex of cell in response to skin injuries

Skin resident cells interact themselves and with immune cells to maintain their homeostasis. A low level of neutrophil and monocyte circulate in the normal condition (Forbes and Rosenthal, 2014; Rodrigues et al., 2019) (Figure 1-2A). During injury, the interaction of cells is critical activated in three overlapping stages: inflammation, proliferation and remodelling (Gurtner et al., 2008)

1.2.3.1 The inflammatory phase

The inflammation is the initial stages of repair, it involves the coordination of hemostasis and immune response (Kolaczkowska and Kubes, 2013). Upon tissue injury, hemostasis occurs immediately after vascular damage, initiated by vasoconstraction of the vessel walls, the platelet plug formation and coagulation. Following wounding and blood rupture, the thrombogenic subendothelial matrix is exposed which can bind to endothelial using via G protein-coupled receptors (GPCR), integrins and glycoproteins on their surface. This subendothelial matrix is important for coagulation, the formation of aggregated platelet plug that prevents blood flow and fluid loses (Figure 1-2B) (Rodrigues et al., 2019).

Neutrophils and mast cells are the first immune cells in host defense. Short-lived neutrophils are activated and recruited into injured tissue. They crucially engulf bacteria, cell debris and dying neutrophils by phagocytosis (Niethammer et al., 2009). Initially considered the derivative from innate immune system, mast cells secre chemoattractants, recruit eosinophils, monocytes and release the anti-microbial peptides that prevent infection of the skins (Skaper et., 2014).

Resident tissue macrophages are supplemented by recruited monocytes, actively release pro-inflammatory cytokines or support an anti-inflammatory response (DiPietro et al., 1995). Activated macrophages control the clearance of neutrophils at the later phase which remains a critical resolution of inflammation (Chen and Rogers, 2007)

1.2.3.2 The proliferative phase

Formation of connective tissue occurs during the proliferative phase, together with several other processes including neovascularisation, immunomodulation and re-epithelialisation (Figure 1-2C). Granulation tissue is mainly formed by fibroblasts that newly synthesise ECM, which in turn serves as a scaffold for other cells. Neovascularisation is also critically important for wound healing as vessels function to deliver nutrients and supply oxygen. New blood vessels are then generated by proliferation of vascular endothelial cells (Gurtner et al., 2008). The basic layer of granulation tissue associated with the sprouts of capillaries via fibroblasts and macrophages. Together they replace the fibrin matrix and create a new substrate for keratinocyte migration, maturation and finally restoration of the epithelium (Werner and Grose, 2003).

1.2.3.3 Tissue maturation and remodelling

Once re-epithelialisation occurs, most of the endothelial cells, macrophages and myoblasts undergo apoptosis. Furthermore, some of granulation tissue, mainly fibroblasts continue to reconstitute the tissue. These cells together bring about the accumulation of a mass of fibrotic tissue (Figure 1-2D). The acellular matrix is dynamically remodelled by the lysis of collagen III, which is partially replaced by type I collagen, followed by re-organisation and further turn over of the ECM (Szabowski et al., 2000). This process is carried out by fibroblasts which secrete matrix metalloproteinases (MMPs), while the impaired regeneration can be due to upregulation of tissue inhibitor of metalloproteinases (TIMPs) leading to scar formation. Finally, an imbalance between MMPs and TIMPs can cause abnormal modification of ECM and chronic wounds (Gill et al., 2003; Telgenhoff and Shroot, 2005).

The aberrant tissue repair of wounds commonly results in fibrotic tissue. Fibrosis is referred to as an excessive deposition of connective tissue components. Fibrotic tissue is dysfunctional, formed mainly fibroblasts which are surrounded by a disorganised, inappropriate ECM, they produce. At tissue level, it often disrupts the physiological architecture, which may lead to organ malfunction (Distler et al., 2019).

Figure 1-2. Model of cellular responses during wound healing in the skin, triggers the synchronisation of subcellular compartment in distinct phases of repair. A) In the uninjured skin, circulating a low level of neutrophil efflux and monocytes are constantly transport to the tissue. **B) Upon tissue damaged**, epithelial wall is devastated, releases damage-associated molecular patterns (DAMPs), hydrogen peroxide (H_2O_2) and chemokines. These molecules provide initial signals for the recruitment of inflammatory cells and factors, especially neutrophil influx and activated monocytes. The inset (Box B) illustrated when primary hemostasis occurs, liberates vasoconstrictors that cause temporarily stop of bleeding. Hemostasis plug is then established from platelet bind the subendothelial matrix using surface receptors (e.g. GPCR, integrins and glycoproteins). **C) The restoration phase of wound healing**, proliferative activities of keratinocytes, and fibroblasts continue to reconstitution of epithelial layer and granulation tissue. In the event of chronicity, T cells plays role in reduction of chronic inflammation. **D) Maturation and remodelling at the late phase of regeneration**, excessive scarring occurs as a result of continued activation of inflammatory cells, leaving fibrotic mass and impaired epithelial restoration (adapted from Forbes and Rosenthal, 2014; Rodrigues et al., 2019).

Regenerating and fibrotic tissues often have different mechanical properties which in turn can activate cells via mechanotransduction (detailed in the next section) (Wells, 2013)

1.3 Cell mechanics: force transmission through elements of the cytoskeleton and the links to the nucleus

For most cells sensing and tuning in to their physical environment underpinning mechanical processes in forces-bearing molecular events confer the interconnection between surroundings and their cellular response (Guilluy et al., 2014). These external forces are in parts detected and transduced at the cell surface and in parts linked to the cytoskeleton, to the cytoskeleton and via the nucleus (Maniotis et al., 1997). As a result, the nucleus can undergo substantial deformation and this change in shape can facilitate essential activation of transcriptional activity and chromatin re-organization (Khatau et al., 2009; Driscoll et al., 2015; Ramdas and Shivashankar, 2015). Force-induced nuclear deformation is transmitted across the nuclear envelope to the nuclear interior through the 'linker of nucleoskeleton and cytoskeleton' (LINC) complex (Parson et al., 2000; Crisp and Burke, 2008; Lele et al., 2018). The mechanically intricate relationship between the intact cytoskeletal networks, nuclear mechanics and their surrounding environment is particular important for contractile cells to promote higher-order structure (Steinberg, 1963). In the emerging views of force transmission, the processes namely mechanotransduction that transduce both physical and mechanical cues into a biochemical signals and act on cellular behaviours (Frantz et al., 2010; Vining and Mooney, 2017).

1.3.1 Mechanical forces, environmental response and plasticity of cells

From microenvironment to cell functions, cells generally interact with their local environment via mechanical response of cells to forces both generated intrinsically and externally (Marjoram et al., 2014). Two types of mechanical forces and their actions on a cell are summarised in Table 1-2. The detection of physical forces by cells has been widely recognised as well as that forces are routed and transmitted to and between cells across a wide range of lengths (Yusko and Asbury, 2014) and integrated over time (Giannone and Sheetz, 2006). Thus,

the mechanical interactions mediated by adhesion to ECM and cell-cell junctions influence many cellular processes including cell movement, progression and development (Walma and Yamada, 2020). The mechanical action within the cells occur in the event of self-generating forces that produce intrinsically forces in cytoskeletal building blocks. The organisation of cytoskeleton such as contractile actomyosin units in response to external forces significantly impact cell motility and drive changes in their shapes (Kumar et al., 2006). Cell-extrinsic tensile, shear and compressive forces are applied forces through external loading (Wang and Li, 2010). The mechanical response of a cell to deformation is monitored by aspects of the cytoskeleton, which also provides resistance to these forces (Smeets et al., 2019). Upon mechanical loading, the relationship between the force and deformation determines the rheological properties of the cell, mainly focus on the elastic modulus of its cytoskeleton (Riveline et al., 2011; Unal et al., 2014). The force-deformation link to the elasticity of materials that stores energy during transfers of the stress or strain. The stress-strain relationships have been used to identify these features (Haase and Pelling, 2015), termed as described in detail see Box1-1 (Paluch and Discher, 2015). In elastic solids, there is a linear relationship between stress and strain energy. Young's modulus of an elastic material is the slope of the stress-strain curve, which defines the mechanical response when a material is subjected to a force (Vining and Mooney, 2017) and followed by reversible return to their original state during removal of load applied (Banerjee et al., 2021). Some synthetic polymers used in biomaterial applications show highly elastic properties, this includes rubbers and some hydrogels (Song et al., 2018).

The relevance of such universal mechanics at subcellular level is wide ranging, the cells properties can vary between viscoelastic and elastic behaviours. The plasma membrane is apparently inelasticity as it withstands deformation by relatively large external forces (Hochmuth and Waugh, 1987).

Table 1-2. Externally applied and intracellular generated forces in cell mechanics: the actions, diagrams and definitions.

Mechanical force	Diagram & force vector		References
I. Extrinsic forces			
Tension		• Magnitude of a force applied perpendicular to the membrane surface resulting in expansion.	Goldyn et al., 2009
Compression		• Compression force is stress that pointing inward on the object experiencing the force. • It causes compaction of affected area.	Lessey et al., 2012
Shear stress		• Applying a force parallel to the surface of the cells deform a structure at the local area where is compressed. • Force field extends an object in the orthogonal direction.	Matamoro-Vidal and Levayer, 2019
II. Intrinsic forces			
Actomyosin contractility		• Myosin motors that exerted forces by pulling on F-actin anchored to their matrix adhesions. • Adhesion sites are responsive to counter-force and directs the balance between disassembly and maturation.	Wozniak and Chen, 2009; Gomez et al., 2001
Actin-protrusion		• Membrane tension antagonises the growing actin filaments at the leading edge to protrude the membrane, potentially maintains polarity during cell migration.	Diz-Munoz et al., 2013
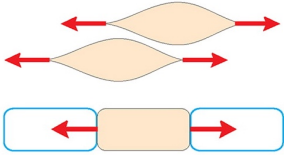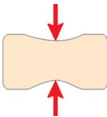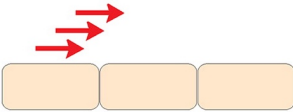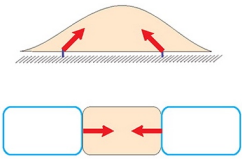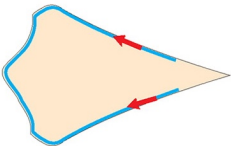
However, most cell inner components exhibit a viscoelastic nature, thus termed due to behavior that conforms both to solid-like elastic and fluid-like viscous properties, as dynamically balanced by creeping deformation and relaxation following application of intermittent mechanical forces (Kuznetsova et al., 2007; Haase and Pelling, 2013). The apparent load-induced stress-stiffening followed by reversible softening of cells is attributable to entropic elasticity and plastic yielding events according to Chaudhuri et al. (2007).

Box1-1. Mechanical terms and concepts, uses in elasticity

Using the kinematic relations represent the geometry of deformations and stresses in the structure, the stress-strain curve can be used to explained the behaviour of an elastic material in which the contribution of relative force acts on material, is likely to vary in mechanical properties.

The load-displacement relate to stress-strain relationships

Being area forces, stress (σ) is a force distributed over the initial surface area, measures this internal force and quantified connect to strains in termed as constituted law which generalised Hookes's law of elasticity. Strain (ε) is a measure of deformation dependent load and relative change in size in response to stress. Strain can be calculated by

the ratio between changes in length and the original length ($\varepsilon = \Delta l/l_0$). Schematic diagram of stress-strain relationship is linear until the stress reaches the proportional limit. With increasing load, the slope of the curve decreases and continuously transition to plastic range beyond the elastic limit. This phenomenon is explained the nature of elastic material relative to applied forces.
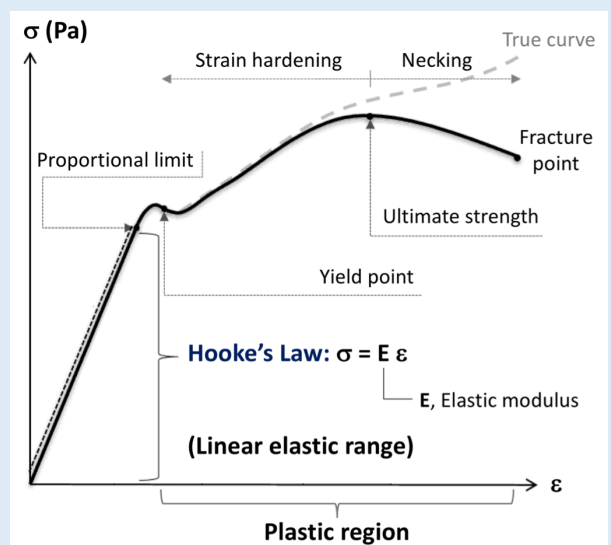
The power-law exponent (β) characterizes the solid or fluid states of a cell, A step increase in external force, ΔF closely leads to the deformation d(t) of the cell. A relative force over times follows a power law described using equation 1 (Bonakdar et al., 2016).

$$d(t) = c\Delta F(t/t_0)^{\beta} \qquad\qquad (1)$$

The value of the power-law exponent β reflects the dynamic of force-bearing structures and indicates elastic and dissipative behaviours (Fabry et al., 2001). If β approaches 0, this implies a purely elastic solid and if β = 1 the mechanical behaviour can best described as a purely viscous fluid. In cells, β values are typically between 0.1 and 0.5, representing a viscoelastic entity (Kollmannsberger et al., 2011).

1.3.2 Integrating the cytoskeletal dynamics, cell-matrix adhesions and cellular tension

In migrating cells, forces are generated by both actin polymerization (at the leading edge) and myosin II-dependent contraction of F-actin networks, with the later creating tension at attachment sites, that then subsequently lead to their maturation into focal adhesions (Ciobanasu et al., 2012). Actin-mediated protrusions drive a leading edge of the plasma membrane forward, which interacts with adhesions as shown in Figure 1-3. Myosin II functions to assist cell migration, traction forces that are generated by the contractility of myosin II are linked through the actin networks to the substrate via integrin-mediated adhesions to the extra cellular matrix (Mitra et al., 2005). Extending protrusions are further stabilised by the formation of new adhesions at the cell front, parallel with disassembly of adhesions at the cell rear (Parsons et al., 2010). These adhesions which are dynamic assemblies of structural and signaling proteins, in turn, stimulate Rho GTPases in the associated cytoskeletal complex (Geiger et al., 2009).

Figure 1-3 in this thesis contains material whose copyright belongs to a third party.

See figure 3 available on:

Geiger, B., Spatz, J. P. and Bershadsky, A. D. (2009) 'Environmental sensing through focal adhesions', *Nat Rev Mol Cell Biol,* 10(1), pp. 21-33.

Figure 1-3. An interconnected feedback loop of the actin machinery and focal adhesions (FA). Forces that are generated by the assembly of an F-actin and myosin II-dependent contractility (step 1) affect actin-binding FA proteins such as talin and vinculin, the integrins and the signalling module. These interacting networks integrate the signals to the actin cytoskeleton (step 2), and is associated with the extracellular matrix.

Consequently, the activated signalling leads to activation of small G proteins (Step 3).

Thus, modulating cytoskeleton-regulating proteins in actomyosin contractile (step 4) and further link to force-generating machinery (step 5) (Geiger et al., 2009).

1.3.3 Actin dynamics control nucleocytoplasmic shuttling a transcriptional co-activator

As a cytoskeleton-regulated factor, myocardin-related transcription factor A (MRTF-A) generates a unique link from actin dynamics to gene encoding components of the cytoskeleton (Speight et al., 2016). Recently, the MRTF-A transcription factor, Yes-associated protein (YAP) and its transcriptional co-activator with PDZ-binding motif (TAZ) showed a significant impact on skin regeneration through nuclear re-localisation.

MRTF-A and its mechanosensitive co-activator serum response factor (SRF) are both growth factor-responsive and directly link to activation of the Rho family GTPases together with their effectors, sufficient to induce fibrillar actin (F-actin) assembly (Jaffe and Hall, 2005; Weissbach et al., 2016). The canonical MRTF-SRF dependent pathway is outlined in Figure 1-4; stimuli that activate transmembrane receptor proteins e.g. integrins, G protein-coupled receptors (GPCR) and growth factor receptor (GFR), trigger assembly of polymeric actin (Olson and Nordheim, 2010; Moya and Halder, 2019). The Rho GTPases effector protein: ras homolog

family member A (RhoA) regulates polymerisation equilibrium of globular actin (G-actin) and (F-actin) in the cytoplasm (Geiger et al., 2009). Activated Rho-GTPase signalling cascade promotes actin polymerisation via downstream signalling through Rho-associated protein kinase (ROCK)-LIM kinase along the (LIMK)-cofilin pathway (Olson and Nordheim, 2010). The enhanced actin polymerisation reduces the G-actin pool that binds myocardin-related transcription factor A (MRTF-A) that in turn translocates to the nucleus and bind its transcription cofactor serum response factor (SRF).

In the meantime, the activation of core of the Hippo pathway composed of Ste20-like kinase (MST1 or MST2), large tumour suppressor kinase (LATS1 or LATS2) and their co-factors Salvador 1 (SAV1) and their transcriptional co-activator MOB1 via phosphoinositide 3-kinase (PI3K) mediator of RTK receptor. Phosphorylated YAP/TAZ are exported from the nucleus. When the activated kinases are inhibited by F-actin, driven YAP/TAZ accumulation in the nucleus (Moya and Halder, 2019). Finally, the MRTF-SRF and YAP/TAZ-TEAD complexes initiate the alteration of cytoskeletal gene expression (Connelly et al., 2010).
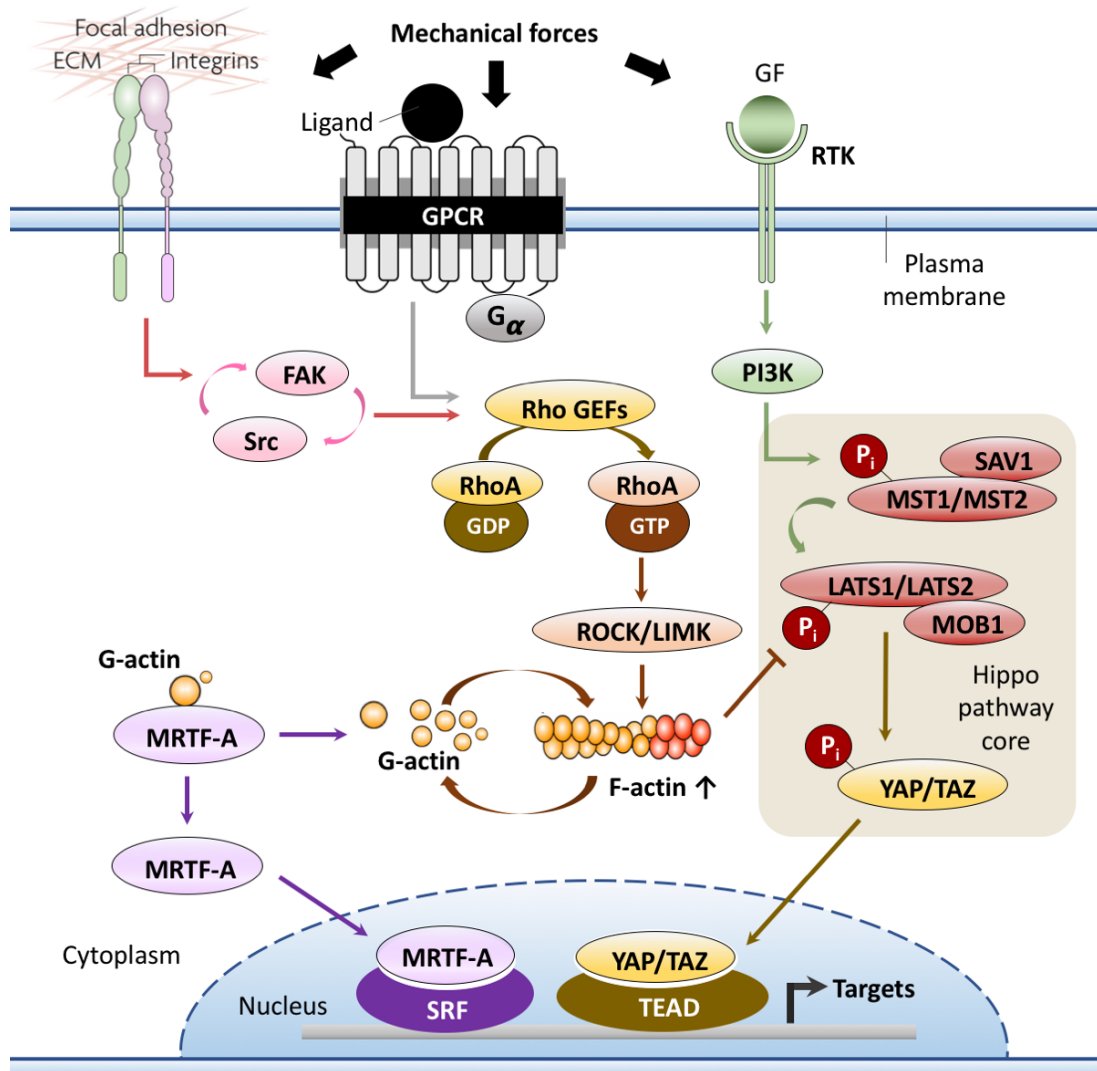
Figure 1-4. Rho-dependent pathway activated MRTF-A and YAP/TAZ relocalisation to the nucleus. Stimulation of receptors e.g. integrins, GPCR and RTK, regulate the activity of Rho GTPases via Rho guanine nucleotide exchange factors (GEFs). These effectors induce the activation of RhoA bound GDP to GTP which in turn to trigger Rho-associated protein kinase (ROCK)-LIM kinase along the (LIMK)-cofilin pathway, a major regulation of polymerisation equilibrium of g-actin and f-actin. The enhanced actin polymerisation reduces the g-actin pool bound to MRTF- A. The role of f-actin is also mainly participated in the Hippo pathway by inhibition of phosphorylated LATS1/ LATS2. Unbound MRTF-A and YAP/TAZ are then translocated to the nucleus and bind its transcription cofactor i.e. MRTF-SRF and YAP/TAZ-TEAD complexes target several genes which can modulate actin dynamics (adapted from Olson and Nordheim, 2010; Moya and Halder, 2019).

1.3.4 ERK signalling and activity in cell migration

The proteins extracellular signal-regulated kinases (ERK1/2) are the downstream components of a structurally related kinases, called mitogen-activated protein kinases (MAPKs). The signalling cascade of ERK regulators trigger fundamental cellular processes including cell survival, proliferation, growth, metabolism, migration and differentiation. The prototypical MAPK/ERK signalling pathway has been cover in reviews (See examples; Roberts & Der, 2007; Mendoza et al., 2011). In the case of ERK activation initiates a motility programme, occurs during cell cycles in single cells, expanded in collective cell migration and in complex tissues, where waves of ERK activity propagating across cycles of edge protrusion, adhesion and cell body contraction (Samson et al., 2022). These coordinated movement events are mainly orchestrated by the stimulation of Rho GTPases and their phosphorelation pathway that are driven by serum or growth factor-induced signals. Rho GTPases-linked transcriptional cofactors that promote growth have shared complex relationship to the action of SRF via SRF-MRTFs or SRF-TCFs (Figure 1-5) (Lavoie et al., 2020). The two classes of transcriptional coactivators MRTFs and ternary complex factors (TCFs; Elk-1, Elk-3 and Elk-4), regulated several cytoskeletal associated genes and cell proliferation, respectively (Zohn et al., 1998). For the ERK regulation of MRTFs, MRTFs are controlled by F-actin formation driven nucleoplasmic shuttling. ERK signalling can be neither a general activator nor inhibitor that precisely controls membrane trafficking in actin-dependent manner. Upon stimulated Rho family proteins, Rho triggers F-actin polymerisation which reduces the pool of G-actin (Muehlich et al, 2008; Panayiotou et al., 2016). Thereby, tethering of MRTFs translocation to the nucleus regulate organisation of actin cytoskeleton and related gene expression such as vinculin, zyxin, integrin α5 and tropomyosin (Salvany et al., 2014; Gualdrini et al., 2016). Upon ERK regulated SRF-TCF cascade complexes, ERK activated the early growth response including EGR1, FOS, JUN by phosphorylating which are robustly support cell proliferation (Fowler et al, 2011; Lopez-Bergami et al., 2010).

Figure 1-5. ERK regulation of cell motility activated ERK proteins and signalling through transcriptional controls of the cytoskeleton factors.

At the transcriptional level, SRF is a conserved transcription factor that mediated both of the serum response elements that induces many of the immediate-early genes (IEGs), and the activation of cell type-specific genes or gene associated cytoskeleton dynamics. ERK stimulates the ternary complex factors (TCFs), comprising ETS domain-containing protein Elk-1, Elk-3 and Elk-4, which is activated by phosphorylation of ERK contribute to switch on the transcription of the IEGs encoding JUN, FOS, MYC and EGR families. The other myocardin-related transcription factor (MRTFs including two isoforms of MRTF-A and likely MRTF-B), contributes to serum regulation via the binding of SRF, which are the downstream effector of the small GTPase RhoA. MRTFs constantly shuttle in and out of the nucleus. In resting conditions, MRTFs localises in the cytoplasm due to formation of RPEL-G actin complex. Upon serum stimulation, Rho GTPase stimulate the actin polymerisation, consequently positively regulate MRTFs nuclear import and activation of transcriptional activity of cytoskeletal genes such as actin, vinculin, zyxin, integrin α5 and tropomyosin (adapted from Lavoie et al, 2020).

1.4 Nuclear envelope remodeling – its role in positioning and functionality of the nucleus

The nuclear envelope (NE) is characterised as a double membrane sheet, that serves as both a protective membrane shell sheltering the genome and a specific site for versatile communication at the interface between the nucleus and the cytoskeleton (Crisp and Burke, 2008). Despites its important structural role in nuclear positioning, the NE is a dynamic and highly adaptable boundary that can remodel its composition and its mechanical stability. It is not only provides immediately repaired upon rupture or damage but also can rapidly disassembles and reforms during and after cell division in open mitosis (Ungricht and Kutay, 2017). NE remodeling is fundamentally involved in cell growth, differentiation and governs numerous biological functions such as determining nuclear size and stiffness, activity and translocation of transcription factors, or even controlling the epigenetic states via interaction with chromatin and also influence cell polarisation and migration (Bryant and Stow, 2005; Lin et al., 2001; Olsnes et al., 2003).

1.4.1 Nucleoskeleton-associated regulatory surface proteins

As a compartment boarder the nuclear envelope (NE) is composed of the outer nuclear membrane (ONM) and the inner nuclear membrane (INM) which have contact points creating membrane pores essential for nucleo-cytoplasmic exchange (Chaumet et al., 2015). These pores are filled with a nuclear pore complexes (NPCs) which constitutes the major gateway for the selective and controlled entry of molecules into interior via bi-directional transport of large molecules and the diffusion of small substances (Raices and Angelo, 2012). The ring-shaped NPC framework is such a large protein complex of membrane-bound proteins containing nucleoporins (NUPs), provides the building blocks for membrane attachment and facility of the protein-protein interactions (Knockenhauer and Schwartz, 2016). For nuclear envelope proteins that form intricate networks and their distribution in the role of dynamically organisation during mitosis and is responsible for nuclear integrity and genome regulation, as shown in Figure 1-6.

Figure 1-6 in this thesis contains material whose copyright belongs to a third party.

See figure 1a & 3a available on:

Ungricht, R. and Kutay, U. (2017) 'Mechanisms and functions of nuclear envelope remodelling', *Nat Rev Mol Cell Biol*, 18(4), pp. 229-245.

Figure 1-6. Nuclear envelope (NE) architecture and mechanism of NE proteins form networks undergoing open mitosis. A) Organisation of the specialised outer and inner membrane sheets (ONM and INM, respectively) of the endoplasmic reticulum (ER) in which an interconnection site is attached to chromatin (dark blue). Underneath the INM lies the nuclear lamina (pink) meshwork and integral membrane proteins provide structural support and mechanically active to the NE and contributes to chromatin organisation by anchoring the lamina-associated domains (LADs). The lamin-binding protein such as lamin B receptor (LBR), tethers heterochromatin to the NE via interaction of modified histones and heterochromatin protein 1 (HP1). Indeed, the LEM-domain (LAP2, emerin and MAN1) proteins associate with nuclear lamins, thereby generating NE-associated nucleoskeletal structure and also link to the chromatin-associated barrier-to-autointegration factor (BAF). The nucleus is connected to the cytoskeletal elements in turn attach to complexes at the NE formed LINC complex containing nesprins and SUN domain containing proteins. Nuclear pore complexes (NPCs) allow for the selectively nucleoplasmic exchange (structural assembly see in box). B) NE breakdown and reassembly, spindle formation is prepared for cell division by the separation of duplicated centrosomes, chromatin condensation and emerin localisation and functionality during the process (see in box) (adapted from Tews 1999; Ungricht and Kutay, 2017).

The nuclear shaping and positioning-regulated functions require transfer of the forces generated within cytoskeletal networks or transmitted through LINC complexes (Luxton et al., 2010). This mechanical interlink of the nucleoskeleton via the LINC complex then enables the transmission of forces via the cytoskeleton from the cell surface across the NE (Starr and Fridolfsson, 2010) into the nuclear interior, perhaps driving changes in chromatin organization or gene transcription (Guilluy et al., 2014; Bissell et al. 1982; and Wang et al., 2009). The LINC complex is formed by two fundamental units. i.e. I, The Sad1/UNC84 (SUN1-3) domain-containing proteins which on the inside of the NE bind to emerin, lamins and nesprins (Mejat and Misteli, 2010; Mellad et al., 2011). SUNs domain embedded at the INM that provide the mechanical link to the adjacent domain in the ONM layer. II, The nesprins, spectrin-repeat proteins, contain the Klarsicht, ANC-1 and SYNE homology (KASH) domain. These protein complexes thereby from the mechanical interlink or bridge between NE and the cytoskeleton (Sosa et al., 2013).

On the inside of the NE the lamina meshwork has gained importance as the ancestral intermediate filaments of the nucleus, which is formed by the A-type or B-type lamins (Shimi et al., 2008). Lamins are involved in the adaptation and remodeling of the NE during cell cycle, development, migration via the adequate balance between deformability and stiffness (Harada et al., 2014; Rowat et al., 2013). Recent insight has developed the role of A-type lamins controlling nuclear rigidity as an increased level of A-type lamins in relation to B-type lamins results in an enhanced stiffness (Ball and Ullman, 2005), while B-type lamins are associated with increased nuclear elasticity (Griffis et al., 2002, Kalverda et al., 2010). Therefore, cells adapt their relative lamins content as a consequence of the demands of the mechanical loads in their surrounding environment (Lombardi et al., 2011) and further integrate lamin's function directly into the NE organisation to reflect or transmit mechanical forces. The dynamic interconnectivity of lamins is well regulated by multivalent membrane-bound proteins linked to chromatin networks where a platform is established via lamina-associated domains (LADs). The structural relationship of laminA/C and LADs provide gene association with heterochromatin (Scaffidi and Misteli, 2006) allows changes to the accessibility of genes and will affect transcriptional regulators (Martins et al., 2012) whereas, euchromatin containing active genes are key region

of silent chromatin site located at the core of the nucleus where they attached to laminA/C at the nuclear periphery (Uzer et al., 2016).

The insight into the nucleoskeletons and LINC complex comprising protein-protein interactions that serve as signaling scaffolds and nuclear regulators for NE tethering or chromatin mobility, are exciting open frontiers in cell biology. The role of cell-type-specific nucleoskeletal proteins remains to be investigated for uncovering the importance of nucleoskeletons relate to gene expression and integrity of the genome, as well as driving some progress towards understanding pathogenesis, development and possible therapies including disease and aging.

1.4.2 EDMD relevant signaling & membrane protein complexes

A concept of force-induced molecular changes in NE organization, describing mechanosensory and mechanotransduction confers conformational and post-translational alternation (e.g. phosphorylation) in membrane proteins (Kirby and Lammerding, 2018). The NE-associated protein meshwork functions in withstanding and balancing an isotropic distribution of forces to maintain NE integrity, thereby preventing nuclear rupture and 'defending' the underlying chromatin (Furusawa et al., 2015; Schreiner et al., 2015). The INM protein emerin contributes to the stiffening of isolated nuclei in response to force application via the LINC complex component nesprin1 (SYNE1) (Guilluy et al., 2014). Tension and emerin phosphorylation linked to the nuclear lamina protein via the accessibility and leading to reduced laminA/C level. Furthermore, force-stimulated phosphorylation of emerin on the relevant Tyr74 and Tyr95 residues driven changes in decrease stress fibre formation (Meier and Brkljacic, 2009), which maybe a crucial aspect of actin remodeling events at the ONM and facilitate chromatin dynamics (Berezney and Coffey, 1997). In this study, the emerin knockout models in cultured human fibroblasts and epithelia (see chapter 4 & 5) used to elucidate the specific pathway that provide linking to cytoskeletal and nuclear binding partners of emerin, highlighting the function of emerin serve as a downstream effector of mechanical force is supported by its biochemical properties. Characterization of emerin is shown in Box1-2).

Box1-2. An integral protein emerin – its function & architecture

Emerin is anchored at the INM, it is encoded by the EMD gene, which consists of 254 amino acid residues with predominantly hydrophilic amino acids and a single hydrophobic region (Koch and Holaska, 2014). Emerin is a 34 kDa, belongs to the family of the LEM-domain proteins which LAP2 and MAN1 which all contain a conserved ~40-set of residues in each family member (Bengtsson and Wilson 2004; Berk et al. 2013). Emerin is expressed in most essentially human tissues. Mutation(s) of emerin can result in a rare degenerative myopathy named X-link Emery-Dreifuss muscular dystrophy (EDMD) with is clinically characterised by progressive muscle wasting contractures of the elbow, neck and Achilles tendons and cardiac conduction defects (Astejada et al., 2007). One of the striking association of emerin structure, is its co-localisation with interacting A-

Figure 1-7. Structure and localisation of emerin. A) A steroview of the superposition of emerin complex with the backbone blocks (left) and ribbon diagram (right). The stoichiometry of structural emerin was characterised by NMR spectroscopy (Cai et al., 2007). B) The GFP-emerin intracellular colocalises with ER marker (MAC256), lysosomal marker (LAMP1) and laminB (red) at the nuclear envelope of C2C12 cells (Fairley et al., 1999) C) Distribution of emerin (green) and its binding partner laminA/C (red) tracking with cell cycle-dependent manner in HeLa cells at the NE staining of DAPI (blue) to visualise the nucleus. (Dubinska-Magiera et al., 2019) Scale bar = 5µm.

Emerin and other LEM-domain proteins family (i.e. LAP2ß, Lem2 and MAN1) bind directly to lamins and barrier-to-autointegration factor (BAF) (Wang et al., 2002), together forming the nuclear lamina (Funakoshi et al., 1999, Gruenbaum et al., 2002). The LEM-domain of emerin interacts individually with a conserved chromatin protein BAF or BAF-DNA complexes which dimerisation of BAF binding to dsDNA non-specifically and thereby bridge DNA molecules (Yuan and Xue, 2015), involve nuclear assembly, dictates higher-order chromatin structure and also represses gene regulatory by inhibiting transcription activators (Brachner and Foisner, 2011; Mans et al., 2004).

1.5 Biomaterial engineering approaches for tissue regeneration

The biomolecular and physical information coded within the complexity of the extracellular milieu and cell-cell interaction are informing the development of novel biomaterials for tissue engineering. This spurs interest in recreating extracellular influences in bioactive structures, to manipulate cell behaviour within a scaffold for functional domains that promote tissue regeneration (Place et al., 2019). Such simple strategies do not offer a universal property for regeneration. The healing response can be restrained by an age-related degenerative population or the intrinsically low generation potential of certain tissues or by pro-inflammatory and scar formation (Li et al., 2023). The use of cells as a therapeutic option provides natural powers of self-organisation and under the combination of biomaterial approaches can trigger signal transduction in which it conveys appropriate cell responses (Chen and Liu, 2016). Furthermore, several techniques of engineering bioactive scaffolds propose therapeutic routes including engineered cell lines, topography, mechanical stimuli, stiffness and dimensionality of the ECM matrix that allows the most effective outcome for a given tissues (Cortese et al., 2009). A graphic architecture of bioactive materials in cell-matrix interactions direct cell recognition and response (Figure 1-8) (Joyce et al., 2021).

Figure 1-8 in this thesis contains material whose copyright belongs to a third party.

See figure 1 available on:

Joyce, K., Fabra, G. T., Bozkurt, Y. and Pandit, A. (2021) 'Bioactive potential of natural biomaterials: identification, retention and assessment of biological properties', *Signal Transduct Target Ther,* 6(1), pp. 122.

Figure 1-8. Material designs and development targets to functional sites on macromolecules, triggers cell recognition and subsequent signalling cascades. The action of cell surface receptors recognise material motif and permit a virtually limitless binding specificity which can activates several lines of cell pathway in the following cascade in response. I, Jak/STAT and NF-κB pathway initiates cell adhesion, movement and endocytic activity. II, Rho-GTPase and MAPK pathway in regulating of cell survival, proliferation, differentiation and ECM deposition. III, PI3K/Akt and TLR pathway related immunomodulatory response, cytoskeleton in fibre or stress organisation and receptor ligand activity (Joyce et al., 2021).

1.5.1 Mechanical stretching activated growth

Several types of mechanical stimulation (e.g. shear flow, osmotic pressure and hardness of substratum) are constantly present in the environment of most living cells and their physical linkage provides transmition of these through cytoskeletal networks to the nucleus (Iwadate et al., 2013; Monemian Esfahani et al., 2019). Static and cyclic strains are essential for the maintenance of physiological conditions of tissues in various organs. Cyclic deformation of soft tissues is mainly present in the heart, blood vessels, skin, muscles, tendons, lungs as well to a lesser extent as others (Kamble et al., 2017). Cells also continuously perceive external passive mechanical stimuli that are transmitted from the elastic substrate to the cell monolayers (Ursekar et al., 2014). Furthermore, uniaxial forces have been shown to enhance skeletal flexibility and physical performance (Lewis 2014; Zakaria et al., 2015). Mechanical strains on cells often cause cell elongation (Kim et al., 2015), stretching fibroblasts leads to the production of ECM and affected to their role of remodeling (Chiquet et al., 2003).

Static stretching triggers the range of motion for a particular resistive torque level (Nordez et al., 2010). The acute effects of applied static strain showed significantly decrease tissue stiffness (Kay et al., 2015) and torque relaxation for prolonged activated field (Bressel et al., 2002). However, unidirectional stretch unable to reach the dynamic balance of torque or stiffness in the tissue (McNair et al., 2001). Constant velocity stretching also known as cyclic stretching, revealed a trend in enhancing tissue strength (Maeda et al., 2017). Changes in passive torque corresponding to their stiffness after cyclic stretching, elicit nearly dynamic balance by adjusting stiffness at the same angular velocity (Maeda et al., 2016).

1.5.2 Topographic pattern of shaped cells and their behaviors

Dynamic culture surface regulates cellular behavior, significantly modulate the molecular metabolism and their cellular functionality (Mirbagheri et al., 2019). Cell culture on three-dimensional (3D) platforms has been widely used to mimic the natural environment and morphology, allows interaction between cells and uniforms a closer distribution of adhesion molecules over the cell surface (Knight and Przyborski, 2015). Study of the cell react to two-dimensional (2D) culture

emphasise the planar and stretched cell morphologies (Alves et al., 2010; Kolind et al., 2012). The difference between 2D and 3D models, confer the platform of choice that suitable for specific application (Duval et al., 2017). However, existing 2D and 3D systems have not captured optimal ECM architectures, such as aligned fiber networks (Ray et al., 2017; Tabdanov et al, 2018). Topographic pattern is highly structured surfaces composed of diverse patterns, referred to as 2.5 dimensional (2.5D) channels. Cells adhered on particular defined patterns such as grooves, posts, and inside pits, guide cell alignment, shape, adhesion and its impact on cell functions (Mirbagheri et al., 2019). Varying the dimension parameters (e.g. width and depth) of applied topography can carry distinct cellular signaling. Grooved surfaces aid cell spreading and the strength of the cell-surface influenced by a particular depth of pattern (Walboomers et al., 1998).

1.5.3 Engineering the cells at a specific gene with the CRISPR-Cas toolbox

The advent of straightforward genome editing using RNA-guided prokaryotic CRISPR-associated (Cas) proteins that harness natural DNA repair mechanisms (Chavez et al., 2023) have gained widespread acceptance for modifying and manipulating the genome more easily and precisely than ever before. Knocking out genes with robust and reliable outcomes is essential to decode the function of a given genes and identifying the roles of key regulatory elements. The breakthrough in genetic manipulation technology originated from targeted immunity present in prokaryotes (Ishino et al., 1987, Mojica et al., 2000). The bacterial genome sequences between the repeats termed clustered regularly interspaced short palindromic repeats (CRISPRs) was characterised by their similarity that matched to parts of phage genomes (Bolotin et al., 2005) and often co-localised with the CRISPR-associated (Cas) proteins (Jansen et al., 2002, Haft et al., 2005). The functional CRISPR/Cas loci at the CRISPR array are comprised of identical repeats intercalated with DNA-targeting spacers that encode the crRNA and Cas proteins with putative nuclease and helicase domains (Chavez et al., 2023) (See graphic structure Figure 1-9).
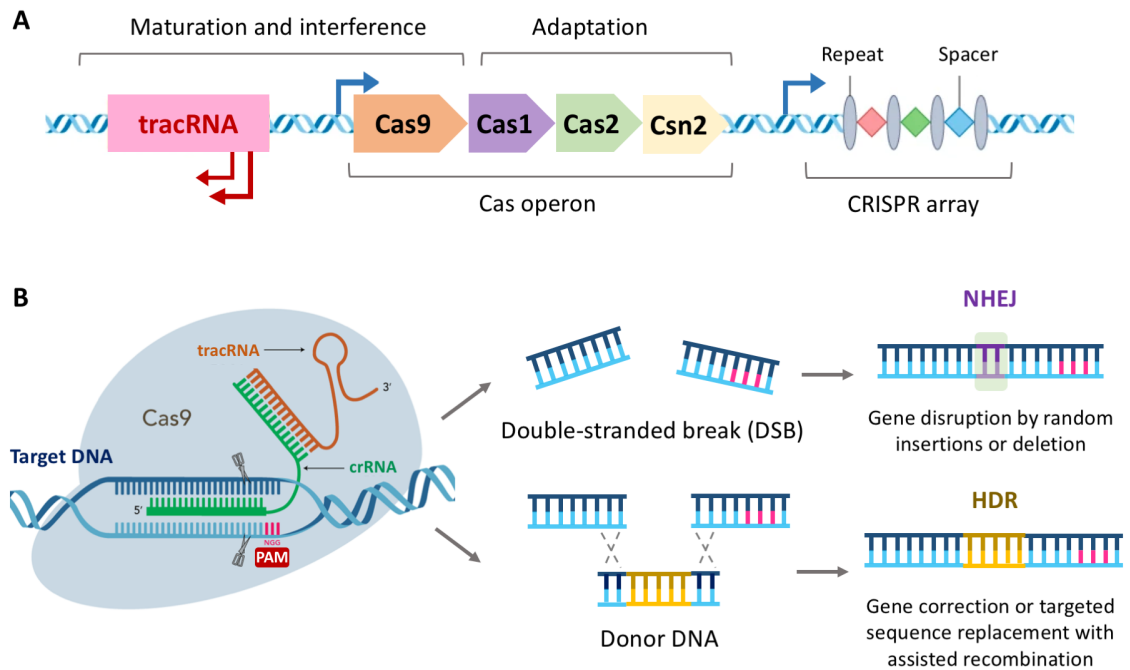
Figure 1-9. The CRISPR/Cas9 system at CRISPR locus and mechanism of RNA-guided cleavage of target DNA triggers repair mechanisms. A) The prokaryotic genome encodes a CRISPR array and Cas gene operon with tracrRNA. A CRISPR array containing spacers separated by repeats, spacers which are short piece of DNA that have match homology to the genome of the invading DNA of pathogens. B) The creation of a DNA double-stranded break (DSB) initially generated by Cas9 enzyme at the genomic locus using its two catalytic activities to cleave DNA target site in both strands adjacent to PAM sequence and matching 20-nt sequence of sgRNA. Nucleases-induced DSBs can be repaired by nonhomologous end-joining (NHEJ) and homology-directed repair (HDR). NHEJ pathway is activated and can lead to efficacy introduction of insertions and deletions (INDELs) or even substitutions at the DSB target site which can perturb the translational reading frame of coding sequence frequently resulting in the disruption of gene function. HDR mediated repair occurs in the presence of exogenously supplied DNA donor templates. The HDR mechanism can be used to introduce specific point mutations or to insert desired sequences through homology recombination which offers precise gene modification such as gene knock-in or correction (adapted from Chavez et al., 2013; Doudna and Charpentier, 2014).

The mechanism of this adaptive immunity to protect against phages and invading genetic elements, simplified occurring in three stages: (I) The acquisition stage, insertion of a short fragments of the foreign DNA as a spacer sequence into the CRISPR repeat-spacer array within the host chromosome, thereby providing a genetic record to prevent reinfection (Barrangou et al., 2007; Amitai and Sorek,

2016). (II) Transcription of the CRISPR array; the CRISPR array is transcribed and followed by its endonucleolytic cleavage of precursor crRNA (pre-crRNAs) that undergoes maturation to generate short mature CRISPR RNA (crRNAs) (Brouns et al., 2008). The crRNAs that each contain a single spacer, further hybridise with a small trans-activating CRISPR RNA (tracrRNA) (Deltcheva et al., 2011). (III) Cas9 nuclease unwinding DNA by generating a double-stranded break (DSB), crRNA-directed cleavage of invading nucleic acid at sites complementary to the crRNA spacer sequence. Once homology is recognised, cutting the DNA and thereby inhibiting from infection (Bondy-Denomy and Davidson, 2014; van der Oost et al., 2014). The CRISPR/Cas9 platform has been used for large-scale genome-wide functional screening and expanded series of Cas applications beyond genome engineering and regulation (Qi et al., 2013). Translating CRISPR into sufficient blocks of activate transcription for gene repression and activation, respectively (Gilbert et al., 2013; Mali et al., 2013). CRISPR-mediated epigenetic modification can be alternatively used to reprogramme the transcription by writing or even erasing changes in histone epigenomic regulators (Nakamura et al., 2021). The CRISPR/Cas complex and repair mechanisms (as illustrated in Figure 1-10) (Chavez et al., 2023).

1.6 Biomaterial-directed immunomodulation

Biomaterials and tissue engineers draw heavily from of crossing range of multi-disciplines to take a holistic view of biomaterial development and investigate cell-material interactions along with biological conditions (Rajagopalan et al., 2013). The transition of biomaterial from bench to clinic have raised biocompatibility concerns (Raut et al., 2020). The study of *in vitro* cell-cell and cell-material interactions and *in vivo* implantation of biomaterials are often used to examine their biocompatibility, to develop functional biomaterials with an appropriate host response in any given application (Ratner, 2019). The foreign body reaction in response to a biomaterial application depends on conditional factors such as contact duration, material chemistry, surface properties, nano- and micro-morphology, degradation rate, porosity and sterility (Anderson, 1988).

Figure 1-10. Application of CRISPR/Cas9 to genome-wide screening and engineering. A) Partial and reversible repression with CRISPR interference (CRISPRi) is capable of targeted gene downregulation via the dCas9-KRAB system for studying gene functions. B) CRISPR activation (CRISPRa) with fusion of dCas9 to transcriptional activators such as VP64 to enabled systematic gain-of-function perturbations at endogenous loci. C) Targeted DNA methylation using DNA methyltransferases such as DNMT3 causing long-termed and heritable gene suppression. D) Removal DNA methylation by the fusion of methylcytosine dioxygenase such as TET to dCas9. E) The epigenetic landscape can be marked by fusing epigenetic modifying enzymes such as p300 or LSD1 in order to modifying histone residues resulting in upregulation or downregulation of targeted genes. F) Fusing dCas9 or nickase Cas9 (nCas9) to creates single-stranded DNA breaks for base conversion of local cytosine to uracil via the action of cytosine deaminase APOBEC1 (Chavez et al., 2023).

Biodegradable materials physicochemical properties are impacted by size, shape, stability and molecular weight along with surface features such as chemical functionality, charge and hydrophobicity (Figure 1-11A) (Andorko and Jewell, 2017). These properties involve in directing immune responses during implantation of materials to the site of injury. The immune system has quickly evolved to recognise pathogens or non-self agents in the body (Janeway and Medzhitov, 2002; Matzinger, 2002). Figure 1-11B provides a temporal sequence of immunogenic cells that become activated over time countering changes in damaged cells and implanted materials (Laskin et al., 2011).

Figure 1-11. Regenerative characters are influence by biomaterial mediated immunogenic features. A) Intrinsic properties of tunable materials comprise size, shape, hydrophobicity, surface charge, and molecular weight aid interaction with the immune system. These factors result in controlling adaptive immune response, stimulation of differentiated macrophages and dendritic cells, recognition and confinement by antibody and complement proteins and even regulating fibrotic formation. B) Temporal sequence of immune and associated cells become activated after damage and also response to biomaterial implantation. This diagram highlights the main cellular players from early phase of infection to late resolution often cause fibrous encapsulation. Targeting sequential interplay with innate and adaptive immune response, associate with local skin resident cells such as fibroblasts (Andorko and Jewell, 2017; Laskin et al., 2011).

The innate human immune system includes neutrophils and mononuclear phagocyte cells: dendritic cells, monocytes and macrophages (Nestle et al., 2009). Neutrophil recruitment is the first line of defense against invading pathogens (Caputa et al, 2019) and are co-opted in the defense against "intruding materials". Macrophages which can be considered as a hallmark of host cell defender due to their plasticity, is then further activated in response to protect the body from potentially harmful agents (Laskin et al., 2011). Skin macrophages are mainly derived from the resident macrophage by recognising damage-associated molecular patterns (DAMPs) and pathogen-associated molecular patterns (PAMPs) or T cells activating monocytes (Rodrigues and Gurtner, 2017). These immune cells are following support granulation tissue in resolution phase, serve as helper in repair or therapeutic intervention.

1.7   Project rational and aims

Despite the advance in skin repair, the source of donor availability, rapid clearance of damaged cells, and activated an adequate regenerative character still remain a challenge (Kanapathy et al., 2016). Cell-based scaffold has revolutionised the capability to direct the program of cells through tunable properties with environmental cues (Liu et al., 2022; Sedimayer et al., 2018). Understanding how cells respond to the mechanics of microenvironments with improved delivery via biomaterial scaffolds, may open fascinating opportunities for tissue regeneration and regenerative medicine.

Recent far-reaching advances in functional and molecular effects of mechanical stimulation of cells, this research project has applied interdisciplinary cooperation of cell-based scaffold and applied tissue engineering approaches to deliver the functional mechanical stimuli to implanted cell populations to activate regenerative activities of skin healing. This thesis adopted a combinatorial approach, employing dermal fibroblasts or epithelial therapies in combination with mechanical force application for skin regeneration and wound healing.

The absence of a precise molecular mechanism of cell mechanobiology and mechanotransduction pathways currently present the major challenge for *in vitro* cell interactions. The focus of this thesis is to investigate the functional consequences of cells interacting to their microenvironment under high and low mechanical forces. Analysis of relevant mechanosensitive regulators including actin polymerisation and interconnected transcription factor, MRTF-A is detected to access the activated mechanotransduction processes. Under dynamic microenvironments, cells were cultured on highly stretchable membranes and incorporated into stretching devices to activate mechanical properties. On the other hand, the system of decreased mechanical forces was generated by the withdraw expression of a key regulator in the actin binding complex inside the nucleus, emerin. The model of emerin knockout cells were created to study in more detail the function of the molecular switches with regard to lower mechanical forces.

The aim of this thesis includes the design and characterisation of cell-biomaterial with altering mechanical forces through topography, stretching, and CRISPR-based gene knockout networks that drive specific biological set points in force transmission from external outputs via cytoskeletal complex or internal force-regulated nuclear organisation and thus, influence cell functionalities. Taken together, the ultimate goal of this work is to propose a biocompatible scaffold with cell-based tissue-engineered therapy to offer a new avenue to clinical application for skin regeneration and fulfill the mechanisms and molecular pathways underlying cell mechanobiology.

CHAPTER 2 MATERIALS AND METHODOLOGY

2.1 Materials

List of Reagents

Surface preparation and modification

Chloroform .... Thermo Fisher Scientific
Ethanol .... Thermo Fisher Scientific
Fibronectin .... Sigma-Aldrich
Polycaprolactone (MW: 80,000) .... Sigma-Aldrich
Polydimethyl siloxane .... Dow Corning Corporation

Cell culture reagents

Dulbecco's modified eagle medium .... Sigma-Aldrich
Fetal bovine serum .... Thermo Fisher Scientific
L-glutamine .... Invitrogen
Medium-199 .... Thermo Fisher Scientific
Sodium pyruvate solution .... Sigma-Aldrich

Immunofluorescent staining

Bovine serum albumin (BSA) .... Sigma-Aldrich
Fluorescein streptavidin .... Vector Laboratories
Formaldehyde .... Sigma-Aldrich
Horse biotinylated anti-mouse IgG .... Vector Laboratories
Horse biotinylated anti-rabbit IgG .... Vector Laboratories
Rhodamine Phalloidin .... Invitrogen, Molecular Probes
Triton$^®$ X 100 .... Sigma-Aldrich
Tween-20$^®$ .... Sigma-Aldrich
Vectashield mounting media with DAPI .... Vector Laboratories

Quantitative real-time polymerase chain reaction

Brilliant III Ultra-Fast SYBR Green qPCR Master Mix .... Agilent Technologies
Deoxynucleotide (dNTP) Solution mix .... New England Biolabs
Phenol/Chloroform .... Sigma-Aldrich
Random Hexamers .... Invitrogen
RQ1 RNase-Free DNase .... Promega
SuperScript^{TM} IV Reverse Transcriptase .... Invitrogen
TRI Reagent$^®$ .... Sigma-Aldrich

Westernblot assay

Methanol .... Thermo Fisher Scientific
NuPAGE$^®$ LDS Sample Buffer (4X) .... Invitrogen

2.1 Materials (Continue)

List of Reagents
Westernblot assay NuPAGE® MES SDS Running Buffer (20X) .... Life technologies NuPAGE® Transfer Buffer (20X) .... Life technologies NuPAGE™ 4-12% Bis-Tris-Gel .... Invitrogen Ponceau S solution .... Sigma-Aldrich Donkey Anti-Rabbit IgG H&L (HRP) preadsorbed .... Abcam Polyclonal Goat Anti-mouse Immunoglobulins/HRP .... Dako

2.2 Substrate preparation and surface modification

2.2.1 Formation of polycaprolactone thin film

To fabricate a thin-sheet of semi-crystallised polycaprolactone (PCL), the membrane was prepared by spin coating on a silicon wafer with 12% (w/v) PCL dissolved in chloroform solution at 1,500 rpm for 30 seconds using spin coater system (Brewer Science, USA). The membrane thickness is approximately $20\mu m$ (measured by a micrometric gauge). To create amorphous PCL, the PCL coated wafer was then heated up to 90°C and subsequently quenched with a high temperature gradient using a liquid nitrogen cooled cylindrical copper block. Membrane was peeled off the wafer and cut into the desired size i.e. 7x30mm rectangles used as a stretchable substrate for unidirectional stretch.

2.2.2 Rapid curing of polydimethylsiloxane (PDMS) elastomer

Dow Corning PDMS (Sylgard 184) was prepared by mixing of PDMS elastomer base component with the curing agent at a ratio of 1:9 weight-to-weight, followed by deaeration under vacuum. Then, the mixtures were poured onto the designed microtopographic pattern (SU-8 masters with $12.5\mu m$ repeated $5\mu m$ deep structures). The curing polymer was incubated at 80°C for 2 hours.

2.2.3 Substrate surface modification

To increase hydrophilicity of the surfaces, the substrates were placed in a plasma cleaner (Harrick Plasma, USA) and exposed to air plasma for 1-1.17 minutes. Beyond providing an adhesive structural support, human plasma fibronectin was

used to modify the surface plasma treated PDMS. The membranes were absorbed with 20 μg/ml of fibronectin for an hour at 25°C before cell seeding.

2.3   Cell culture

Human foreskin fibroblast cells (BJ1, CRL-4001[TM]) immortalised with telomerase reverse transcriptase (TERT) and human epithelial kidney cells (HEK293, CRL-1573[TM]), were cultured in Dulbecco's modified eagle medium (DMEM). The growth medium supplemented with 20% medium-199 (for BJ1-hTERT), 10% fetal bovine serum (FBS), 2mM L-glutamine, 1mM sodium pyruvate and 1% penicillin-streptomycin. The cells were passaged every a few days to maintain exponential growth at sub-confluent levels in a 37°C incubator with 5% CO_2.

2.4   Immunofluorescence assay

For cell staining, the cells were fixed with 4% formaldehyde/PBS and permeablised using 0.5% Triton[TM] X-100/PBS. Next, cells were blocked in 1% BSA/PBS and stained primary antibodies (1:100). In conjugation with phalloidin-rhodamine (1:50), the samples were then incubated overnight at 4°C. Afterwards, cells were washed with 0.5% tween 20/PBS (3 x 5mins) to minimise background labelling. Secondary stains were obtained by addition of horse biotinylated anti-rabbit or anti-mouse IgG (1:50) in BSA/PBS and incubated at 37°C for an hour. After washing steps, Fluorescein isothyiocyanate (FITC)-Streptavidin (1:50) in BSA/PBS was added to samples and incubated for 30 minutes at 4°C. Samples underwent washing stages and were finally stained for DNA with 4'6-diamidino-2-phenylindole (DAPI). Cells were visualised using a semi-automated motorised fluorescence microscope (Olympus BX51, USA) at 10X magnification with Surveyor imaging software.

2.5   Image and statistical analysis

For a calibration scale with an image of 0.01mm stage micrometer, overlay fluorescent images were proceed and exported to measure the cell size via ImageJ/Fiji. Using the threshold tool to optimise the pipeline of cell profiling, images were exported to CellProfiler software. To increase data accuracy, objects touching the cell perimeter were discarded together with selected the cell size-specific measurement. Image analysis is mainly focused on alteration of the phenotypes include cell morphology, intensities, radial distribution and texture

measurement. Figure 2-1 exemplified the overview of image analysis that combine fluorescent imaging into specialised modules for each identified cell or subcellular compartment. For statistical analysis, unpaired two samples Student's t-test where applicable was processed using R software.
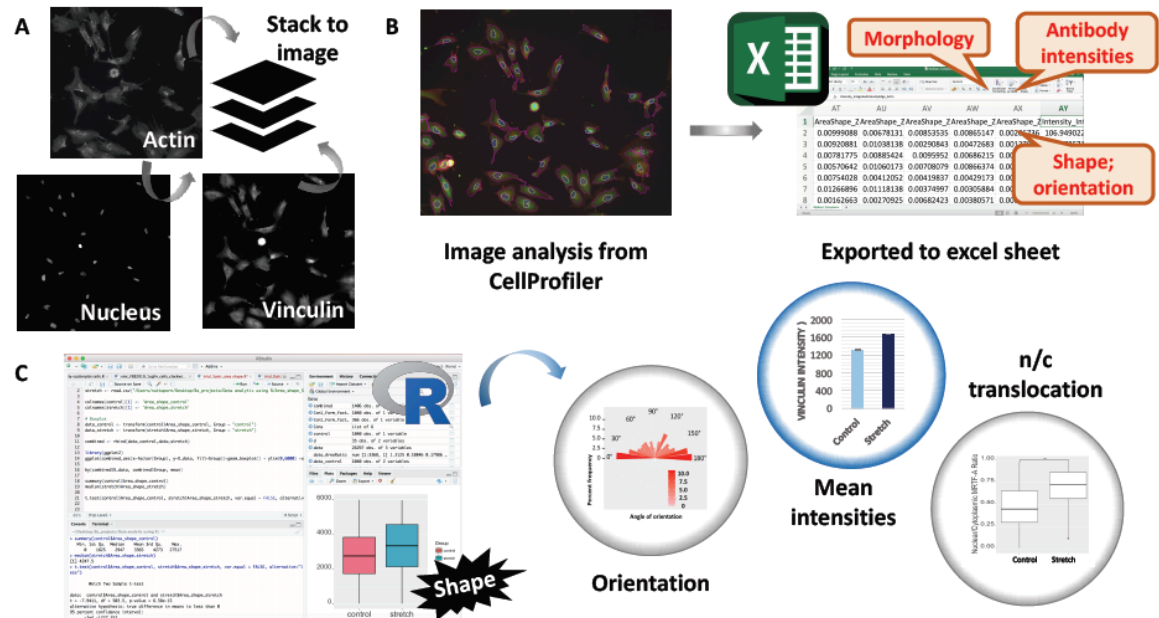
Figure 2-1. Data and image analysis flow diagram. A) Configuration of the cell components and its cytoskeleton. CellProfiler obtained data from the input raw images from all 3 fluorescent channels sampled. B) An example showing identified cells (red outline) and measurement output from the software into an Excel sheet. C) For statistical analysis, sample groups were categorised and compared using R software as well as selected measurements plotted.

2.6 The quantitative real-time polymerase chain reaction (qRT-PCR)

In order to prepare the RNA extraction and cDNA synthesis for qRT-PCR assay, the cells were seeded to reach at approximately 80-90% confluency on tissue culture plate (TCP) or elastomeric substrates before RNA extraction. To isolate RNA from the cells, TRI Reagent® was added to the cells and incubated for 5 minutes at room temperature, centrifuged at 12,000g for 2 minutes. Next, the RNA in supernatant mixtures were purified using Direct-zol RNA Miniprep Kit (Zymo Research Corporation). To eliminate the contaminating DNA in the RNA samples, DNase I treatment was further proceed. The DNA/RNA mixtures were incubated with DNase I/RQ1 buffer at 25°C for 20 minutes. The final step of RNA purification, phenol/chloroform extraction was performed at a ratio of 1:1

(phenol/chloroform:RNA samples) and subsequently recovery of the RNA yields using isopropanol precipitation. The purified RNA was pre-treated with SuperScript^{TM} IV Reverse Transcriptase for cDNA synthesis. The cycling temperature in each process is shown in Table 2-1.

Table 2-1. The steps of Thermal cycling used for cDNA synthesis

Reactions	Temperature (°C)	Timing (mins)
Priming RNA using random hexamer for extension	23	10
Reverse transcription	55	10
Inactivation	80	10

In a qRT-PCR reaction, the Brilliant qPCR master is formulated with Taq DNA polymerase, combined to approximately 40ng of cDNA templates, 300nm forward and reverse primers, 0.3 μl of diluted ROX reference dye and adjusted the final volume with nuclease free PCR grade water into 20μl. The thermal cycle diagram of qPCR experiment is as shown in Figure 2-2. The detection was measured by SYBR green dissociation curve using Mx3000P^{TM} and MxPro software.
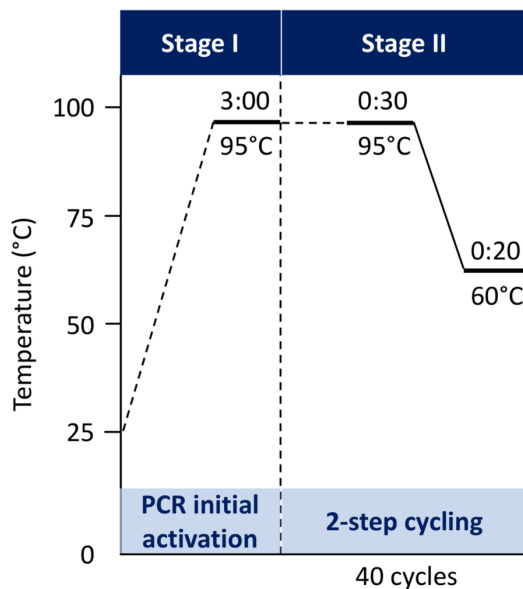
Figure 2-2. A schematic diagram of two-step cycling protocol in qRT-PCR that includes a denaturation step at 95°C, combined annealing/extension step at 60°C and subsequently detect fluorescence data.

2.7   Westernblot assay

Cell lysates were harvested after 7 days of cell seeding. The cells were washed twice with DPBS, subsequently extracted the proteins with 0.5% SDS in Tris-HCl buffer. To control the equal amount of protein loading, the comparative analysis

was performed using Ponceau S staining. Briefly, 20 µg of protein was mixed with sample loading buffer and further denatured at 70°C for 15 mins. In the first step of westernblot, the proteins were separated using Gel electrophoresis. The samples were loaded onto pre-packed 4-12% Bis-Tris-Gel and run with ice-cold running buffer at 200V for 30 minutes using Bio-RAD. Next, the separated proteins were transferred into solid phase via nitrocellulose membrane at 30V for 1.5 hours at 25°C. The blots were then blocked in 5% milk/TBST at room temperature for an hour. Secondly, immunodetection was used to label the following primary antibodies at the indicated dilutions (as shown in Table 2-2), incubated 4°C overnight. The blots were washed with 0.1% tween 20/TBS (3 x 5mins) on a shaker platform. After that, the secondary antibodies: anti-mouse HRP (1:1000) or anti-rabbit HRP (1:3000) were applied to the blots at 25°C for an hour followed by washing with 0.1% TBST (3times). Finally, the membrane membranes were incubated with enhanced chemiluminescence (ECL) at 25°C for 1 min prior to detection using the Fujifilm LAS-3000 imaging system.

Table 2-2. The primary antibody was used in westernblot assay.

Primary antibodies	Product details		Working dilution
	Supplier	Cat no.	
Alpha tubulin polyclonal antibody	Proteintech	11224-1-AP	1:2000
Mouse monoclonal anti-EMD antibody (1H9)	DSHB, University of Iowa	MANEM10	1:130
Phospho-p44/42 MAPK (Erk1/2) (Thr202/Tyr204) (E10) Mouse mAb	Cell signaling	9106S	1:2000
P44/42 MAPK (Erk1/2) (3A7) Mouse mAb	Cell signaling	9107S	1:2000
Rabbit polyclonal anti-Mkl1/MRTFA antibody	Abcam	Ab49311	1:800
Recombinant Anti-Lamin A + Lamin C antibody [EP4520-16]	Abcam	Ab133256	1:5000

CHAPTER 3 MECHANICAL STRETCHING OF FIBROBLASTS

3.1 Introduction

Cells of every living organism exist in a dynamic physiological environment and are constantly subjected to a wide range of mechanical forces such as fluid shear flow, tensile strain and stretching force (Bershadsky et al., 2006; Kirby and Lammerding, 2016). The mechanism that underlie the extraordinary capacity of cell sensing their environment are a cascade of signaling events that happen in response to those microenvironmental features and its deformation (Tajik et al., 2016). Cells not only can actively generate forces (Cai and Sheetz, 2009) but they also being passively mechanically stressed, and these mechanical changes exert measurable effects on cell dynamics, behaviours and eventually cell fate (Ingber 2008). These mechanical cues direct many essential aspects of the cellular machinery during growth, function, development and maintain a homeostatic level of intracellular tension (Watanabe and Mitchison, 2002; Webster et al., 2014).

Insights into the adhesive interfaces between cells and the surrounding matrix, a more biomechanically competent tissue construct is critically needed for optimal controlled cellular mechanical loading. In attempts to create a biocompatible scaffold that can closely mimic the natural environment *in vivo*, living cells are often exposed to aligned architectures. Thus, the cells elongate along anisotropic matrix by a process termed contact guidance (Harrison, 1912; Weiss, 1945). This finding developed the biohybrid materials containing aligned ECM fibres, that contact-guided cell alignment could be replicated by combining synthetic polymers, biomimetic coating and microgroove topography (Curtis and Varde, 1964; Hoffman-Kim et al., 2010).

Mechanical stimulation devices which are commercially available offer limited functional customisation and constrained force measurement capability (Atcha et al., 2018; Raveling et al., 2021). This study proposed stretching systems with an aspect to enhance mechanical forces in the cellular microenvironment, allowing fully customisable devices to meet demanding research. Together, these fulfill the knowledge gap in molecular pathways and how cells respond to mechanical

signals and influence cell behaviours. In this chapter, a series of novel designs of stretching devices were developed with the aim of stimulating cells and their microenvironments by passively pulling the cells through the deformation of biomaterials. It has been hypothesised that applied force externally by stretching is currently associated with mechanosensitive elements of cells and tether cell growth, movement, or even contractile function. To address these mechanobiology studies, the stretching systems have been fabricated to investigate the effect of mechanical stimuli on mechanosensitive mechanisms involve reorganisation of the cytoskeleton, transcription factor regulation, and cell adaptation. Two comparative cell stretching systems have been developed to investigate the local responses of fibroblasts to mechanical loading. Observation of these mechanical processes of human dermal fibroblasts derived from foreskin were used to determine the signal propagation and integration of force within the cells, linked to the nucleus. In this chapter, a uniaxial stretcher was designed and connected to stepper motor that allowed varying rates of unidirectional or cyclic stretching tightly controlling the cell-substrate movement. Cells detected the mechanical environment and adjusted the organisation of their F-actin cytoskeleton; this cytoskeletal redistribution, reinforced linkages and hence the influence of the stretch on cell shape and motility (Vogel and Sheetz, 2006). The growing of evidence from many studies that have evaluated the effect of applied tensile strain at a varying level of up to 20% on cells in connective tissue (Simpson et al., 1999; Shao et al., 2013; Chen et al., 2018). As the cytoskeleton acts as a signal integrator, it is highly sensitive and adaptive to mechanical load. The actin networks and bundles have revealed that they are mechanically interconnected to allow force transmission of these external stimuli across the cells (Schwarz and Gardel, 2012), Protrusion of cell edges, closely related to cell proliferation (Price et al., 1995; Taber et al., 1996; McCain and Parker, 2011) enable cell motion following change shape (Fletcher and Mullins, 2010). Actin-adhesion links to the outside include the cellular extensions that are generated by actin polymerization, filled by a dynamic branching of cytoskeletal components and recruitment by and to the integrins and their link to the ECM via the binding of vinculin (Geiger et al., 2009).

Combining both biomaterials and external mechanical loading allows to answer the demand for a better understanding of the mechanical relationship between the cells and its environment. This chapter describes how dermal fibroblasts on functionalised polymer surfaces are sensitive to mechanical stretching. The forces exerted on the cells trigger a variety of changes and modulation at a molecular level including: (I), the nuclear localisation of MRTF-A, (II), fusiform morphology and alignment of their actin cytoskeleton, and (III), the pattern of cell orientation following the complex interplay between cells on topographical surface and applied forces in parallel or perpendicular to microtopography.

3.2 Materials and Methods

3.2.1 Materials

List of Reagents
Surface preparation and modification
Fibronectin .... Sigma-Aldrich
Polycaprolactone (MW: 80,000) .... Sigma-Aldrich
Polydimethyl siloxane .... Dow Corning Corporation
Superclear silicone sheet .... Silex Silicones
Cytotoxicity study
Alamar blue .... Bio-Rad
Immunofluorescent staining
Fluorescein streptavidin .... Vector Laboratories
Horse biotinylated anti-mouse IgG .... Vector Laboratories
Horse biotinylated anti-rabbit IgG .... Vector Laboratories
Mouse monoclonal anti-vinculin IgG .... Sigma-Aldrich
Rabbit polyclonal anti-Mkl1/MRTFA antibody .... Abcam
Rhodamine Phalloidin .... Invitrogen, Molecular Probes
Vectashield mounting media with DAPI .... Vector Laboratories

3.2.2 Preparation of stretchable membranes

To fabricate a material for unidirectional stretch system, the polycaprolactone (PCL) membranes were prepared by spin coating and perform an amorphous structure (as detailed in section 2.2.2.1) before cutting into 7x30mm rectangles. For cyclic stretching, pre-manufactured 0.8mm thick ultraclear silicone sheet (40° Shore hardness) was obtained from Silex Silicones (UK).

Using a 3D printing (Ultimaker2, Netherlands) blocks were printed as a substrate holder, two 3D-printed plastic blocks (29x19x6.5mm and 29x46x6.5mm) were attached to either end of the membrane using 12% (w/v) PCL/chloroform as a glue or clamping by 3D printed and laser cut parts (29x3x0.9mm). Then, the assembly was exposed to an air plasma for 1-1.17 minutes (Harrick Plasma cleaner, max setting). In order to start cell culture and the actual stretch in the linear plastic flow regime for the PCL sheet, the membranes were pre-stretched to 33%. The assembled clamped silicone sheets were similarly stretched for 20% before coating with 20 μg/ml of fibronectin for an hour at 25°C followed by cell seeding and culture.

3.2.3   Stretcher and cell expansion

3.2.3.1   Stretching device

The custom-designed bioreactor uses a microcontroller controlled stepper motor to apply force on a membrane coupled via 3D-printed clamps. The assembled membranes were inserted into 4 well-cell culture plates and immobilised in the device by screwing one of the block to the structural frame. The other block was held in place by moving cover that was linked to stepper motor, which was controlled with an Arduino. Figure 3-1 outlines A) surface preparation workflow and B) uniaxial cell stretching device.

The second generation of cyclic stretching system was developed to be based on a stretchable PDMS culture plate that could be incorporated into the slightly modified mechanical stretcher system. To prepare the elastomeric culture plate, Dow Corning PDMS (Sylgard 184) and curing agent were mixed, deaerated (see section 2.2.2.2) and poured onto the designed template in 8 well-liked rectangular area coupled to screw holes for clamping system. To pre-pattern the wells with microtopography, a replica of grooves (SU-8 masters with 12.5μm repeated 5μm deep structures) was transferred to a polystyrene sheet via spin coating and attached on top of the 3D blocks. The curing polymer was incubated at 80°C for 2 hours. The substrate was then gently removed from the 3D-template, washed with 70% ethanol and followed by plasma treatment for 1 minute before experiments. Figure 3-2 represents an overview of the stretchable PDMS-based

stretching device, including template design in A) 8 well-like pattern, B) culture plate and C) the detail of their components in the cyclic stretching system.
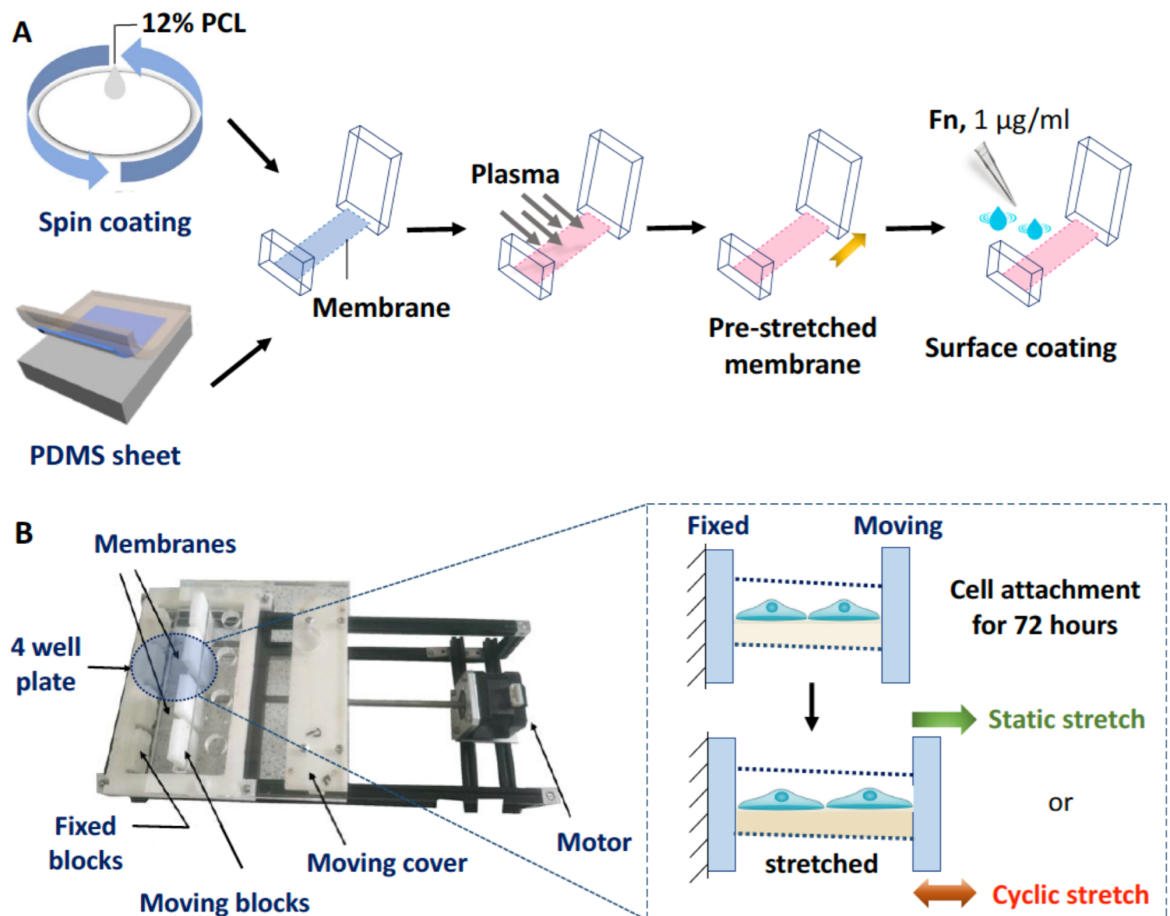
Figure 3-1. Clamping device components and stretch bioreactor. A) Preparation of PCL (obtained via spin coating) and silicone membranes, were glued or clamped to two 3D-printed blocks. Air plasma was applied to increase the hydrophilicity of substrates, as indicated by the arrows. The membranes were then modified by pre-stretching and surface coating using fibronectin. B) The fully assembled mechanical stretching system include a 4 well cell culture plate for substrate insertion, structural clamping tools, moving cover served as culture lid and linked to stepper motor where the external load was controlled by a Arduino microcontroller. Diagram of stretched cells (inset boxB), subjected to unidirectional or cyclic stretch. The directional of cell motion as indicated by the arrows).

3.2.3.2   Cell seeding and stretching

The Cells were seeded at a density of 79 cells/mm^2 in 10 ml culture media on PCL sheet and 315 cells/mm^2 in 5 ml media for a stretchable PDMS culture system. After 72 hours of cell seeding, cells were fed with fresh media and subsequent

applied mechanical load at 4.2% unidirectional stretch or 5% cyclic stretch at 0.05Hz for 24 hours. Each experiment was performed at least in triplicate.
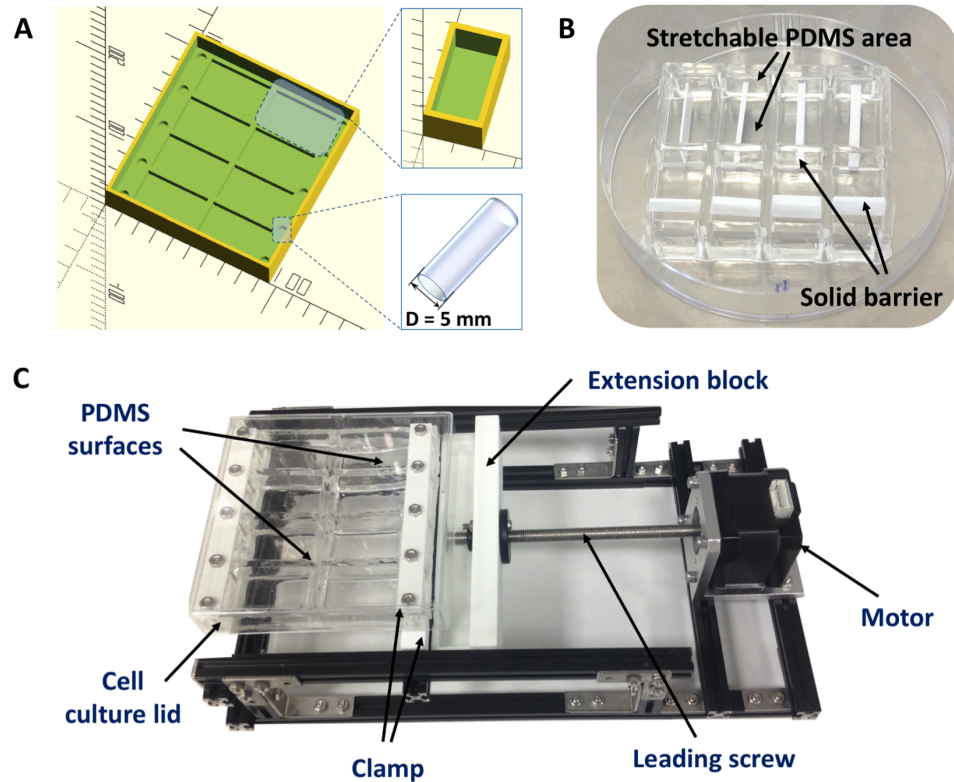
Figure 3-2. Schematic design and fabrication of the stretchable culture plate tracked cyclic stretching. A) CAD design for the PDMS plate-casting mold, which is a three-part object consisting off a baseplate, cylinders and blocks that define the space for the wells, designed in OpenSCAD software. By using a microgrooved PS sheet, the inverse of the topographical patterning was transferred into the culture area. B) Completely 8 well conformation with removable 3D printed blocks that keep aspects cell free to study cell migration. C) The 8-well chamber incorporated into the cyclic stretch device, where the stepper motor was connected to an Arduino for the adjustable amplitude and specific frequency.

3.2.4 Alamar Blue assay

To access the effect of cell viability on PCL and PDMS membranes, cells were seeded for 24 hours. Then, cells were re-fed with 10% Alamar Blue (Resazurin) fluorescent dye in the growth media and incubated at 37°C for 4 hours. Cell viability were quantified by measuring at 570nm and 600nm. The calculation of

the percentage of Resazurin reduction test was done as detailed in the following equation:

$$\% \text{ Difference in reduction} = \frac{(\varepsilon_{ox})\lambda_2 A\lambda_1 - (\varepsilon_{ox})\lambda_1 A\lambda_2}{(\varepsilon_{RED})\lambda_1 A'\lambda_2 - (\varepsilon_{RED})\lambda_2 A'\lambda_1} \qquad (1)$$

Where $\varepsilon\lambda_1$ and $\varepsilon\lambda_2$ are constants representing the molar extinction coefficient in the oxidized (ε_{OX}) and reduced (ε_{RED}) forms of resazurin at 570nm and 600nm, respectively. $A\lambda_1$ and $A\lambda_2$ represent the absorbance of test wells at λ_1 (570nm) and λ_2 (600nm) respectively, whereas $A'\lambda_1$ and $A'\lambda_2$ represent absorbance of media control at the same wavelengths (Al-Nasiry et al., 2007).

3.2.5   Immunofluorescent staining and data analysis

Human dermal fibroblasts immortalised with TERT were cultured for 72 hours and then stretched for 24 hours. The cells were fixed, permeablised and blocked in 1% BSA/PBS buffer. Then the membranes were stained either with primary rabbit anti-MRTF-A and mouse anti-vinculin antibodies (1:100) and conjugated with phalloidin-rhodamine (1:100) in order to labelling their local actin filaments (F-actin), the samples were then incubated overnight at 4°C and further stained for secondary and Tertiary antibodies (See section 2.2.4 & 2.2.5).

3.3   Results

3.3.1 Substrate characterisation and biocompatibility

The amorphous PCL membranes are formed to allow uniform extension and avoid the development of ordered surface structures in the polymer via fast freezing method. The assembled membranes are subjected to a pre-stretch of 33% to reach the plastic flow regime such that in the following they are evenly mechanically loaded. The strain field was previously tested by digital image correlation (DIC) technology to characterise the mechanical behaviour of PCL membranes. The full-field surface strain measurement displayed homogeneity of the strain field of the substrates subjected to mechanical loading, PCL sheets underwent deformation at the plastic flow with a rate of applied force in the range between 32±1% to 270±84%. To evaluate the biocompatibility of modified membranes, the viability of fibroblasts was followed on different surfaces comparing non-treated and

plasma treated samples. The effect of plasma treatment on PCL sheets was, that the cells showed an increase in cell viability and proliferation to 98±2%, whereas cell density observed on the non-treated film was at around 15% less than on the plasma-treated group of films. For result on PDMS, non-treated and plasma treated showed a slight rise in cell viability after treatment, were 72±2% and 78±3%, respectively. To enhance cell adhesion fibronectin was adsorbed onto the membrane surface after plasma treatment in order to improve cell growth via fibronectin specific activation of cell surface receptors. The results from Alamar Blue test for cell viability indicated that fibronectin-coated substrate promotes cell proliferation to nearly 100% of cell viability (Figure 3-3). Treating the plasma oxidized surface with fibronectin is required for the optimal cell compatible PDMS surface.
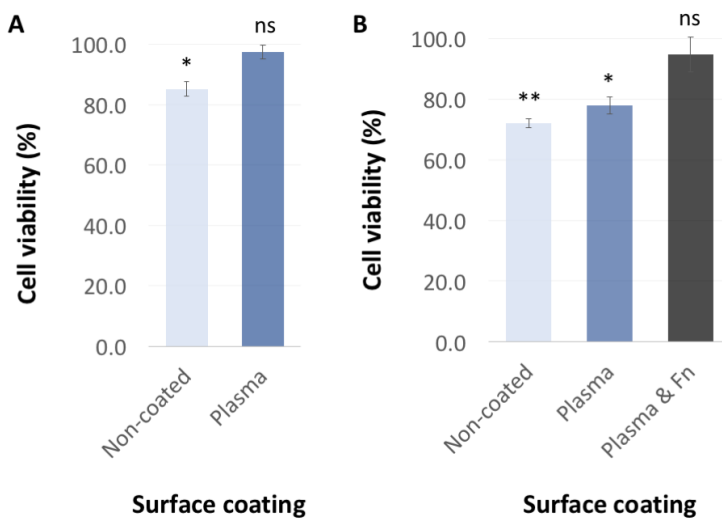
Figure 3-3 The percentage of viability in fibroblasts increased with modifying the surface of substrate by plasma treatment and fibronectin-coating.

Analysis of the cell viability in BJ1 cells on synthetic materials A) PCL and B) PDMS membranes via Alamar Blue assay, compared to cells on TCP as positive control (n_{Bio}=3). Data were represented as mean ± SD. * indicated p<0.05 and ** indicated p<0.01. The cell culture on plasma-coated PCL and plasma/Fn-coated PDMS reliable ns; non-significant showed biocompatibility surfaces to BJ1 cells.

3.3.2 Unidirectional stretch regulated phenotypes and shaped in fibroblasts

3.3.2.1 Temporal control and selective activation of nuclear MRTF-A translocation

Mechanically stretching fibroblasts triggered nuclear accumulation of MRTF-A, an actin-dependent transcription co-factor that forms a complex with cytoplasmic g-actin. Following stretch stimulation appear the more translocation of MRTF-A in the nucleus, nuclear MRTF-A signals are based on timing of stimulus. The

nuclear/cytoplasmic (n/c) ratio of MRTF-A expression in stretched cells are examined using immunofluorescence staining. As a result of stretch-activated growth at 4.2% of uniaxial strain, the n/c MRTF-A ratios increased approximately 11±4% when the cell was subjected to continuous stretch at a rate 41.7μm/h of for 12 hours compared to a non-stretch group as a control. After 24 hours of continuous unidirectional stretch, MRTF-A did further translocate to the nucleus to around 31±9%. However, the rate of n/c MRTF-A signals regressed to 3±5% after 48 hours of stretch. Figure 3-4 illustrated the mean integrated intensity of n/c MRTF-A ratio under applied strain for 12, 24 and 48 hours on the PCL thin films supported growth of dermal fibroblasts.
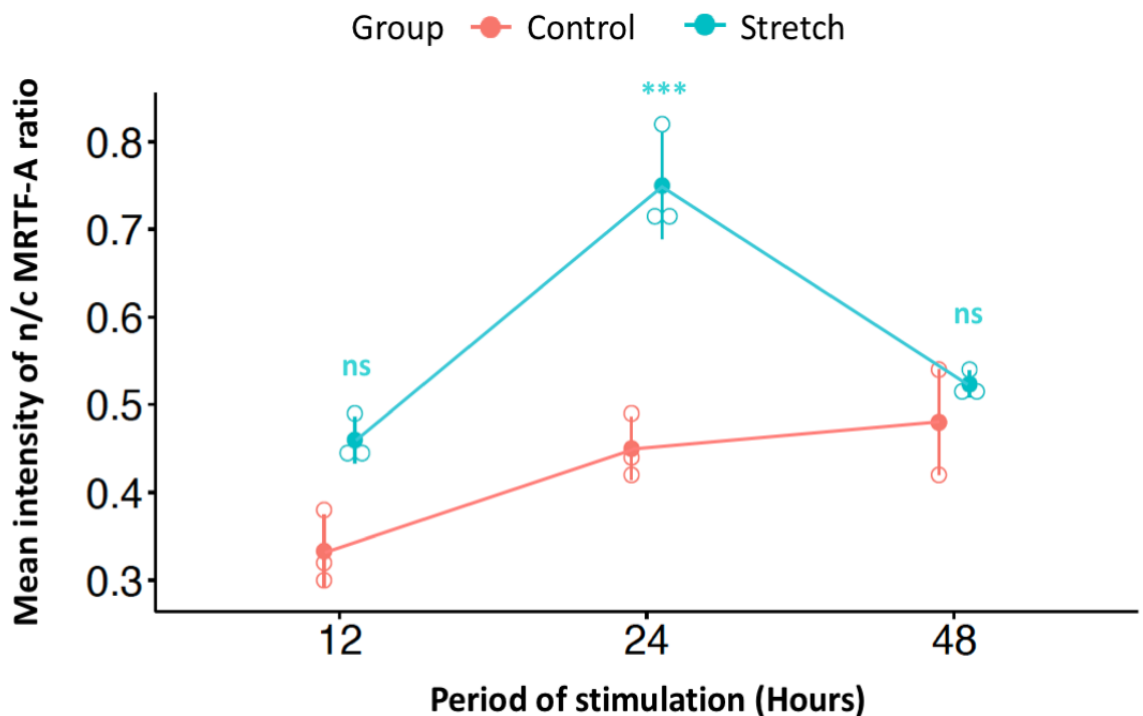
Figure 3-4. Spatiotemporal analysis of stretch-induced nuclear translocation of MRTF-A over 12, 24 and 48 hours. The average of integrated intensity of n/c MRTF-A ratio was analysed and compared between stretched (cyan line) and non-stretched (red line). Upon unidirectional stretch, the relocalisation into the nucleus of MRTF-A gradually increased during 12 hours of stretch compared to control. Double expression of nuclear MRTF-A was measured in the cells respond to stretching for 24 hours whereas the signal decreased within 48 hours of stimuli observing a similar MRTF-A localisation as compared to stretched group for 12 hours. The nuclear MRTF-A signalling in non-stretched cells appeared at a range from 0.33 to 0.48 during cell growth on PCL sheet. Error bars represent standard deviation in the cell population; N_{Cell} = 1,695-4,114 cells per substrate, n_{Bio}=3. The stretched cells (cyan line) were calculated the mean intensity of MRTF-A where is significantly difference compared to non-stretched (red line) (*** p<0.001 and ns – non-significant).

The quantitative analysis demonstrated that the MRTF-A translocation was at a peak after less than 24 hours of stimulation. Here it is observed that this leads to an around two-fold increase of nuclear relocalisation of MRTF-A. Figure 3-5 displays the stained cells tracking MRTF-A expression and the localisation in the nucleus and the cytoskeleton via an immunofluorescence assay allowing comparison between control and stretched samples.
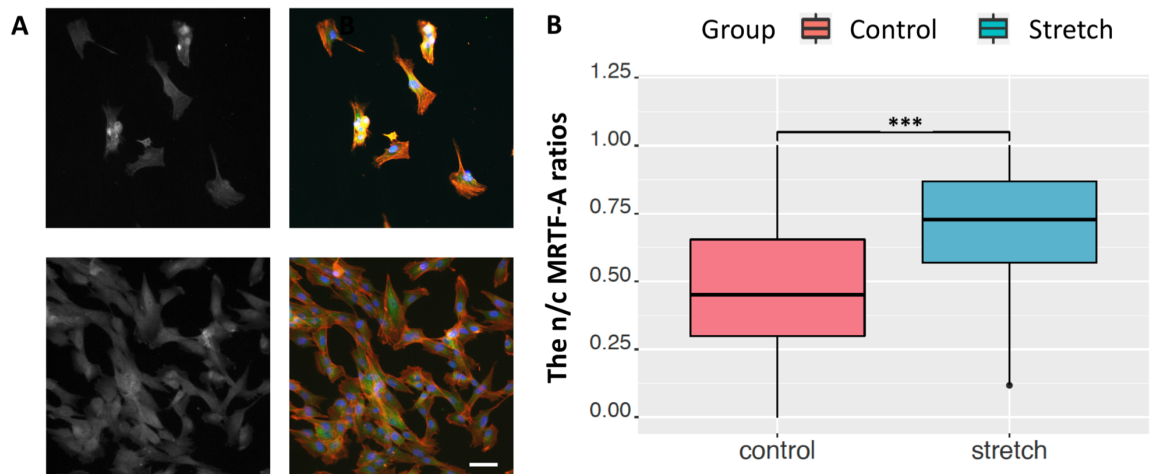
Figure 3-5. Effect of unidirectional stretching on MRTF-A translocation into the nucleus after 24 hours of applied load. A) Images of immune-stained cells in control (top) and stretched group (bottom). Monochromatic images of BJ1-hTERT cells stained with anti-MRTF-A (left panels) and structural components of cells in RGB colour scheme (right panels) for F-actin (red), MRTF-A (green) and nucleus (blue). Scale bar is 20µm. B) quantitative analysis of MRTF-A localisation, the integrated intensity of MRTF-A ratio was measured and calculated in the relative of n/c form. Targeting at the distribution of MRTF-A in cells on PCL surfaces, there was significant increase in accumulation in the nucleus. For statistical analysis, Unpaired two-samples t-test indicated as ***$p<0.001$. Experiments were repeated at least 5 times (N_{cell} = ~5,000 cells/replicate).

3.3.2.2 Elongated cells and remodeling of actin filaments in response to stretch

To measure the level of elongation when cells were subjected to unidirectional stretch, the aspect ratio of the projected cell area was measured as the ratio between the major and minor axis of the best-fitted ellipse around the outline of the cell, as based on the phalloidin stained F-actin image. The results showed significant increase in the length of the major axis of the stretched cells (Figure 3-6A). The effect of static stretching on actin remodeling and distribution was

then assessed by analysis of the intensity of phalloidin stained F-actin. The quantitative image analysis of F-actin formation and localisation in whole cells, together with the redistribution or accumulation of F-actin around the cell edges as shown in Figure 3-6. Interestingly, in the non-stretched group of cells F-actin was observed at a width range of whole cell position. However, stretched cells generated actin filaments in a pattern that was similar between the overall cytoplasm and the margins of the cells. The images were used to extract data in order to compare the polymerisation of actin around the plasma membrane under different conditions. The data showed no significant difference in the F-actin arrangement between control and stretched groups.
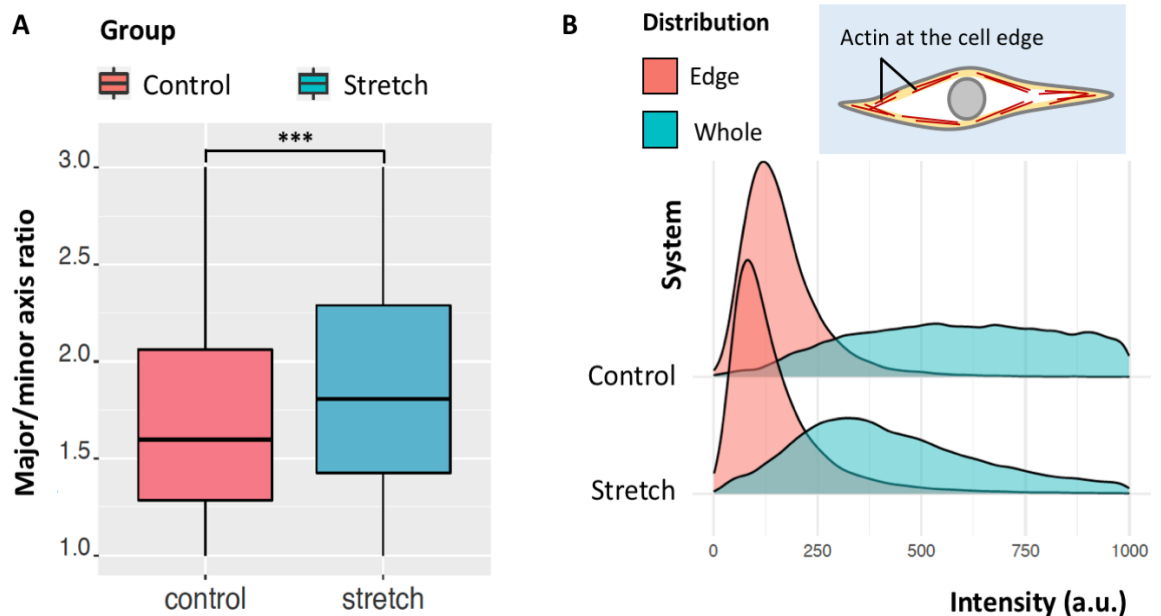
Figure 3-6. The effect of stretch-mediated with the aspect of the length of cells and distribution of f-actin. A) The elongation rate of cells enhanced significantly as a result of stretching. The cell length was normalised with the distance in the major to minor axis ratio. For statistical analysis, *** indicated where the p-value less than 0.001. B) Expression of F-actin, frequency plot over the intensity in the main distribution of actin around the edge (red-filled) and on the overall area of cell shape (referred to whole cell, cyan-filled), N_{cell} = ~5,000 cells/replicate, n_{Bio}=5. The inset box, B) shows a sketch of cell with specified area of cell edge (~25% of coverage area) as boundary highlighted in yellow, together with example of red line distribution of F-actin.

3.3.2.3   Unidirectional stretch alters morphology of fibroblasts

In order to evaluate the effect of passive stretching experiments influence shapes and arrangements of cytoskeletal texture. A set of quantitative measures has been selected to address the physiological state of the cell. Definitions and descriptions of selective shape parameter are detailed in Table 3-1. These measures include geometric parameters such as area and perimeter that can be used to calculate then the value of two derived variables: form factor (equation 2) and solidity.

$$\text{Form factor} = \frac{4\pi A_p}{P_p^2} \tag{2}$$

Equation (2) Where A_p represents area of the particle and P_p represents perimeter length of the particle. The image of cell is projected to convexity in the form known as solidity which can be calculated by the proportion of the object or particle area (A_p) divided by the convex hull area. A bounding of smooth convex hull is defined where the values to closed to 1.

Table 3-1. Summary of shape parameter used in Image-based quantitative analysis.

Parameter	Sensitivity	Description
Area	Spreading	By using the actual number of pixel in the region.
Perimeter	Form and Spreading	The total number of pixels computed around the boundary of each cell region.
Form factor	Form and roughness	Measure of nuclear circularity.
Solidity	Roughness (morphological)	Measure of the regularity of objects boundary.

Stretched cells had a smaller footprint or spreading area compared to non-stretched controls (See Figure 3-7A). The result from this selective measure suggested that the contractility occurs within their cytoskeletons in response to 4.2% unidirectional mechanical load for 24 hours. The change in the circumference, the perimeter of the cells on stretching revealed a slight decline in response to stretching (Figure 3-7A and 7B). The data on nuclear shape, where the circularity of the nucleus declined dramatically with stretch, indicates that

strain had a measurable impact on the nucleus. The effect of mechanical load triggers the nuclear flattening, resulting in the deformation in reducing its degree of solidity (Figure 3-7C and 7D).

3.3.2.4 Stretched state leads the cell to reoriented on the whole-cell level

Due to substrate stretching, adhered cells were stretched continuously for a day during which the polymer films were extended by around 1mm (which is equivalent to 4.2%).
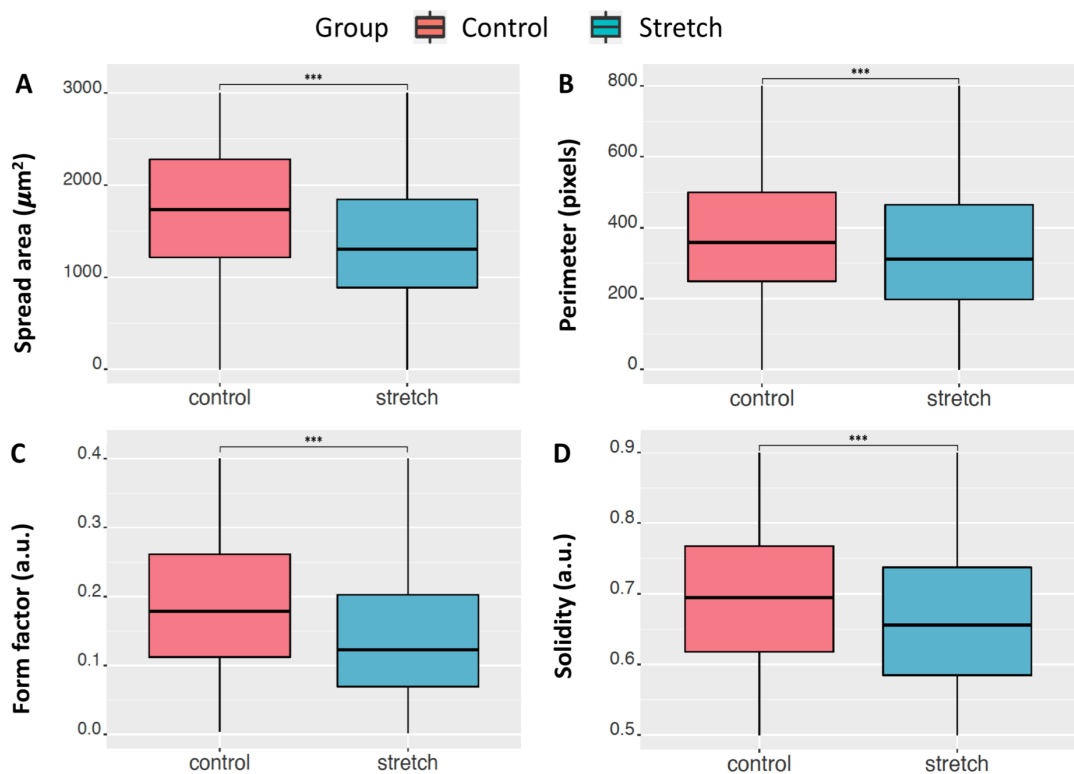
Figure 3-7. Morphology changes of cells in response to uniaxial static stretching at 1mm/day. A) Area of the cell spreading decreased substantially in response to applied forces. B) Cell perimeter, showed a slight decrease in the stretched state. C) The shape of the nucleus as assessed by circularity, showed a dramatic drop in this form factor. D) Solidity – a measure of shape regularity, was also reduced after stretching. For statistical significance; Student's t-test ***, $p < 0.001$ (N_{cell} = ~5,000 cells/replicate, n_{Bio}=5).

To study how the cells as a whole changed their orientation on the stretched films, cell orientation can be described by the orientation of the smallest ellipse that can be fitted around the projected cell shape as determined by analysing f-actin images. Actin bundles are another major influence involved in the determination of the corresponding global orientation of cell. Figure 3-8 illustrates the cell-

substrate adhesion and reaction on cell stimulated by mechanically stretching. Instantaneous position of the cell in Figure 3-8B, denotes θ as a function of orientation angle with respect to horizontal axis of strain field. Non-stretched and stretched cells polarised on PCL film displayed in Figure 3-9, an angle histogram representing the frequency contribution with regard to angular orientation of the individual cell.

A

Actin located around the edge of cells

Cell-substrate adhesion

Direction of applied forces

B

Actin bundles & stress fibers

Fitting ellipse

Stretching

θ

Major axis
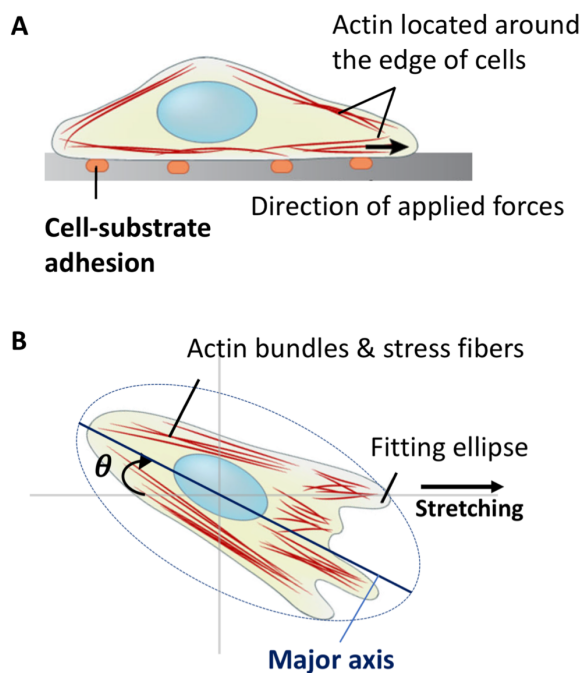
Figure 3-8 Schematic drawing of cell-substrate interactions and response to mechanical loads. A) The model of cell motion and adhesion to substrate, arrow indicates the directional of stretch on substrate. B) Illustration of the angle of cell orientation relative to applied stretching direction. The major axis of an ellipse cell rotated at an angle θ in degree relation to stretching parallel to x-axis.

In control group, an orientational patterning showed that over 48% of cells were polarised with the angle that they form with the direction of the applied strain close to being in parallel to the stretch direction. The number of cells that are aligned with the direction of the applied strain are calculated from the cells that are aligned between 0°-30° and between 150°-180° (Figure 3-9A). The results suggested that the cells oriented along the horizontal axis without additional applied force. This observed apparent orientation may be caused by the alignment of the material during the pre-stretching stage. When further stretched to the extent of 4.2% by unidirectional stretch, the cells reorient to lose alignment being oriented almost equally in every angle of orientation with an average of 5.8±1% (as shown in Figure 3-9B).
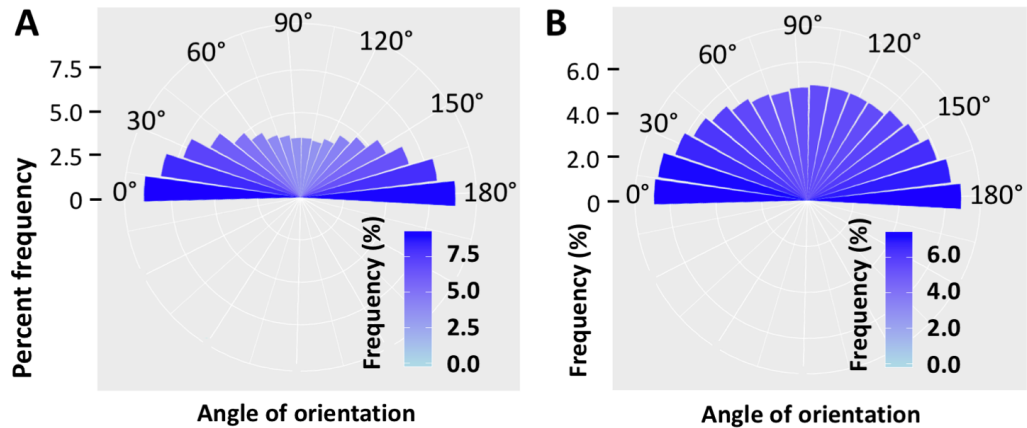
Figure 3-9. **Angle histogram of orientational response between control and stretched cells.** A) Non-stretched cells spread close to horizontal axis with nearly half of cell population, the other cells align at around 5% in each degree of orientation. B) Cells subjected to stretching. The cell reoriented themselves to the direction perpendicular to dynamic load, hence of an equivalent of cell polarization from 0°-180°.

3.3.3 Cyclic mechanical stretching of cell on biomimetic coating surface

3.3.3.1 Acute stretch-mediated recruitment of vinculin to focal adhesions

Cell embedded on substrates and its interaction are known to effect focal adhesion formation (Fraley et al., 2010). The cytoskeletal protein vinculin was examined in order to test if the applied tension initiates vinculin recruitment to adhesions, stretched cells were stained to detect the amount of this focal adhesion protein after 24 hours of stimulation over a range of 1-5% cyclic stretching. Surprisingly, immunofluorescent staining displayed that stretched cells increased vinculin intensity to $105.6\pm4.2\%$, $169.5\pm8.5\%$, and $202.1\pm11.0\%$ during 1%, 3%, and 5% of cyclically mechanical loads (See Figure 3-10). The vinculin signals in stretched cells were compared to non-stretched control.
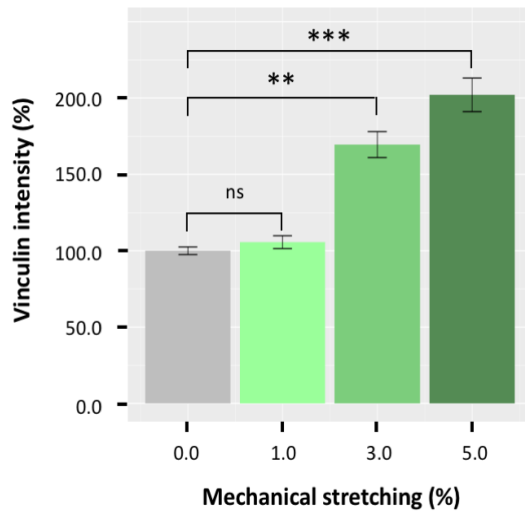
Figure 3-10. vinculin signals respond to cyclically mechanical stretching at 1%, 3% and 5% stimulation. The more intense vinculin expression was observed with an activated level which proportion to higher mechanical loading. The percentage of fluorescently labelled vinculin significantly increased subjected to 3% and 5% stretching, as indicated **p<0.01 and ***p<0.001. However, the cells exposed to 1% stretch have a slight rise of vinculin intensity with non-significant (ns). The unpaired t-test is used to compare fluorescent images between stretched cells and non-stretch (0% stimulation). Experiments were repeated at least three biological repeats.

To assess the resulting images (Figure 3-11), the integrated intensity of vinculin signal was measured at a single cell level when the cells were exposed to a magnitude of 5% cyclic tensile stretch at a frequency of 0.05Hz.
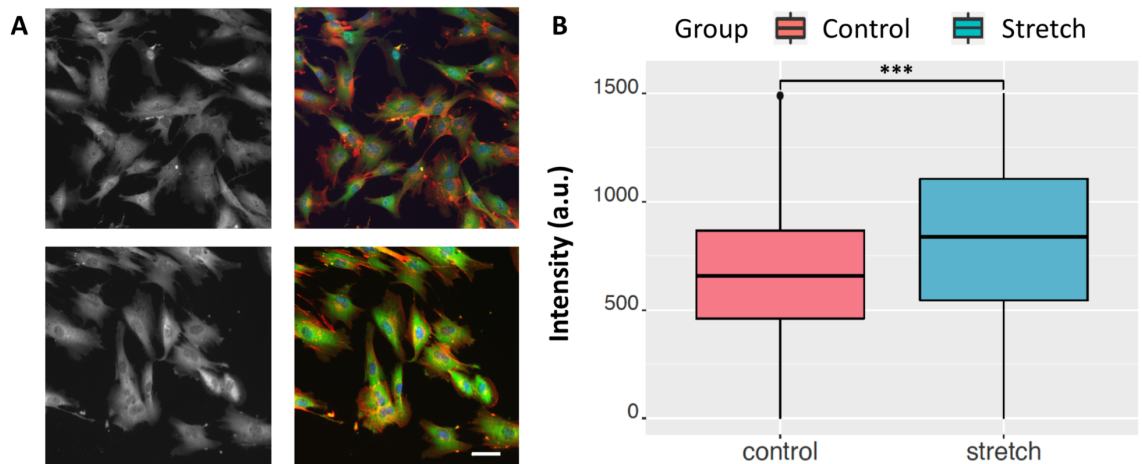
Figure 3-11. Applied stretch stimulates vinculin recruitment to focal adhesion under 5% cyclically load at 0.05Hz for 24 hours. A) Stained cells in relax (top panel) and stretched (bottom panel) substrates, vinculin was visualised with mouse anti-vinculin antibody (left panels). For RGB images (right panels) were labelled with anti-vinculin antibody (green), Rhodamine-phalloidin targeting F-actin (red) and DAPI staining of nucleus (blue), Scale bar = 20μm. B) Quantification of vinculin intensity, a double-expression of vinculin enrichment was detected upon cyclic stretching and normalised to non-stretched cells. N_{Cell} = ~1,051-3,202 cells/replicate, n_{Bio}=3; independent experiments. Two unpaired student t-test; ***, p<0.001.

The data showed that vinculin intensity increased two-fold in adhesion plaques in response to cyclic stretch (5%, 0.05Hz).

3.3.3.2 Cyclic stretching of cells leads to translocation of MRTF-A in Rho-A dependent manner

To study the response of cell and their actin cytoskeleton that under repeated stretch application. Cell were grown on fibronectin-coated elastomers for 72 hours followed by acute stretching for 24 hours. MRTF-A did not relocalise to the nucleus after 5% cyclic stretching at 0.05 Hz, as the data resulting from the image analysis of immunofluorescent staining revealed that, it had no significant effect. As there were some cells that did respond and others that did not the assumption was that this may have been due to the cells respective shape or spatial orientation with respect to the direction of the applied cyclic stretch. I therefore modified the surface using microgroove topography to pre-align cells with respect to the direction of substrate movement either perpendicular or parallel to the applied strain. Fibroblasts seeded on microgrooves displayed a relatively higher nuclear translocation of MRTF-A at about 8±2% when the scaffold was pre-patterned with microgroove master aligned perpendicular to the directional stretch. However, cells on grooved surface patterning in parallel to the stretch axis did not exhibit an enrichment of MRTF-A localisation in the nucleus. Figure 3-12 demonstrating that the cell sensing cyclic tensile stretch manipulated nuclear translocation of MRTF-A on the different surface textures.
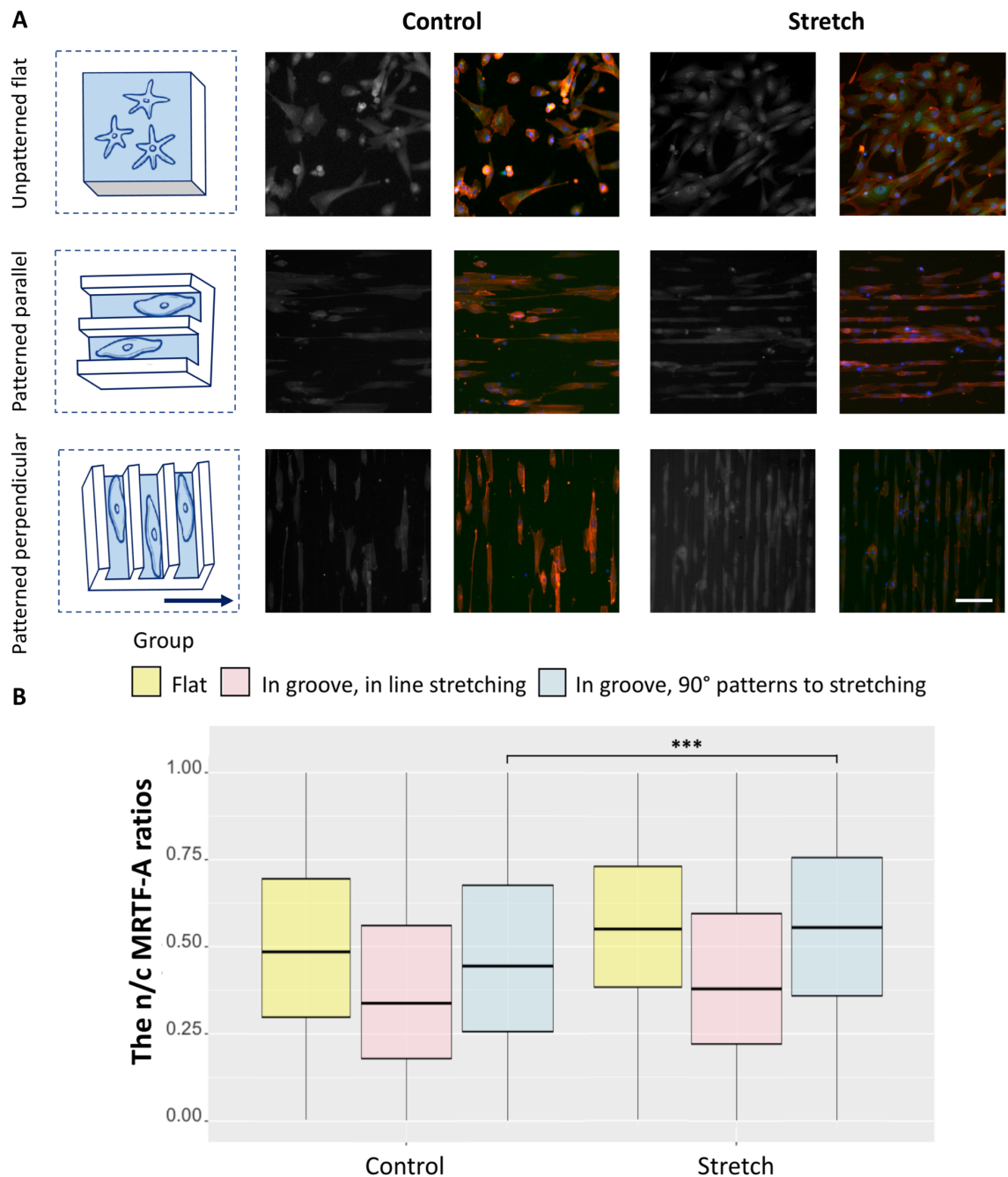
Figure 3-12. Activation of MRTF-A gene expression with 5% cyclic stretching on grooved PDMS surface aligned perpendicular to the direction of applied force. A) Schematic and immunofluorescence images of cells comparing between control and stretched groups on flat and grooves (aligned either parallel or perpendicular to stretch axis, arrow as indicates the direction of applied strain). Multilabel immunofluorescent staining of MRTF-A (Greyscale single-channel images, or green in RGB images), F-actin (red) and nucleus (blue), Scale bar = 20μm. B) The n/c MRTF-A remained stable after stretching in flat PDMS and in grooved which pre-patterned along the stretch axis. The study of statistical significance highlighted that the proportion of nuclear MRTF-A translocation rose significantly in response to applied force where the microgrooved guides the cell align perpendicular to the directional of stimuli. The unpaired t-test indicate significant differences between control and stretch; $p < 0.001$. N_{Cell} = ~4,940 cells/sample, n_{Bio} = 3.

3.3.3.3 Cells on the microgrooves elongate and establish a meshwork of actin-enriched at the edge

Due to the competition of g-actin binding to MRTF-A molecules, which binds in the same area of MRTF-A where the RPEL motif is located, which leads to nuclear translocation. More f-actin presumably leads to a lower amount of g-actin available to bind to and retain MRTF-A in the cytoplasm, assuming constant amounts of action being made. The composition and microstructure of the actin cytoskeleton determines the shape of the cell, topographic cues enforce the cell orientation to the underlying topography. The changes in their shape instructed by mechanical stimulation are reflected in an increased elongation factor (Figure 3-13).

Directional tension had elongation effect mechanical performance, describing that exposure of cells to uniaxial cyclic stretch results in augment in the axial ratio (elongation factor) with groove textured surface and directional of tension applied. Elongation was calculated by forming the ratio of the length of cells in the major over the width of the cells in their minor axis. Cells strongly exhibited an area of cell expansion in response to cyclic stretch, microgroove pattern only had an influence on the aspect ratio of cell length when topography was combined to stretching system. The results from dual-stimulation by stretching and topography, revealed a gradual increase in the cells elongation (Figure 3.13). In accordance to the direction of the topography, the stretched cells on the grooved samples elongated more pronounced where the cells were stretched at 90° to the grooves and with that their main or long axis.
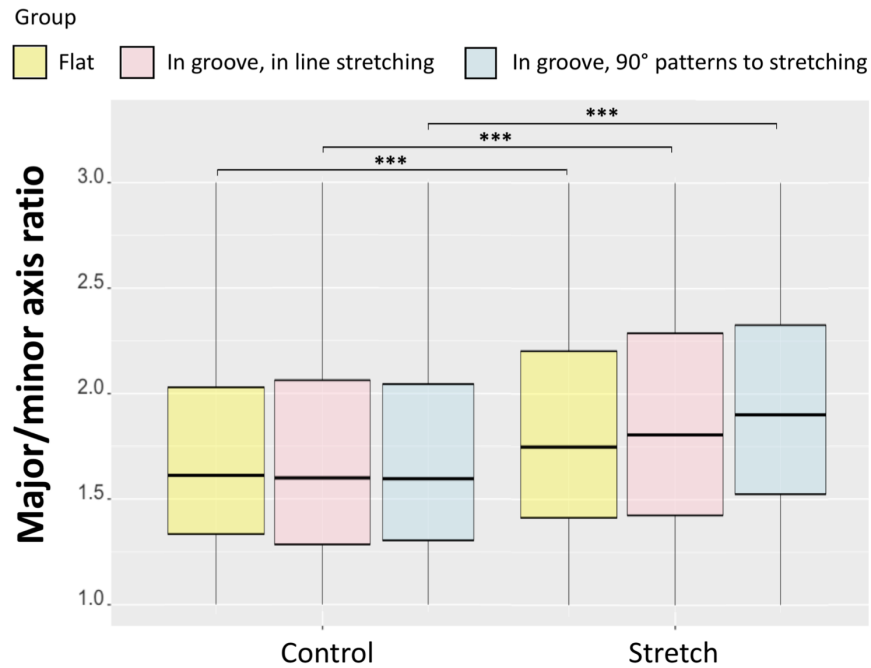
Figure 3-13. Elongation index of cells, measuring the tensile strain stimulates cell expansion. Assessing the aspect ratio (major/minor) of axis length, revealed that the action of force and topographic texture required to enhance the mobility coupled with elongation. Three independent experiments were set up and calculated the statistical analysis where it is significant differences between groups as determined by an independent t-test ***, $p<0.001$. N_{Cell} = ~4,940 cells per sample, n_{Bio} = 3.

Taken together, the alteration of the actin cytoskeleton in response to 5% of cyclic stretching at 0.05Hz and topographic patterning in relation to the area of actin accumulation: The results showed that the grooved substrates, that guided cell alignment, activated the collective formation of actin filaments at the cells edge. In contrast, cells cultured on flat unpatterned substrates displayed a higher amount of F-actin overall the whole cells. These observations indicate that tension applied on flat surface revealed that it had no effect on formation of actin associated with the edge of cells, a slight increase of total actin cytoskeleton around the cells in stretched group (Figure 3-14).
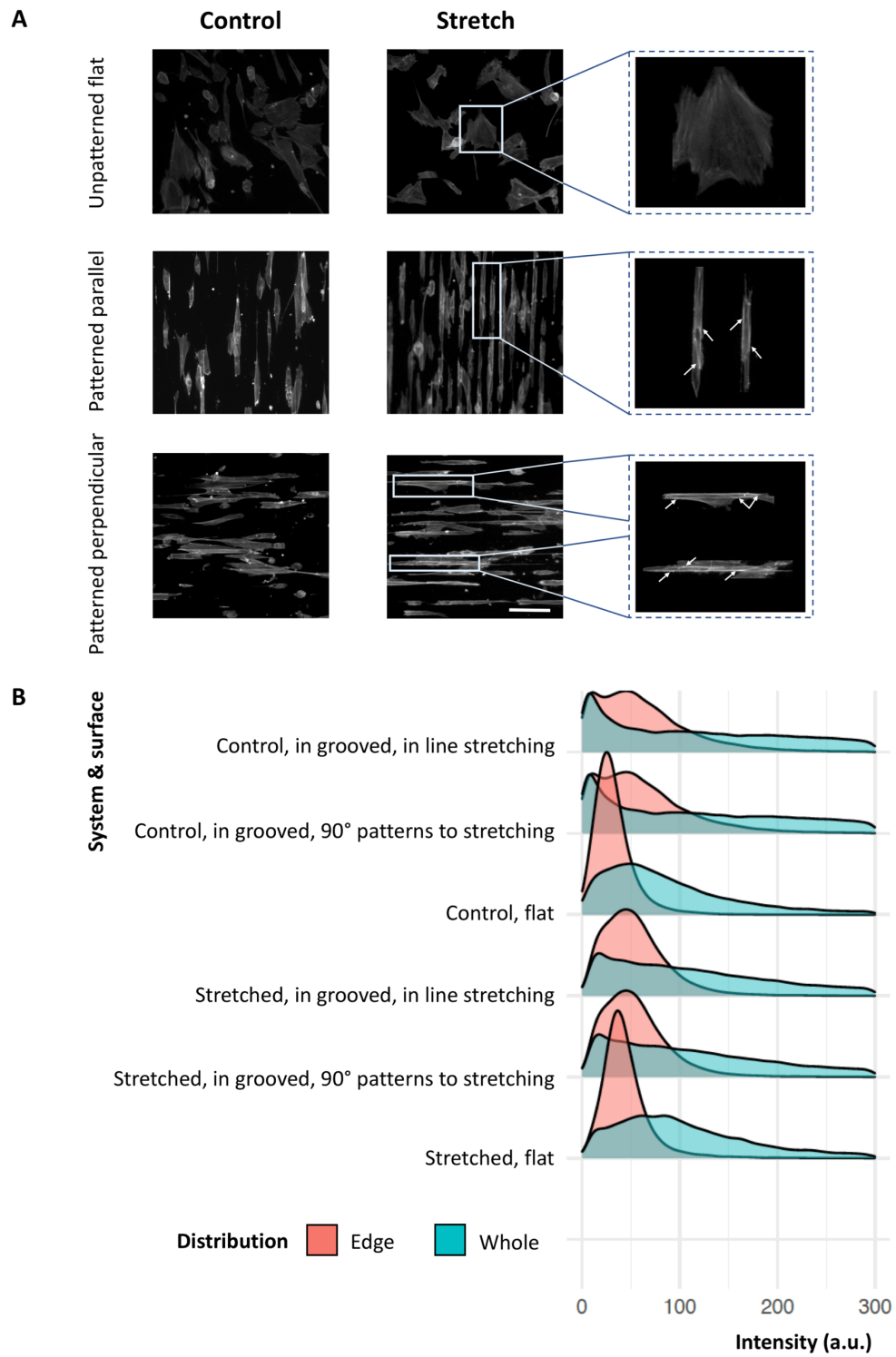
Figure 3-14. Evaluation of the amount of f-actin assembly near the edge of cells compared to whole cell surface area. A) Actin filaments staining with fluorescent dye-labelled phalloidin comparing between controls (left panels) and stretched cells (middle panels). Examples of F-actin (right panels) upon cyclic stretching (5%, at 0.05Hz) were selected to represent a higher intensity of actin around the edge of cells on the microgrooved surface (as indicated by arrows). Scale bar is 20μm. B) Histogram plot explained the major distribution of cells containing actin-rich at the edge as a response of cell adaptation on the grooves.

3.3.3.4 The morphological features of the cells sense mechanical cues

A total of four selective morphological shape measurements were used to explore the influence of acute cyclically loading that cause cell deformation. By characterising the shapes and a subset of measures that characteristically change in line with the degree of cell deformation: the cells spreading area, their perimeter, form factor and solidity were analysed as shown in Figure 3-15.
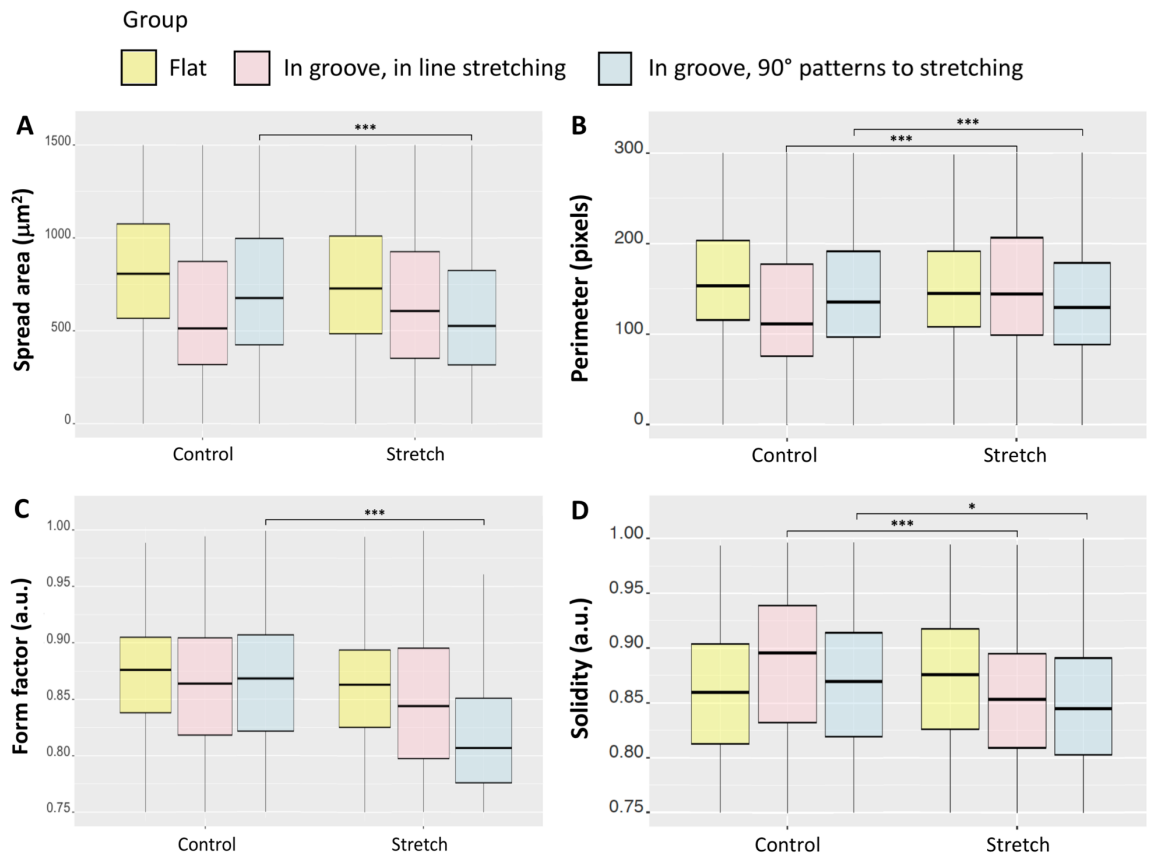
Figure 3-15. Stretching enables the cell morphology on grooved PDMS, aligned perpendicular to the directional of stretch. Stretched cells on flat and grooved patterning in parallel to stretch axis also have some changes despite being less pronounce. Several physical measurements A) Spread area B) Perimeter C) Form factor and D) Solidity indicated a significant decreased, particularly in the nuclear deformation via a measure of circularity. Besides the cell on grooved substrate that align in parallel to applied force showed a sharp variation of their perimeter and solidity after 24 hours of stretch. Flat PDMS maintained their morphological nature after mechanical stimuli. For statistical significance; *, $p<0.05$; ***, $p<0.001$ (N_{Cell} = ~4,940 cells per substrate, n_{Bio} = 3).

A set of selective measurement, which determines local differences based on the areas and boundaries of the cell and in the nucleus, indicating the largest

difference in patterned grooves samples aligned opposite to the directional of stretch at 90°. If cells were grown on flat or microtopography cell elongation (major axis/minor axis) changed accordingly to increase on the microgrooves. In combination of both stretching and microtopography, a significantly lower area of cell spreading was observed in grooved samples at 90° stretching. However, there was no significant change in samples that had been stretched if pattern and direction of stretch were aligned. It was obviously that a reduction of cell elongation factor is influenced by applied force and the directional of topography in respect to stretching axis.

In accordance to increase data accuracy, perimeter around the cell membrane were further analysed to define their shape. Interestingly, it is likely that the role of microtopography regulate cell elongation or contractility in the manner of directional surface patterning where subjected to stretching. These two ways of manipulation resulted in a significant reduction in the cell perimeter when the grooves rotated to 90°(perpendicular) to the direction of stretch. On the other hand, the perimeter was longer when the cells were located on the grooves that aligned along the stretching axis. Next to the level of cell deformation, the results displayed that nuclear flattening increases with engineered substrates. The circularity of nucleus was decreased in all conditions. There was a gradual decline of the form factor in response to stretching especially on grooved samples aligned at 90° to the direction of stretch. Furthermore, a dramatic nuclear deformation occurs in the groove prior to stretching (Figure 3-15C). The solidity of the nucleus showed a reduction of its compactness in the stretched cells on the microgrooves (Figure 3-15D).

3.3.3.5   Comparative analysis of cyclic stretch and unidirectional movement

Two cell stretching experiments were performed in cyclic direction and unidirectional stimulation. For cyclic stretching, cells were cultured on assembly membranes and subsequently exposed to cyclic stretch with an amplitude of 5%, at a frequency of 0.05Hz. The strain energy in relation to stretching frequency on stretchable substrates is illustrated in Figure 3-16. Graphic representation of relative displacement of extended membranes throughout cyclically applied force monitoring in a seesaw motion. The direction of cyclic stretch was plotted and

compared to unidirectional stretch which acts on membrane movement continuously with increased distance over time per an hour. Both stretching systems were then operated for 24 hours before force measurement.
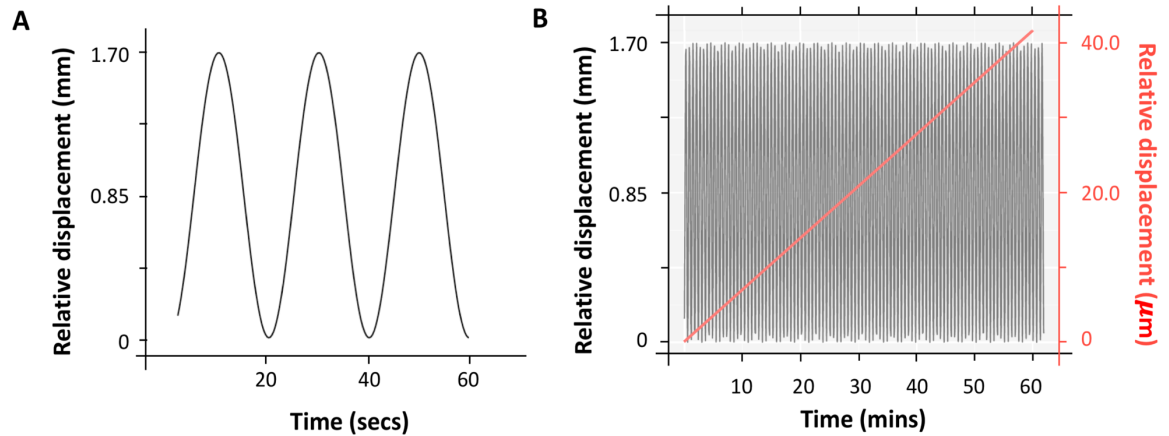
Figure 3-16. Regulation of the stretch frequency A) Plot of relative displacement of the deformed substrate over time using dynamical equation of motion launching the corresponding in R. The force was performed at 5% strain with a frequency of 0.05Hz. B) Comparative analysis of stain magnitude between cyclic stretching (black line) and uniaxial static stretch (Red line). The graph outlined a relative displacement that in stretching systems over an hour (scales dedicated force action in details).

3.3.3.6 Cyclic stretch reorients cell alignment nearly in parallel to the direction of the tension axis

In order to assess directional reorientation of the actin cytoskeleton to elongate under the regulation of dynamic cyclic loading. As the intrinsic properties of the substrate are found to cause some orientational patterning of cells at 120°-180° (Figure 3-17A). Upon 5% cyclic stretching at 0.05Hz, applied force contributes to a much higher population of cell alignment in parallel to directional of stretch (Figure 3-17B). The result from alignment in direction from 0°-30° and 150°-180°, revealed that over 45% of stretched cells oriented close to the directional of stretch. For results in minor population, the distribution of cell alignment exhibited almost equality number of cell orientation at the defined range degree of orientation with a mean of 13±3% oriented to 30°-60°, 60°-90°, 90°-120° and 120°-150° degree, respectively.
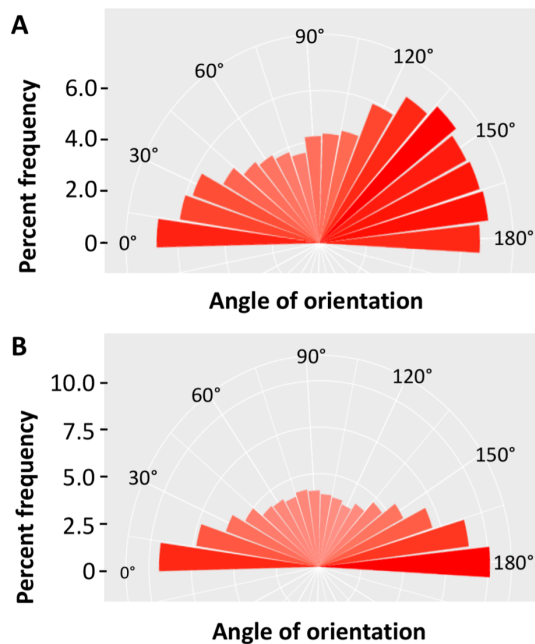
Figure 3-17. Frequency histogram of cell orientation relative to tensional applied in the horizontal axis. Number of cells normalised and expressed as the percentage of the radial distribution (0°-180°) within 10° bins. A) The orientational observed for the non-stretched group, these are characterised by a random orientation and having some preferential alignment at 120°-180° B) Cyclically stretched cells, here nearly half of stretched cells reorient close to the direction of the tension axis. The data assessment was analysed from five biological repeated experiments.

3.4 Discussion

Based on physical properties of the biomaterial, PCL and PDMS substrates possess a universal appeal over other materials such as simple fabrication, biological inertness and gas permeability (Hutmacher et al., 2001; McDonald and Whitesides, 2002; Sia and Whitesides, 2003). In the application of cell stretching experiments, a high elastic module is required for dispersion and its flow rate under force field. The PDMS also exhibits the designed characteristic feature for a robust ability to mediate mechanical loads owing to its tunable elasticity (Zhang et al., 2013). In contrast, the PCL polymer contains a lower elastic content as compared to PDMS surface. In this study, semi-crystalline block technique was used to enhance the plastic flow rate of PCL. Amorphous structure was thus obtained under the thermal regulation, showed richness in the transparency of fibres with high rubbery flow rate. Similar to the amorphous block of copolymers based on ε-caprolactone in the previous study by Ninago et al., 2013, suggested the action of conformational changes may be regulated by spherulite growth mechanism and isothermal crystallization kinetics. The spherulitic initiation is typically enhance a growth of mineral aggregation and later crystallization between fibres. All of these strengths convey to polymer transformation include extrusion and melt spinning among others.

In the context of biocompatibility of material surfaces, both of PCL and PDMS polymers appear to favour of cell microenvironment (Desmet et al., 2008). Whereas, there are highly hydrophobic surfaces in its native state that can easily be modified for hydrophilic interactions via plasma treatment, self-assembled monolayer coating and polymer/peptide grafting techniques (Love et al., 2006; Hui and Pang, 2019). This finding proposed air plasma treatment to render the hydrophilicity of materials. The results of this work demonstrated that the treated PCL and PDMS with plasma can drastically diminish wettability, gain a larger number of hydrophilic groups. Several studies support this function of energy density. For instance, the water contact angle of the untreated PCL surface is approximately 74° and subsequently decrease to 52° within 5 mins of air plasma treatments (Jacobs et al., 2011). A group of De Geyter et al. (2013), identified that the treat PCL film dramatically decrease the contact angle to 38° within a few minutes after plasma surface treatment in argon compared to the normal circumstance before plasma time linked to 74° of water contact area. It was found that the effect of the plasma technique on the polymer surface caused by the incorporation of oxygen-containing groups (i.e. C—O, C=O and O—C=O bonds). The impact of plasma is more likely that the hydrogen abstraction present in the discharge state which mainly composed of oxygen atoms and OH radicals. The concentration of oxygen-containing groups hence intensely rose (Dorai and Kushner, 2003). For results, cytotoxicity assay of fibroblasts is tested between substrates in relation to surface plasma treatment. The growth rate of cell greatly responds to cell-to-plasma treated surface interactions, the cells were grown on PCL sheet with approximately 98% of cell proliferation rate after plasma treatment. The viability of cell on PDMS membranes displayed a slight increase in their growth subjected to plasma, while around 22% of reduction related to growth was observed in this manner. Next, fibronectin coating of plasma treated PDMS substrates were apply in an aspect of the maximum growth rate close to tissue culture plastic (TCP; positive control). In the following aspect, fibroblasts were observed to have attached and spread on fibronectin over 95% of cell population. In comparison, sheet of PDMS coating at the same concentration used exposing around 93% adhere of arterial endothelial cells. It was observed the attachment and proliferation of less than 20% of the cells on non-coated membranes (Cornelissen et al., 2013). An interesting case studied by Rea et al. (2009),

highlighted that utilising immobilized fibronectin at 83.3 μg/ml supports cell adhesion due to the $\alpha_5\beta_1$ binding domain. The viability of NIH/3T3 mouse fibroblasts significantly enhanced the efficacy of intracellular trafficking.

By characterising the cell behaviour under stretching and particularly subtype of adhesion interactions expressed by fibronectin coating surface in this work, the fluorescent intensity of MRTF-A in the nucleus was measured to determine the strength of force in the localisation of mechanosensitive transcriptional regulator. In this study, the results from stretching experiments reported that continuous process of unidirectional amorphous PCL thin film at 1mm/day reinforced MRTF-A moved to the nucleus in 24 hours of stretching. There was observed that cell in stretched state results to an inward displacement of the nuclear MRTF-A signal with a twofold increase upon tension. Temporal analysis of stretched cells become activated in the range between 12 hours to 24 hours of mechanical loading, assessed a peak of nuclear accumulation of MRTF-A at 24 hours and thus subsequently decline and return to a basal level of MRTF-A at 48 hours similarly to non-stretched controls (Figure 3-4). Supporting this issue, an insight into dynamics of MRTF-A relocation upon mechanical stimulation is maintained over time associated with the homeostasis of mechanical functions (Montel et al., 2019). Harper and co-workers (2023), illustrated that application of cell exposure to increase mechanical force in the microenvironment, cells sense and respond to mechanical cues that trigger mechanosensitive regulatory system and cell remodeling, thereby enable the adaptation process to the mechanical challenges of their surrounding environment and quickly return to the original state in order to maintain homeostasis.

As discussed in chapter 1, the role of MRTF-A in particular are expected to correlate with MRTF-actin interaction, implicating predominantly cytoplasmic of MRTF-A localization (Guettler et al., 2008; Miralles et al., 2003; Vartiainen et al., 2007). The formation of actin filament is thus targeted to evaluate the effect of stretch-mechanisms in promoting actin polymerisation. It had no remarkable impact on F-actin intensity between stretched and control groups. A study by Montel et al. (2019), pointed out that the level of g- and f-actin are regulated by an adequate strain and transient for short duration of stretching. It is likely than

the cells in 10% static stretching showed an increase in the ratio of F-/G-actin intensities whereas 30% applied forces cause a reduction of F-actin forming immediately after stretching. The temporal studies indicated that an actin cap was stimulated and returned to its similar level of control after 25 mins of further stretch. In the same study, application of 10% strain, 100 mins is in focus with a major localisation of MRTF-A, with around 38% promoting in nuclear accumulation.

The second stretching system is operated on stretchable PDMS culture plate under 5% stretching cyclically at 0.05 Hz for 24 hours. Having confirmed the sensitivity to passive stretching, our experiments reported the nuclear MRTF-A relocalisation enhanced significantly when the cells were stretched on microgrooved surface with 12.5 μm repeat 5 μm deep structures at 90° to stretch axis. In comparison, Cui et al. (2015) highlighted that the PDMS substrate under 5% cyclic stretching with the optimum frequency at 0.1 Hz can induce MRTF-A translocation approximately threefold in nuclear accumulation. The distribution of MRTF-A in this manner reported that there was peaked of nuclear MRTF-A after 2 hours of stretching and maintain accumulated up to 8 hours before cessation. Next, alternation of cytoskeleton complex requires several proteins that localize to focal adhesion. This finding selected the intensity of F-actin and one of the structural proteins vinculin localise to focal complex, representing the deformation of the fibronectin coated layer and cytoskeletal reorganisation under cyclic stretch. The cells were grown on flat PDMS and stretched for a day, revealed that stretched cells in fibronectin coated matrices formed adhesion plaques with a double expression in vinculin recruitment. A similar observation was found by Freeman et al. (2016), suggested that endothelial cells on 2D fibronectin coated silicone polymer enhanced the amount of vinculin around twofold under acute 10% equibiaxial stretch. In uniaxial stretch system, cells exhibited a small vinculin forming structure after 24 hours of stimulation. As the integrin-binding proteins are widely acted to mediate cytoskeletal linkage, our results displayed stretch activated actin polymerisation at the edge of cells on grooved texture despite having some actin-rich only found in unpattern stretched substrates on the whole surface area. Newly polymerised actin at the leading edge of cells is found to enriched as its corresponding to vinculin-rich focal-contact-like structures upon tension applied (Freeman et al., 2016). Evidence supported in the published work

by Ahm et al. (2010), claimed that myoblasts were grown on microgroove consisted of patterned lines with 40 μm intermediate width and exposed to 7% stretching cyclically at 0.5Hz, it had been observed the formation of its actin stress fiber is dominantly regulated by stretch applied at 90° to the micro-contact grooves. Further to this, in the 45° grooves subjected to tension applied were shown full-length complex of myotube with a dense actin network.

As well as determining cell mechanical state and morphophysical features change, the impact of cytoskeleton mechanics can be used to investigate the cell behavior and adaptation as a consequence of interaction between cell and their microenvironment when the tension was applied. In relation to the field of mechanobiology, fiber tension extends stress fiber and thus enables focal adhesion alignment in spreading cells (Lu et al., 2008). The results from elongation response factor of cells exposed to tensile strain have been shown to represent the protrusion machinery or contraction in the cell sensing of strain energy. This finding reported that the overall cell spreading significantly rose with 4.2% level of PCL deformation and 5% cyclic stretching of PDMS substrate on fibroblasts. Similar behaviour was suggested an increase of cell shape factor (major axis/minor axis) that occurred in stretched substrate as compared to static conditions (Chowdhury et al., 2010; Aragona et al., 2013). Differences observed in spreading area between the stretched cells could be attributed in variation in strain rate-dependent manner. In this work, experimental results exhibited the decrease of cell area in response to continuous (4.2%) and cyclic (5%, 0.1Hz) stretch. The robust decline of spread area had found in the cells perceived mechanical stretching perpendicular to the grooves. Similar to the cells subjected to higher stretching frequencies described in the previous work by Hsu et al. (2010), over 80% of their original area was diminished significantly within an hour of applied cyclic equibiaxial stretch at 1Hz in 10% magnitude. Greiner et al. (2013), also identified a similar trend of cell spreading rate and area that stretched cells had a significant lower in the kinetic of spreading and maximum cell area at the uniaxial cyclic tensile strain at 8% with the frequencies of 1Hz and 3Hz. However, cells exposed to low stretching frequencies of 0.1Hz and 0.5Hz in the same study, there were not significant reduce in the cell area between stretched state and control group.

Based on the alignment of the cell cytoskeleton as a structural adaptation to mechanical loading, this alignment has characteristically been attributed to the stress fiber reorganisation of the adherent cells to resist deformation forces (Zielinski et al., 2018). Das and co-workers (2022), created a system that mechanically coupled the cytoskeletal stress fiber to the direction of cell alignment with cell morphologies in response to applied cyclical stretching. Cells tend to reorient perpendicular to the direction of applied strain, the researchers suggested that the phenomenon of cell and cytoskeleton alignment, is a consequence of the cell reducing its free energy in order to cyclic strain avoidance. The model proposed by Kaunas et al. (2010), the disassembly of actin stress fibers upon mechanical stretching trigger a stabilisation and formation of cellular structural orientation. Based on the results carried out in this chapter regarding to orientation response. It was noted that some patterned orientation of cells in static condition aligned close to the direction of pre-stretching stage. After 24 hours of applied unidirectional stretch, cells tend to orient away from the longitudinal stretch with an average of cell alignment equally at every angle of orientation. In comparison to, Steward et al. (2010) explained the orientational behaviour of cells and their actin cytoskeleton were polarised after 3 hours of high strain in 20% magnitude. The cell alignment was observed that an increasingly in population reoriented to the direction of stretch axis over period of applied force with 85% of cell alignment upon 24 hours of stimulation. In the following part of cyclic stretching system (5% at 0.05Hz), orientation behaviour of cells revealed that almost half of actin aligned parallel to stretch direction. As described in the work by Jungbauer et al. (2018), an upward of the speed and frequency upon periodic stretching guide the maximum value of cell orientation in the model using variation of level of stretching toward rat embryonic fibroblasts. At higher amplitudes and frequencies, many studies suggested cells polarised perpendicular with respect to stretch axis (Costa et al., 2002; Kaunas et al., 2006; Nadruz et al., 2005). For instance, the dynamic of cell reorientation perpendicularly in response to the cyclically stretched substrates from 10-15% with relative ranging frequencies at 0.5-2Hz (Chen et al., 2017; Qian et al., 2013; Shao et al, 2015). In contrast to cell alignment when subjected to low frequency, a case reported by Hsu et al. (2010), there were no significant difference in stretched state at 0.01-

0.1Hz. It is highly possible that this response occurs as a relaxation when the cells was exposed to decreasing the strain rate below the activated stage.

The substrate-stretch combined micro-patterned surface was widely motivated in this research area (See examples; Lim and Donahue, 2007; Andalib et al, 2016). Stretchable topographic guidance could be more affected to activate cell signaling and alignment. As part of this work, it was intended that stimulated cell is more pronounced when the fibroblasts confine with the grooves perpendicular to stretch applied. A similar trend to be address by Houtchens et al. (2008), vascular smooth muscle cells exhibited increased cell alignment on grooved surface that influence the direction of cell spreading perpendicular to stretch axis. Due to limited orientation response of cell on patterned lines parallel to mechanical load, the microgroove data from experiments in fibroblast did not alter their alignment in response to stretching (Wang and Grood, 2000; Wang et al., 2004; Loesberg et al., 2005). All of these supportive data of cell alignment reflect the interaction and balancing of the contractile force dipole generated by the actin, focal adhesion and respond to their surrounding environment including external mechanical loading (Kito et al., 2000; Kumar et al., 2006).

3.5   Conclusion

Two generations of novel custom-built stretchers had successfully developed which allow multiple analyses, force measurement capacity, and fully adjustable monitoring uniaxial direction of stretch (e.g. unidirectional and cyclic stretch). The advantage of a second-generation stretcher containing a stretchable cultured area which compatible to combine surface modification techniques, the stretching system was incorporated into topographic pattern on substrates that carried both passive and active stretch at the same time to cells for a robust outcome. These contributed to a precise study of the mechanical mechanisms for stimulating mechanosensitive elements including dynamics in actin polymerisation, nuclear accumulation of MRTF-A (a crucial regulator of activated mechanosensitive gene circuits for cell movement and maintained cell/tissue homeostasis). The morphometric parameters of cell shape and size were also analysed to fulfill the geometric features and re-orientation to access cellular spreading and adhesion in response to applied stretch.

CHAPTER 4 EMD GENE ENGINEERING USING THE CRISPR/Cas9 SYSTEM

4.1 Introduction

Cells use mechanotransduction mechanisms to convert mechanical forces into biochemical and molecular events and impact on cellular and nuclear functions (Wang and Li, 2010). *In vitro* model systems contain a powerful ability to control experimental conditions of mechanical properties of the cell and its microenvironment (Kim et al., 2002; Li et al., 2004). The concept of this project is that monitoring the cellular environment under high and low mechanical forces can alter the mechanobiological responses of the cells affecting functions. The systems include increased mechanical force via applied stretch (chapter 3) and decreased force via withdrawal of a protein at the nuclear membrane that may be involved in nuclear mechanical properties (chapter 4). Emerin, an integral membrane protein was selected as a candidate in this chapter to generate cells-lacking emerin via CRISPR/Cas9 platform which is linked to actin capping protein and chromatin remodelling. Therefore, the functional consequences of lowering mechanical forces in emerin-null cells were analysed both downstream and upstream effectors of alterations in intracellular pathway and gene expression patterns in chapter 5.

The aim of the generation of cell-lacking emerin in this chapter is to investigate how networks of mechanical switches under low mechanical force microenvironment, contributed to cell behaviours. A key aspect of this study focuses on the mechanoregulation of the nucleus that considers cell mechanics as a single mechanical unit via physical connections from cytoskeletal filaments and nuclear lamin to chromatin. Graphic representation of mechanoregulation studies in molecular adaptive responses of cell mechanics including (1) the balance of G-actin and F-actin formation, (2) the control of the nuclear entry of transcription factor MRTF-A, (3) the effect of mechanical properties in chromatin remodelling, (4) transcription factor activities (in Figure 4-1), and comparison of cell mechanic between microenvironments subjected to high and low mechanical forces.
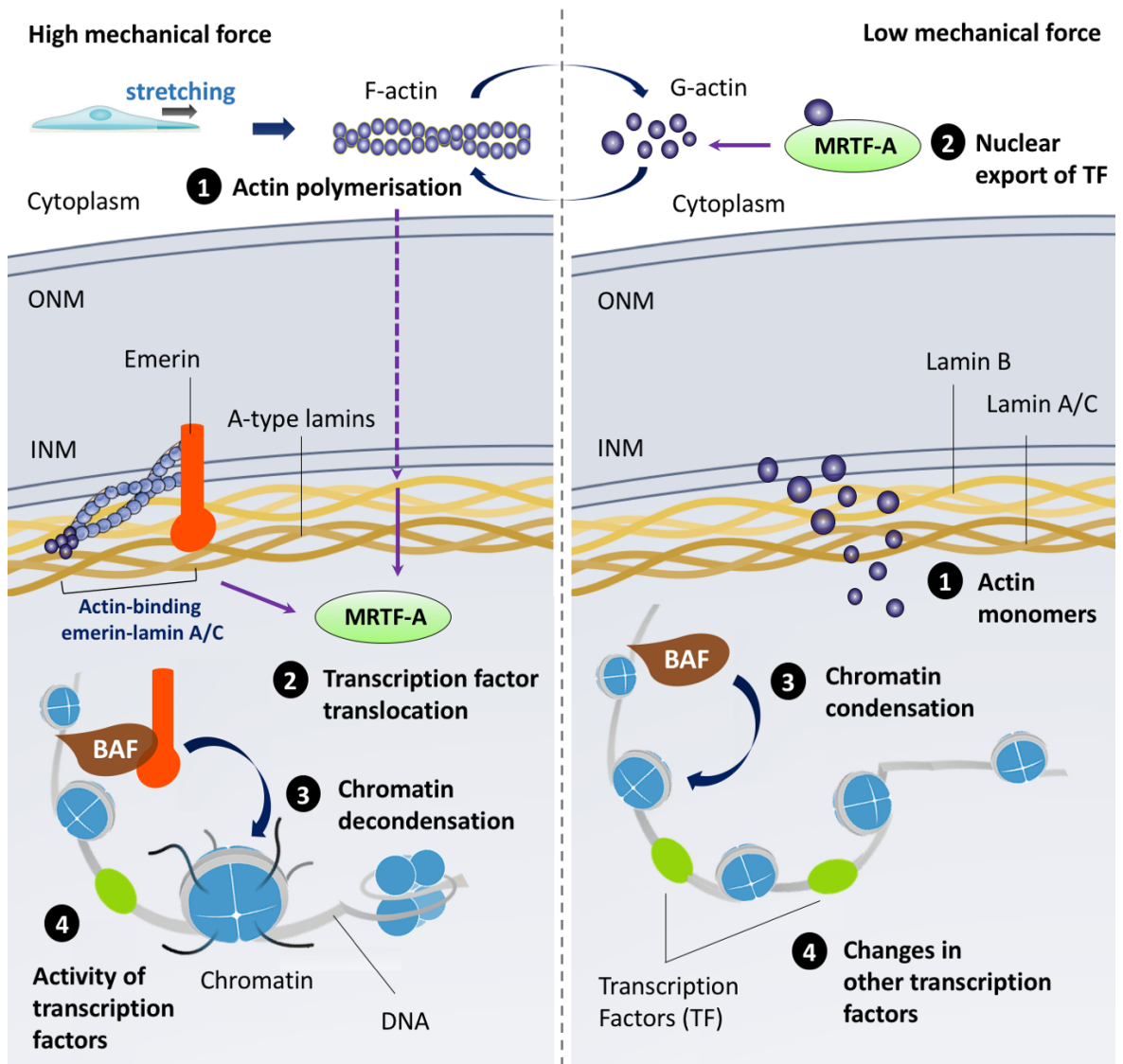
Figure 4-1. The contribution of altering the mechanical properties to functional adaptive responses of the nuclear deformations. A relationship between changes in mechanical force and nuclear reorganisation can affect a series of molecular events regulating components of the nuclear structure. (1) Mechanically induced actin polymerisation: high mechanical force increases the activity of F-actin formation and low mechanical force promotes monomeric actin. (2) Force regulated localisation and activity of mechanosensitive transcriptional activators, such as MRTF-A. An increased force susceptibility to trigger nuclear import of MRTF-A while export of MRTF-A can occur under condition of reduced force. (3) Nuclear force linked deformation may reposition or locally modify chromatin decondensation and confer their associated transcriptional activities. Chromatin accessibility under high mechanical force may cause the fold of chromatin complexes while under condition with low force could unfold chromatin domains. (4) Dynamic networks of regulatory transcription factor subjected to microenvironmental cues. Transcription factor that may activate in response to mechanical stimuli and activation of other transcription factors for compensation under low mechanical force (Adapted from Simon and Wilson, 2011; Kirby and Lammerding, 2018; Kalukula et al., 2022).

To investigate genotype-phenotype relationships, genetic manipulations with precise and robust outcomes are essential tools. They help to identify gene function. Particularly using gene deletion can unlock not only an individual role for a gene, but also help characterise multiple gene interactions (Jakutis and Stainier, 2021). In this chapter, the bacterial immune system-derived CRISPR/Cas9 system was used for genetic manipulation in a sequence-specific manner. The type II CRISPR/Cas9 pathway can be repurposed as a customised RNA guided DNA binding platform in order to suppress the transcription of almost any gene of interested (Qi et al., 2013). To reprogram the strength of nuclear envelope in a cell line I aimed at modifying a conserved protein, emerin, encoded by the EMD gene, and generated the knockdown and knockout models.

The CRISPR/Cas9 system has transformed the selective modification of targeted DNA sequences by utilising a programmable single-guided RNA (sgRNA) to locate and bind to specific regions directly adjacent to the protospacer adjacent motif (PAM) of strand DNA backbone (Jiang and Doudna, 2015; Nishimasu et al., 2014). Structurally sgRNA-DNA duplex is then recognized by Cas9, where Cas9 nuclease induces double-stranded breaks (DSBs) primarily determines the mode of gene editing via either gene deletion, knockout, correction or insertion, followed by mechanistically conserved cell intrinsic DNA repair processes (Foley et al., 2022).

Two genetic repression approaches via CRISPR-Cas9 toolbox have been applied directly to the specific sequence of the target locus (see overview Figure 4-2). An inducible CRISPR interference (CRISPRi) offering a transient knockdown of gene expression without changing in the target sequence (Larson et al., 2013). While, CRISPR-based knockout systems are the state-of-the-art tools to abrogate the gene expression by generating loss of function mutations through the creation of insertions or deletions (INDELs) that ideally permanently silence the target gene (Vitor et al., 2020). The transfection with a proper CRISPR-Cas9 delivers site-specific changes. Multiple selection steps (i.e. a drug-selectable marker, monoclonal selection and Sanger sequencing) then allowed their expression to be confirmed and validated transfection efficiency.
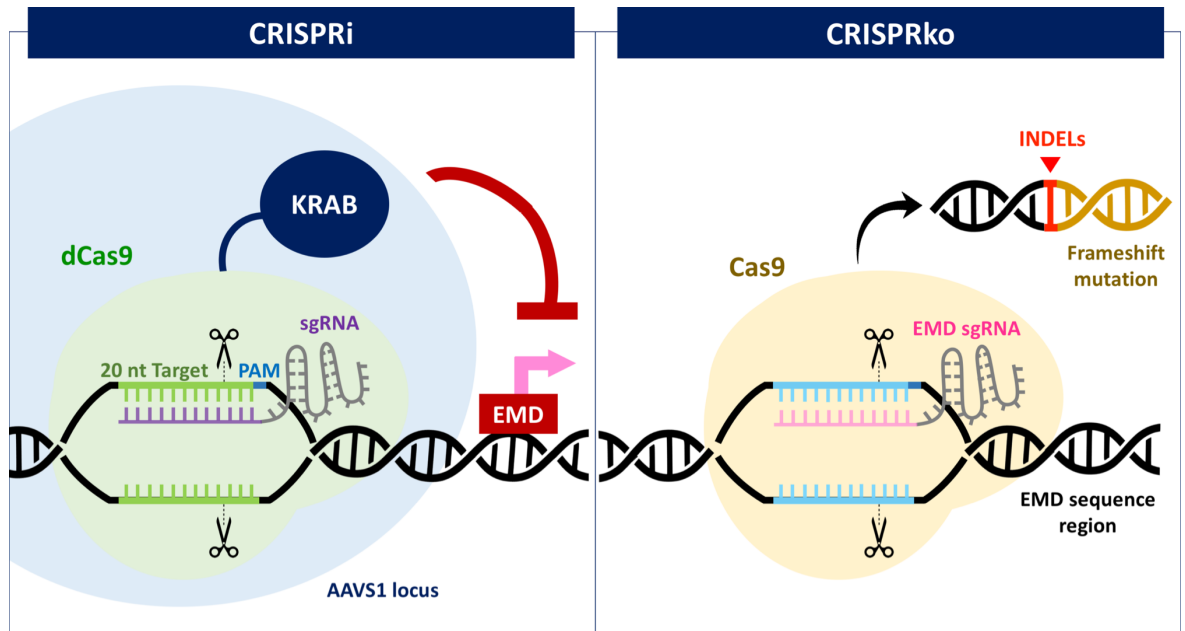
Figure 4-2. Two-way CRISPR/Cas9 model used for gene disruption of EMD expression. CRISPR interference (CRISPRi)-mediated sequence specific cleavage at the AAVS1 locus, dCas9-KRAB repressor domain which will act as a roadblock the elongating RNA polymerase to targeted EMD gene. CRISPR knockout (CRISPRko) targeting the gene of interest directly at the transcribed EMD sequence. The Cas9-sgRNA complex recognises target DNA via Cas9 nuclease activity to generate double-stranded break (DSB) adjacent to the PAM recognition site. Next, repair mechanism with creation of insertions or deletions (INDELs), often lead to frameshift mutation and abort EMD transcription. Thereby, inactivating protein coding of the target gene product.

Beyond translating CRISPRi to repress transcription into mammalian cells, the sgRNA-guided localization of catalytically inactivated Cas9 (dead Cas9, dCas9) to inhibit endogenous gene promoters near transcription start site (TSS) (Mitsunobu et al., 2017; Schuster et al., 2019). The promoter blockage can further improved by fusion of dCas9 to various repressor domains such as Krüppel-associated box (KRAB) (Wang et al., 2016). This transfection complex was delivered into the common sustainable gene transfer site in human non-pathogenic adeno-associated virus integration site 1 (AAVS1), referred as "the genomic safe habours" for integration that ensured the function predictably and improved the safety of modification applications (Hayashi et al., 2020; Papapetrou and Schambach, 2016; Samulski et al., 1991).

As using CRISPR knockout strategy outperforms CRISPRi, the former have become to be a mainstream focus in specific sequence alterations which can reverse the function of its gene transcripts and pathways (Sander and Joung, 2014). Generating knockout model by introducing a donor template sequence used sgRNA-targeting directly at the first exon of EMD, this allows the correction of defective endogenous genes to remove or insert an exogenous strand of DNA. The full CRISPR-mediated functional knockout (KO) genes in their open reading frames (Yang et al., 2016; Cullot et al., 2019), are only ensured a depletion of expression, occurred upon disruptive mutations of both alleles of the gene (Evers et al., 2016).

The CRISPR-based disruption of gene expression strategy described in this chapter, provides the explanation of how this RNA-guided system works and how it has been applied to disable the expression of emerin, or more precise disrupt the EMD locus. The model of cells defect in EMD/emerin expression in human dermal fibroblasts and epithelial-like cells have been proposed, and also described is how the system can be repurposed to study other gene functions.

4.2   Materials and Methods

4.2.1   Materials

List of Reagents

sgRNA construction and delivery
Oligonucleotides .... Sigma-Aldrich
T4 DNA ligase .... Promega
T4 DNA ligase buffer.. Promega
T4 phosphonucleotide kinase .... Biolabs
T4 phosphonucleotide kinase buffer .... Biolabs

Bacterial culture reagents
LB broth or agar .... Agilent Technologies
Plasmid Midi Kit .... Qiagen
StrataClone Competent cells .... Agilent Technologies
SOC medium .... Agilent Technologies

Gel electrophoresis
0.08% SDS/Gel Loading Dye .... New England Biolabs
1 kb DNA ladder .... Invitrogen

4.2.1 Materials (Continue)

List of Reagents
Gel electrophoresis UltraPure^{TM} Agarose .... Invitrogen
Restriction enzyme digestion Buffer E .... Promega HINDIII .... New England Biolabs NEBuffer 4^{TM} .... New England Biolabs SspI-HF® .... New England Biolabs
Cell transfection EnGen® Spy Cas9 NLS .... New England Biolabs MessengerMAX^{TM} Reagent^{TM} transfection reagent .... Thermo Fisher Scientific

4.2.2 sgRNA construction and delivery

To identify potential single-guide RNA (sgRNA) to each region of interested, primers were designed using Chopchop tool. The sgRNA sequences were guided by 4 nt window to U6 promoters for the EMD-gene of interested and CMV promoters for the AAVS1 – genomic safe habours, followed by spacer (20-24-bp target). Forward and reverse primers used to amplify designed gene-edited sequence are shown in Table 4-1 (Synthesized oligos from Sigma-Aldrich).

Table 4-1. Primers for cloning reaction are listed

Oligo Name	Length	MW	Tm°	GC (%)	Sequence (5'-3')
EMD sgi 1F	24	7237	80.6	62.5	CACCGCCCAAACGTCATCAACGCG
EMD sgi 1R	24	7409	76.5	54.1	AAACCGCGTTGATGACGTTTGGGC
EMD sgi 2F	24	7376	76.7	58.3	CACCGTTGATGACGTTTGGGCTCG
EMD sgi 2R	24	7269	72.4	50.0	AAACCGAGCCCAAACGTCATCAAC
AAVS1 cut 2F	27	8107	74.5	59.2	CTTACCAATCCTGTCCCTAGTGGCCCC
AAVS1 cut 2R	27	8431	83.3	70.3	CGCGGGGGCCACTAGGGACAGGATTGG

To perform phosphorylation modifications of synthesized oligos at the 5'end, the sgRNAs were phosphorylated using T4 phosphonucleotide kinase and buffer (1hour incubation at 37°C), annealed in a thermocycler for 15 mins at 65°C, and ligated

into pTetCRiRosa1 plasmid. For DNA construction, the pTetCRiRosa1 vector was generated to knockdown the expression of EMD via transcriptional suppressor at the KRAB domain. A schematic representation of restriction map of pTetCriRosa1 plasmid (See Appendix Figure A-1). The pTetCriRosa1 vector backbone was digested with BsmBI and ligated together with the phosphorylated and annealed oligo duplex (1:50 dilution) using T4 DNA ligase and buffer. The reaction was incubated at room temperature overnight. Assembled plasmids containing the co-delivering of EMD and AAVS-1 inserts, were then transformed into *E.coli* competent cells and plated on Amplicilin selection plates with 2% X-gal on each plate.

4.2.3 Bacterial culture

Competent cells were purchased from Agilent Technologies (StrataClone Competent Cells, #200185). For PCR cloning, 2 µl of the ligation reaction was added to the competent cells and incubated at 4°C for 20 minutes. Upon Heat-shock transformation, the mixture of cells and plasmids were heat-pulsed by placing in it a water bath at the 42°C for 45 seconds. The cells were then cultured in SOC medium and incubated at 37°C for 1 hour, followed by Blue/White screening antibiotic resistance using Amplicilin for selection. The plasmid midi-preps was performed using Plasmid Midi Kit (Qiagen, Germany) and further quantified the DNA concentration by Spectrophotometer (Nanodrop, Thermo fisher scientific, USA). The plasmids were then analysed by Sanger sequencing to confirm proper sgRNA assembly.

4.2.4 The polymerase chain reaction (PCR) amplification of vector insert

Primer pair AAVS1 cut 2F and EMD sgi 1R/2R was used to amplify EMD insert carrying AAVS1 from pTetCRiRosa1 plasmid (~2,000 bp). For qPCR colony screening, the reaction containing 200nM of primers, 1x master mix (DNA polymerase, dNTPs and $MgCl_2$) and colonies on the Amplicilin-resistant plates with the following protocol: 99°C for 15 minutes, 99°C for 15 seconds, 55°C for 15 seconds, 34 cycles and a final 30 seconds extension at 72°C. To analyse the products of conventional PCR, gel electrophoresis was used as a read out of DNA fragments using 1% agarose/0.5X TBE buffer. Gels were run in a horizontal

electrophoresis at 150V for 30 minutes at room temperature using Bio-RAD. Each gel was stained for 20-30 minutes in 0.01% ethidium bromide/0.5x TBE buffer and further imaged using Fuji-film.

4.2.5 High-fidelity Cas9 provides high specificity in the targeting AAVS1 construct

To verify the efficiency and specificity of Cas9 that generates the double stranded break in the DNA at the seed region adjacent to PAM sequence in the AAVS1 locus. Plasmids were double digested with HindIII, cleave the DNA into 2 fragments comparing between fragment containing PAM specific sequence and another fragment used as a reference. In brief, 2µg of plasmid DNA were digested with HINDIII/buffer E for an hour at 37°C. Then, the mixtures were cleaned up using PureLink® PCR purification Kit (Thermo fisher scientific, USA). To verify the high specificity of a single cut size of the target and vector by Cas9, *in vitro* digestion between the pre-digest products with HINDIII and 100-300 nM of EnGen® Spy Cas9 NLS were incubated at 37°C, overnight. Finally, the reactions were heat inactivated the Cas9 in 0.08% SDS/Gel Loading Dye at 65°C for 5 mins before running a gel electrophoresis.

4.2.6 Lipofection of Cas9 mRNA-sgRNA complexes

Two transfection approaches used to generate knockdown and knockout cells at the EMD target sequence in BJ1-hTERT and HEK293 cells. Liposome-based transfection using Lipofectamine MessengerMAX™ Reagent™ transfection reagent in a combination with Cas9 mRNA, programmable sgRNA and Puromycin selectable region. An outline and time course of transfection complex components for the sgRNA-Cas9 deliveries, conserved region od designed drug selectable marker and screening for targeted gene disruption is summarised as shown in Figure 4-3.
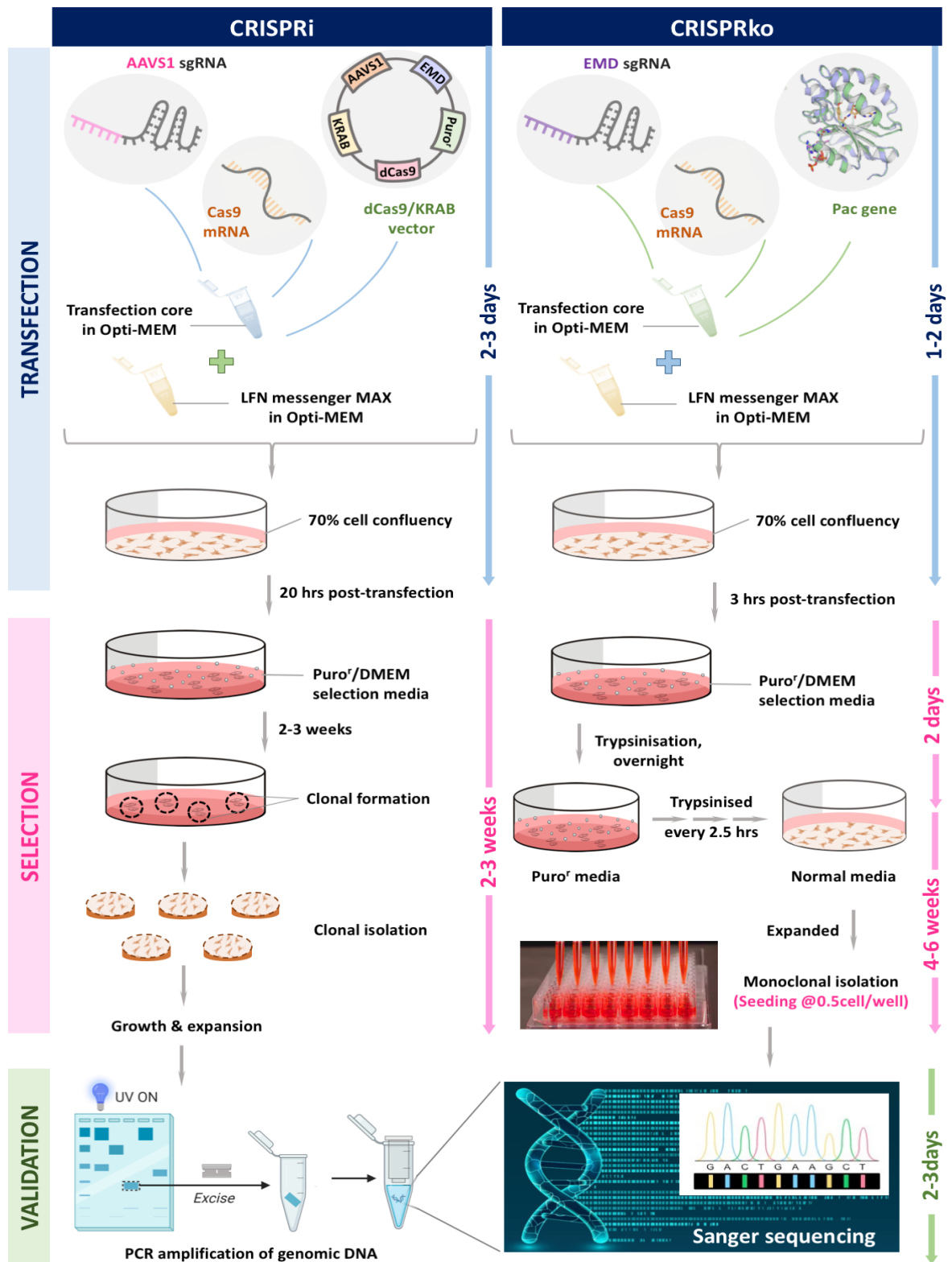
Figure 4-3. The workflow of transfection strategies used to generate the model of EMD gene disruption in human cell lines. CRISPRi components (AAVS1 sgRNA, Cas9 mRNA & plasmid) are co-delivered via LFN messengerMAX into 70% pre-seeded cells, followed by Puromycin selection at 20 hrs post-transfection and then allowed the clonal formation in 2-3 weeks. Finally, isolated clones were validated by PCR amplification and DNA sequencing (left panel). For CRISPRko, direct target transfection via sgRNA-guided EMD sequence and selected cells resistance to Puromycin condition (confers to pac), followed by trypsinised cycles, cultured in normal media for screening and validation steps (right panel).

4.2.6.1 CRISPRi-based plasmid DNA transfection & integration into AAVS1 site

Cells were transfected with mRNA-lipid complex in the proportion as follows: The lipofectamine (LFN) MessengerMAX was diluted in Opti-MEM medium at 3:50 volume ratio and incubated for 10 mins at RT. The combined plasmid DNA and Cas9 mRNA were substantially mixed with AAVS1 sgRNA or without sgRNA as a control. An approximately 1 μg of DNA-RNA complex (720 ng of Cas9 mRNA, 100 ng of pTetCri_AAVS1 vector and 1pM of AAVS1 sgRNA) was also carried in 50 μl of Opti-MEM medium, incubated and further added to the premixed LFN Messenger MAX followed by 5 min-incubations. Finally, cells at 70% confluency in 12-well cell culture plate were transfected with the mRNA-lipid complex for 20 hours before changing into selection media at 3 μg/ml of Puromycin/DMEM. The transfected cells were refreshed the media every 2-3 days until performing the single colony before isolation using Pyrex ring-vacuum system.

4.2.6.2 CRISPR-mediated gene knockout approach

The Cas9 mRNA was performed by A. Hamilton and kindly gifted for transfection. In brief, plasmid-coding Cas9 template was in vitro transcribed in a reaction containing T7 polymerase, dNTPs (ATP, CTP, UTP and GTP) followed by harvesting and column purification of the RNA yields using Purelink® PCR purification Kit (Thermo fisher scientific, USA).

For transfection, the cells were seeded at 5×10^4 cells/well for BJ1 and 2×10^5 cells/well for HEK293 in 24-well cell culture plate, incubated at 37°C with 5% CO_2 for 18-24 hours before transfection. The mRNA-lipid mixture according to cell transfection was performed and incubated at 25 °C in each step of premixed reaction mixes as follows: 3 μl of LFN MessengerMAX and nucleic complexes (720 ng of Cas9 mRNA, 0.75 pM of EMD sgRNA and 180 ng of pac) were prepared in a separated tube and diluted in 50 μl of Opti-MEM medium, mix well by vortex and incubated for 10 minutes. Next, the complex mixture of nucleic acid/Opti-MEM were added to diluted LFN MessengerMAX and incubated for 5 minutes before dividing and adding into 2 well of cells. The media was changed into selection/normal media after 3 hours post-transfection. The cells were cultured in 5μg/ml of puromycin/DMEM media for 1 hour, trypsinised and neutralised with puromycin/DMEM overnight. Then, cells were trypsinised for 2-4 rounds every 2.5

hours before changing into normal cultured media until they reached 70-80% confluency in 6-well cell culture plate before validation at the sgRNA-targeted site using DNA sequencing. In order to screening of monoclonal selection for an individual knockout clone, cells were seeded at 0.5 cell/well in 96-well cell culture plate.

4.2.7 PCR reaction and Sanger validation

To targeting coding region, libraries/profiles in the genomic DNA which amplification of PCR products using designed primer pairs directing at least 150 bp away from the sgRNA cut site. In addition, the transfected cells using pTetCRi_AAVS1 was also performed the junction PCR between AAVS1 integration site and 20 nt of either 5' or 3'end of the transfection vector. Table 4-2 showed the properties and sequences of primers used to verify the efficiency of transfection at the cut site. The PCR products were then run in 1% agarose/0.5x TBE at 150V and purified using PureLink™ Quick Gel Extraction Kit (Thermo fisher scientific, USA). The Sanger sequencing was synthesized by Eurofin, the resultant DNA sequence was verified by the Synthego ICE analysis tool.

Table 4-2. Primers used to target the sgRNA cut sites.

Oligo Name	Length	MW	Tm°	GC (%)	Sequence (5'-3')
AAVS1 for	20	5964	64.4	55	AGTCTTCTTCCTCCAACCCG
AAVS1 rev	20	6271	62.7	55	GGGAAGTGTAAGGAAGCTGC
pTet for	20	6327	62.3	60	GAGGGTAGGAAGTGGTACGG
pTet rev	20	6062	63.1	55	GATGTAACCCACTCGTGCAC
EMD Ex1i for	20	6133	63.2	55	AGCCTACGAGTTGATCCTGG
EMD Ex1e rev	16	4916	68.9	68.7	GGCCGTGACGCGACAA

4.2.8 qRT-PCR assay of the Doxycycline-inducible transgene expression system

In order to evaluate the efficiency of knockdown expression of EMD in HEK293 cells, an inducible Tet-Off system which allows the silencing of gene expression by pre-administration of Tetracycline-derivatives like Doxycycline (Dox) (Das et al., 2016) in the cells was used to access via qRT-PCR assay. The non-transfected and transfected cells were treated with 1 µg/ml of Dox/DMEM culture media for 12, 24 and 48 hours (37°C, 5% CO_2). Next, the cells RNA was extracted using Direct-

zol^{TM} RNA Mini Prep Kit (Zymo Research, USA), followed by cDNA synthesis and qRT-PCR reactions as detailed in Section 2.2.6. Table 4-3 showed the primers used in qRT-PCR reaction which were designed in the exon-exon boundaries for EMD and GAPDH as a housekeeping gene and optimised primer pairs from part of the plasmid for dCas9 and KRAB.

Table 4-3. Primers used in a transient gene knockdown and access level of expression via PCR assay.

Oligo Name	Length	MW	Tm°	GC (%)	Sequence (5'-3')
GAPDH for	20	6253	66.3	55	AGGCAGGGATGATGTTCTGG
GAPDH rev	19	5718	63.5	57.8	GCACCACCAACTGCTTAGC
dCas9 for	20	6209	65.9	55	CAGAAGGGAAACGAACTGGC
dCas9 rev	20	6093	64.6	55	GCACCTTGTCCAGATTAGCG
qEMD for	20	5979	62.8	50	TCCTTGCACTCCTCTTCAGA
qEMD rev	21	6384	60.1	52.3	AGAGAGCTACTTCACCACCAG
KRAB for	21	6390	58.1	47.6	GATGCTAAGTCACTAACTGCC
KRAB rev	20	5875	61.8	55	CTCTTCTCCCTTCTCCAACC

Abbreviations; Ex – Exon, for – forward, rev – reverse, q(qEMD) – Quantitative.

4.2.9 The validation of protein repression using IF staining and westernblot analysis

In order to validate the knockout clones of EMD gene toward their expression in the protein level, the cells or proteins were harvested followed by immunospecific labelling using anti-EMD antibody at 1:50 for IF staining or 1:130 for WB assay. (See section 2.2.4 & 2.2.7 for detail).

4.3 Results

4.3.1 Validation of the multiple sgRNA cloning

To clone multiple sgRNAs into a single expression vector for CRISPRi target site, the cloning vector was digested using type II restriction enzyme sites (BsmBI) for robust assembly of the EMD and the AAVS1-targeting sgRNAs. Figure 4-4 represented the schematic diagram of cloning vector used pTetCRiRosa1 plasmid backbone and insertion of AAVS1 and EMD genes at the double divergent BsmBI cut sites. In multiple cloning sites, the vector was then assembled cassettes for oligonucleotides ligation of protospacer sequences using T4 DNA ligase. The

ligation reaction was transformed into competent *E.coli* cells and selected using Amplicilin selection marker.
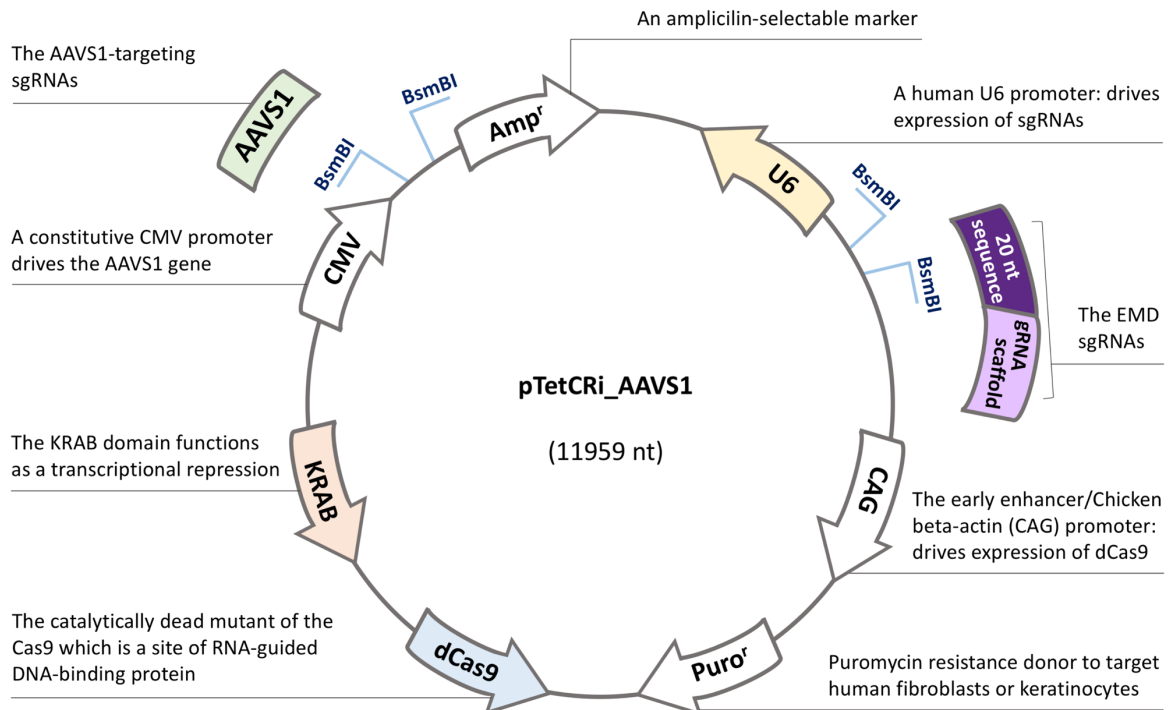
Figure 4-4. Schematic diagram for cloning of the guide sequence oligos into a plasmid. The cloning vector containing the Krüppel-associated box (KRAB-containing zinc-finger repressor proteins), two sgRNAs (light green and purple boxes)-encoding DNA was appended onto the either U6 or CMV primers and an extended DNA oligos containing 20-24-bp targets preceding 5'-NGG PAM in genomic DNA. The restriction site BsmBI TypeII restriction sites (DNA clevage site as outlined in light blue) is inserted to the sgRNAs expression cassette to facilitate cloning of annealed oligos. The sgRNAs expression plasmid composes of a U6 promoter with an annotated amplicilin-selectable marker (Amp^r) and contains a puromycin-resistance (Puro^r) gene controlled by the CMV promoter.

In order to validate the vector insert and evaluate the transformation efficiencies of the recombinant plasmids, individual transformant colonies were analysed using qPCR. The desired size of the PCR product is approximately 2,077 bp. Interestingly, the results from qPCR detected the expected band at around 2,000 bp as compared to DNA standard using 1kb DNA ladder. Next, the plasmid DNA was isolated from recombinant *E. coli* cultures and purified by using an alkaline lysate procedure, followed by binding of plasmid DNA to an anion-exchange resin column. Finally, the resultant plasmids were washed ou and then validated to confirm the desired sequences by Sanger sequencing (Figure 4-5).
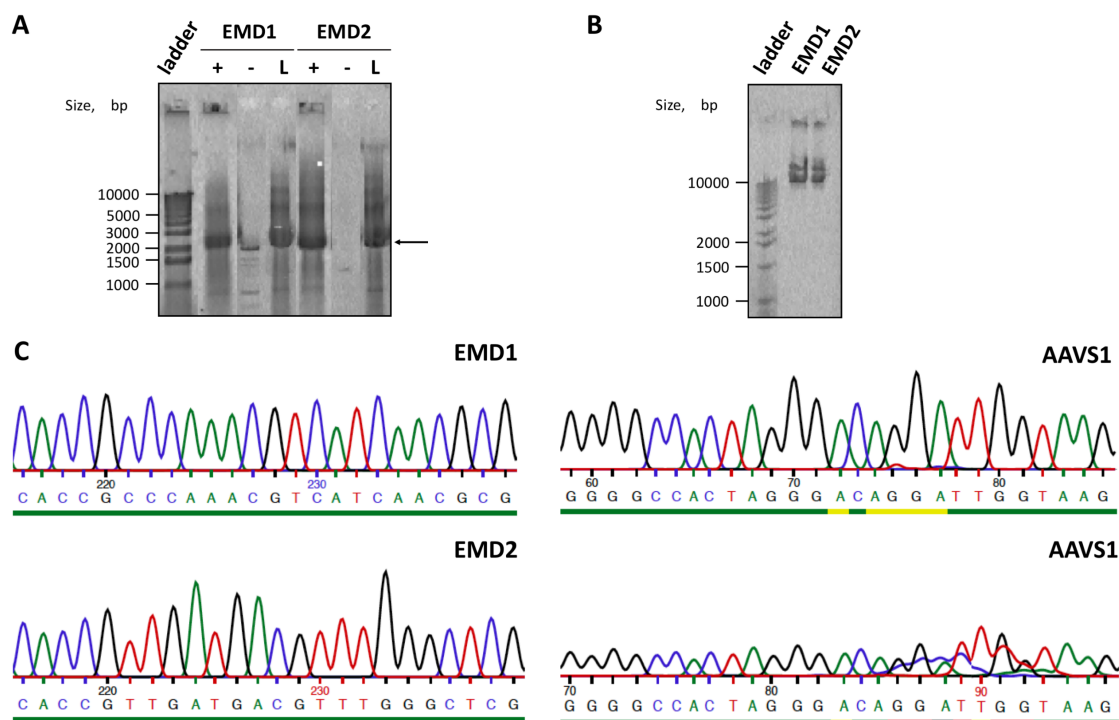
Figure 4-5. PCR and Sanger sequence analysis of the plasmid that contains the gene of interest. A) The qPCR amplification of inserted DNA fragment. The plasmid DNA was then separated using agarose gel electrophoresis together with ethidium bromide staining. Black arrow indicates expected fragment sizes for each insert. B) Photograph of a supercoiled DNA showed correct size vector assembly. Two new vector inserts were joined with the cloning vector. C) Primer sequences of sgRNAs cloning site, the complete nucleotide sequence EMD1/2-sgRNAs matches to the original design of primers (left panel), the chromatograms of AAVS1-sgRNAs used to co-delivery with EMD1/2 (top right – EMD1, bottom right – EMD2). The sequences were shown as an anti-sense strand that perfectly matched to the primer design. For gel electrophoresis images; ladder, 1 kb DNA ladder was used as a standard marker; +, Positive transformed colonies; -, Negative control; L, Ligation reaction of EMD1/2.

4.3.2 Site-directed determinant of Cas9 specificity

To verify the target specificity that incorporate to Cas9 nuclease activity, the enzymatic digestion and gel assay were monitored as follows: the on-target DNA cleaving Cas9 enzyme, an all-in-one vector was double-digested with HindIII and EnGen® Spy Cas9 NLS followed by observing the DNA fragment products using Agarose electrophoresis. The assemble plasmid vector was pre-digested with HindIII, this resulted in 2 fragments; a unique segment carrying a protospacer adjacent motif (PAM) region and the other DNA segment used as a reference. The

cleavage map and electrophoresis showed in Figure 4-6, validated that the Cas9 can selectively determine the appropriate target recognition site and cleaved specific. Thereby, it should be sufficient for transfection.
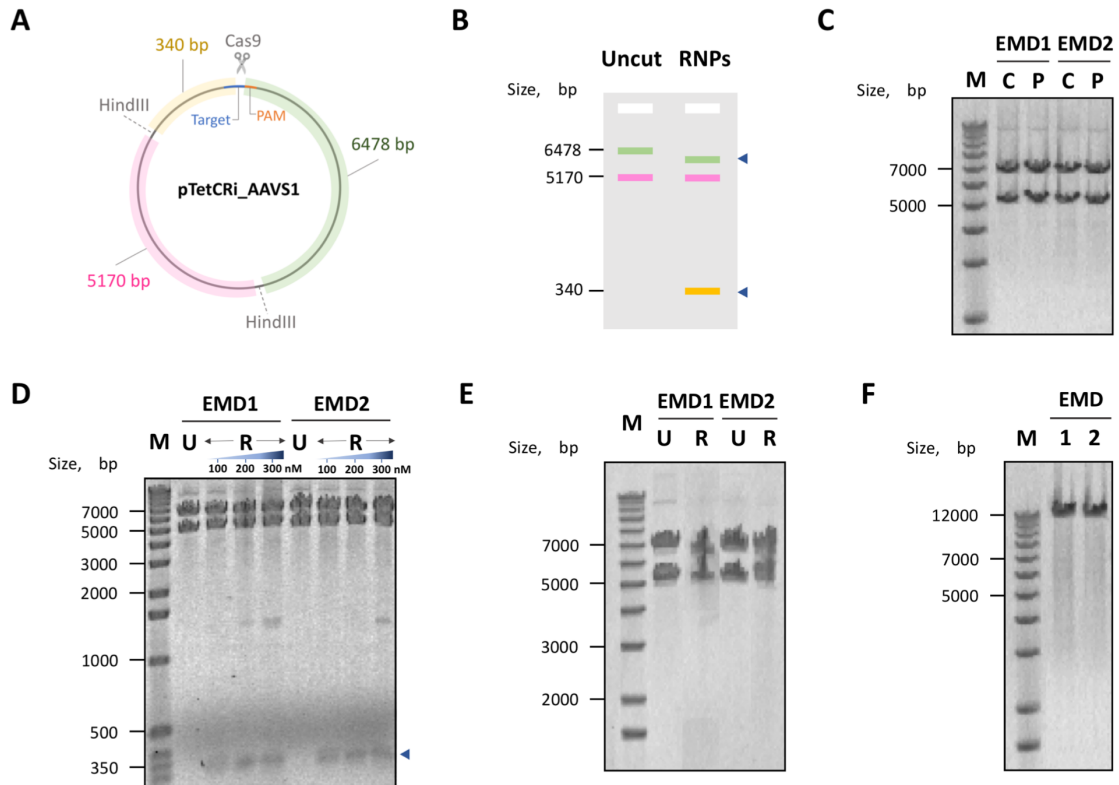
Figure 4-6. Cas9-catalysed cleavage of target DNA at the recognition PAM site. A) an overview of double-digested plasmid with HindIII and Cas9 enzymes, generated the three linearised plasmid fragments. B) Comparison between uncut plasmid and ribonucleoprotein (RNPs) complex, the precise cut sites appeared as a distinct band on an agarose gel. C) The resulting digested DNA by HindIII, separated into two pieces. D) the RNPs complex formation when it was fused to 100-300nM of Cas9, produced an expected fragment visible as a band at ~340bp. E) Assessment of Cas9-RNPs decomposition, Cas9 specifically break the DNA target at the PAM site containing in the top band without interfering the band below that can be used as reference band. F) A linearized plasmid product of the circular plasmid using SspI. The DNA Marker (M) on the left panel and the following lanes: U, Uncut; R, Ribonucleoprotein (RNPs); C, Cut; P, Purified DNA.

4.3.3 Direct target integration into the AAVS1 site

The plasmid used for transfection encoded a sgRNA targeting the endogenous AAVS1 locus and dCas9 worked in concert with a synthetic AAVS1-sgRNAs and Cas9 mRNA, the PCR amplification target was designed to characterise the insertions

or deletions (INDELs) polymorphism that can occur after transfection, followed by puromycin selection and single clone isolation (Figure 4-7).
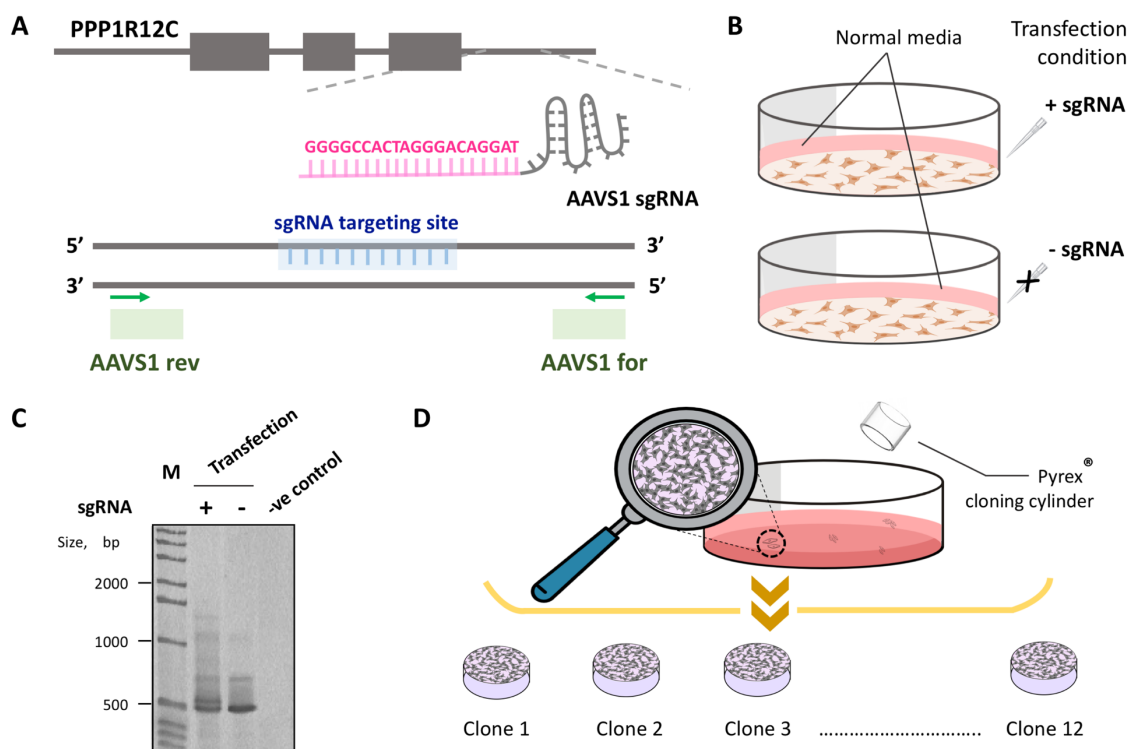
Figure 4-7. Transient transfection, selection and expansion of clonal post-transfection. A) Targeted transgene CRISPR/Cas9 expression into the human AAVS1 safe habour locus, PCR amplicon of interest was designed to evaluate the transfection efficiency B) Tracking the transfection into the designed transgene integration site, the foreign plasmid DNA was delivered with Lipofectamine MessengerMAX reagent in the present/absent of sgRNA targeting AAVS1. C) The PCR product at post-transfection in HEK293 cells, appears as a two-core bands in the condition of delivery with AAVS1 sgRNA and a band in transfection control without AAVS1 sgRNA. D) Isolation and expansion of single clone, the transfected cells were screened in Puromycin selection media after 20 hours of transfection. Twelve-clones were observed and isolated using Pyrex$^{®}$ cloning cylinder.

In order to verify targeted insertion into the defined loci, the PCR primers were designed (at least 150bp) upstream and downstream region from transfected boundaries by AAVS1-sgRNA targeting. The sequencing and interference of CRISPR edits (ICE) detection validated target insertion resulting in the percentage of %INDELs at a frequency of 11% without drug selection from transfected HEK293 cells. For normalisation of precise targeted insertion, the transfection control delivery without sgRNA exhibited some random cut of DNA with 19% of INDELs

score at a low R^2=0.23 (See appendix Figure A-2). Next, the first wave of the screens was performed on transfected cells in culture with 3 μg/ml of Puromycin supplementary media, followed by clonal isolation and expansion. Then, the region targeted by AAVS1-sgRNA, was further validated and confirmed the integration by the junction PCR between the insert sequence and donor plasmid. Figure 4-8 displayed the schematic illustration of the core of transfection at the target site and designed PCR primer position, PCR junction products and sequence alignment. The results from junction PCR showed that 7 out of 12 clones from isolation were screened for junction PCR, 5 out of 7 (71.4%) tested clones were 5'/3' junction PCR positive bands. In clone 9, 10 and 12 (subjected to 42.9%) which displayed the junction PCR positive clones in both 5'/3' genome-donor boundaries, were then selected to validate the sequence (Fig 4-7D).

The hard-to-transfection BJ1-hTERT cells were subjected to lethal Puromycin selection media (n_{Bio}=2). The cells were also transfected with equal amounts of an eGFP–expressing plasmid, here I observed less than 1% eGFP positive cells at post-transfection.

4.3.4 CRISPRi-mediated targeted silencing of EMD gene

To generate the dox-inducible dCas9-KRAB-EMD expression in HEK293 cells, the clonal population was treated with 1 μg/ml of Dox which was added to the cultured media. The qRT-PCR analysis identified clones (Figure 4-9A) that highly expressed dCas9 in clone 10 and clone 12, but no observed enrichment expression of dCas9 in clone 9. Following the dCas9 overexpression, ~87-fold to 88-fold upregulation occurs after 12 and 24 hours of Dox treatment in clone 10. In clone 12, exceed 200-fold activated expression of dCas9 was measured between 12-24 hours post-treatment of Dox. However, the EMD expression was reduced slightly in all tested clones at approximately 0.4-0.8-fold downregulation in dox-inducible cassette expression. To ensure reproducibility of the results and limit false positives, the clone 12 that exhibited the highest expression of dCas9 was selected and performed two-independent biological replicates and prolonged treatment of the screen by added Dox to the knockdown-derived clone 12 for 72 hours.
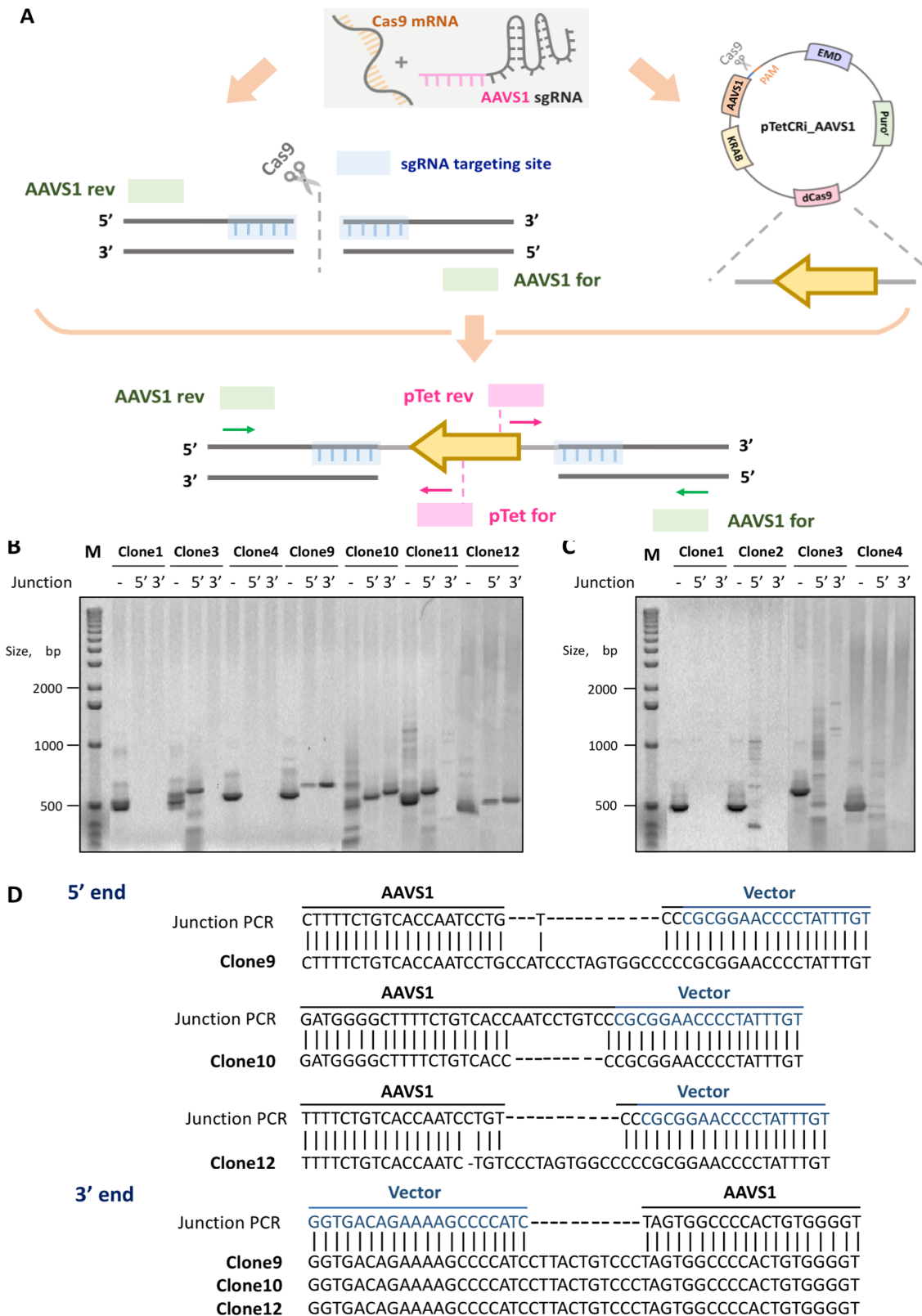
Figure 4-8. Targeting sgRNA-Cas9 intracellular elements and delivery for gene knockdown into the transgene insertion AAVS1 site. A) Illustration of the sgRNA target genome and cleavage site. B) Agarose gel of 5'/3' junction PCR on clonal isolation at post-transfection. C) 5'/3' Junction PCR in control of transfection without sgRNA. (5'/3' indicates direction of transcription, - referred to AAVS1 genome reference) D) Sequence alignment confirmed insertion, validated from Sanger sequencing and Junction PCR blast alignment to the ideal cut.

In replicates, expression levels of dCas9 were overexpressed while the EMD expression remained at a similar level compared to untreated control (Figure 4-9B-C).
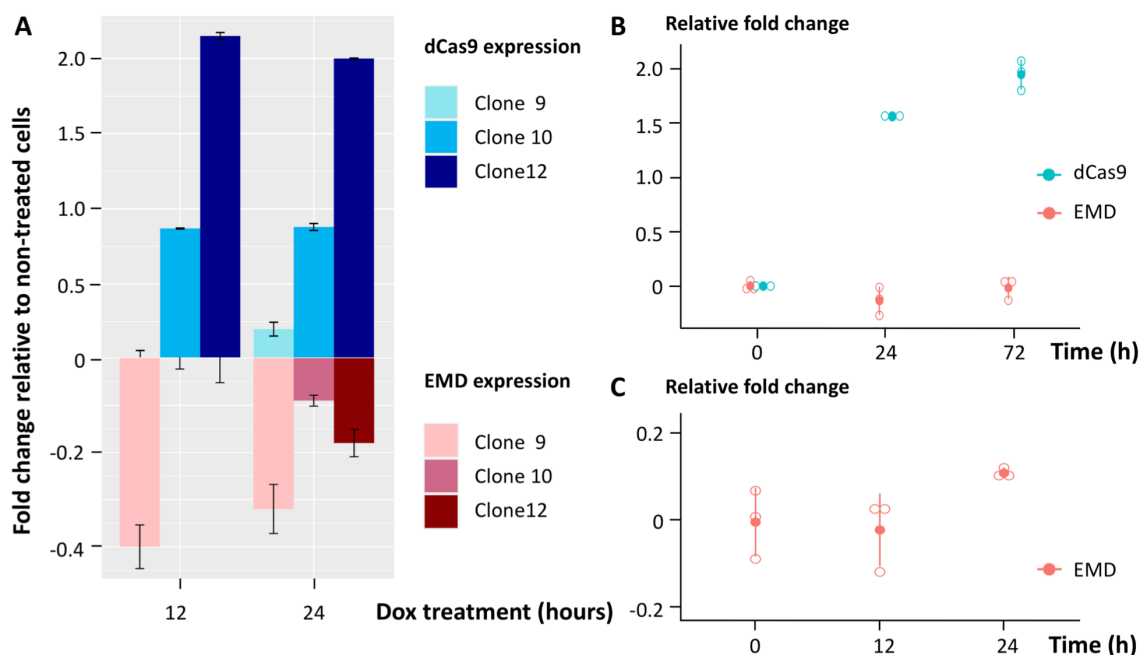
Figure 4-9. Transient effects of AAVS1-mediated dCas9/KRAB gene silencing under regulation of tetracycline (Tet)-inducible systems. A) RT-qPCR expression of dCas9 and targeted EMD in transfected HEK293 cells, represented as a 10-fold (log10) changes between Dox (1 μg/ml) treatment and untreated control. B) Log10 fold change between dCas9 and EMD in clone 12 at a prolonged time course of Dox treatment to 72 hours. C) A relative fold changes in log10 of EMD expression in non-transfected cells during 0-24 hours of Dox-inducible manner. Error bars represent standard deviation of the mean of the reaction replicates.

4.3.5 CRISPR-based gene knockout influences permanently silencing the EMD

Purposeful disruption of the EMD gene at the first exon via CRISPR knockout (CRISPRko) could introduce loss-of-function mutations, given that INDELs to alter a coding frame or even generation of a premature stop codon. The transfection performed in human BJ1 or HEK293 cell lines, the sgRNA targeting EMD locus was selected and designed for functional knockout of EMD. Besides wt-CRISPR-Cas9 expression, the application uses mRNA-encoding Cas9, sgRNA targeting EMD with 20nt complementary base pairing and Pac (confer to puromycin selection) deliveries into cells and PCR primer designs for on-target validation in Figure 4-10.
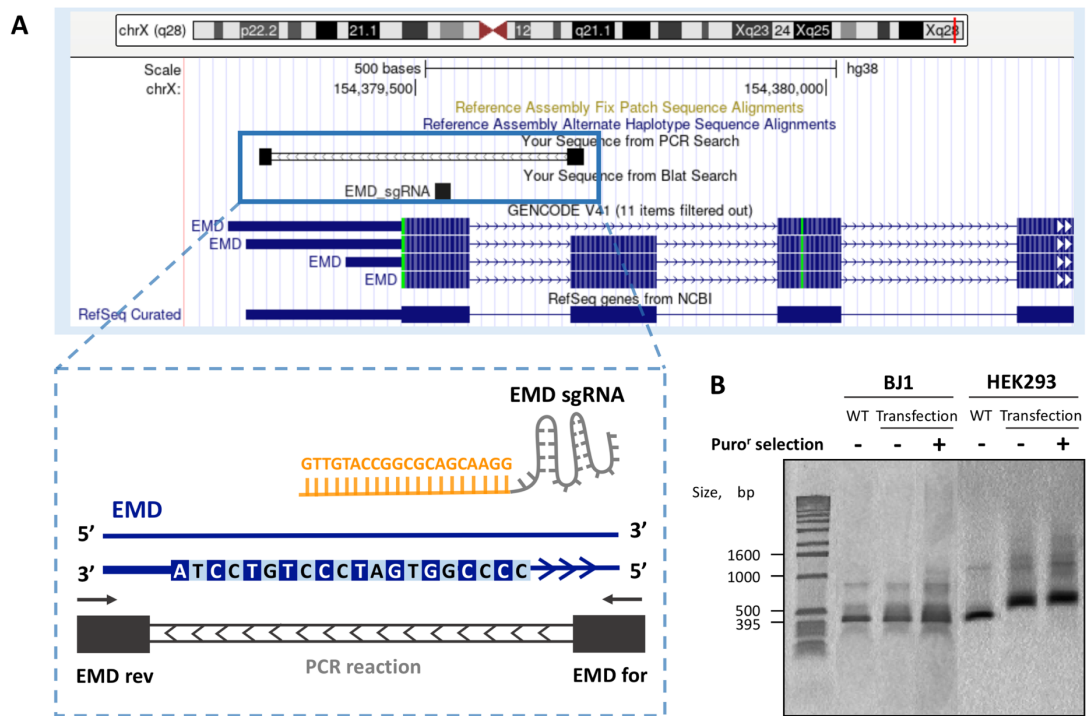
Figure 4-10. Targeted edition carrying gene knockout directly at the first exon of EMD locus. A) Designed sgRNA targeting EMD (labelled EMD_sgRNA), predicted localisation and PCR primer used to identifies DNA cut sites B) Agarose gel of wild-type (non-transfected), transfected cells before and after Puromycin selection.

To further consolidate the CRISPRko library screening in BJ1 cells, the resultant of PCR amplification from genomic DNA at post-transfection followed by Sanger sequencing. The DNA sequences can be used to infer directly to the targeted genome loci that are being disrupted by the Cas9-sgRNA heteroduplex, the sequencing analysis revealed that in approximately 5% of transfected cells INDELs were introduced to the define cleavage site. While, 93% of transfections retained the original DNA sequence when they were cultured in normal media. The transfected cells were further selected in 5 µg/ml of Puromycin, the %INDELs of transfected population subsequently increased to 53±1% (n_{Bio}=2) after trypnising twice. Most impressively, the enrichment of selection by addition of the trypsinisation steps showed reasonably higher %INDELs at up to 65% after 4 rounds of passage in selection media. Figure 4-11 displays an assessment of CRISPRko in targeted location of endogenous EMD silencing, transfection efficiency and the results of Sanger sequencing.
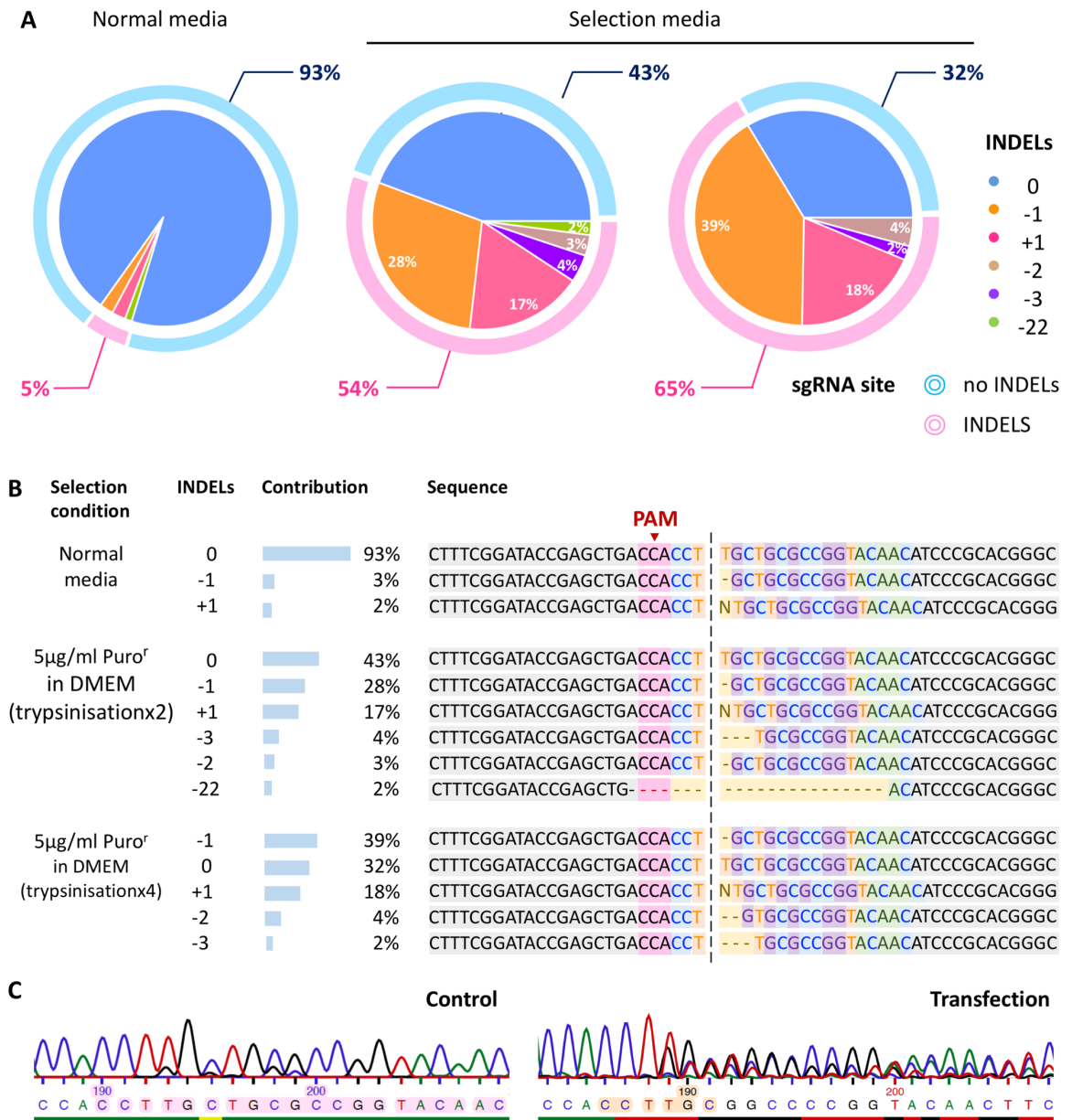
Figure 4-11. EMD gene harbouring a mutant knockout on-target editing in transfected BJ1-hTERT cells. A) The effect of CRISPR-introducing INDELs and divergent distribution of the sequence at editing EMD location between normal and Puromycin selection media. In selectable condition, 54% (left) and 65% (right) of INDELs occurs after 2 rounds and 4rounds of trypsinisation prior to culture the cells with normal media. B) Genomic sequences of CRISPRko-edited EMD site, colour labelling indicates the predicted PAM and 20-nt of sgRNA used in transfection. C) Chromatogram of DNA sequence alteration in mixture at post-transfection comparing between control (normal media) and transfection (obtained in selection media), colour box indicated where sgRNA is defined to target region. The Sanger sequencing results input was analysed by ICE detection, only first available of transfection in selection media (x2times), was shown and further processing the monoclonal selection (n_{Bio}=2).

Next, the assessment of CRISPR-induced mutation in HEK293 cell line was also examined at a similar location of the sgRNA-guided transfection (See Figure 4-12). Due to the innate characteristic of HEK293-easy to transfect classified cells, the successful transfected cells were appeared to 22% for facilitating sgRNA import and subsequent repairs, with a majority (14%) of a single base insertion (+1) at the targeted EMD site. Indeed, the cultured cells in supplemented-Puromycin growth media at 5 µg/ml, resulting INDELs at 81% after 2 cycles of trypsinisation.
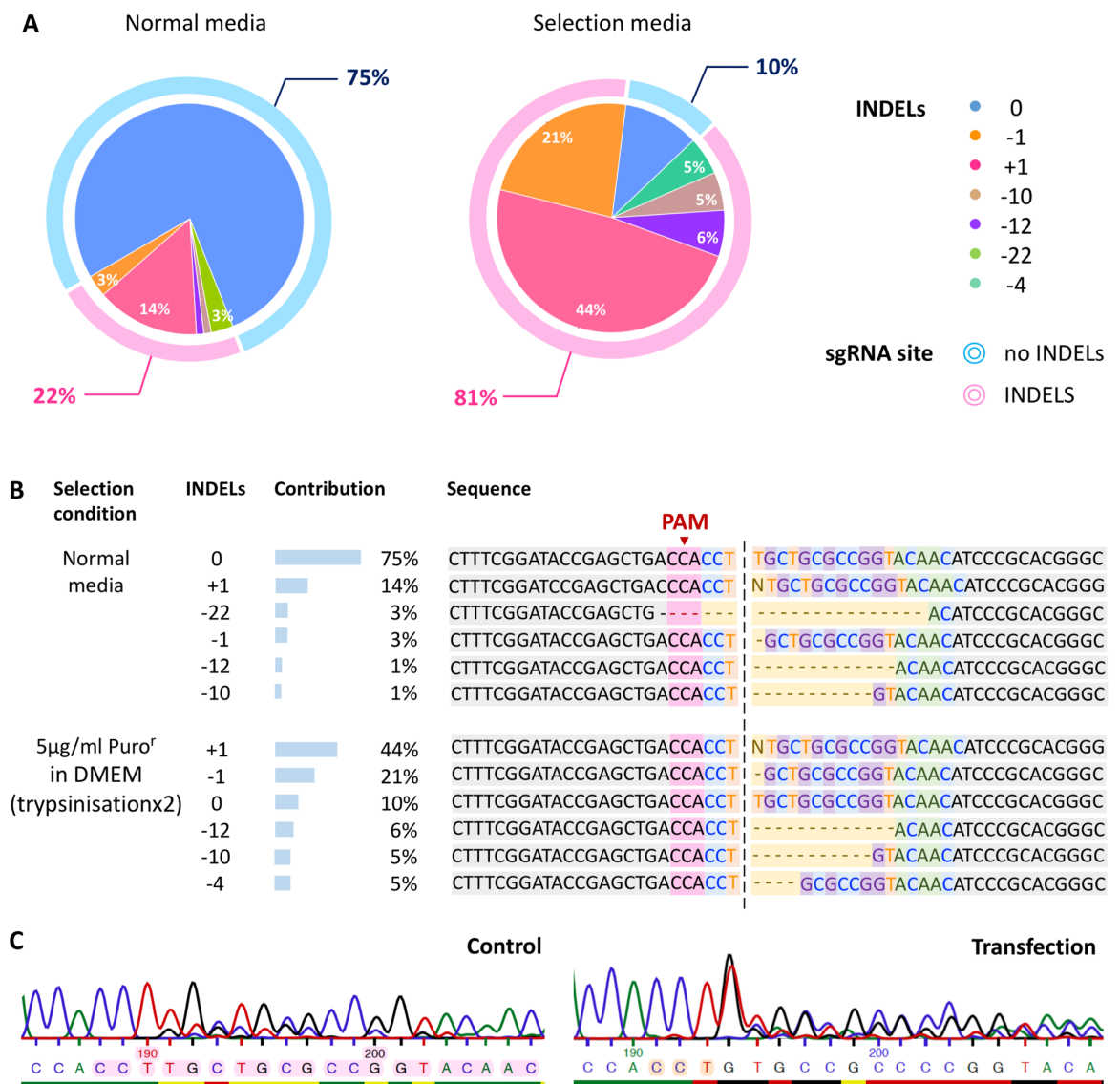
Figure 4-12. Characterisation of site-specific sequence diversity on-targeting EMD in HEK293cells at post-transfection via CRISPRko-Cas9 platform. A) Overview of INDELs observed with or without selection media. B) INDELs frequencies and sequences in normal cultured media and cell pools subjected to Puromycin-resistant cells. C) Mixed Sanger sequencing chromatogram exhibited a distinct sequence phenomenon after transfection.

91

In addition, the transfected HEK293 cell pools screening, observed that the more variants of genotypic alteration outcomes as a result from DNA repair.

4.3.6 Evaluation of the CRISPRko approach across AAVS1-based sgRNA

To validate an approach used to knockout functional expression that can flexible target almost any gene via reprogrammable sgRNA, a former sgRNA confers to part of intron1 of AAVS1 that used in complex with CRISPR knockdown in this chapter was repurposed to transfecting the BJ1 and HEK293 cells for comparison of the transfection efficiency and compatibility of the cells facilitate the other gene locus instead of targeted EMD region. A series of transfection set up by using Cas9-mRNA, pac and 320ng of AAVS1 sgRNA, causing alteration of the percentage of INDELs in BJ1-hTERT cells around 3% without selection media and 42% subjected to 5 μg/ml of Puromycin/DMEM media, respectively (as shown in Figure 4-13A).
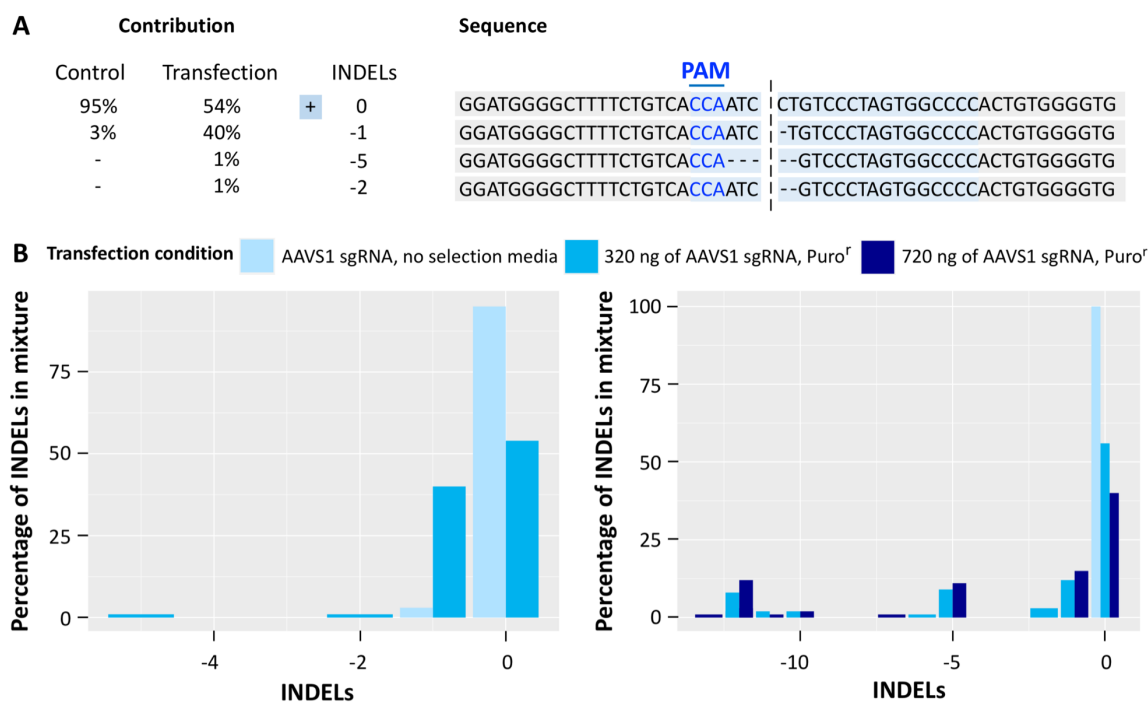
Figure 4-13. Detection of INDELs generated by CRISPRko via AAVS1-mediated sgRNA sequence. A) DNA sequencing confirms the cleavage DNA, generates point mutations (1 to 5bp deletion) within the sequence of AAVS1-sgRNA (Blue) in BJ1 cells. The contribution of transfected population was compared between transfection control and transfection with puromycin treatment. B) Alteration of AAVS1-sensitised cells to increased concentration of sgRNA delivery in BJ cell line (left) and HEK293 cells (right).

The enlarge scale in exploration of varying concentration of used sgRNA in BJ1 and the data for HEK293 cells is represented in Figure 4-13B, this indicates that the higher concentration of sgRNA used for transfection can improve the transfection efficiency.

It was observed that over one-sixth of transfected cells increased when doubled the concentration of sgRNA used in transfection to 720ng. The transfection efficiency from two different sgRNAs toward HEK293 cells was found that it is variable, with reduced efficiency from 81% to 61% compared to transfection targeting at the EMD region when using AAVS1-sgRNA at a similar ratio of Cas9-sgRNA complex for transfection.

4.3.7 Anticipated depletion of EMD expression at the protein levels

To examine the diversity of monoclonal selection, the transfected BJ1 cells with 54% of INDELs during Puromycin treatment was expanded and isolated by seeding at an average of 0.5 cells/well using 96-well plates ensures that cells derived from a single cell in all detected wells. DNA sequencing identifies clonal structure of EMD disruption in BJ1 cells (as shown in Figure 4-14), suggesting genetic homogeneity under clonal selection. The percentages of mutation in the mutated EMD loci was found at 83.3% (calculated from 5 out of 6 obtained clones), yields 4 clones with small INDELs (exert 1-4 base deletion or insertion) and an unexpected large (~100bp) deletion.

A series of single cell isolation was also performed in modified HEK293 cells, resulting mainly 'frame deletion' and only a single pure knockout clone with 12bp deletion was observed (namely 1D1). For 10 out of 11 clones, the cell pooled in frame deletion full sequences referred to the supplementary Figure A-4. For an example of graphic sequencing distribution in the mutated clonal-derived from HEK293 cells without the mixture of wild-type sequence remaining as shown in Figure 4-15A. In order to obtain more insight in the level of clonal heterogeneity, together with enrichment of clonal selection, the resultant clones with high percentage of ±1base editing from candidate clone 2D2 (See Figure 4-15B) was doubled-screening by seeding at 0.2 cells/well and confirmed by DNA sequencing.
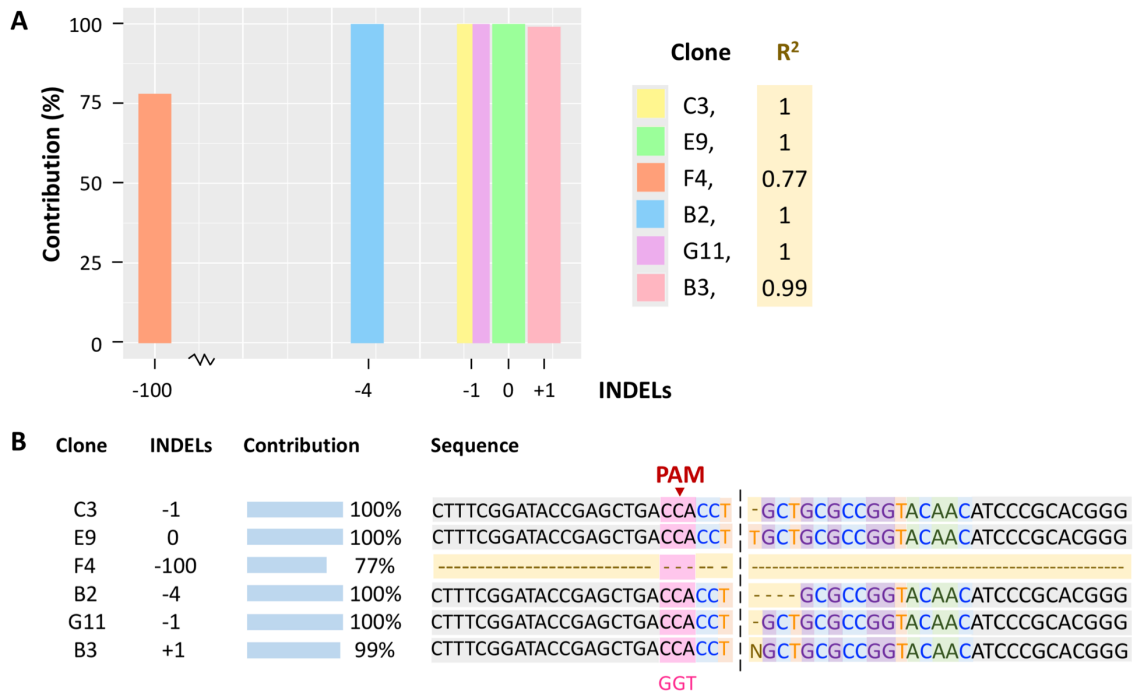
Figure 4-14. Sequence-based gene editing analysis of single cell-derived knockout clones at the EMD transcripts in BJ1 cells. A) Contribution of the genomic sequence similarity of each individual clone. B) Sanger sequencing of the anti-sense DNA strand from monoclonal knockout cells targeting EMD coding sequence. The colour base represents the define match localisation targeting by 20-nt sgRNA used in transfection with adjacent PAM – TGG (as indicated by an arrow).

The second identification of subclonal sequencing data revealed that a major (88-91%) of a single base insertion and minor (~7-10%) of point mutation with 4 base deletion, in all tested accordingly. For testing the inhibitory phenotypes, the clone 1D1 and subclone H5S were cultural expanded and extracted of the whole proteins with sheering the nucleus for westernblot analysis. Next, to examine the hypothesis that the EMD knockout mutants generating frameshift or even null mutation can completely inactivating the gene product. The experimental analysis in the protein expression level in CRISPR-editing BJ1 and HEK293-derived clones were examined by westernblot assay, the immunoblot identified clones exhibited that harboured INDELs-introducing at the EMD exonic sequence, leading a full depletion of Emerin expression.
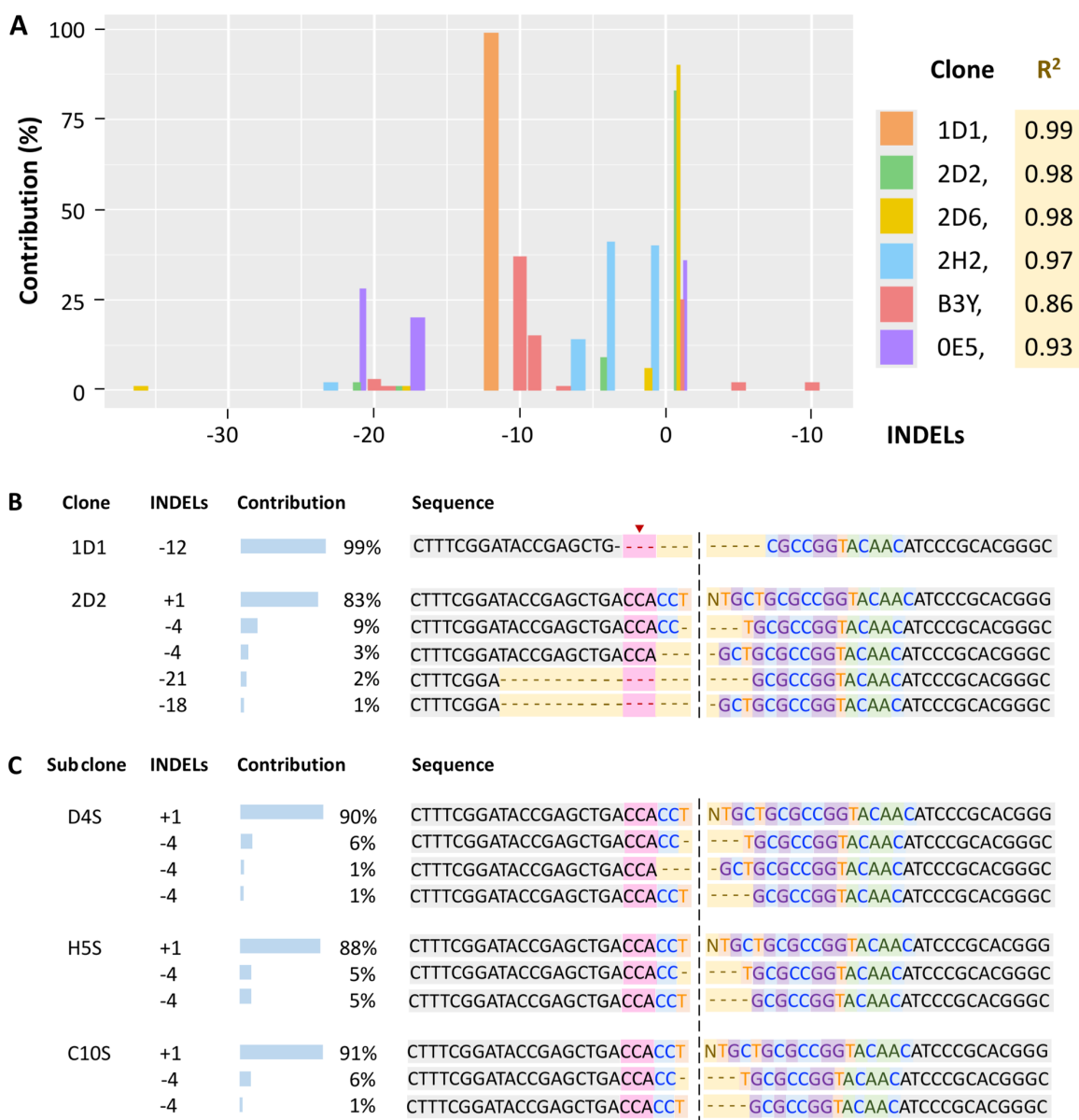
Figure 4-15. Heterogeneity and frequency of genomic sequences in mutated HEK293 cells, obtained frame-deletion in coding region of EMD gene. A) Mutation generated by CRISPRko after clonal selection. The sequencing background in B) Selected clones and C) Sub-clonal populations for further confirming the phenotypic loss-of-function. The red arrow and box highlighted the PAM site with colour box of 20 nt-guided by sgRNA at transfection.

With these CRISPR/Cas9 knockout models, the further test clarified the underling mechanism by which Emerin/EMD gene loss could reactivates the MAPK/ERK signalling pathways. Preliminarily data based on immunodetection established that activation of ERK phosphorylation was observed in the screened, confirmed EMD BJ1 cell knockout clones. While, knockout of EMD in HEK293 clones showed there was no detectable bands of pERK production in either wild-type or EMD knockout cells. Figure 4-16 westernblot analysis showed that the confirmation of EMD knockout with no visible bands reacted with primary anti-EMD MANEM10 (1H9) antibody in all tested clones, by measured the reactive protein production of Emerin. Thus, in turn to stimulates of pERK expression in BJ1 cells.
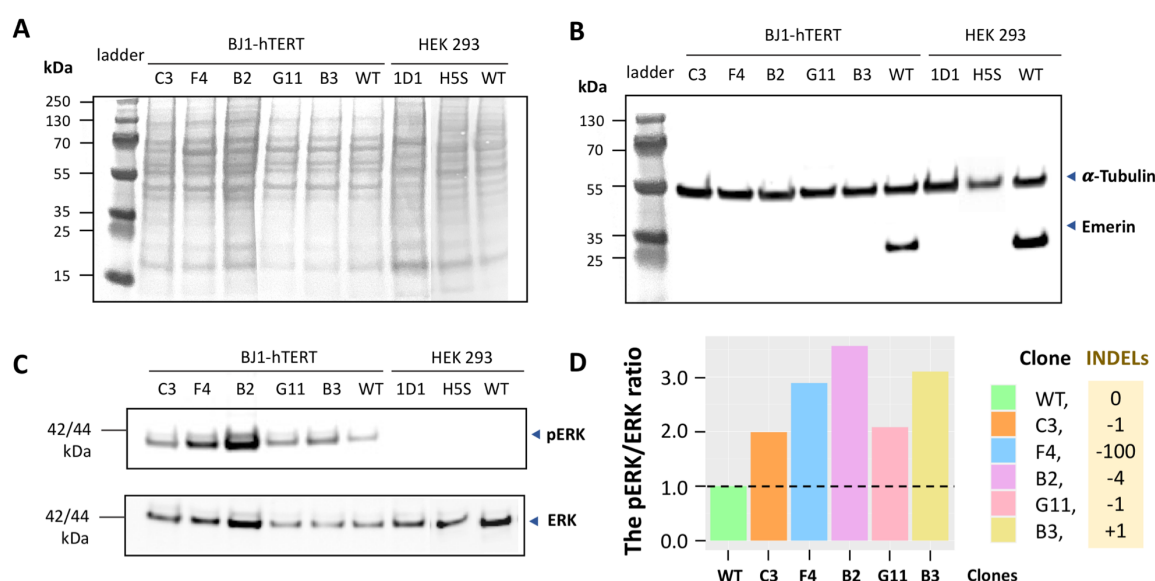
Figure 4-16. Disruption of EMD gene harbouring a frameshift-inducing deletion or insertion on target CRISPR knockout, effect on depletion of translated-Emerin protein (encoded by EMD gene). A) Total protein visualisation by Ponceau staining prior to westernblot assay. B) Immunospecific-labelling detection of clonal (C3, F4, B2, G11 and B3)-derived from BJ1 and clonal (1D1 and H5S)-derived from HEK293 cells, compared to positive control under normal expression in wild-type cells (WT). C) Westernblot analysis of pERK/ERK against knockout EMD cells D) The quantification of pERK/ERK ratio, a relative fold-change activation was represented and double normalisation with alpha-Tubulin and ponceau signals.

4.4 Discussion

Due to the rapid development of natural CRISPR molecules and engineering of its associated Cas proteins, offering a powerful and versatile approach for genome regulation, including alter transcription, create precise mutations or modified change in the epigenetic level that enable writing site-selective on the genome. In this work, CRISPR/Cas nuclease function-based platform was utilised to perturb the targeted EMD expression in human BJ1-hTERT and HEK293 cell-lines.

The proposed gene knockdown model using CRISPRi in HEK293 cells was successful, transfected into the AAVS1 locus, it generated INDELs at approximately 11% in cells pooled at 20 hours post-transfection with Cas9-sgRNA delivery system. The present targeting efficiency remained relative low, similar to other findings reported the transgene perception with transfection efficiency between 10% to 30% (Chu et al., 2015; Xu et al., 2018). While, some research groups have shown increased efficiency with improved delivery in polypeptides or organoids from nearly 50% up to 70% (Wang et al., 2018; Sun et al., 2021). In this study, uses the most common available transgene integration site with AAVS1-based delivery of the Cas9 complex due to their mild immune response and its ability to target non-dividing cells (Gaj et al., 2016). However, the gold standard 'hot spots' or genomic 'safe habours' loci for human transgene editing is highly demand that should ideally allow high and stable transcription-linked to expression level of targeted gene without disrupting genes and essential regulatory elements.

It is also ordinary to set up transfection without sgRNAs delivery for normalisation and validation of the target integration. The non-targeting sgRNAs, Cas9 mRNA and Cas9-based repressor (dCas9^{KRAB}) were transfected to HEK293 cells, resulting in 19% INDELs with no statistically significance. Many studies have informed extensive genome-wide off-target which may occur in the dCas9-binding events (Duan et., 2014; Kuscu et al., 2014; Polstein et al., 2015). These studies have shown the bound Cas9-sgRNA complex confirmed by ChIP sequencing and other supported assays with binding from tens to thousands at off-target sites, although most of the analysed complexes bind to the off-target sites with leaky affinity (Wu et al., 2014). The case by O'Geen et al (2015) & Wu et al. (2014), suggested that off-target binding events were largely due to the limited chromatin accessibility

of targeted regions. Of note, only a small subset of these off-target binding is generated by Cas9 cleavage. In agreement with the result from systematic digestion, Cas9 nuclease activity created a selective and site-specific cleavage as shown in Figure 4-6. Future work should use additional assays to determine how local chromatin or epigenetic status can affect genome target binding and regulatory activities within the transcribed DNA. For cloning steps, two sgRNAs were individually cloned into separate plasmid vectors as an alternative option for transfection. It is highly possible that the true on-target binding, could be enhanced when combining two different sgRNA hits per gene as a cut-off genomic region of interested, because it is unlikely that two sgRNAs targeting the same part of the genome would (with different sequence characteristics) share similarity of the off-target effects.

The repression assay with CRISPRi may be less effective due to its 'multi-component' systems that required packaging of the large protein, the gRNAs and all regulatory elements that control their inducible expression, especially affects transcriptional efficiency but not either mRNA or protein stability. The results from the drug selection screens, where only the cells with resistance to puromycin media condition survived resulted in twelve surviving clones that could be isolated. Out of seven tested clones three had both 5'/3' junctions PCR positive and could be confirmed by deep sequencing shown in Figure 4-8. The doxycycline (Dox) derivatives of Tetracycline (Tet) regulated inducible systems was added to measure the repression of target EMD gene and dCas9 expression via qRT-PCR. There were two clones which had high expression of dCas9 transcripts with an increase of nearly 90-fold in clone 10 and an activation of over 200-fold in clone 12. Likewise, levels of the target transcript in both clones were unaffected, levels of the EMD transcript decreased 1-fold and 2-fold after addition of 1 μg/ml of Dox for 24 hours, in clone 10 and 12, respectively. Of note, Dox-induced reactivation of reversible expression of EMD remained at similar levels as compared to wild-type after having been exposed to Dox for 72 hours in the knockdown-derived clone 12. As mentioned above, the inducible expression is under operation subjected to 1 μg/ml of Dox. In agreement with applied antibiotic Dox commonly uses at a concentration between 0.01 - 1 μg/ml (Randolph et al., 2017; Xia et al., 2008), described that it was sufficient to activate the Tet-inducible expression

system that alter cellular metabolism without detectable inhibitory affects or impairment of cell growth (Luger et al., 2018). Whereas, the expression level of targeted gene was no affected, suggesting that CRISPRi inefficiency occurred during the cell compensation or adaptation at post-transfection.

In line with experimental CRISPRi-based plasmid DNA delivery, it takes several weeks to obtain clonal resistance to selection media. By that time the CRISPRi plasmids that are critical regulate the repression systems may have been diluted out of the cells during division and thus have turned into already-present molecules regulating the annotated transcripts, mRNA and proteins for the target gene before the repression are measured. To improve their effective application, it is best suited to redesign the repression assay to minimise the time for the assessment to between 24-48 hours after transient transfection (Gilbert et., 2013). In addition, the regulatory elements of the CRISPR multi-components are approaching the packaging limit of the preferred AAVS1-based vectors such as the larger SpCas9 (Truong et al., 2015; Wright et al., 2015; Zetsche et al., 2015). These unfavourable conditions with a large size of plasmid to cognate promoter sequences, localisation signals, donor DNA or additional sgRNAs for gene perturbation, may cause the experiments become less effective when using CRISPRi in regulating human cell-lines.

For selection screens, it was decided to select the clone formation that survived in the selection growth media supplemented with Puromycin, followed by deep-sequencing analysis. This work was only carried out with transfected HEK293 cells which acquired 3 clones of junction PCR positive in both 5'/3'direction and validated by Sanger sequencing. The transfected BJ1 cells died without forming any colony; this observation was similar to a case reported by Sun et al. (2021), where no colony forming of human foetal lung cells after transfection with a CRISPRi complex could be observed. Due to the naturally resilient characteristics of the HEK293 cell line, which can form viable aggregates, is able to grow in suspension as well as attached (Jang et al., 2022; Malm et al., 2020). For this reason, the results from clonal screening is slightly speculated that the cell clumping of each clone generated from the variety of cell population in mixture (i.e. cell perceived donor plasmid in 5'/3' direction from a different cell, cell

adapted to Puromycin-resistance contains a wild-type like outcome). Some researchers suggested that the selection criteria used for screening could be associated with certain promoting cell surface markers that are either positive or negative for cell adhesion and survival (Cong et al.; Parnas et al., 2015). A potential technique to actively select expressing cells would be fluorescence activated cell sorting (FACS).

Moving forward to the CRISPRko approach where complete loss of function mutations are the desired outcome – here the desired CRISPR effect is directed at the coding sequence of the target gene to permanently silence it. As the usage of short and fast action of transfection and Puromycin selection that was completed within 2 days, this improved the recovery of transfected cells at post-transfection delivery with sgRNA-Cas9 complex and pac gene. Although both gene amplification and increased stringency of selection allowed the identification of mutations that occurred by INDELs, the transfection efficiency varied depending on the sgRNA and cell types used as well as the structure of the target site (Shi et al., 2015). In this study, the creation of effective sgRNAs with their desired effect being to disrupt as much of the EMD expression as possible ideally by instigating a frameshift mutation targeting an early exon where PAM cleavage sites can be targeted. The DNA sequencing results show that the sgRNAs generated detectable ranges of INDELs from 5% to 54%, in normal and selection media followed up with trypinisation twice in BJ1-hTERT cells. Compared to the transfected cells with the same tested sgRNAs and conditions, the percentage of INDELs displayed at 52-54% (n_{Bio}=2), 81% and 91% in all screened of BJ1, HEK293 and MCF-7 cells, respectively. Next, the addition of trypsinisation cycles into cell pooled after a prolonged period of growth in puromycin selection media, showed cells enriched for mutants to over ~10%. The full rate of transfection efficiency leaned towards three; represented human cell-lines can be found summarised in Table A-1 in the appendix. A case study by Caputo et al. (2021), supported the stably transfected HEK293 cells from pac-derived mutants with the higher secretion of a soluble and recombinant target protein by 3-fold increased levels and productivity. Using CRISPRko strategy with beneficial features in this study, have impacted to achieve the high transfection efficiency above average. Compared with the CRISPR/Cas9 complex induced INDEL mutations with typical success range of between 16% to

58% via NHEJ and 7.4% to 27.8% via HDR-repair mechanisms was also found by others (Cristea et al., 2013; Ramakrishna et al., 2014; Lee et al., 2015). A case study by Ranjbar (2022), observed that transfection efficiency reached around 30% in HEK293T cells with guide RNAs targeting to knockout the ß2-microglobulin (B2M) gene, which was confirmed by measuring the number of (co-transfected) eGFP expressing cells.

This work underscores the importance of functional screens to characterise the complete EMD knockout clones for studying the phenotypic changes of its co-worker. The knockout candidates with a sign of editing from INDELs in their DNA sequences were selected to be confirmed by IF and westernblot analysis. Although, the CRISPR/Cas9 knockout yielded multiple unique mutants (e.g. with small and large INDELs) in both BJ1 and HEK293 cells, westernblot results confirmed that no expression of emerin (protein encoded by EMD gene) in all tested clones see Figure 4-16.

In this chapter, two different techniques to repress/eliminate EMD regulation via CRISPRi and CRISPRko models were purposed and serves as an option resource for loss of function assay tailored in human cell study, represented in the presenting BJ1 and HEK293 cells. Partial and reversible effects from CRISPRi system have shown less effective. However, it is especially useful for studying essential gene functions which cannot be done with knockout approach due to permanently and completely deletion of genes causes a lethal damage to the cell and prevent most functional assays.

The advance of current technologies has been the production of highly specific genome modifications with excellent efficiency and precisely than ever before. The results as stated above in this study, have shown that the enrichment steps include the increase of selecting steps and concentration of drug selectable marker can effectively improve the selection of successful transfected cells up to 100% regardless with transfection efficiency. Nevertheless, it is still importance to underline the transfection efficiency as it can represent the effectiveness of CRISPR tools, especially partially loss of function using CRISPRi. There are several ways to improve the transfection delivery that have proposed elsewhere. One

avenue to upgrade with transfection yields, a case reported by Zuris et al. (2015), adapted cationic lipid transfection reagents compatible with the most favourable form of anionic Cas9-sgRNA complex. This method allowed gene activation/repression of up to 80% in cultured cells compared to other finding from 40%-60% reduction using CRISPRi (Li et al., 2020; MacLeod et al., 2019; Ran et al., 2015). Furthermore, the trade-off in efficiency should still gain the awareness, several practical concerns arise in relationship between cleavage efficiency (on-target binding) and specificity (off-target binding). At high concentration of the Cas9-sgRNA complex, identified more detectable off-target binding events (Pattanayak et al., 2013). It is needed to call for cautions of the ratio between Cas9 and sgRNA in transfection. Our work displayed that the increase of Cas9-sgRNA complex concentration enhanced transfection efficiency (as shown in Figure 4-13). Similar to the many studies such as Fu et al (2013) & Hsu et al. (2013) that lowering the concentration of Cas9-sgRNA complex illustrated less number of off-target effects and efficiency.

Regarding to the CRISPR/Cas9 technique is such a powerful method owing to its several advantages across other strategies. While, some limitation is still challenging and need more efforts to address. The simplicity and predictability of CRISPR system provides a host-independent platform for site-selective and transformed from complicated protein engineering problem to a RNA-guided coding problem, instantly making CRISPR a robust and more reliable tool for genome engineering researches. Examples of programmable genome editing machine include zinc-finger nucleases (ZFNs) and transcription activator-like effector nucleases (TALENs) in which construction of protein-DNA interactions are comprehensive complex to build for each of the unique sites (Garg et al., 2012; Sanjana et al., 2012). In comparison between targetable nuclease platform regarding to their recognition site, the CRISPR/Cas system is determined by single-base pairing whereas, the ZFNs/TALENs recognise different 1-bp or 3-bp per module with protein engineering at target is needed (Carroll, 2014). Alternatively, RNAi provides a convenient approach but it is limited to transcripts (Kim and Rossi, 2008), whereas CRISPR can design to target elements across the entire genome including promoters, enhancer, introns or directly at exons (Larson et al., 2013). However, the successful CRISPR is varying depend on PAM targeting site and

specificity. The requirement for an NGG triplets of PAM sequences limits the availability of target site and its recognition determine the target interference (Jiang et al., 2013). The targeting specificity is determined by RNA chimera and the target DNA which recognised by 14-nt long region for spacer acquisition and can lead to off-target effects (Carroll, 2014).

4.5   Conclusion

Cells reside in a complex and dynamic microenvironment. This chapter mainly focuses on manipulating internally generated force inside the nucleus via the nuclear actin-binding protein, emerin which directs cell behaviours. CRISPR knockout clones of emerin were successfully generated to study the role of emerin which represented lowering mechanical properties of the cell microenvironment. These knockout cell models, open the window to test the functional consequences of loss-of-function in the emerin-null cells through mechanical links of emerin to nuclear regulation regarding cytoskeletal and nucleoskeletal reorganisation activated transcription factors, and chromatin remodelling via histone deacetylase 3 (HDAC3) activity (referred to chapter 5).

CHAPTER 5 THE MECHANICS OF EMERIN-NULL CELLS

5.1 Introduction

Every living cell receives physical signals (e.g. forces generated by cytoskeletal protein complexes, mechanical stimulation) from its microenvironment. The activated force-generation machinery of the cells is then transduced into biological signals in a process known as mechanotransduction (Goult et al., 2022). Much of this mechanotransduction is achieved by mechanical linkages functioning via force transmission between the cytoskeleton and nucleus that impact cell behaviours (Gautel, 2011; Goult et al., 2018; Margadant et al., 2011).

The nucleus is not only a destination hub for signalling cascades, its nuclear envelope (NE), which establishes as a shielding barrier and separation between nuclear and cytoplasmic compartments, has also been attributed to be a sensory element, and therefore its direct mechanical coupling to the cell architecture and across the plasma membrane to the extracellular matrix (ECM) is important (Uzer et al., 2016). The linker of nucleoskeleton and cytoskeleton (LINC) complexes that bridges between the inside of the nucleus and the cytoskeleton both provides mechanical integration of nucleus into the cell (Mika and Rost, 2005) and connects to extracellular mechanical environment (Sastry and Burridge, 2000). The LINC complexes, forms a robust meshwork of protein-protein interactions that couples the nuclear lamina to the cytoskeleton (Stroud, 2018). One integral protein, emerin is a functionally important binding partner of the LINC that localises predominantly at the inner membrane of the NE (Manilal et al., 1996). In this chapter, the reprogramming of the nuclear mechanical properties was the focus – ideally disturbing the balance between stiffness and deformability. Although, the loss of emerin expression may reduce the nuclear stiffness, an isotropic force guiding the cell-nucleus alignment is provided by the change in cell shape induced by placement of the cells on Fn-coated microgrooved substrates.

Emerin is an actin capping protein and promotes accelerated actin polymerisation (Holaska et al., 2014). Under low mechanical force, the emerin knockout cells were generated in the chapter 4 to withdraw expression of emerin in cell microenvironment. The role of emerin was then investigated using emerin-null

cells to establish how this protein is involved in the organisation of the intracellular cytoskeletal network. The gene activities in the cells that lacked emerin was observed in relation to their response in their expression levels or even direct controlling gene accessibility to heterochromatin via HDAC3 and action of transcriptional regulators via Rho-A dependent manner. Next, the preliminary results have shown the activation of phospho-ERK expression in emerin knockout clones from BJ1-hTERT (as shown in Figure 4-16), similar to stimulated pERK signals in emerin-knockdown HeLa or C2C12 cells (Muchir et al., 2009). These observation lead to the hypothesis looked at in this chapter of this study, that depletion of emerin may influence nuclear stiffness, and thus could promote pERK causing hyperproliferation.

For aspect of study the response of emerin-depleted cells to external challenges see graphic overview of hypothesis and scope of experimental testing (see Figure 5-1), the screening of gene/protein expression is in line with the following;

I, emerin binding proteins that directly interact with lamins and a conserved chromatin protein (BAF) was detected to be present and forming a major component of the NE-associated nucleoskeleton, also known as the nuclear lamina (Dechat et al., 2008).

II, two classes of transcriptional coactivators, myocardin family of proteins and ternary complex factors (TCFs), which are major regulator of several gene encoding components of the actin cytoskeleton through the canonical serum responsive factor (SRF)-dependent activity.

III, ERK in cell motility and shape via the classically dynamic of actin polymerisation, activating Rho GTPases by phosphorylation on ERK.
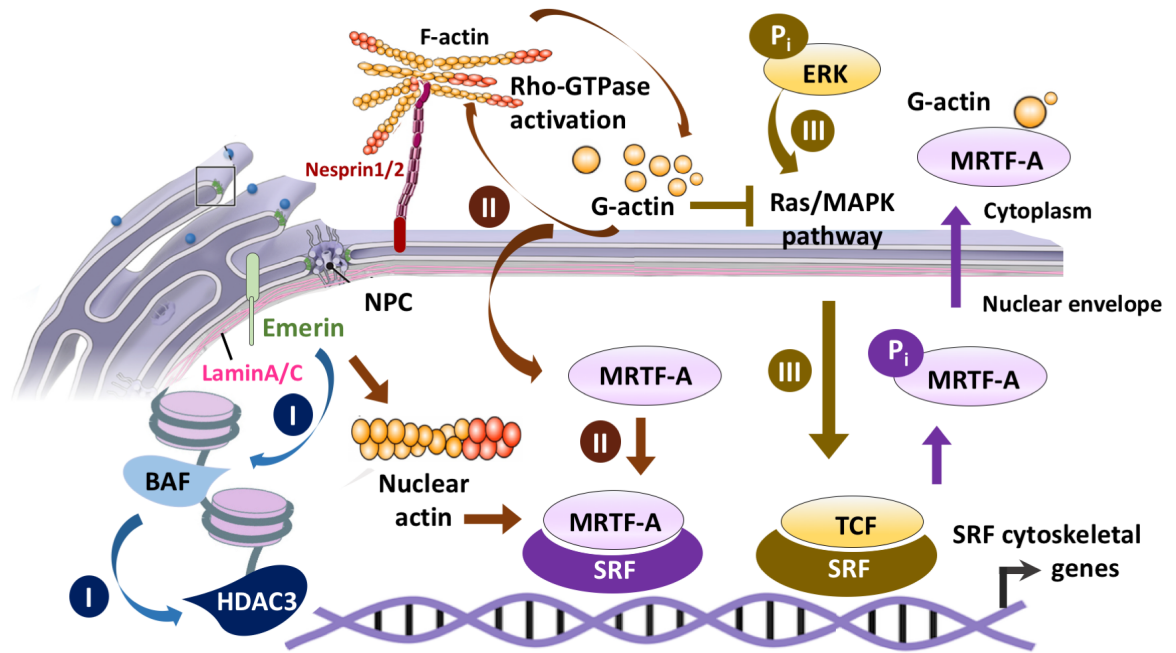
Figure 5-1. Proposed scope of the study of mechanisms for how cell nucleus could respond to emerin-depleted signalling, particularly underlies the direct binding complexes of protein-interacting to emerin and cytoskeletal organisation via RhoA dependent manner. (relative position of components to underline connections, not physical location) Three molecular paths were categorised to discover whether emerin could interact with multiple genes and transcription regulators implies that it might alter their transcription activity, and further lead to cell behaviour including cell growth, morphology and proliferation or migration. The signalling route of study in emerin association as the following; I, a network of nuclear protein-protein interactions in both nuclear lamin (mainly focus on laminA/C) and the indirect link to chromatin with LEM domain proteins via binding of barrier to autointegration factor (BAF), which could provide contact network to the histone modification enzyme histone deacetylase 3 (HDAC3). II, manipulating the nuclear force via emerin deletion on geometric topography affect nuclear actin which can modulate dynamic export between monomeric-polymeric actin and influence on translocation of the transcriptional regulator MRTF-A (also known as MKL1). III, disrupted force acting inside the nucleus via emerin could activate the ERK/MAPK signalling, and reinforce their transcriptional activity switch from activation of MRTF-A/SRF to alternative activation of TCF/SRF activity, thereby promoting MRTF-A phosphorylation and attenuating its interaction with pairing to actin driven nuclear export. For further abbreviation; NPC, nuclear pore complex illustrating the selective channel for permeability barrier between the nucleus and cytoplasm. P_i, displayed refer to site of phosphorylation where its binding was promoted as a consequence of phosphorylated signalling (adapted from Gau and Roy, 2018; Kirby and Lammerding, 2018; Stroud, 2018).

The ultimate goal of this chapter is to present a mechanical view of the cells under low mechanical force via emerin knockout cells where the assembled emerin binding complexes working together represent a mechanosensitive network of nucleoskeletal protein emerin to mechanical switches for cellular function including:

I, reorganisation of emerin binding partner complex (i.e. laminA/C and BAF) and contribute to altering histone acetylation via assessing of HDAC3.

II, nuclear translocation of the actin-regulated MRTF-A, which is a crucial regulator of mechanosensitive transcription factor and influences cell contractility and proliferation.

III, mechanosignalling associated with the transcription factor under equilibrium. In the absence of emerin and low tension, is there an alternative to switch on the activated stage of other transcription factors for compensation?

5.2   Materials and Methods

5.2.1 Materials

List of Reagents
Real-time PCR analysis Custom DNA oligos .... Sigma-Aldrich
Immunofluorescence & westernblot assay Alpha tubulin polyclonal antibody .... Proteintech Mouse monoclonal anti-EMD antibody (1H9) .... DSHB, University of Iowa Phospho-p44/42 MAPK (Erk1/2) (Thr202/Tyr204) Mouse mAb .... Cell signalling P44/42 MAPK (Erk1/2) (3A7) Mouse mAb .... Cell signalling Rabbit polyclonal anti-Mkl1/MRTFA antibody .... Abcam Recombinant Anti-Lamin A + Lamin C antibody .... Abcam

5.2.2 Immunofluorescence staining

The BJ1-hTERT and HEK293 cells were seeded at 5,000 cells/well in 24 well fibronectin (Fn)-coated plastic culture and 13mm of PDMS non-/patterning PDMS Fn-coated area for 2 days. Next, the cells were fixed, permeabilised and stained with primary anti-EMD (1:50) or anti-MRTF-A (1:100) in conjugation with

Phalloidin-Rhodamine (1:100) followed by secondary antibodies specific staining and DAPI to visualise the nuclear composition. For the full protocol see the detail in section 2.2.4.

5.2.3 Real-time PCR assay targeting MAPRK/ERK signalling pathway

The 3.0×10^4 of BJ1-hTERT cells or 1.5×10^4 cells of HEK293 seeded on plastic, PDMS (non-/pre-patterning with 12.5μm repeated 5μm deep) Fn-coated surfaces, 7days prior to RNA extraction. The RNA isolation, cDNA synthesis and qRT-PCR techniques were explained in chapter 2 (See section 2.2.6). To target expression of nuclear associated protein and MAPK/ERK pathway linked emerin-deficient cells, primers used as shown in table 5-1.

Table 5-1. Primer used to study the relative gene expression in emerin-KO cells via the nuclear associated protein and MAPK/ERK pathway.

Oligo Name	Length	MW	Tm°	GC (%)	Sequence (5'-3')
Banf1_For	20	6053	67.8	55	CTTTCAGCCATTCCCGGAAG
Banf1_Rev	20	6244	66.3	55	CTGGCTGGGATTGGTGAAGT
Elk-1_For	18	5364	65.2	61.1	CACCAGTCCAAGCCCCTT
Elk-1_Rev	20	5933	65.9	55	CCGCAACTTCCAACTCTTCC
Elk-3_For	19	5869	65.2	57.8	CAGACTGGGGATTGGCACT
Elk-3_Rev	20	6099	65.9	50	TGGATTGCTTCTGACTCCGA
Elk-4_For	20	6237	65.4	50	TTTTGCAGGCAGAAGAGGTG
Elk-4_Rev	20	5988	65.6	50	TCAATCCTGCCCACTGTCAT
GAPDH_For	20	6253	66.3	55	AGGCAGGGATGATGTTCTGG
GAPDH_Rev	19	5718	63.5	57.8	GCACCACCAACTGCTTAGC
HDAC3_For	20	6084	65.1	55	CCTCGGGTGCTCTACATTGA
HDAC3_Rev	20	6182	61.8	55	GGGCACGTTCAGACAGTAGT
LMNA_For	20	6253	65.4	55	GGGTGAACTTTGGTGGGAAC
LMNA_Rev	20	6367	66.6	60	TGGAGGAGGTGGATGAGGAG
MAPK1_For	20	6047	63.8	60	CCTACTGCCAGAGAACCCTG
MAPK1_Rev	20	6170	61.6	50	GCTGAGGTGTTGTGTCTTCA
MAPK3_For	20	6071	63.3	55	GATCCTGAGCATGACCACAC
MAPK3_Rev	20	6133	64.2	55	ATCCAGGTAGTGCTTGCCAG
RPL13A_For	22	6726	69.8	54.6	CTCAAGGTGTTTGACGGCATCC
RPL13A_Rev	22	6655	67.5	54.6	TACTTCCAGCCAACCTCGTGAG

5.2.4 Immunospecific westernblot assay

The proteins were isolated and immunoblotted for specific antibodies: anti-EMD (1:130), anti-ERK (1:2000), anti-pERK (1:2000), anti-Lmna (1:5000), anti-MRTF-A (1:800) and anti-Tubulin (1:2000) was used as an internal control (See section 2.2.7).

5.3   Results

5.3.1 Genotypic background with translated protein in emerin mutants

Two EMD mutant lines in each of the CRISPRko models from transfected BJ1 and HEK293 cells were selected for studying the effect and adaptation of cell in response to the environmental in the absent of functional emerin expression.

Firstly, two CRISPR knockout-derived mutants from BJ1 cells, one with a 1-bp deletion (clone named C3) and another with 4-bp deletion (knockout EMD clone B2) in the DNA-binding domain of EMD gene at the first exon generating a frameshift mutation, resulting in the loss of emerin expression confirmed by Sanger sequencing (Figure 4-13) and westernblot analysis (Figure 4-15). Prior to moving forward with these two selected knockout clones, the peptide array analysis (as shown in Figure 5-2) was performed as a double-screening in line with the mutant sequences.
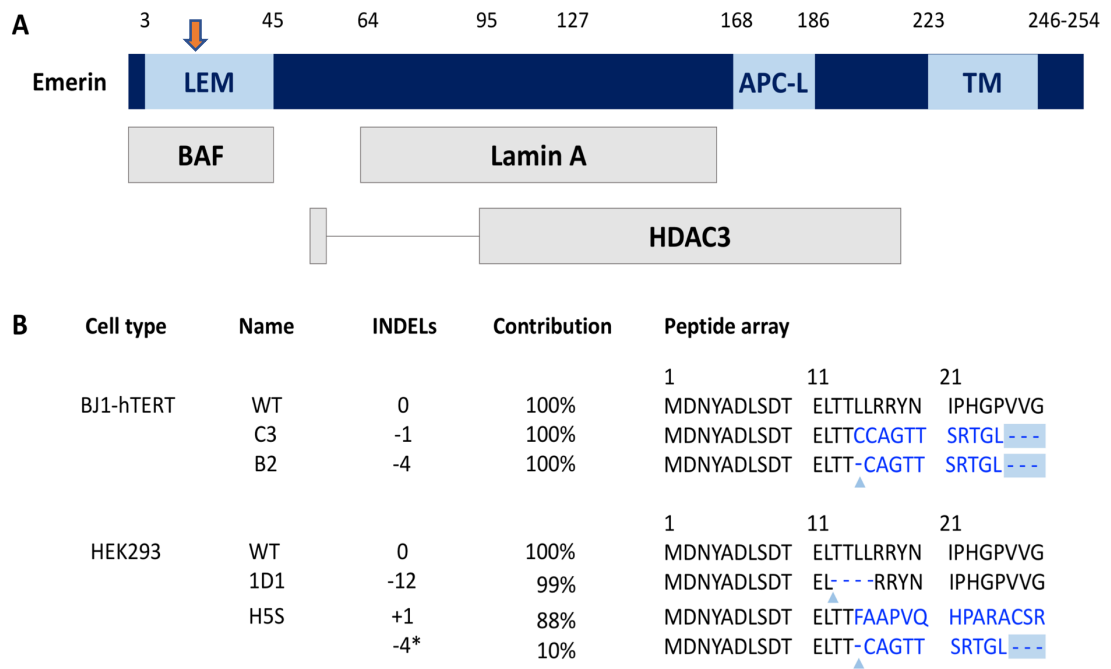
Figure 5-2. Polypeptide mapping and array of human emerin. A) Localisation of emerin binding partners (BAF, LaminA and HDAC3) binding motif where the specific residues interact to emerin polypeptides consisted of LEM-domain (LEM), APC-like domain (APC-L) and transmembrane domain (TM) (Adapted from Berk et al., 2014); approximate position at which deletion starts indicated by orange arrow. B) Amino acid sequences alignment of wild-type (WT) human emerin and mutant clones (i.e. C3 & B2 for BJ1-hTERT and 1D1 & H5S for HEK293) undergoes post-translational modification. The light blue arrow indicates the cleavage site during CRISPRko edition, causing INDELs and initiated a pre-matured stop codon. -; 'Deletion', *; pulled from 2-distinct genomic sequences that resulting in a similarity at protein translational level.

Interestingly, both mutant of EMD gene with a frameshift lead to a premature stop codon at residue 26 wherein the disrupted location served for LEM-domain binding. Next, the validation in the protein translation of the expressed transcript from HEK293 mutants, suggests an 'In-frame deletion' and a 'frameshift mutation', tested in clone 1D1 and H5S, respectively. For detailed deep sequencing and westernblot detection as shown in Figure 4-14 & 4-15, clone 1D1 with 12-bp deletion and clone H5S introducing +1 and -4 frameshifts that alter the reading frames encode emerin expression.

5.3.2 Emerin null immortalised fibroblasts in nuclear content

To characterise the loss of emerin in knockout clones and access the nuclear shape quality and quantitatively. The cells were grown on tissue culture plastic for 2 days before fixing, followed by immunospecific labelling with primary mouse anti-EMD, green fluorescent secondary, in conjugation with rhodamine phalloidin and DAPI staining as detailed in Chapter 2. The results from IF staining analysis exhibited that normal expressed emerin in wild-type BJ1-hTERT cells, mainly localised inside the nucleus. The emerin knockout (EMD^{KO})-derived clone C3 and B2 in BJ1 cells displayed that there was no detectable fluorescent signal of emerin staining which confirmed the cells complete absence of emerin expression as shown in Figure 5-3. The EMD^{KO} BJ1 cells retained their normal cellular and nuclear shape in either C3 clone or B2 clone. DNA content analysis by DAPI stains revealed that EMD^{KO}-C3 clone had two mainly distribution of DNA intensity proportion in the cells that bind in stoichiometric manner, similar to wild-type cells. However, the EMD^{KO}-B2 clone had a significantly one peak of DAPI fluorescent signalling at a higher intensity nearly 200 units (See Figure 5-3B). To simplify the measurement of how rapidly that the cells in the absence of emerin can be divided, the result from DNA stain showed that the role of emerin was involved in nuclear assembly and cell cycle progression. It was a clear evident that the cells lack of emerin caused a delay of cell-nuclear division. Whether two nuclear characteristic exist in this experiment, further study via assay with prolonged timeframe observation or live imaging would contribute to a more precise nuclear regulation and potential mechanism to bridge this knowledge gap.
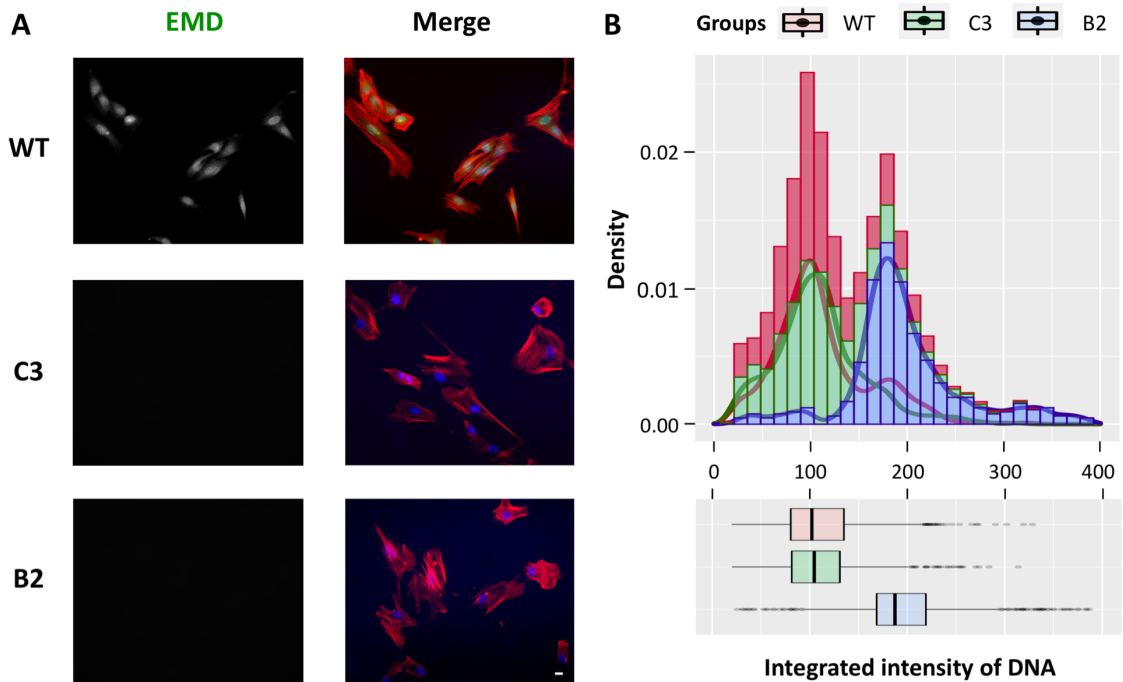
Figure 5-3. Depleted expression of emerin in BJ1-hTERT cells and association of nuclear DNA replication. A) Localisation of wild-type expressed emerin in BJ1 cell-line at fixed on Day 2 on tissue culture plastic and stained by immunofluorescence using anti-EMD antibody and no detectable fluorescent signals in either mutant cell line (clone name; C3 and B2), the overlay fluorescent channel (as shown in the right panel) for the nucleus (stained by DAPI, in blue), actin (appeared in Rhodamine-phalloidin - Red) and EMD signal (green). Scale bar ~20μm, n_{Bio}=3. **B)** Quantification and distribution of nuclear intensities, measured by DAPI staining the DNA bind the dye stoichiometrically, and thus visualised the amount of DNA present in each cell. The frequency of integrated intensity of DNA displayed 2-peaks for wild-type (WT) and clone C3, while only a relevant peak occurs in clone B2.

5.3.3 Regulation of nuclear shapes in EMD KO mutants of fibroblasts on grooves

It is known that nuclear function is integrated with alteration of its morphology during cell cycle which in turn reflects on genome size, duplication state or ploidy and life span (Deolal and Mishra, 2021). Here I opted to quantify how the changes in nuclear size and shape contribute to this phenomenon by determining how nuclear shape fluctuations are cell cycle dependent. In this system, the nuclear shape of each single cell was analysed in fixed cells at day 2 of culture, followed by IF staining for different markers. Two key parameters i.e. spreading area and aspect ratio of the nucleus were used to define nuclear size and shape to

establishing nuclear deformation and rigidity in response to the absence of emerin and with or without topographic patterning.

Upon observation of EMD knockout clones, the nuclear area was shown to increase in cells lacking emerin and microtopography. Figure 5-4 displayed nuclear architecture and coverage area of spreading of cells grown on flat or patterned materials with EMD disrupted cells compared to wild-type.

In order to compute the difference of area of the nucleus toward cells alignment on groove compared to their relative nuclear area on flat attachment, a simple mathematic equation was used to describe the portion of which are change carrying out along grooves compared to flat due to loss of emerin synthesis. For the degree of changes in spreading area are given to their relative contributions as follow;

$$\Delta A = \frac{Ao(Groove) - Ao(Flat)}{Ao(Flat)}$$

The overlapping area between flat and groove islands was cropped by estimated middle quartile to explain the nuclear enlargement of spreading along the grooved surface represented as ΔA for is the nuclear surface to area expansion. To account the best possible of estimated area, the average of nuclear size located at the lower and upper quartile of spreading area when $A_{O(Groove)} > A_{O(Flat)}$. The $A_{O(Groove)}$ is variable of wild-type and EMD mutants compared with a constant of $A_{O(Flat)}$ where is a coverage of area of the nucleus in wild-type group on flat surface adhesion. Table 5-2 summarises the representative nuclear area of emerin-deficient cells on microgroove attachment and size distribution in lower and upper quartile toward wild-type growth. The effect of emerin-disrupted BJ1 cells on grooves had significantly enlarged nuclear areas were 22±4.8% and 31±5.5%, in C3 and B2 knockout derivatives, respectively.
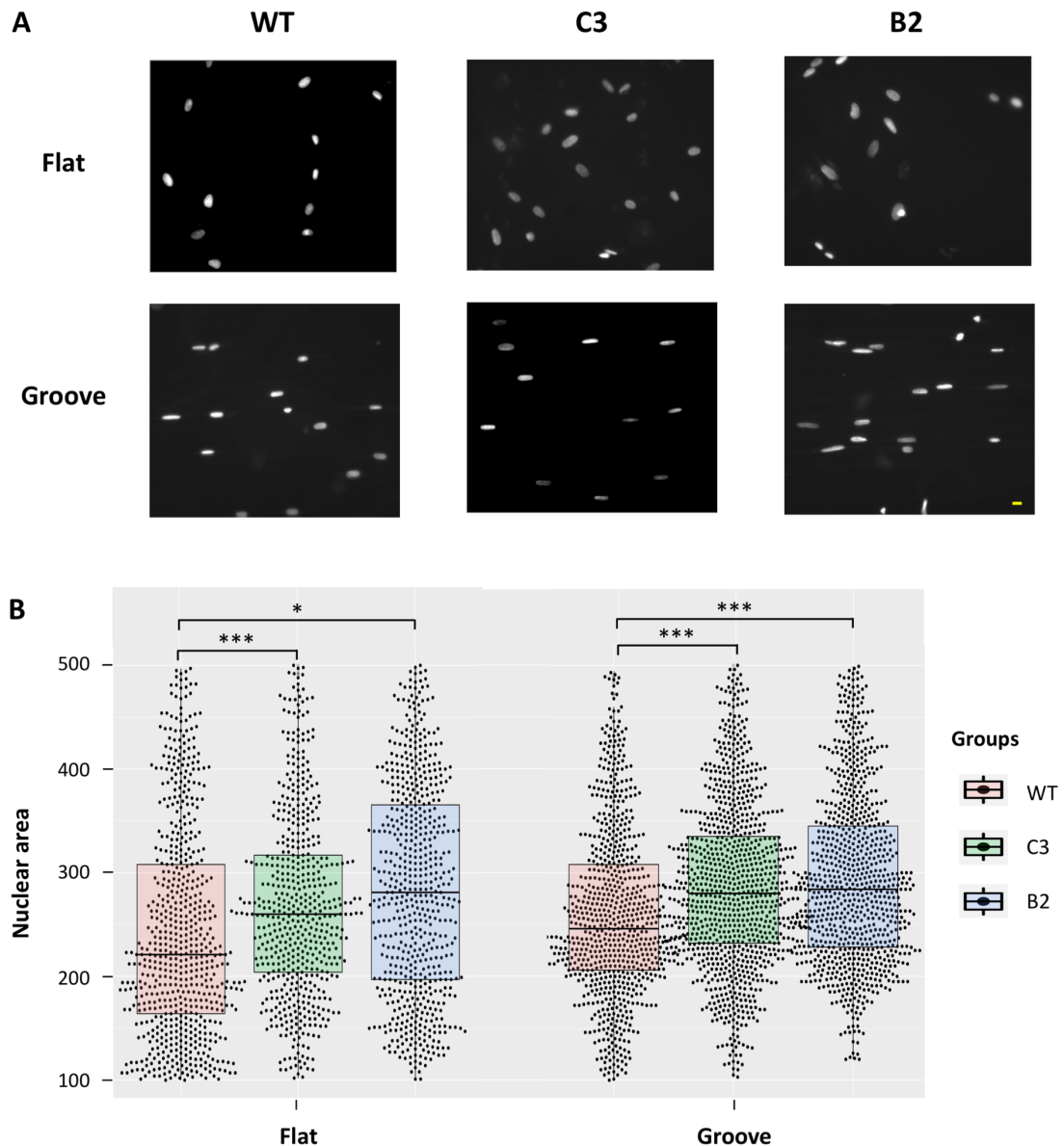
Figure 5-4. The nuclear morphology and their relative physical area of hTERT-immortalised fibroblast cells that were grown on two surfaces comparing between adhesive non-patterned (flat) and micropatterned (12.5μm groove). A) The microscale of cell nucleus expressing EMD in their normal level in the wild-type (WT) and completely lack of the EMD signal in the clone C3 and B2, observed in BJ1 model that fluorescently labelled of the nucleus by DAPI. The nucleus is maintained their shape in normality which are unaffected as a consequence of the EMD disruption. Scale bar ~20μm. B) EMD mutants influence nuclear surface area extension, the spreading area of nucleus was significantly increased in all tested groups compared to wild-type. Three separate experiments with the range of N_{cells}= 485-735 cells/replicate of cell imaging were analysed and indicated where is statistically difference; *p<0.05, **p<0.01 and ***p<0.001. Welche's T-test, n_{Bio} = 3.

Table 5-2. The spreading area of nucleus in emerin null hTERT-BJ1 cells on grooves compared with wild-type on non-/patterned surfaces.

Groups	Nuclear area (μm^2) on grooves		The difference of area of the cells on groove toward wild-type cells on flat
	Lower Quartile (Q1)	Upper Quartile (Q3)	
Wild-type (WT)	206±5.5	308±2.0	14±2.9%
EMD^{KO}-clone C3	222±2.0	335±2.5	22±4.8%
EMD^{KO}-clone B2	211±5.5	340±8.0	31±5.5%

Indeed, the analysis comparison of nuclear area of wild-type compared across the difference between flat and groove, displayed there was significant increase at approximately 14±2.9% of nuclear area on groove as compared to flat substrate.

To further evaluate the nuclear characteristics, their shape, the aspect ratio, the length of major to minor axis ratio was calculated as a shape factor. The analysed aspect ratio's increased when the nucleus of EMD knockout clones deviate from a roundness (a perfectly circular ratio is equal to 1) to a more ellipse with a higher degree of elongated shape along the grooves. A higher percentage of aspect ratios was shifted away from 1:1.5 as an effect in cells lacking emerin; the frequency and individual measures of aspect ratio shown in a scatter plot/boxplot as shown in Figure 5-5. The frequency distribution of nuclear aspect ratios was found to increase roughly by 5-10% at each of 0.5 unit of extension i.e. various aspect ratio away from 1:2, 1:2.5 and 1:3.0 of mutant cells on grooved substrates (Figure 5-5A) and more observations of aspect ratios of the nucleus at a similar surface texture (Figure 5-5B). However, the nuclei of EMD mutants on flat fibronectin-coated control material formed a round nucleus with lower relative aspect ratio compared to WT and those on anisotropic substrates.
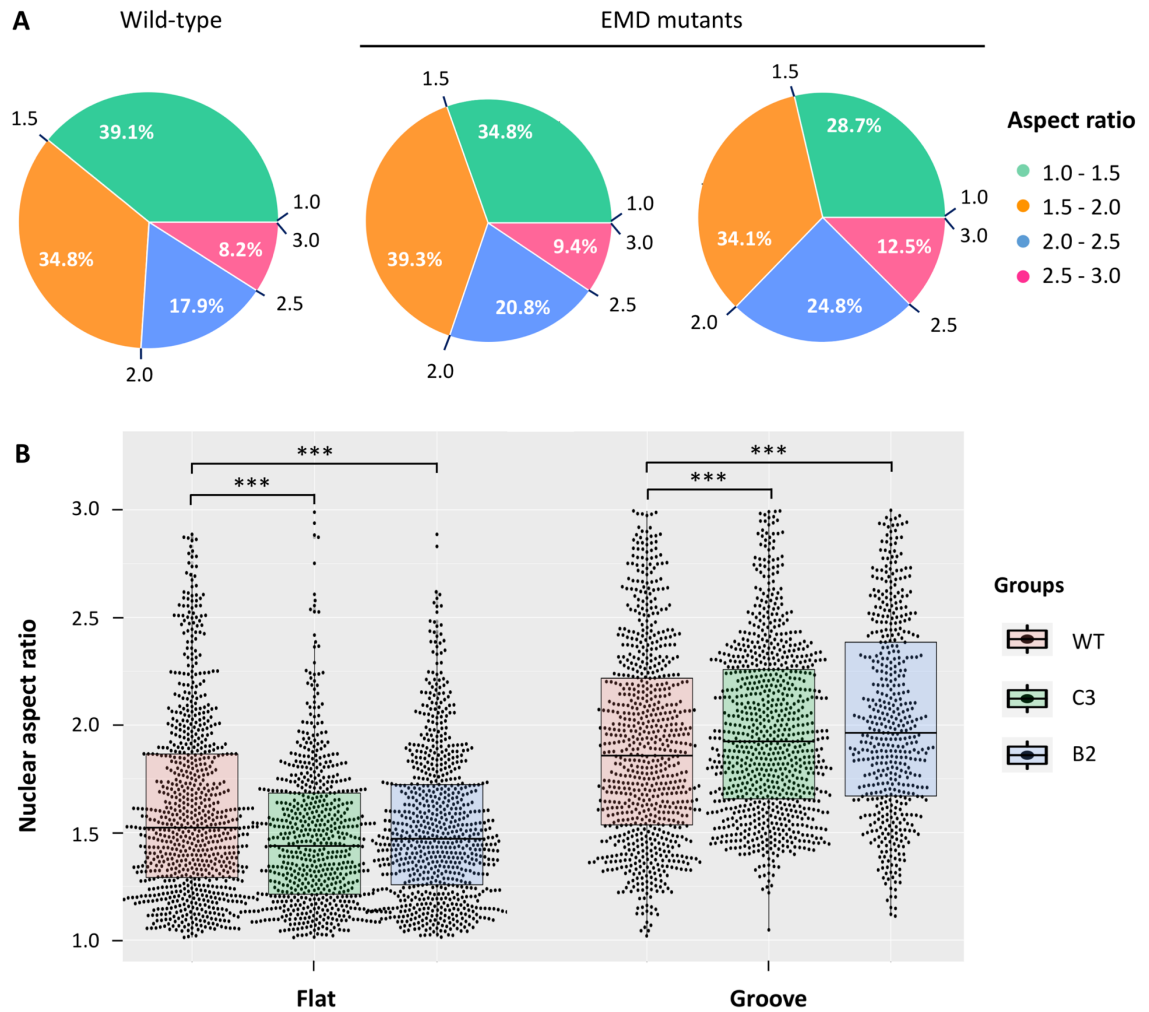
Figure 5-5. Quantification of nuclear shape and elongation of hTERT-BJ1 cells on Fn-coated substrates. A) Frequency and distribution of aspect ratio in the degree range from one to three, a higher density of nucleus shifting from spherical to ellipse position in the EMD-deficient cells on grooves. B) Boxplots and corresponding dot plots of nuclear aspect ratio in mutants showing a more pronounce of circularity of their nuclear shape, while mutants on groove were found to be more elongated as measured of increasing of nuclear aspect ratio. Unequal variances t-test used for statistic significance; *p<0.05, **p<0.01 and ***p<0.001, (N_{cells}= 485-735 cells/replicate, n_{Bio}=3).

To test whether changes in nuclear shape can regulate the cell cytoskeleton and morphology fluorescent staining of actin filaments was used to demarcate the cellular periphery, a relative link between the cytoskeleton and the nucleus were provided in a cell-to-nuclear aspect ratios of individual cells as displayed in Figure 5-6. Measuring if nuclear size and aspect ratio (calculated from net major to minor axis length) is proportional to the cell aspect ratio, to investigate the correlation between cell and nuclear shape. For varying cell-to-nucleus aspect ratio of cell on flat substrate, the nuclei remained highly elongated, almost independent of the ranges of measured cell length/aspect ratios in wild-type, while both nucleus and surrounding actin become less spread in EMD knockout clones where nearly identical effects were found on EMD^{KO}-C3 clone. The effect of micropatterned anisotropic surfaces, used to control and study how spatial coordination between cell and nuclear shape were changed, were then analysed, suggesting that the nuclear position may involve a diffusible cytoplasmic factor and directly contribute to cell elongation in the absence of emerin.

The slope of cell aspect ratio versus nuclear aspect ratio of below 1 appears the relationship of cell-type regulated specific nuclear morphology in both EMD mutants, whereas wild-type cells in confined grooved geometry are less pronounced implying the nuclear proliferation of which indicated as a slope of 2.8 with cellular widespread in its aspect ratio.
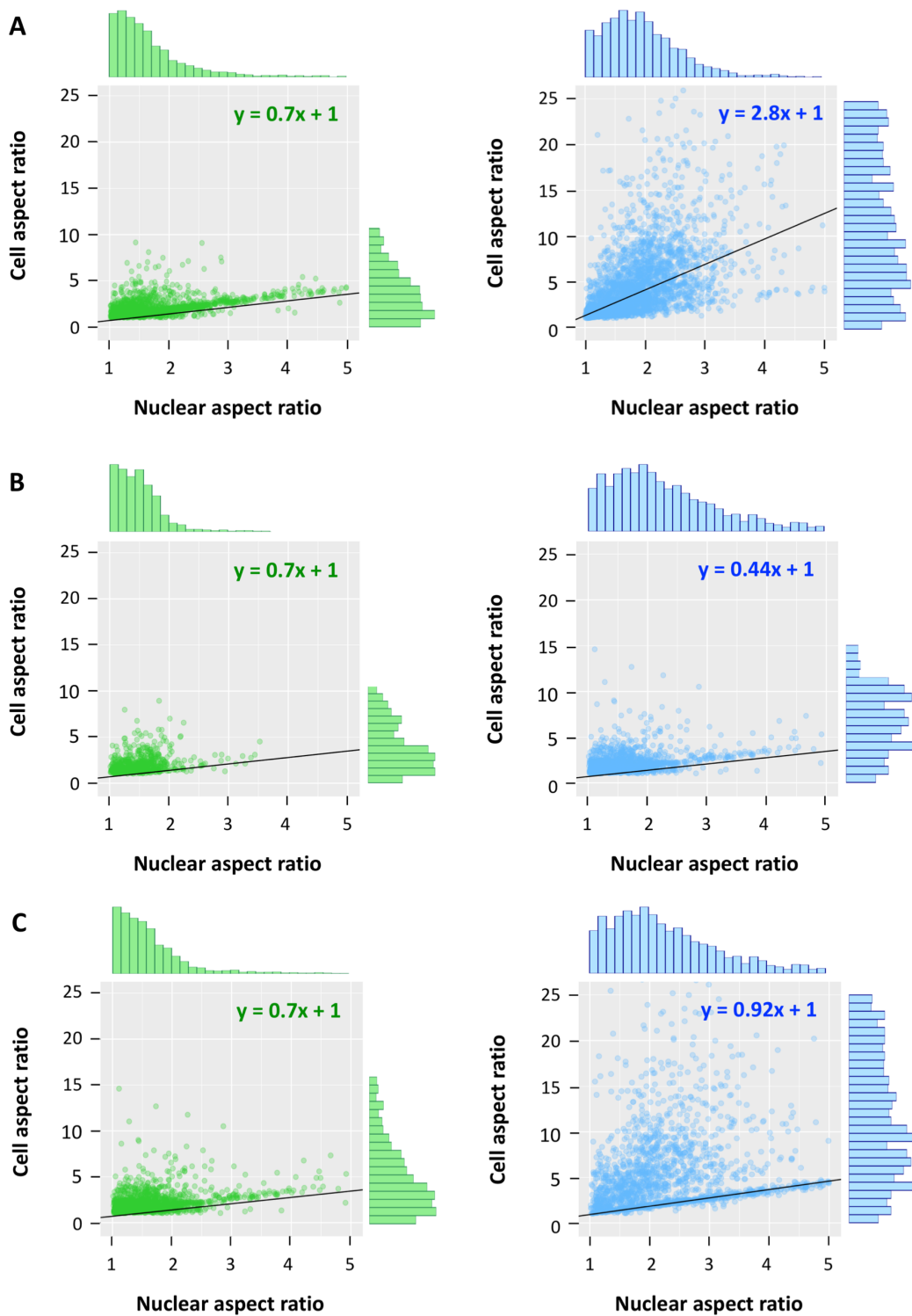
Figure 5-6. Correlation between cell and nuclear aspect ratio in A) wild-type BJ1 cells B) knockout clone C3 and C) mutant clone B2. The BJ1-hTERT was seeded on flat (green plot) and groove (blue plot) PDMS coated with Fn and fixed at Day2, followed by Immunofluorescent staining. For cell number and replication; N_{cells}= 485-735 cells/replicate, n_{Bio}=3.

5.3.4 Nuclear response in HEK293 cells lacking emerin

In order to confirm the expression of emerin-depleted cells and access the alteration in nuclear shape and deformation. The fluorescence maps the nuclear assembly and emerin signals using IF assay. The results from fluorescently labelled nuclei and emerin in the fixed cells on day 2 of culturing showed that the correctly localisation by assembly of emerin around the nucleus in wild-type cells. While, the completely loss of emerin expression as a result from knockout expression using CRISPRko approach, denoted no detectable fluorescent signal of emerin in mutant clones in either EMD^{KO}-1D1 or EMD^{KO}-H5S cells. Figure 5-7 displayed the fluorescent images of emerin expression in wild-type compared to mutant clones of HEK293 cells-tagged nucleus using DAPI. With the nuclear staining images, allow to access the local shape fluctuation that may occur as a consequence of emerin disruption in HEK293 cells. On the contrary to EMD^{KO}-BJ1 cells on plastic-coated surfaces, the knockout model in HEK293 cells had significantly increase of nuclear aspect ratio which facilitated to a more deformable nucleus in response to the lack of internally expressed emerin. Upon disruption of emerin on non-/patterned-PDMS coated substrates, microgrooves tracking alignment dominantly drive the deformability of nuclear position which transformed their bounding from a round to flattened ellipse and a more elongated shape associated with emerin-null cells. However, there were no difference between wild-type and mutants in the measurement of nuclear aspect ratio, suggesting the maintenance of its circularity on non-patterned flat control in all tested groups.

Using the nuclear images, the DNA visualised with DAPI allowed from its binding in a stoichiometric manner to deduce their DNA content; this allowed to determine the cell cycle state and comparison how emerin influenced cell cycle progression. The number of averagely two peaks in DNA intensities and distribution was observed in all tested cells either wild-type or knockout emerin phenotypes toward three different surfaces cultured in pre-coated Fn on plastic, flat and grooved PDMS materials (Figure 5-8), this suggested that disruption of emerin in HEK293 cells were not affected to divided nuclei of HEK293 cells, or even it alter in a slight effect that it was not sensitive to read out using this IF assay.
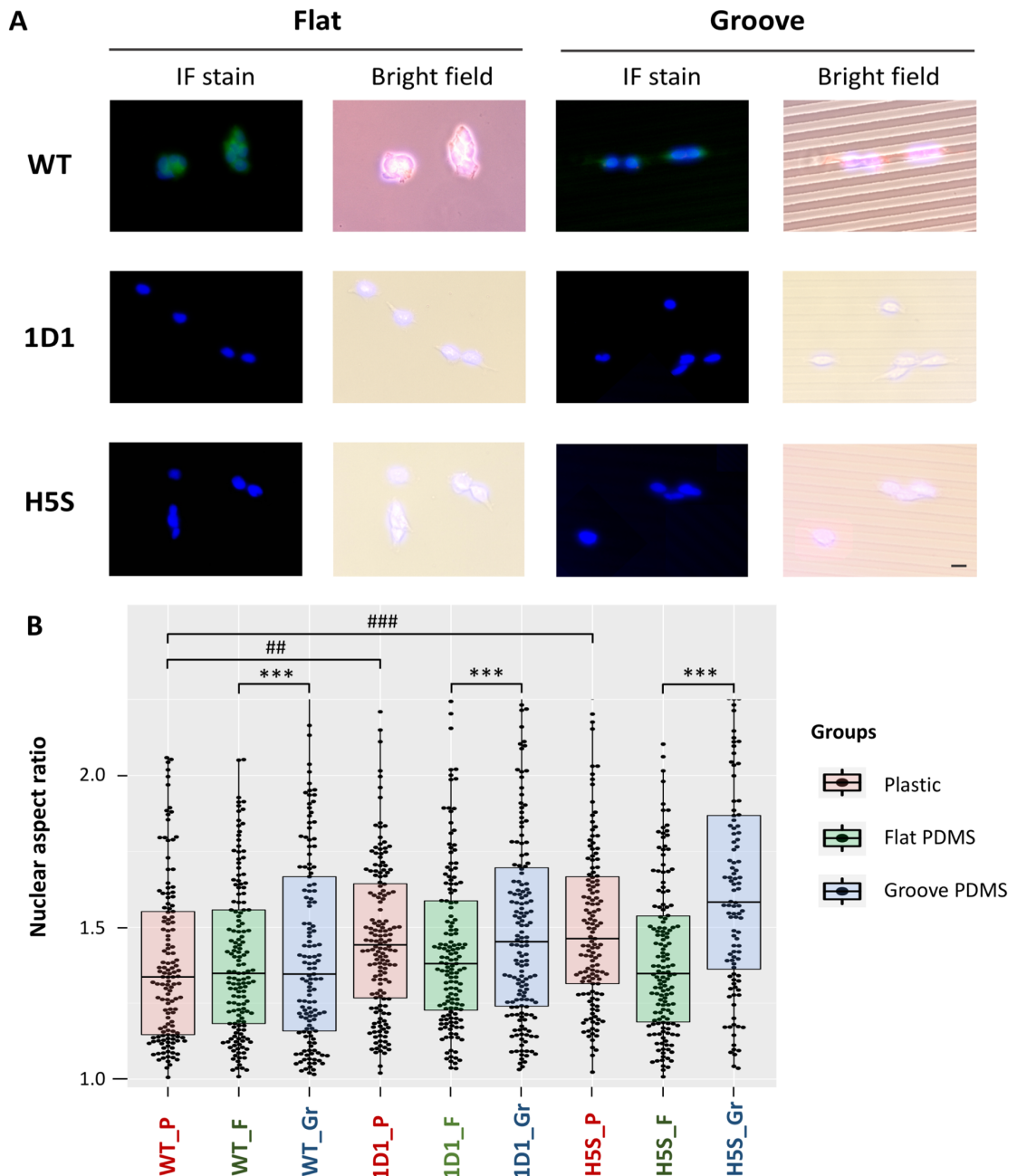
Figure 5-7. Characterisation of emerin-null HEK293 cells influence nuclear shape. A) Immunofluorescent images of wild-type normal expressed emerin and absence of signal in knockout clone 1D1 and H5S. For fluorescent labelling; EMD – green, DAPI – blue. Scale bar ~20μm, n_{Bio}=3. B) The aspect ratio of the nucleus in wild-type (WT) and mutant strains (clone 1D1 and H5S). The occurrence of elongation at the NE boundary relative to nuclear aspect ratio, have significant increases where extensions of NE were measured in mutants on grooves as compared to distributed nuclei of wild-type with a similar surface geometry. For the suffix abbreviations note of surface culture in plastic (P), flat (F) and groove (G). Three individual experiments were performed and analysed of at least N_{cell} = ~200-280 cells/replicate. Two ways of statistical analysis including t-test between EMD-expressing and EMD^{KO} cells on TCP surface as indicated in $^{##}p<0.01$ and $^{###}p<0.001$. Then, the unpaired t-test that compares the group sample difference between flat and grooved surface as indicated in ***p<0.001.
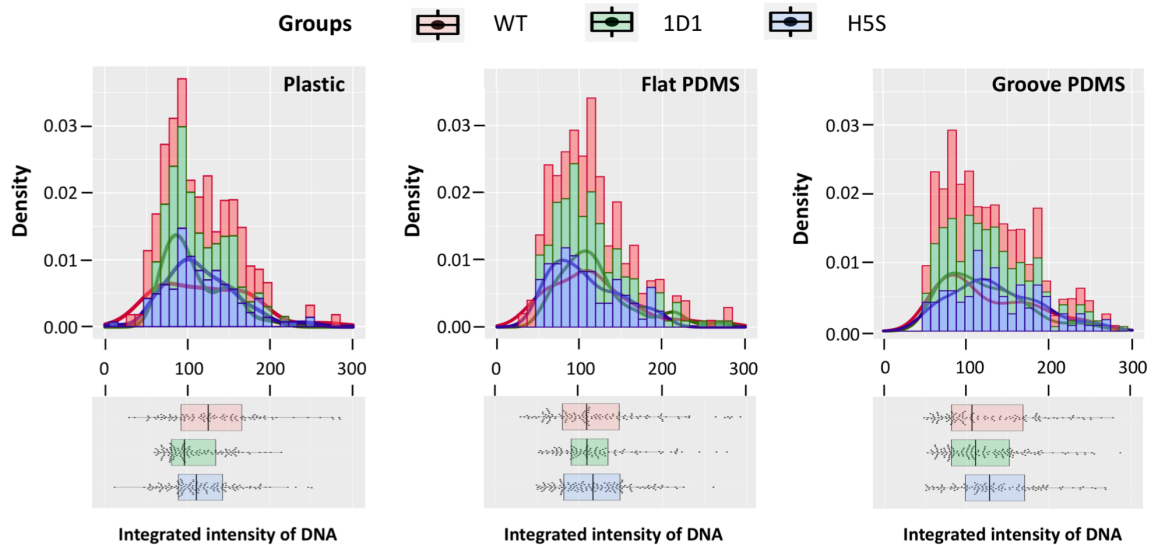
Figure 5-8. Histograms and boxplots of DNA intensity visualised by DAPI staining of HEK293 cells. Frequency distribution of DNA density in wild-type (red), EMD^{KO}-1D1 (green) and EMD^{KO}-H5S (blue) cells. The cells were grown pre-coated surface with fibronectin and on tissue culture plastic (left), flat PDMS (middle) and grooved PDMS substrate (right), (N_{cell} = ~200-280 cells/replicate., n_{Bio} = 3).

5.3.5 Global characterisation of gene activity in emerin-associated functions

Such of some changes detected in the nuclear shape, which houses the genetic material within double membrane layer. This study is next examined the gene production that are altered in the absence of emerin, three overlapped signalling cascades with candidates in each way that have been drawn to validate the expression changes of some representative target genes by qRT-PCR assay with two internal controls for data consistency. The cells were grown on plastic with Fn-coated surface for 7 days of culturing to allow the cell spreading and cell-cell interactions before RNA extraction followed by cDNA synthesis and proceeding qRT-PCR (For full experimental conditions and detailed methods see section 2.2.6). Figure 5-9 showed overall trend of target gene expression toward gain-/loss-of-function in emerin expressed BJ1-hTERT cells. Firstly, the relative of gene associated emerin-bound proteins including; histone deacetylase 3 (HDAC3), laminA/C (two isoforms predominantly encoded A-type lamins regulated by Lmna) and BAF (encoded from Banf1) were measured and normalised to GAPDH control (Figure 5-7A). All three of these genes (HDAC3, Lmna and Banf1) expression were

substantially reduced to 48±5.7%, 50±18.0% and 70±13.5%, respectively in EMD^{KO}-C3 clone as compared to wild-type. Similar to these observations in the EMD^{KO}-B2 clone, there was a reduction to 46±10.2%, 49±10.1% and 52±19.9% in the expression levels of HDAC3, Lmna and Banf1, respectively. Given that the role of emerin function connected closely to MAPK/ERK signalling, the ERKs; Erk1 and Erk2 were next measured, the results showed that both Erk1 and Erk2 remained stable expression to the baseline of their expression in either C3 or B2 mutants. Finally, the ternary complex factors (TCF) which formed the ETS domain containing proteins includes the subset of Elk-1, Elk-3 (also known as SAP2 or Net) and Elk-4, (also called as SAP1) have reported as one of coactivators of SRF that link transcription of gene encoding several cytoskeletal components in RhoA-dependent manner (Gau and Partha, 2018) and also was promoted by signalling via MAPK/ERK cascades (Gineitis and Treisman, 2001). The qRT-PCR analysis of gene encoding TCF family proteins revealed an induction of Elk-1 and Elk-4 to around 223±31.0% and 261±17.1% in EMD^{KO}-C3 clones. Similarly, activation was also observed in EMD^{KO}-B2 clones with an increased expression of both Elk-1 and Elk-4 to 189±37.0% and 264±38.5%, respectively. However, a reduction of Elk-3 expression was found in both EMD^{KO}-C3 or EMD^{KO}-B2 cells with expression levels observed to be 46±5.7% and 49±14.3%.

The effects of fibroblasts lacking emerin with an applied isotropic force using grooved PDMS was further determined and compared to cells on non-patterned (flat) PDMS surfaces. For the emerin binding proteins, the activity of HDAC3 significantly decreased by ~0.5-folds in all tested mutants and for all surfaces (Figure 5-9B). Indeed, the level of HDAC3 expression in wild-type was shown to have substantially decreased as a result of the softer surface for cells grown on flat/grooved PDMS when compared to normal TC plastic. Next, two major interaction of emerin which are mainly component in the structural formation of the nuclear lamina; Lmna and Banf-1 had decreased expression levels in emerin KO/mutant cells. There were 0.57-fold and 0.38-fold decrease of Lmna expression in the C3 clone grown on flat and grooved surfaces, and a 0.46-fold and 0.55-fold decrease of Lmna observed in B2 clone (Figure 5-9C).
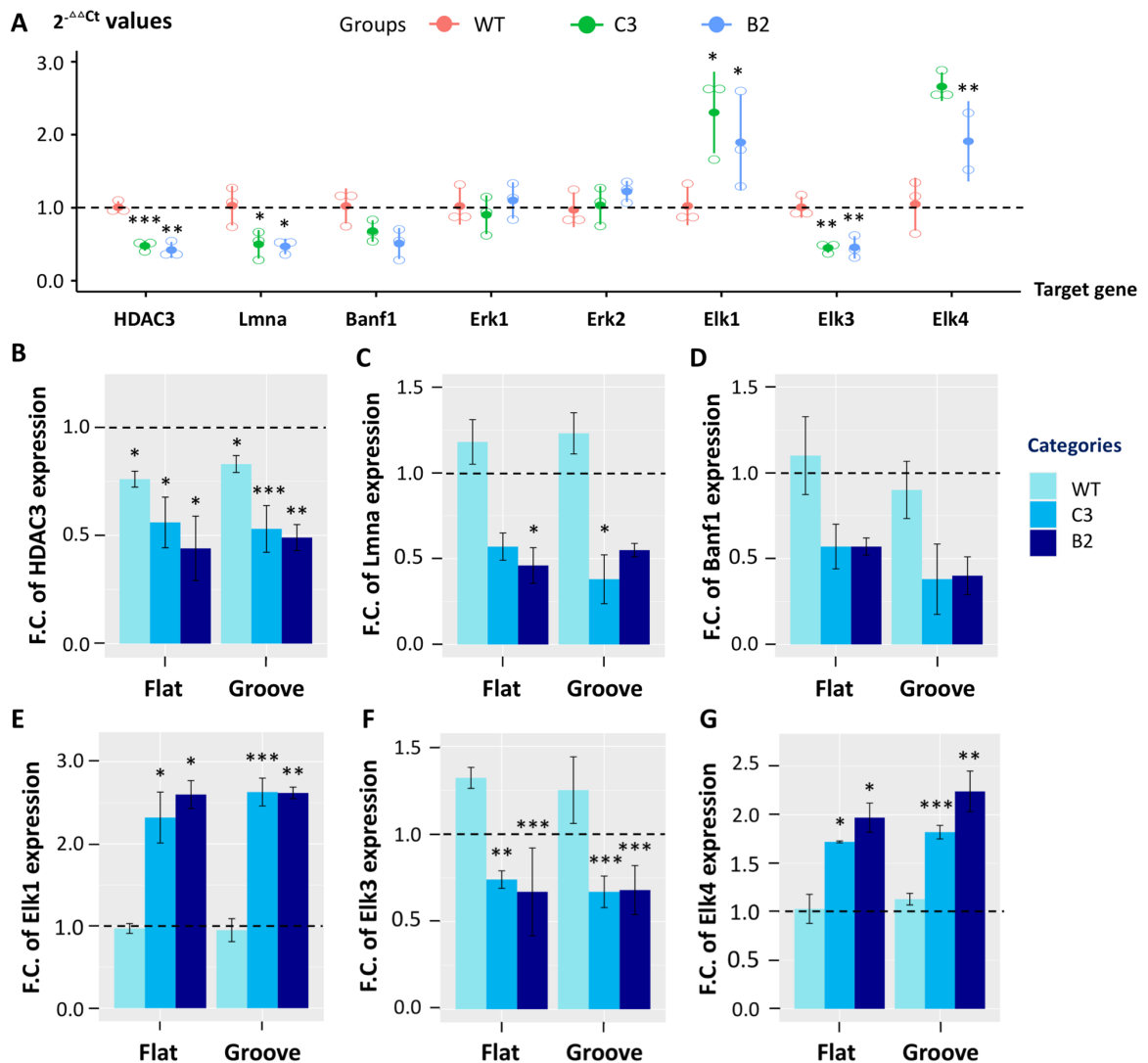
Figure 5-9. Gene expression profiles of emerin dependent target genes in the emerin-depleted cells (knockout C3 and B2 clones) in BJ1-hTERT cells. A) Comparison between normal and disrupted emerin expression regarding the level of target associated gene expression. Target genes expression was calculated and represented as the $2^{\Delta\Delta Ct}$ values. Samples of three independent experiments from cells on Fn-coated plastic surface for 7 days of culturing. Error bars represent standard deviations. For colour indication of wild-type (WT, red), EMD^{KO}-C3 (C3, green) and EMD^{KO}-B2 (B2, blue) cells. B-G; Barplots of target gene expression from cells culturing on flat and grooved PDMS surfaces. Fold-change (F.C.) of genes compared to each control group were grown on plastic-coated Fn in the following; I, groups of emerin's binding partners in B) HDAC3, C) Lmna and D) Banf1 reduced expression. II, Ternary complex factors include E) Elk-1, F) Elk-3 and Elk-4, the activation of Elk-1 correlated with Elk-4, whereas the corresponding Elk-3 was decreased. Dash lines aid vision for normal expression of unique genes. Three separate experiments with statistic indication; *p<0.05, **p<0.01 and ***p<0.001. All target gene were initially normalised to GAPDH as a cell internal control, and then to WT cultured on TCP.

Banf-1 was suppressed in KO cells if grown on grooved PDMS with ~0.39-fold decline across two tested mutants, and ~0.57-fold decrease of Banf-1 expression when the cells were grown on flat PDMS (Figure 5-9D). Then, the results from target genes which are subset of TCF complexes (See graphic evaluation in Figure 5-9E-G) revealed that Elk-1 and Elk-4 were overexpressed in the emerin-KO fibroblasts. There was a 2.30-fold to 2.60-fold increase of Elk-1 and a 1.72-fold to 2.24-fold rise of Elk-4 in the emerin KO clones C3 and B2 on both flat and grooved surfaces. With an exception, the Elk-3 was found to have a reduced expression in the absence of emerin, resulting in a decrease in the range between 0.67-fold to 0.74-fold, regardless of surface topography.

With regards to confirm and minimise the variation that may be caused by the limitation of qRT-PCR or alteration of mutants, the results were also alternatively normalised to RPL13A across all candidate target genes as displayed in Figure 5-10A which shows the data for cells grown on TC-plastic coated with Fn for 7 days. The trend of gene expression, normalised against RPL13A was strongly correlated to their expression when normalised to GAPDH, only small variations were measured; for example, as noted the plastic adhesion in this scenario, HDAC3 expression was decreased to 42±11.3% and 36±5.3%, in C3 and B2 clones, respectively. Likewise, Lmna, Banf-1 and Elk-3 expression was relative similar to levels when their expression was normalised to either GAPDH or RPL13A. There was a decrease in Elk-3 expression to around 36±9.3% and 36±5.3%, in C3 and B2 mutants, respectively. For comparison of gene profiling level of BJ1-hTERT lacking expressed emerin, there were similar alterations of expression levels in proteins involved in downstream signalling comparing the normalisation using GAPDH and RPL13A with no more than approximately 10% variablity. Examples of graphic gene expression level of selected targets normalised with RPL13A toward non-patterned or patterned surface are shown in Figure 5-10B-G.
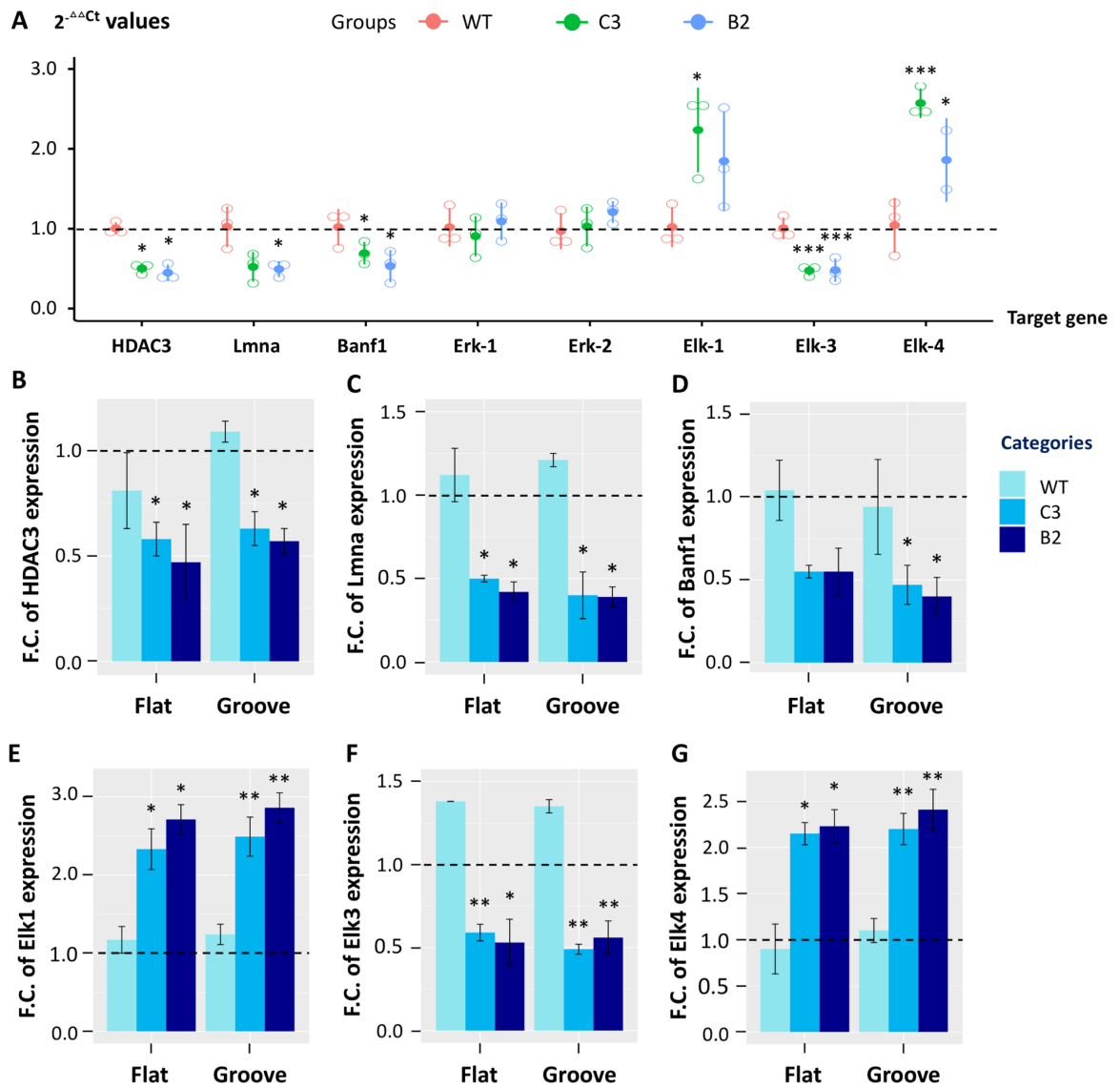
Figure 5-10. Evaluation of gene activity in the emerin-null immortalised fibroblasts toward pre-coated non-/patterned PDMS materials with Fn when all target genes were normalised to RPL13A for data consistency with at least three separate experiments. A) Expression levels assessed by qRT-PCR assay with the $2^{\Delta\Delta Ct}$ values of all target genes, observed from cells on Fn-coated plastic plate. B)-G) Fold-change of gene (HDAC3, Lmna, Banf-1, Elk-1, Elk-3 and Elk-4) expression from cells grown on PDMS. Dash lines for visual aids of normally expressed basement of genes in this cell-line. Error bars represent standard deviations of three individual experiments. For statistic significance; *p<0.05, **p<0.01 and ***p<0.001.

The ERKs expression levels in emerin KO mutants remained similar to the normal expression in wild-type cell. As expected, the stimulation of Elk-1 and Elk-4 were observed in both KO lines with 269±34.0% and 261±24.0% respectively in the C3 clone, and with 202±36.5% and 217±31.5% respectively in the B2 clone.

Therefore, Erk1/2 expression correlated to the previous annotation from two mutants which observed behaviour from cells on plastic cultures, there were no change of Erk expression in response to the KO of emerin comparing the cells responses to non-patterned/patterned PDMS (Figure 5-11).
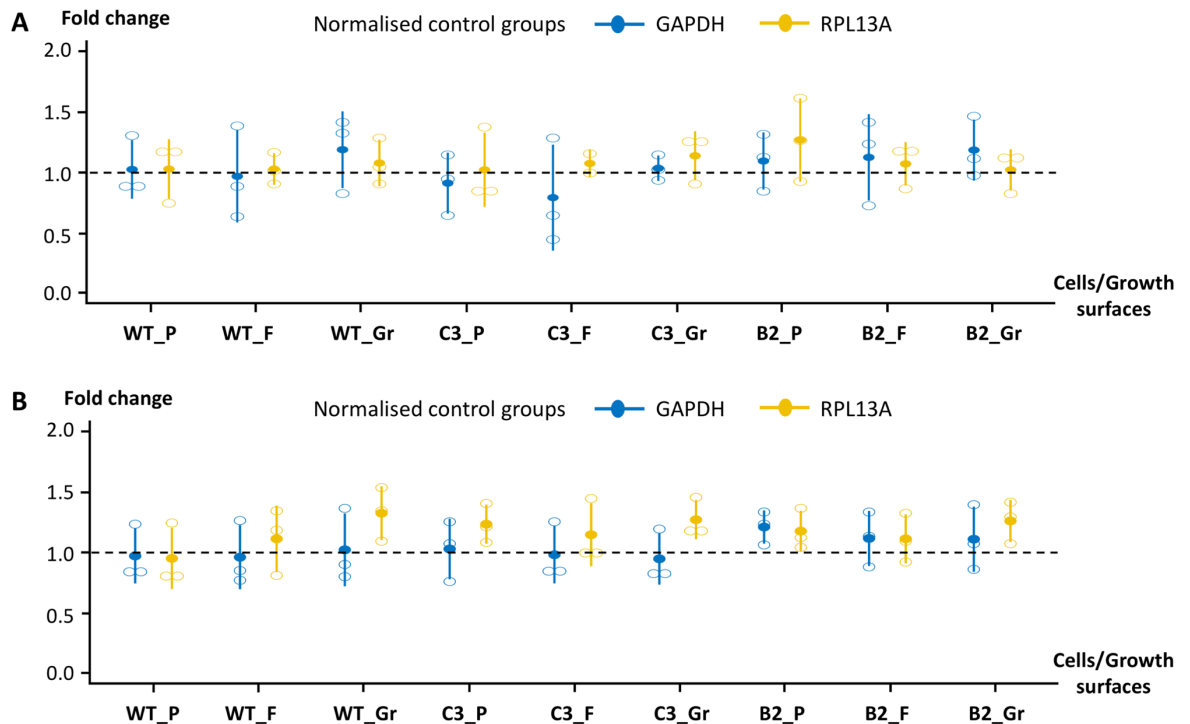
Figure 5-11 Expression of Erk-1 and Erk-2 levels were not affected in the emerin-null cells in BJ1 fibroblasts. The measurement of A) Erk-1 and B) Erk-2 expression remained stable in all tested cells or cultured surfaces. The results from three biological repeats were performed for analysis and double normalisation with two internal house-keeping genes; GAPDH – blue and RPL13A – yellow.

5.3.6 Gene expression profiling analysis in HEK293 cells lacking emerin

With a similar study design as above shown for BJ1 cells, the comparative mRNA expression analysis was performed in HEK293-WT and EMD KO mutants using qRT-PCR measurements. The cells were grown for 7 days on fibronectin-coated surfaces across three different textures i.e.: TC-plastic plates, flat and grooved PDMS prior to gene analysis study. The PCR data were normalised to GAPDH control for each group and expressed as fold-change relative to wild-type control on plastic-coated surface. Three genes associated with and known functional binding

partners of emerin: HDAC3, Lmna, and Banf-1 were downregulated by half of their normal expression in both EMD KO cells across all substrates used; plastic, flat and grooved substrates compared to wild-type grown on plastic culture as shown in Figure 5-12 (in left panel).
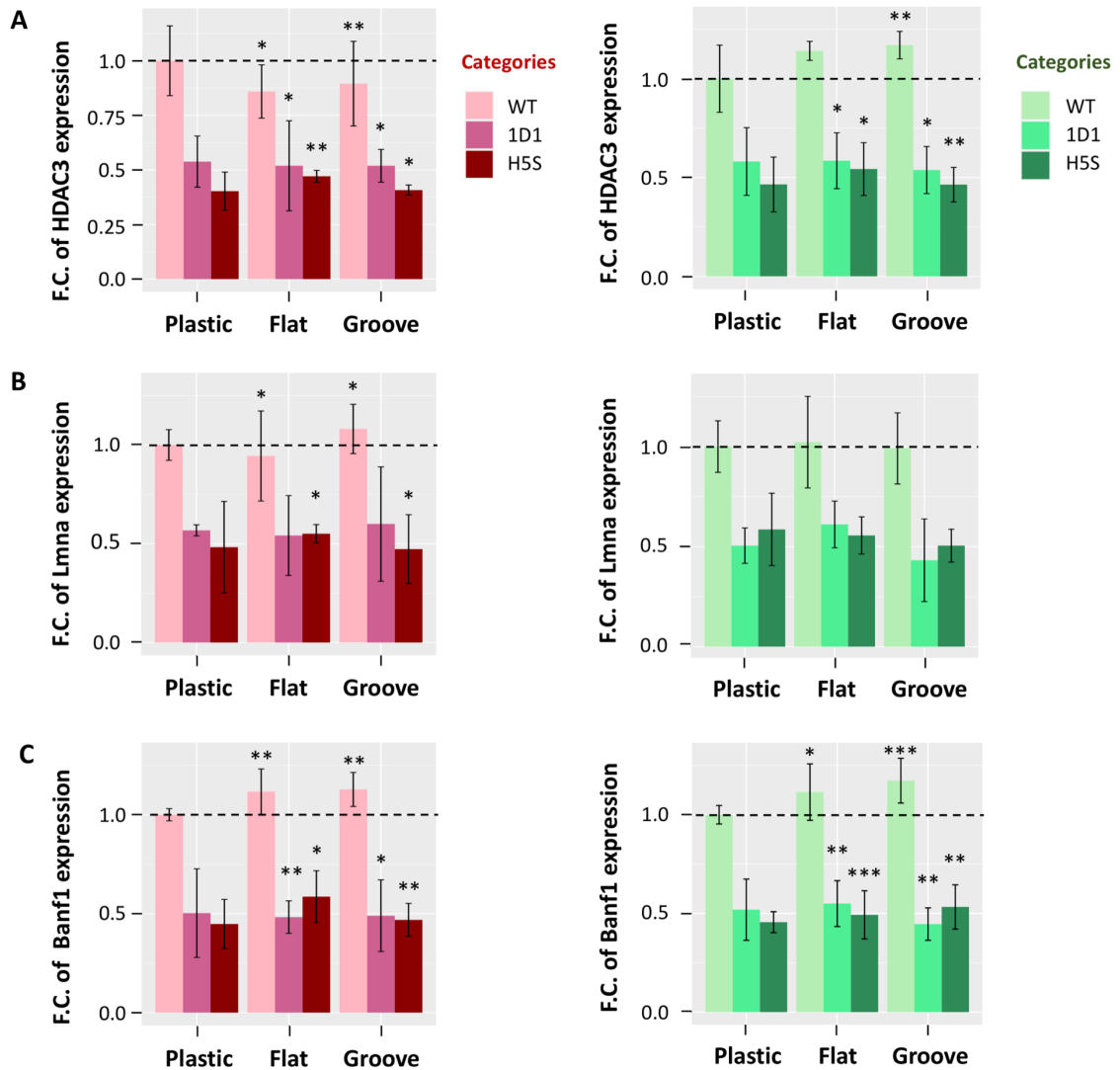
Figure 5-12. Gene expression analysis of functional binding groups of emerin-associated gene factors expressed in HEK293 knockout EMD (encoding emerin) cells. All of three downstream competitive binding of EMD mutations toward A) HDAC3 B) Lmna and C) Banf1 expression level were substantially reduced where the fold-change compared to wild-type on plastic were significantly difference at 7 days post-seeding shown in *p<0.05, **p<0.01 and ***p<0.001. Regulatory internal control under normalisation with) GAPDH (left panel) and RPL13A (right panel) used as house-keeping genes. All represented data was performed independently from three biological replicates.

As expected the comparative target expression was very similar to that calculated when normalised using RPL13A as an internal control instead of GAPDH. These data indicate that the effect of altered gene expression was due to actual changes in the cells response to EMD KO rather than any non-specific variation between mutants. Graphic illustration of results normalised to RPL13A are shown in the right panel parallel to each individual gene profiling (See Figure 5-12, right panel).

Next, the results indicated an activation of a MAPK pathway via Erk-1 have in EMD knockout HEK293 cells. The expression of Erk-1 transcript was upregulated in the emerin KO clone 1D1 by 2.41-fold on plastic, 2.53-fold on flat PDMS and 2.72-fold on grooved PDMS, respectively. These results were consistent with those seens for another tested EMD^{KO} clone; H5S, as for 1D1 an increase in Erk-1 by 2.72-fold on plastic, 2.66-fold on flat substrate and 3.08-fold on grooved substrate (normalised to GAPDH, RPL13A and represented as a net average of fold-change compared to wild-type control on TC-plastic). Interestingly, the differences in activated Erk-1 expression between flat and groove surface texture from wild-type control and EMD^{KO} cells were enhanced by approximately 7.5% and 15.8%, in 1D1 and H5S clones when cultured on grooves. The increased expression of Erk-1 but not Erk-2 was detected only in EMD^{KO} cells (Figure 5-13, top panels).
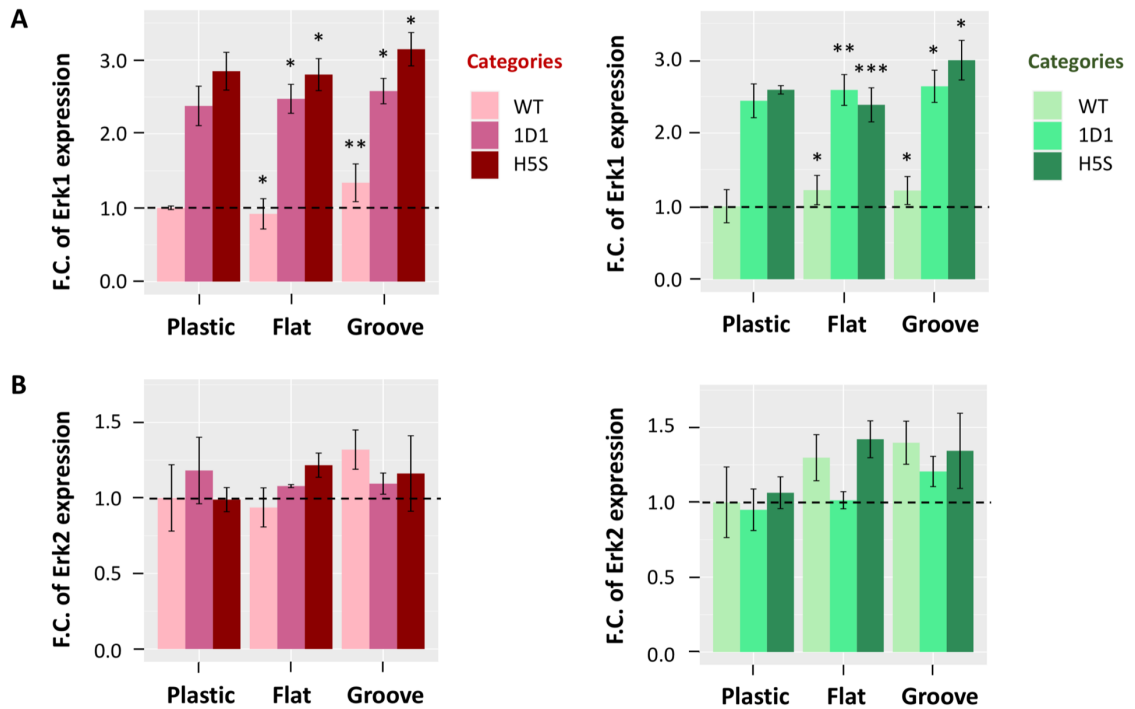
Figure 5-13. Knockout of emerin in ERKs branches of MAPK signalling. EMD mutant clones in A) Erk-1 and B) Erk-2 expression measured using RT-PCR from RNA extracts after 7 days of culture. Quantitative analysis of gene encoding Erk-1 had significantly enhanced. While, the Erk-2 level remained nearly stable in emerin-null HEK293 cells compared to control of each group. The fold-change was calculated and compared with wild-type on plastic culture surface, two internal controls used GAPDH (left panel) and RPL13A (right panel) were used for normalisation of results. Values are means ± standard deviations for n_{Bio} = 3 samples, t-test was used to compare to WT on TCP, *indicates p<0.05 and ***indicates p<0.001).

Finally, the alteration of target gene expression series of ternary complex signatures in EMD-null HEK293 cells appears in a similar trend compared to BJ1 fibroblasts of increased Elk-1 and Elk-4 whereas, the Elk-3 was subjected to declined level of its transcript by ~50% reduction (Figure 5-14).
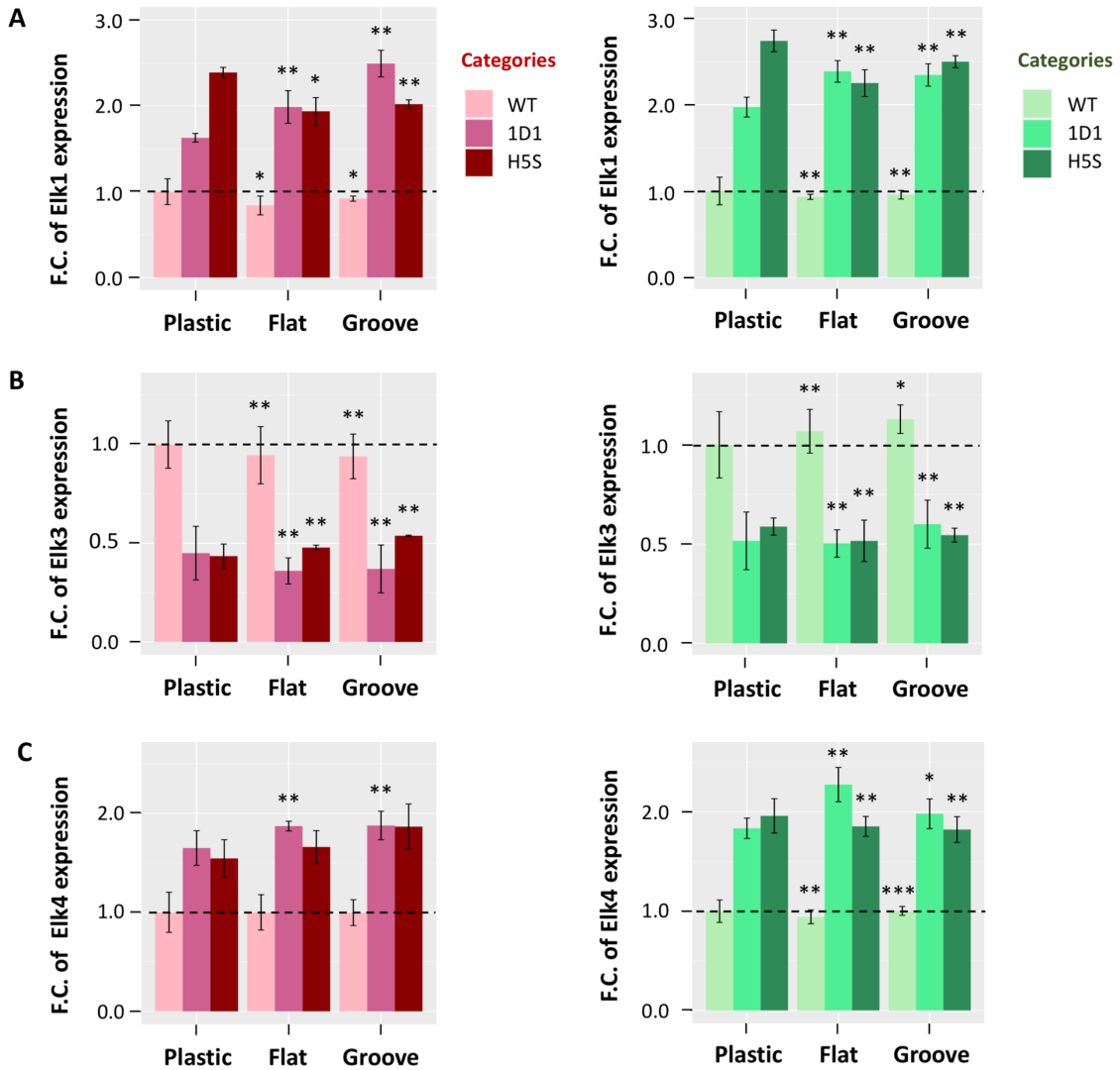
Figure 5-14. Transcriptional targets of TCF family of SRF-linked ERK/MAPK signaling pathway analysis using real-time PCR. The mutation of EMD gene in HEK293 can alter the expression level of the gene encoding transcription factors including A) Elk-1 B) Elk-3 and C) Elk-4. The cells were grown on PDMS with non-patterned (flat) or patterned (groove)-coated Fn on PDMS material compared to their normal growth in tissue culture plastic-coated Fn of each groups. The cells were allowed growth for 7 days before testing of related gene expression in transcriptional machinery. The fold-change was shown in comparison to wild-type cell grown on plastic culture and normalised to GAPDH (left panel) or RPL13A (right panel). All values of gene expression of transcripts were calculated from three separate experiments where were significant indicated as *p<0.05 and **p<0.01.

For stimulated Elk-1 expression, there was an increase level detected in the emerin KO clones 1D1 (1.80-fold on plastic, 2.29-fold on flat PDMS and 2.42-fold on groove PDMS) and H5S clone (2.57-fold on plastic, 2.10-fold on flat PDMS and 2.26-fold on groove PDMS). The overexpression of Elk-4 was calculated to be 1.64-fold (with respect to TC-plastic), 1.97-fold (with respect to flat PDMS) and 1.83-fold (with 12.5 μm grooved PDMS) from 1D1 knockout of EMD, overall activated at a range from 1.65-fold to 1.74-fold rise from H5S mutant toward all tested surface of culture adhesions.

5.3.7 Depletion of emerin impacts on the protein levels of known interaction partners

The global influence of emerin KO on three distinct signalling routes with known protein interactions with emerin were examined in hTERT-BJ1 fibroblasts and HEK293 cells. A candidate protein representative of each group was immunoblotted as detailed in the following;

I, Direct binding observed in laminA/C-bound emerin. Molecular underlying transcription factors link actin cytoskeleton were also assessed via

II, phosphorylated ERK1/2 which is crucial for Ternary complex formation (TCFs) and

III, master regulator of actin dynamics through MRTF-A remodelling and nuclear redistribution.

To determine how fibroblasts lacking emerin in the distribution of its binding interaction, knockout clones of emerin-null BJ1 cells were western blotted; Ponceau S staining allowed to assess the protein pattern isolated; followed by immunospecific detection of laminA/C, pERK/ERK and MRTF-A compared to the respective wild-type cells (as shown in Figure 5-15). Quantitative analysis by band densitometries then allowed to assess the level of each individual target protein present; this data was normalised to an internal control, α-Tubulin and checked for similar loading by Ponceau S staining. As shown in Figure 5-16, the data for laminA/C, pERK/ERK and MRTF-A were plotted to establish the effect of emerin KO on signal transduction. This is supported by a representative image of MRTF-A localisation.

Firstly, the results from relative fold change of immunoblotting with antibodies that recognised laminA/C (Figure 5-16A) displayed a decline of half expression in A-type lamins in EMD^{KO}-B2 clone but not EMD^{KO}-C3 clone in cells grown on plastic-coated Fn compared to wild-type.
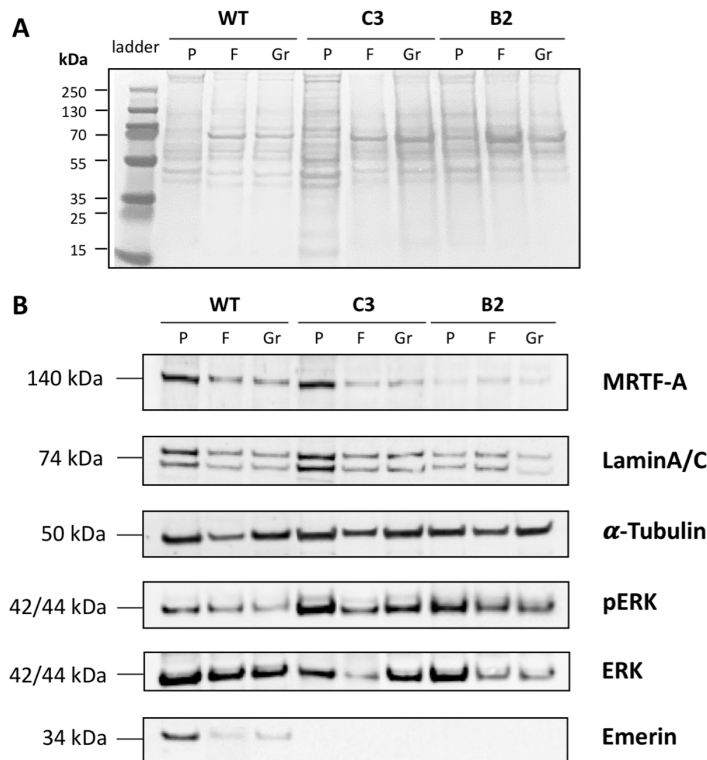
Figure 5-15. Loss of emerin in human fibroblast cells induces changes in protein expression of its interaction partners.

A) Characterisation of total protein identified by Ponceau S staining, 20 μg of protein lysates were denatured in LDS sample buffer and loaded in each lane prior to membrane transfer. Ponceau S staining is used as reference control and for evaluating of the transfer efficiency.

B) Target protein detection representing the specific functional classes of protein sharing role to emerin containing MRTF-A, laminA/C and pERK/ERK in knockout of emerin in BJ1 cells (clone C3 and B2) compared to wild-type (WT). Endogenous emerin was immunoblotted with mouse monoclonal anti-EMD antibody (1H9) for confirmation of knockout clones. Westernblot of α-Tubulin was also labeled and normalised for quantitative analysis. The representative blot is shown (n=3). Each group of cell tested in three cultured surfaces − P; tissue culture plastic, F; flat PDMS, Gr; grooved PDMS which are subjected to Fn-coating for cell adhesion, and harvested the cells after 7 days of experiments.

LaminA/C production by cells grown on flat PDMS substrates was further examined and compared to calculate fold change with respect to that in wild-type emerin cells grown on Fn-coated TC-plastic, approximately 70±17.5% and 55±2.5% of laminA/C expression were detected in emerin KO clones C3 and B2, respectively. Next, the role of mechanical stress by shaping the cells, mainly nuclei was then added by pre-patterning the PDMS substrate with microgrooves for comparison of cell behaviour. On the grooves, a similar trend was observed for changes in

laminA/C in emerin KO cells; a reduced expression of laminA/C of around 64±13% in EMD^{KO}-C3 and 42±12% in EMD^{KO}-B2 when it was compared to basal line of WT emerin (+ve) cells on TC-plastic.

Secondly, the degree of ERK1/2 activation was analysed by measuring phospho-ERK1/2 (pERK1/2) normalised to the ERK1/2 signal. As shown in Figure 5-16B, the ratio of pERK/ERK revealed that phosphorylated ERK on plastic coated surface was about 2.27-fold higher in the emerin KO clone C3 and 1.74-fold higher in the emerin KO clone B2. In addition, pERK signalling seems stimulated on topographic patterning compared to flat control, this is likely to an induced activation of ERK by phosphorylation compared to KO clones on TC-plastic at almost similar activation of ERK phosphorylation of around 2.23-fold in EMD^{KO}-C3 and 2.14-fold in EMD^{KO}-B2. Without microgrooves, cells lacking emerin were found to have less pERK with a slight drop when compared with the same cells on grooved surfaces. pERK was detected to be ~1.71-fold and ~1.32-fold increased in clone C3 and B2 on flat substrates. These small differences in regression of activated pERK at about 56±11.5% in EMD^{KO}-C3 and 82±39% in EMD^{KO}-B2 subjected to groove-guided nuclear alignment, respectively.

Lastly, the functional dichotomy between the sub-interactomes of transcription factors associated with emerin depleted cells toward actin cytoskeleton connectivity was assessed as one of representative measurement via MRTF-A signalling by quantified immunoblotting and immunofluorescence assays. Loss of emerin in hTERT-BJ1 cells revealed a significant decrease in aggregation of nuclear MRTF-A, confirmed in both tested knockout clones. However, the comparative analysis of substrate guidance cells via immunoblotting did not displayed a difference in change subjected to surface textures. Westernblot analysis of EMD^{KO}-C3 pools showed a reduction of nuclear MRTF-A translocation to around half of expression toward plastic, non-/patterned microgroove substrates compared to the basal level in wild-type control. The declined signals of MRTF-A, predominantly in the nucleus of EMD^{KO}-B2 was found similarly with a slightly higher impact of reduction to ~34±12.5%, 33±6% and 33±7%, in plastic cultured, flat PDMS and grooved substrates, respectively (as shown in Figure 5-16C – comparison of KO cells to WT; wild-type cells). Therefore, examples of IF images illustrated the

localisation of MRTF-A levels in nuclear and cytoplasmic distribution as shown in Figure 5-16D – combined staining of MRTF-A, nucleus with DAPI followed by actin with Phalloidin for cellular compartmentation.
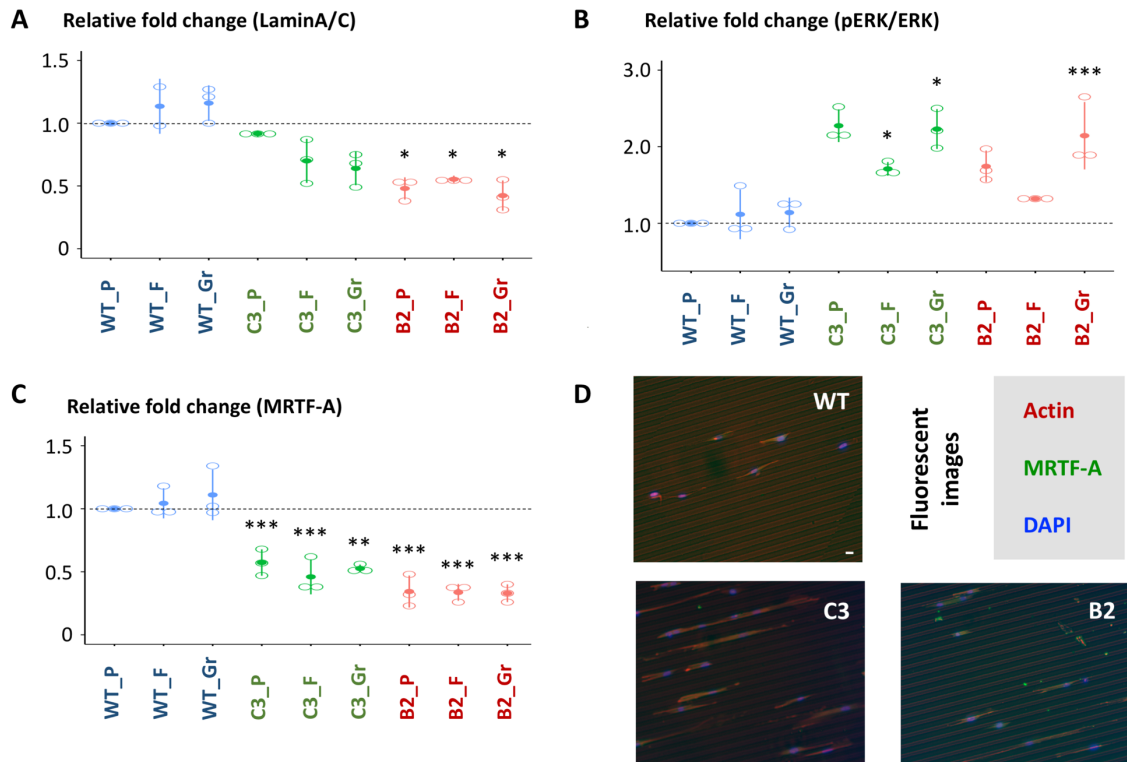
Figure 5-16 Quantitative analysis of targeted protein expression in fibroblasts lacking emerin. Quantitation of A) Lamin A/C B) pERK/ERK and C) MRTF-A production were westernblotted in control (tested by wild-type, WT) and knockout BJ1 cells which are mutated in EMD gene (observed in C3 and B2 clones) after 7 days of culture on Fn-coated plastic (P) surface, flat (F) and grooved (Gr) patterning of PDMS. The relative fold change of selected protein expression was calculated and compared to the basal expression of wild-type on TCP/plastic coated Fn. Results are from three independent experiments. Data show ± SD where the evaluation is statistically significance, markly indicates in; $*p<0.05$, $**p<0.01$ and $***p<0.001$. D) Representative images of fluorescently labelled MRTF-A displays the localisation of MRTF-A (green), together with nuclear structure (blue) and actin cytoskeleton (red). The examples of IF staining are shown from cells on grooves. Scale bar ~20μm.

Consistent with the above tested results in emerin knockout clones, the impact of emerin associated protein expression of selected interaction partners was also determined in emerin KO HEK293 clones. The results from western blotting of total proteins with Ponceau S staining (Figure 5-17A) and immunospecific antibody

labeling of MRTF-A, laminA/C, pERK/ERK, together with loading control α-Tubulin and confirmation of completed knockouts against anti-EMD measurement (as displayed in Figure 5-17B). In wild-type expressing emerin and candidate knockout clones, pERK was not detectable from the nuclear extracts of HEK293 cells. Densitometric quantification of intensities for MRTF-A and ERK were analysed to observe the alteration as influence by the deletion of emerin-expressing cells (Figure 5-17C).
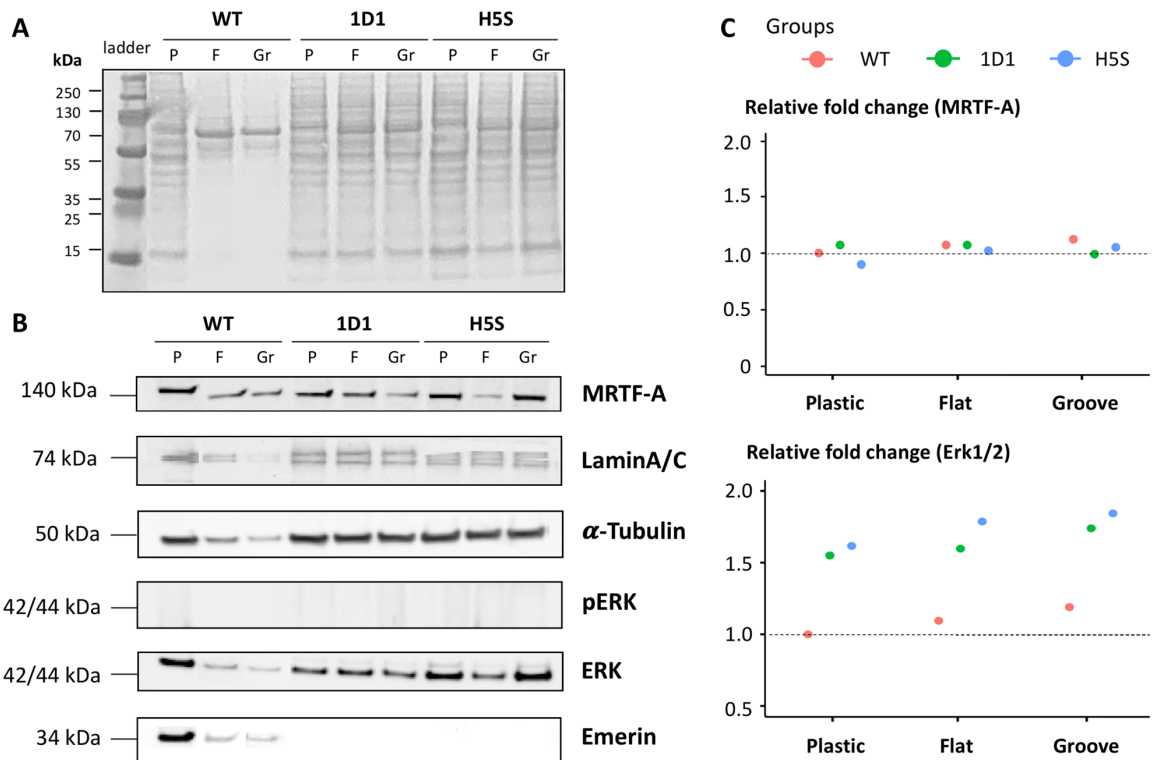
Figure 5-17. Mapping the changed protein network in emerin knockout HEK293 cells via westernblot analysis in wild-type (WT) and two representative clones (1D1 and H5S). A) Total proteins from cells on plastic (P), flat (F) and groove (Gr) PDMS from 7 days of cultures were loaded at ~20 μg and visualised the denatured protein separation using Ponceau S staining. B) Targeted protein expression of MRTF-A, laminA/C, pERK and ERK are immunoblotted against antibodies. Westernblot also used to shows the absence of emerin protein in knockout clones, α-Tubulin represents as positive internal control. C) Quantitative values of protein expression of the indicated protein MRTF-A (top) and Erks (bottom), are calculated and compared in their relative fold change of targets compared to wild-type on plastic. Data is plotted from n=1 sample per group. The protein extract in each genotypic group is tested across three culture surfaces.

The nucleoplasmic MRTF-A of emerin knockout 1D1 and H5S clones remained stable expression similarly to wild-type controls with no difference in three cultured surfaces observed in hard plastic, PDMS substrates with/without pre-patterning topography. Interestingly, ERK1/2 levels were next sought to measure to represent in the protein levels upon knockout of emerin in HEK293 cells. The loss of emerin activates ERKs expression with an increase in relative fold change of ERK1/2 intensities from nuclear extracts of emerin depleted cells compared to wild-type grown on plastic-Fn coating.

The quantified level of ERKs in EMD^{KO}-1D1 clones showed a rise level to ~1.58-fold, 1.63-fold and 1.78-fold stimulation in plastic, flat and grooved substrates. The observation of ERKs in EMD^{KO}-H5S was found correlated link of activated level to ~1.65-fold, 1.83-fold and 1.89-fold, as observed in cells growing on Fn-coated surfaces of plastic, non-grooved, grooved PDMS, respectively. A gradual increase of ERKs upon an influence of micropatterned substrates was detected at about 15% and 6% with grooves in comparison with flat substrate in 1D1 and H5S clones, respectively.

As an unaffected nuclear MRTF-A level in response to emerin knockout clones assessed by westernblot analysis, the immunofluorescence assay was further examined to confirm their expressed intensities and indicated of nuclear localisation (Figure 5-18). The integrated intensities of MRTF-A tagging by CellProfiler where the MRTF-A signals overlapped with the nuclear architecture via DAPI staining were detected. The results from IF images exposed that the MRTF-A expression was not alter upon emerin depleted HEK293 cells.
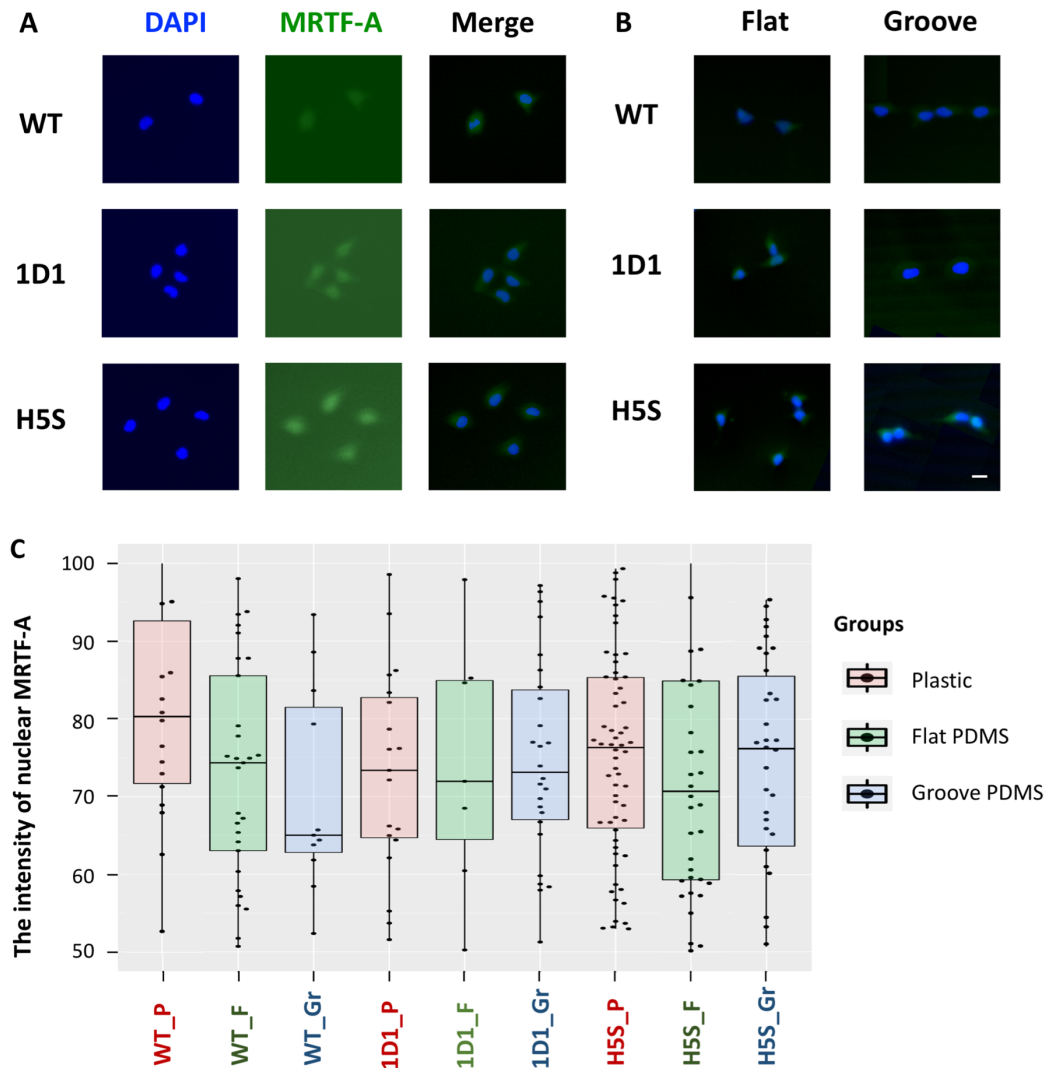
Figure 5-18. Immunofluorescence staining of MRTF-A localisation and intensities in wild-type (WT) and mutants (clone 1D1 and H5S) of EMD knockout models from HEK293 cells. A) Nuclear localisation of MRTF-A signalling of cells on TCP coated with Fn after 2 days of culture. The MRTF-A is then tracked after fixing followed by fluorescently labelled of individual channel uses DAPI for nucleus and MRTF-A conjugated with FITC for MRTF-A. B) Examples of MRTF-A accumulation and comparison between non-/patterning substrates. Scale bar ~20μm. C) MRTF-A intensities are measured and mainly aligned its localisation in the nucleus demonstrated similarity of nuclear MRTF-A intensities scored from around 200 nuclei in each tested group. Values are plotted from two independent experiments.

5.4 Discussion

The mechanical roles of inner nuclear membrane (INM)-destined integral membrane proteins and their functions have been often explored in research activities which are referred to as the "structural" and the "gene expression" hypotheses (see examples; Cohen et al., 2001; Osmanagic-Myers et al., 2015; Salpingidou et al., 2007; Samson et al., 2018). In this chapter, the type II INM protein emerin has focused on the study of cross-linked and interdependent regulation in the knockout of emerin modelled in human dermal fibroblasts and epithelia. The route of investigation not only provided insights into emerin self-contribution and an interface function of its domain binding partner but also elucidate the alteration of how a mutation in gene encoding emerin affects gene regulation in cytoskeletal elements. As such, emerin and other INM proteins are highly co-translationally inserted into the ER network and the LINC complex which establish a bridge between nuclear lamina to the actin cytoskeleton.

Supporting the structural hypothesis, experimental studies are accumulating results that emerin-null cells represent a complete knockout emerin expression in the degree of nuclear rigidity, also implicated in size, shape and measures of DNA contents which link to the cell-cycle division and progression. Such changes correspond to e.g. genome duplication and condensation of chromosomes in emerin-null cells, the images of fluorescently labelled DNA stoichiometry observed in EMD knockout fibroblast displayed variance that a delayed cell division occurred in one of tested EMD mutant (namely B2 clone) with no observation of a newly formed nucleus with the timing of nearly 48 hours. However, DNA content distribution appeared regular in EMD^{KO}-C3 which is similar to wild-type (as shown in Figure 5-3). It has also been found that embryonic stem cells lacking lamin A/C and or emerin lost pluripotency and ability of differentiation under retinoic treatment (Smith et al., 2017). On the contrary, emerin and A-type lamin-deficient mouse fibroblasts had a significantly higher fraction of polyploidal nuclei as analysed by flow cytometry compared to cell nucleus distribution in immortalised cells (Lammerding et al., 2005). The image analysis from emerin-null HEK293 cells appeared normal distribution of DNA content with no difference between wild-type and mutants (Figure 5-8). So that, the role of emerin in cell cycle stage is needed for further studies that allow determine the change of NE

material properties during duplication. A case reported by Dubinska-Magiera et al. (2019), provided evidence of the role of emerin which interacting mitotic spindle microtubules and invagination sites linking centrosomes during mitosis, together with associated membrane proteins to condensing chromatin using laser confocal microscopy, GFP-emerin and fluorescently marked emerin. This finding illustrated an association of emerin distribution in a culture model in HeLa cells and some examples of deletion mutants. The presence of emerin fraction at mitotic spindle microtubules and centrosomes which is found entering early mitosis from prophase, prometaphase and metaphase. In anaphase cells, a major emerin fraction follows "core-regions" on chromatin and condensing chromatin with a small amount of bound emerin in centrosomes. The same study also indicated that emerin interacting proteins; the main nuclear lamina-A type lamin and the chromatin associated BAF in participate sharing interface features and distribution in cell-cycle dependent recruitment of membranes to chromatin at the onset of mitosis. In addition, some EMD mutants were generated which observed fragmented nuclei or structural DNA/chromatin outside the nucleus. In consistent with the results as determined by the DNA content (see Figure 5-3), the resultant from emerin-deficient cells affecting nuclear characteristics or phenotypes vary and are mutant dependent. It is more likely that depleted emerin-expressing cells cause quiescence, rather than more severe negative impact such as apoptosis, along with minor differences in cell cycle phases. Four cases studied of the emerin deletion mutants from Dubinska-Magiera and co-worker, demonstrated variable levels of cellular phenotypes: abnormal, cut and apoptotic and cell phase in represented deletion mutants (E70, E176, E70-140 and E1-254) – position of amino acid residues where it was disrupted in emerin-expressed cells. It was found that full-length deletion of emerin protein (E254 also known E1-254) had around 10% of mild abnormality with a declined number of cells in S and G2 phases. While all three partial deletion mutants resulted in a larger scale of abnormal features. For general control of mitotic entry and exit, E70 mutant exhibited a lower population in the sub-G0 phase, and E70-140 gave rises in G0/G1 and phases but decreased at the later stage in G2 phage. Indeed, a more population of cells abnormality had detected in three partly mutations by around half of the cell pooled. Combining all the above report with the results from EMD^{KO}-clones tested in hTERT-BJ1 cells are potentially enough to delay cell

cycle progression. However, the impact is varying due to the site of emerin mutation. Especially, the experimental tested in this chapter using knockout cells at residue 15-254, displayed no statistical differences between emerin mutants and control which correlated to the finding observed in E254. It was also confirmed that lacking expression of emerin is unlikely to cause apoptosis (Lammerding et al., 2005), along with minor issues in nuclear division differences during cell phase (Dubinska-Magiera et al., 2019). An in vivo study supported by Ozawa et al. (2006), both emerin-null mice and the double knockout with additional lamin A/C have similar weights and are not significantly affected at post-development defects.

Next, the assessment of size and shape of individual nuclei that were positioned and attributed to local changes in membrane rigidity and implying chromatin's compaction. Upon emerin depletion during fibroblast's growth, nuclear area increases with a more circular shape as shown in decreased measurement of the analysed shape's aspect ratio in cells on flat culture. Therefore, the nuclear enlargement in emerin-depleted cells was also observed on grooved surface, while the shape factor deviates from a circular to bounding ellipse was influenced by micropatterned-tracking cell nucleus alignment (Figure 5-5), along with nuclear deformability in which resulting in a more elongated shape using mutants with microscale-topography. This is consistent with reports of nuclear deformation which led to an increase in nuclear size driven oval shape upon lacking emerin expression, characterised by lung adenocarcinoma (Kobayashi et al., 2018), ovarian epithelial cancer cells (Watabe et al., 2021) and mouse embryonic fibroblasts (Lammerding et al., 2005). Emerin mutants in HDFs, combined with micropatterns suggested that Q133H and P183H mutations influence nuclear deforming it to its characteristic ellipsoid shape in 15 μm patterns, as confined structure and altered nuclear strength in 10 μm patterns became more pronounced differences in adaptive nuclear deformation (Fernandez et al., 2022). The same finding by Lammerding et al. (2005), indicated that there was an increased in size and roundness of nuclear membrane, analysed by lower values of the nuclear length/width ratio and contour ratio (4π x area/perimeter^2) during suppression of emerin in fibroblasts. Supporting the outlined morphology, nuclear emerin can alter size or shape by cell type-specified. Apart from mild effect of nucleus size variation, an over 3-fold increase in ovarian epithelial cancerous cells

(Malpica et al., 2004; Vang et al., 2009; Ramalingam, 2016) whereas smaller nuclear area was found in breast cancer cells (Liddane et al., 2021). Following the trend observed in Figure 5-7, the shape fluctuations of emerin-null cells in HEK293 were detectable without change in relatively nuclear aspect ratio. For the size-wise nuclear area, a wide range of these cells were crowded, unevenly distributed nuclei driven the measurement was not reached.

Taken together, the impact of emerin-null cells reflected fluctuations of nuclear morphology. Some of degree of proliferation or chromatin protrusion has been shown to validate the deformation-driven motility and extensive membrane expansion. Most recent researches often compare the loss of emerin with lamin A/C, which have shared features but emerin had a much weaker impact on nuclear stability and integrity. Loss of function in lamin A/C mutants often leads to emerin mislocalisation affecting distorted nuclear membranes and shedding of cell-nuclear compartmentation (Sullivan et al., 1999; Raharjo et al., 2001). There was evidence by Reis-Sobreiro et al. (2018), informed that emerin depletion promotes nuclear instability and is widespread in prostate cancerous cells and increased metastatic sites which are confirmed by metastatic cells of epithelial origins. The nuclear rupture is very rare due to lack of emerin, no difference observed in fibroblasts (Lammerding et al., 2005), a case example of appeared DNA damage in highly expressed emerin tissue detected in skeletal myoblasts (Earle et al., 2020). However, chromatin protrusion (or nuclear blebs) in emerin knockout cells has found less severity than in lamin A/C mutants. An article from Earle's group, reported the prevalence of chromatin protrusion and elongated myonuclei, consistent with clinical translating reports from patients with laminopathy (Tan et al., 2015) and Lmna KO mice (Gnocchi et al., 2011). Beyond NE proteins and proliferation, stretch-induced proliferation was examined as its mechanobiological beneath the inner nuclear proteins, emerin and lamin A/C. The proliferating VSMCs cells had significantly increased in emerin- and lamin A/C-target siRNA in response to 5%-15% cyclic stretch, with more pronounced under 15% stimulation (Qi et al., 2016). The absence of emerin under strain application at 3%, 5% and 10% biaxial strain in fibroblasts confirmed that no significant effect on apoptotic cells (Lammerding et al., 2005).

Mechanisms based on emerin scaffolds are known to contribute to gene expression patterns via the direct interaction of emerin with lamin A/C or BAF complex formation. Lamin A/C interactions with emerin, the NE protein whose anchorage at the nuclear rim could belong to the nuclear lamina and further regulate the gene expression (Brachner & Foisner, 2011). Other gene-regulatory partners BAF utilise emerin scaffolds for their mediated activities involved in chromatin remodelling through its ability to link DNA regions and to binding interaction at the core histone H3 (Maraldi et al., 2006; Montes de Oca et al., 2005). Thus, the interaction of emerin as a support role for the complex inside the nucleus could influence on altered gene expression by chromatin remodelling complexes (CRCs) and histone deacetylases (HDACs), in turn recruited by transcriptional regulators (Chau & Wang, 2003). In this study, the lack of influences of emerin-null cells as models emphasise disruption of the nucleoplasmic region of emerin that affect the level of productivity and stability. The qRT-PCR experiments detected Lmna expression differences around half production in both emerin mutation tested in BJ1 and HEK293 cells with a similarity across three cultured surfaces in plastic, flat and grooved-Fn coat substrates as compared to normal expression in wild-type cells. In addition, westernblot analysis confirmed reduced expression of lamin A/C in BJ1-hTERT cells in the absence of emerin signal in either EMD[KO]-C3 clone or EMD[KO]-B2 clone. Compared with lamin A/C-deficient cells in emerin synthesis, it has been reported that an increased intensity and upper band of emerin was measured during laminA/C suppression conditions in combination with mevinolin treatment which used to induce an upstream production of a precursor protein prelamin A. The higher accumulation of emerin was found to increase as correlated to the level of prelamin A observed in human skin fibroblasts, HeLa and HEK293 cells (Cenni et al., 2020). In addition to emerin binding partner BAF – a conserved protein involved in chromatin remodelling, the lack of emerin regulating BAF expression was shown to significantly decline to 0.7-fold on plastic, 0.57-fold on flat PDMS and 0.39-fold on grooved PDMS in Banf1 expression of emerin knockout BJ1 clones normalised to wild-type grown on plastic culture. The onset of emerin-BAF complex could likely decrease the affinity of BAF-DNA interaction (Park et al., 2015), the resultant of soft material and topographic pattern guiding emerin knockout BJ1 candidates were more pronounced when the cell nucleus is forced under mechanical stress. A report from Snyers et al. (2022),

suggested that mutation of emerin strongly conveys its potential to disrupt BAF accumulation with topological/oriented defects at the core region. Next, the point in emerin interaction to HDAC3 provides the existence of crosstalk between HDAC3, lamin A/C and BAF molecular association under emerin supply regulating their control inside the nucleus. Emerin related to one of chromatin-modifying complexes, so-called the nuclear co-repressor (NCoR) complex which is an HDAC3-containing complex, providing a mechanism by which loss of emerin might be connected to repressed chromatin and consequent to decreased heterochromatin formation (Holaska & Wilson, 2007). The gene expression data from cells lacking emerin impact HDAC3 expression by reduced production. Emerin-null BJ1 cells declined levels of HDAC3 ~0.47-fold confirmed by two EMD-knockout clones in plastic adhesive surface coating with Fn. An influence of soft matrices resulted in a 24% and 17% decrease in HDAC3 levels of normally expressed EMD in wild-type progenitor on non-patterned and microgrooved patterning PDMS-Fn coated islands, respectively. When the expression of HDAC3 was measured, normalised to GAPDH and compared their relative fold-change to wild-type cells grown on hard surface (TCP-coated area). These reduced HDAC3 expression subsequently enrichment of HDAC3 levels equates to no more than 0.17-fold higher HDAC3 on PDMS cultures with/without topography compared to plastic rigid control cultured EMD^{KO}-clones. A similar trend of observation in HEK293 cells, the lack of emerin caused a lower HDAC3 level in the range of 41% to 52% across three cultured surfaces tested, the difference between soft and rigid surfaces is noted when wild-type cells were grown on plastic in comparison with PDMS substrates. Evidence provided by Demmerle et al. (2012), support the role of emerin-HDAC3 binding in regulating HDAC3 activity. This finding suggested that mutation of emerin inhibited HDAC3 activity while an enrichment of HDAC3 was found at 2.7-fold activation subjected to wild-type emerin-bound HDAC3. It was also found that localisation of HDAC3 is less at the nuclear lamina under emerin-depleted conditions. According to changes in HDAC3 levels, epigenetic status of H4K5 acetylation which is the preferred target of the NCoR complex followed its activation with few of the previous publications (Demmerle et al., 2012; Collins et al., 2017). A case reported by Collins et al. (2017), indicated that emerin-null myogenic progenitors enhanced levels of H4K5ac nearly 2-fold via westernblot analysis. This finding also confirmed that a stimulated statue was subjected to

HDAC3 activity related to emerin depletion by treatment with an HDAC3-specific activator using Theophylline. Treatment with theophylline caused a 54.9% and 35% reduction in emerin-null cells and wild-type myoblasts, respectively. Several lines of evidence demonstrate the alteration of a coordinated process link to HDAC3-binding emerin mutants dependent upon epigenetic mechanisms in response to lacking emerin signals. Emerin-null cells display similar epigenetic features as those seen in the loss of HDAC3 resulting in increased H3K9ac, H3K4me3, but decreased H3K9me2/3 and H3K27me3 levels (Bhaskara et al., 2010; Demmerle et al., 2012; Marano & Holaska, 2022).

An increasing evidence suggested that the ERK pathway and its upstream p38 MAPK signalling are upregulated in emerin-null cells and exhibited stronger effects in laminA/C mutants (Favreau et al., 2008; Koch & Holaska, 2012). A biphasic ERK regulates cell progression, depending on whether ERK is activated or inhibited. ERK activation is required for cell proliferation whereas ERK inhibition is necessary for differentiation to initiate myogenesis (Tiffin et al., 2004; Jo et al., 2009; Yokoyama et al., 2007). In the experimental system, quantitative analysis of ERK expression and activated ERK kinases by phosphorylation are evaluated in emerin-null cells association to ERK activity. In BJ1-CRISPRko EMD clones, ERK expression detected via qRT-PCR analysis displayed there were unaffected in ERK1/2 level in immortalised fibroblasts in the absence of emerin across all tested clones and surface cultures. BJ1-hTERT fibroblasts downregulated for emerin were further accessed in the phosphorylated stage, westernblot results revealed that phosphorylation and nuclear translocation of ERK1/2 were significantly enhanced in the range between 1.3-fold to 1.7-fold activation relative to ERKs levels for normalisation in two EMD knockout clones on non-patterned Fn-coated substrates. In adding microgrooved surface cultures, the activated pERK/ERK levels were promoted by 56-82% stimulation (which referred by over 2-fold increase), which equates to a similar activated of phosphorylation in cells on TCP in comparison to EMD deletion without grooves. In line with this agreement, the activated phosphorylated ERK1/2 was observed by around 2-fold and 3-fold in hearts from EMD knockout mice and Lmna knockout mice, respectively (Muchir et al., 2007). A few findings confirmed ERK activation by treatment with ERK inhibitors in emerin-null myogenic progenitors. Emerin-null cells treated with either U0126 or

PD98059 caused approximately 70% reduction in pERK levels (Collins et al., 2017). Supporting this hypothesis, treatment with p38 MAPK-specific inhibitor SB203580 reduced p-p38 MAPK levels by 66% (Koch & Holaska, 2012). Next, the qRT-PCR analysis revealed that ERK1 expression was statistically significantly increased by an average of 2.6-fold and 2.9-fold when two of EMD-null HEK293 clones were grown on flat and grooved surfaces, respectively. However, the ERK2 expression in the gene level was not altered in EMD-null cells observed in HEK293 samples. The protein examination of activated ERKs was measured by westernblot analysis and exhibited that expressing EMD mutants from HEK293 cells resulted in 1.73-fold and 1.84-fold induced activation of ERK1/2 on flat and groove PDMS compared to wild-type normally expressed emerin. Supporting these activated ERKs, it was also described that a gradient of activation and diffuse fluorescence pattern of ERK1/2 was more intense and predominantly located in the nucleus when the test was performed in the cells and mice without emerin (Muchir et al., 2007). The westernblot results did not show a signal of ERK phosphorylation when the tests were carried out in HEK293 cells, there was also reported that pERK expression was not detectable in wild-type of HeLa cells and weakly (~8% of nuclei) from HeLa cells treated with EMD siRNA (Muchir et al., 2009).

The transcription factor SRF (serum response factor) was lastly focused as it represents the convergence point to couple gene transcription to growth factor associated with Rho GTPase-actin and Ras-ERK signalling (Gineitis & Treisman, 2001; Miralles et al., 2003). The SRF recruits two families of coactivators, the TCFs family of ETS domain proteins (Elk-1, Elk-3 and Elk-4) and the MRTFs to toggle between regulating cell proliferation and orchestrating actin cytoskeletal and contractile movement (Xie, 2014). The knockout cells expressing emerin, combined with gene expression analysis via qRT-PCR technique; TCFs dependence of a complex of transcription factors linked to Ras-ERK activities including Elk-1 and Elk-4. These genes were highly expressed in EMD mutants from BJ1 fibroblasts similar to those in HEK293 of EMD^KO-cells. The results revealed that loss of emerin triggered ~2.5-fold upregulation of both Elk-1 and Elk-4. In agreement with this, the expression of Elk-1 and Elk-4 was enhanced by 2-fold to 3-fold when HeLa cells were treated with EMD or Lmna siRNAs (Muchir et al., 2009). Supportive evidence provided by Esnault et al. (2014), illustrated the role of TCF-dependent signature

overlap with Elk1-SRF targets in HeLa cells that were defined by ChIP-chip and ERK-dependent genes activated serum responsive manner in fibroblasts. However, the qRT-PCR displayed expression of Elk-3 declined by around 50% by EMD^{KO}-cells in either fibroblasts or epithelia (tested in HEK293 cells). The result is unsurprised as Elk-3 (also known as Net), was found as a transcription inhibitor (for reviews or case studies see Sharrocks et al., 1997; Wasylyk et al., 1998). The study by Ducret et al. (2000), suggested that Net transcriptional activity suppressed transcription. Increasing the amount of Ras can stimulate Net activity, examined by luciferase reporter assay. For the transcriptional activity of MRTF-A (or MKL1) regulated by emerin, immunoblotting results from nucleoplasmic extracts in EMD knockout cells displayed that relative expression of MRTF-A was dramatically decreased by nearly 70% observed in fibroblasts lacking emerin in comparison to normally expressed emerin in wild-type control. The protein expression level of MRTF-A showed similar expression when the cells were grown in plastic, flat and grooved PDMS materials with no difference between soft or adding topography and hard surface cultures. Several publications reported in agreement with the data in this study reverse the focal adhesion defects reported in EMD^{KO} fibroblasts which further related to a constitutively active form of MRTF-A/SRF-dependent gene expression manner (Willer & Carroll, 2017). Supporting evidence in the aspect of MRTF-A subcellular localisation, dominant mutations in EMD or Lmna are driven to impaired nuclear translocation of MRTF-A in fibroblasts and myoblasts (Sidorenko & Vartiainen, 2019; Le Dour et al., 2022). Collectively, a case study by Ho et al. (2013), investigated the role of emerin regulates nuclear actin polymerisation and transcriptional activity of MRTF-A in emerin-deficient and Lmna-null cells. An ectopic increase expression of emerin is markedly improved nuclear translocation of MRTF-A tested in Lmna mutants. Meanwhile, emerin mutants were unable to bind actin and failed to restore MRTF-A translocation into the nucleus. Taken together, the same study provided the correlation between MRTF-A and ERK1/2 activity. Inhibition of the ERK1/2 using treatment of Lmna and EMD mutant mice with MAPK inhibitors, subsequently induced nuclear localisation of MRTF-A. These indications supported the results of activated phosphorylation of ERK1/2 in the absence of emerin affected to reduced nuclear localisation of MRTF-A by increasing its nuclear export.

5.5 Conclusion

The molecular pathway characterised the cell behaviour changes upon low mechanical force conditions in the emerin knockout clones was proposed which is essential to fulfill understanding in cell mechanics. The illustration in the results of signal transduction revealed how mechanical switches influence the nuclear machinery functions including emerin linked to nuclear actin binding complexes and chromatin, activities and translocation of transcription factors, and changes in some of key molecular regulators by downstream and upstream signalling.

Using such cell-bioengineered tools, the distinct and overlapping effects of nuclear regulatory proteins and mechanical forces in the cellular microenvironment contribute to changes in cell shape including the degree of spreading. These effects regulated by cell shape were dependent on intracellular contractile force generation via RhoA-directed MRTF-A translocation while, an increase in the cell spreading correlated directly with the abrogation of cytoskeletal complexes and links to MAPK/ERK signalling regulated traction force generation. The results of nuclear localisation of MRTF-A and TCFs by associating with SRF revealed that inhibited MRTF-A accumulation under the regulation of cellular contractility whereas, activated Elk-1 and Elk-4 expression of TCFs which promote hyperproliferative activities of cell spreading.

CHAPTER 6 CONCLUSION

6.1 Closing remarks

Patients with severe skin injuries rely on the use of tissue engineered skin due to insufficient donor tissue and a lack of adequate regenerative characters (Sheikholeslam, 2021). Tissue engineering has emerged as a revolutionary field that combines cell interaction, scaffolds, biomaterials, and biologically active ingredients to create functional tissues (Eldeeb et al., 2022). Local cells in the skin including dermal fibroblasts and epithelia display remarkable plasticity and can undergo reprogramming or functional changes depending on their environment (Liu et al., 2012; Tata et al., 2021; Salminen, 2023). In this thesis, cell-based biomaterials incorporated into tissue engineering approaches were developed to offer tissue-engineered skin regenerative materials that can effectively translate to clinical applications in a proper cellular microenvironment. However, the mechanisms of cellular mechanotransduction by which cells convert mechanical force signals from microenvironmental cues into biochemical signals to regulate cell functions remain incompletely understood. To overcome this challenge, the cell scaffolds were cultured under dynamic microenvironments generated by mechanical stretching (chapter 3) and gene engineering (chapter 4) for mechanobiological studies of networks of mechanical switches and coupled to all regions of the cell nucleus (chapter 5).

A global overview of the cell-based biocompatible scaffold with applied tissue engineering to regulate cell motility via mechanosensitive Rho GTPase pathway and ERK signalling cascade was major lines to investigate the mechanotransduction of dermal fibroblasts and epithelia (as shown in Figure 6-1). Combinatorial tissue engineering approaches were applied to optimise a microenvironment favour of cells with biomaterial cues that are influence by internal material properties (e.g. topography, surface charge, scaffold adhesion, and mechanical properties) and external mechanical force application via stretching systems. A detailed summary of each tissue engineering approach used in the following;

I, Material-controlled cell geometry via micropattern topography to guide cell alignment under anisotropic mechanical regulation of cell shape.

II, Surface modification that used a combination of plasma treatment to increase the hydrophilicity of scaffold and ECM (i.e. fibronectin) coating for providing an efficient adhesion of cell-ECM interactions

III, Mechanical manipulation in the nucleus was reduced by inhibition of emerin linked to actin binding complex via CRISPR/Cas9 gene editing tool.

IV, Stretch-activated growth that applied force to passively pull the cells.
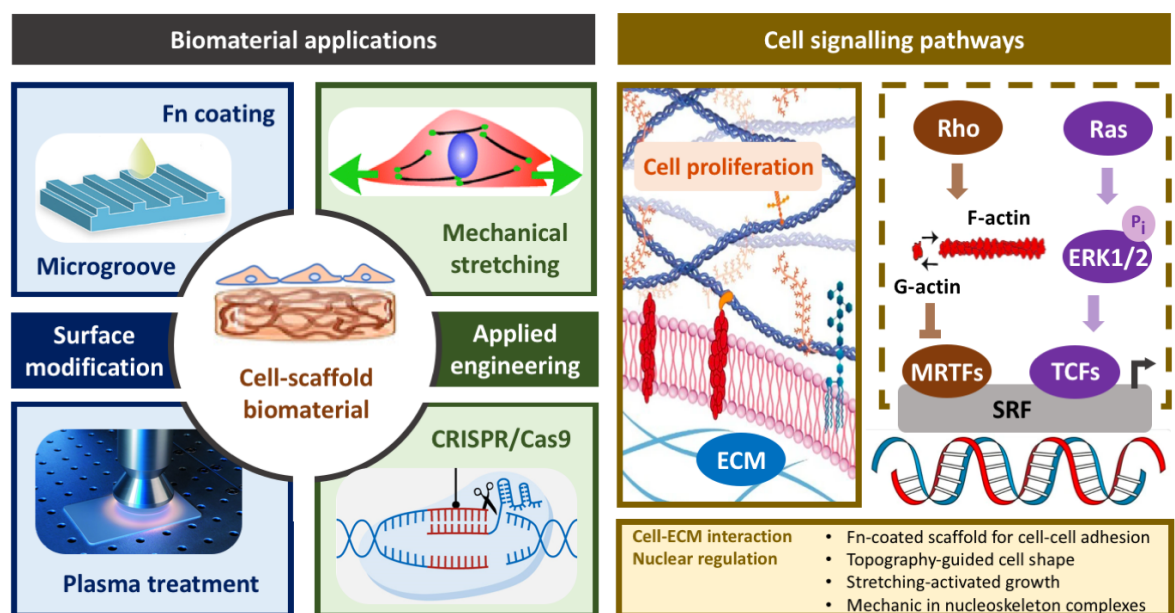
Figure 6-1. Integration of biomaterial strategies used in this research project and signalling cascades in Rho-GTPase and Ras/MAPK-dependent manner. For cell-scaffold biomaterial in tissue engineering, biomaterial approaches used surface modification including soft lithography pre-pattern of substrate with grooves for guidance of cell shape/alignment and plasma treatment with ECM coating surfaces for adhesive properties. Two engineering approaches applied to manipulate the cell growth used mechanical stretching and CRISPR/Cas9 gene editing systems. A selected pathway highlighted the coaching in the nucleus linked to cytoskeleton under competitive binding site of SRF transcription co-factor at the action of MRTFs (MRTF-A/B) and TCFs (Elk-1, Elk-3 and Elk-4).

In a comparative study of cells under dynamic microenvironments, smart responsive biomaterials (in chapter 3) and engineered emerin knockout cell models (in chapter 4) represented the cellular environment under high and low mechanical forces. Mechanical coupling between the cell surface and the nucleus through transmembrane receptors and cytoskeletal filaments that connect to the nucleus, can convey mechanical signals to alter cell functions (Wang et al., 2009; Zhang and Habibovic, 2022). Mechanosensitive transcription factor MRTF-A activity is controlled by Rho GTPase signalling and has a profound effect on the dynamic balance of G-actin and F-actin formation (Esnault et al., 2014). Mechanical stimulation promotes nuclear entry of MRTF-A signalling. The results from varying mechanical properties of the cellular environment showed that the nuclear translocation of MRTF-A was dependent on the force-regulated microenvironment (Figure 6-2).
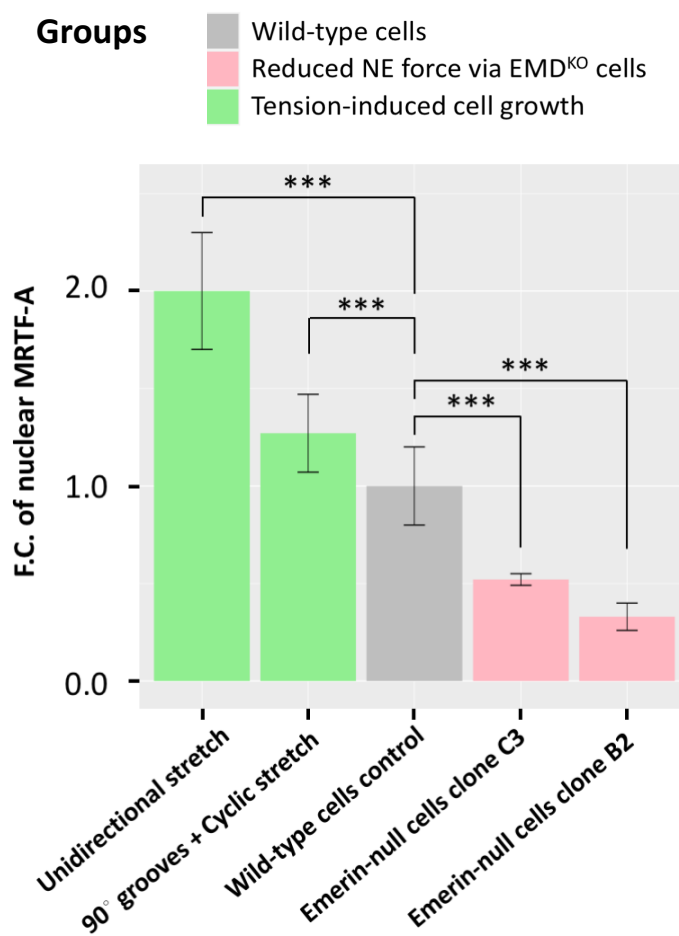
Figure 6-2. Emerin expression and stretch signals regulate nuclear translocation of MRTF-A in BJ1 dermal fibroblasts. Under high mechanical properties, stretched cells exposed to unidirectional stretch and cyclic stretch (5%, 0.05Hz and 90° grooves) had significantly increased nuclear accumulation of MRTF-A were around 2.0-fold and 1.3-fold, respectively. The fold change (F.C.) of nuclear MRTF-A in stretched cells were compared to non-stretched group. By lowering mechanical forces via emerin mutants, there was significant decreased nuclear MRTF-A to the range between 0.3-fold and 0.5-fold compared to cell-expressing emerin on Fn-coated tissue culture plastic (TCP) control. Unpaired two-samples t-test indicated as ***$p<0.001$. The results from at least three independent experiments were performed.

Under mechanical stimulation (chapter 3), mechanical stretching was applied to the cells on Fn-coated PDMS sheets and compared to non-stretched control, there was a significant in increase nuclear accumulation of MRTF-A to approximately 2.0-fold and 1.3-fold subjected to unidirectional stretch (4.2%) and cyclic stretch (5%, 0.05Hz and 90° grooves) for 24 hours, respectively. A prolonged stretching experiment for 48 hours displayed that nuclear MRTF-A had dramatically declined to the basal level of their normal expression compared to non-stretched groups. A temporal sequence of mechanical stimulation provides evidence of activated mechanobiological responses in a timely manner. Therefore, the cell adapted to microenvironment cues and quickly return to their original status to maintain tissue homeostasis. Under reduced force conditions via the generation of cell-lacking emerin (chapter 4 & 5), the nuclear export of MRTF-A was observed in emerin mutants confirmed by two knockout clones. All of characterisation of cell deformation on PDMS substrates were analysed on flat and grooved substrates and compared to TCP control.

Furthermore, the study for the role of emerin and mechanoresponsive elements examined the molecular pathways (chapter 5) in the following;

I, The activity of transcription factors TCFs including Elk-1, Elk-3, and Elk-4 that have shared transcription co-factor binding motifs at the SRF binding sites to MRTF-A. The real-time PCR showed that Elk-1 and Elk-4 were activated to around 2.0-folds and 2.6-folds in emerin knockout cells when the nuclear MRTF-A significantly declined.

II, The nuclear mechanoregulation under low mechanical properties via protein interactions of emerin including lamin A/C, BAF, and HDAC3 that contribute to changes in the nuclear lamina, DNA and acetylation of histone. Half expression of lamin A/C, BAF, and HDAC3 were detected by qRT-PCR assay which implied a lower nuclear stiffness.

This study has developed well-constructed multifunctional biomaterials with stretch stimuli or genetically modified driving microenvironmental cues for mechanobiological studies to improve outstanding outcomes in skin regeneration. The line of studying has addressed mechanoresponsive regulators that act as mechanical switches of gene/protein regulatory networks to control nuclear

deformation and cell mechanics in altering signal transduction-induced cytoskeleton filaments oraganisation, transcription factor activities, histone remodelling via acetylation status of HDAC3 levels and influence cell behaviours.

6.2 Future directions

Base on the project concept, cells based-scaffold with engineering approaches have been proposed to serve as bifunctional material composing therapeutic and regenerative ability. Cell-scaffold interactions have investigated in two-subtypes for skin equivalents that studied on behaviour of human dermal fibroblasts and epithelia cell-lines. Skin covers the body's entire external surface, the cells not only can be used by co-culturing as core structure for skin regeneration, but they can also be adapted to facilitate other applications via cell-cell interactions such as bone, nerve or vasculature systems for designable clinical translation outcomes. For the main focus of biomaterial view, stretch induced- or CRISPR-responsive PDMS biomaterials have created engineered platform carrying modification of phenotypic and regenerative characters of cells. In particular, signalling cascade induced cell motile including proliferation and contractility have been shown that deserve a future consideration of integration of complexity for the best possible functionalise biomaterial with a given propose. Examples of combined the generating biointerfaces science and engineering in this research project as following;

I, The use of CRISPR-responsive biomaterial with smart stimuli (i.e. stretching) to augment its advantage that unlock the biological and mechanical properties of the cellular microenvironment.

II, Developing of the CRISPR-multiplex system that can activate or inhibit expression of gene regulatory complex and the consequent phenotypic behaviours from a known effect in stretch-activated growth.

These tools have been exploit and hold promise as alternative biodegradable scaffold with biological/functional actives for tissue replacement and regeneration. This is open-window for clinical translation especially skin regeneration and would healing. Though significant progress has been made, there is still a need to explore these complex microenvironments, particularly in in vivo

study to defined microenvironment that compatibility and response to innate immune system to generating powers of organisation and self-repair.

Appendix I

CRISPR/Cas9 Transfection Delivery

Appendix I. CRISPR/Cas9 Transfection Delivery

A.1 Plasmid Vector Construction
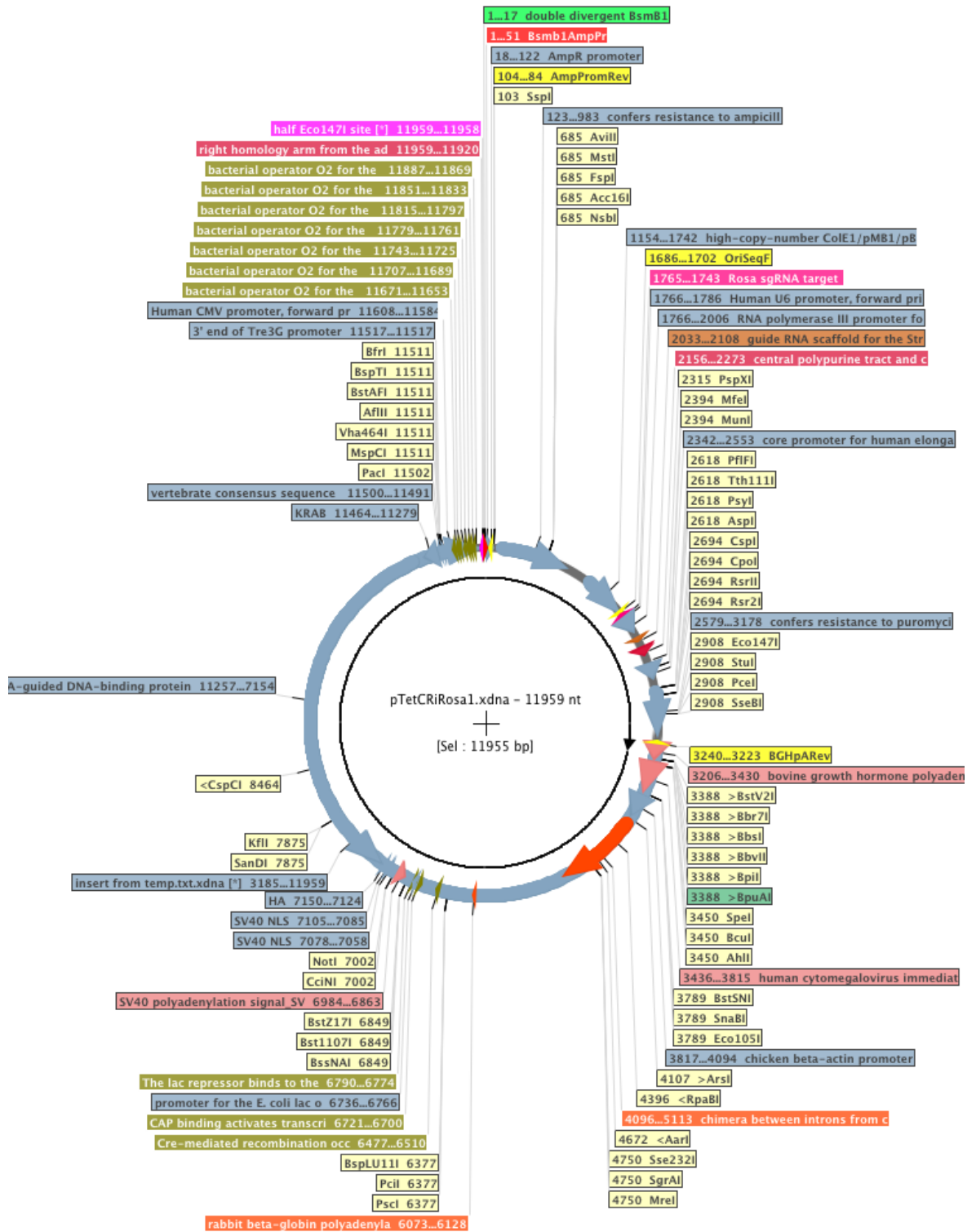
Figure A-1. Full graphic map of pTetCriRosa1 vector used to transfect the cells via CRISPRi system. The order and connection of sequence conformation were plots on Serial Cloner. The mainstream focus such as cloning site for AAVS1 (position 1-17) and EMD insertion site (position 2033-2108), sequence specific region for Puromycin resistance (position 2579-3178), KRAB (position11279-11464) and restriction enzyme cleavage sites (e.g. HINDIII) were highlighted.

A.2   Transfection efficiency in HEK293 cells via AAVS1 sgRNA
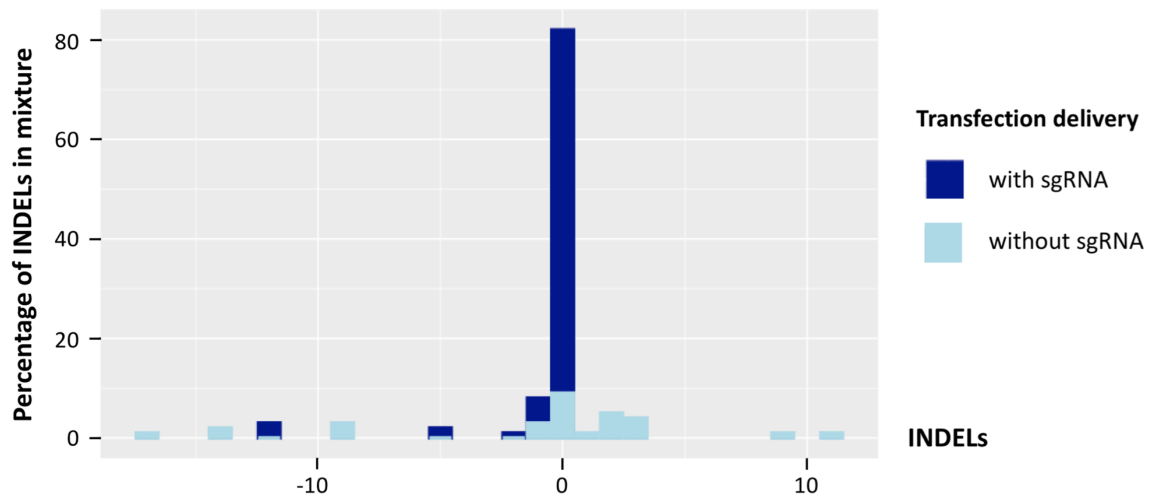
Figure A-2. Efficient transfection of HEK293 cells, delivered into AAVS1 transgene insertion site. The cells were transfected with core complex including mRNA encoding Cas9 and dCas9/KRAB plasmid together with AAVS1-sgRNA (dark blue) and without AAVS1-sgRNA (light blue) as a control.

A.3   PCR bands of monoclonal selection
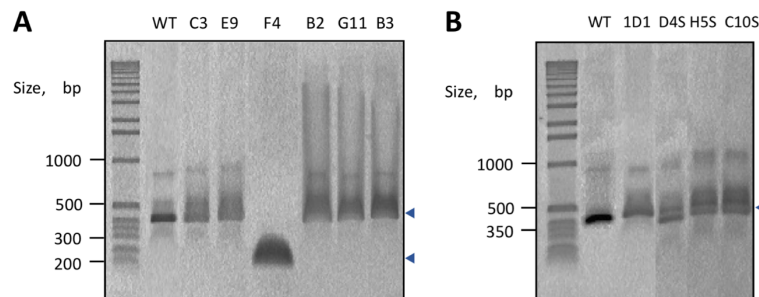
Figure A-3. PCR products after selection of transfected A) BJ1-hTERT B) HEK293 cells in 1% agarose gel/0.5x TBE buffer. The transfected cells were seeded at less than 1 cell/well in 96well-plate, expanded and gel extraction (arrow indicates the location of area bands for DNA sequencing). Abbreviation; WT, wild-type and EMD knockout clones (C3, E9, F4, B2, G11 and B3 for BJ1 cells and 1D1, D4S, H5S, C10S for HEK293 cells).

A.4 Selection and screening from the transfected HEK293 cells

Number	Clone	INDELs	Contribution	Sequence	
1	0E5	+1	36%	CTTTCGGATACCGAGCTGACCACCT	NTGCTGCGCCGGTACAACATCCCGCACGGG
		-21	28%	CTTTCGGATACCGAGCTGA------	--------------ACATCCCGCACGGGC
		-17	20%	CTTTCGGATACCG-----------	-----CGCCGGTACAACATCCCGCACGGGC
		-17	6%	CTTTCGGATACCGAGCTGACC----	-------------CAACATCCCGCACGGGC
		-17	1%	CTTTCGGATACCGAGC---------	-------CGGTACAACATCCCGCACGGGC
		-17	1%	CTTTCGGATACCGAGCTGA------	----------TACAACATCCCGCACGGGC
		-17	1%	CTTTCGGATACCGAGCTGACCAC--	--------------ACATCCCGCACGGGC
2	B3Y	-10	37%	CTTTCGGATACCGAGCTGACCACCT	----------GTACAACATCCCGCACGGGC
		+1	25%	CTTTCGGATACCGAGCTGACCACCT	NTGCTGCGCCGGTACAACATCCCGCACGGG
		-9	15%	CTTTCGGATACCGAGCTGACCACCT	---------GGTACAACATCCCGCACGGGC
		-20	3%	CTTTCGGATACCGAGCTGAC-----	---------------ACATCCCGCACGGGC
		+10	2%	CTTTCGGATACCGAGCTGACCACCT	NNNNNNNNNNTGCTGCGCCGGTACAACAT
		+5	2%	CTTTCGGATACCGAGCTGACCACCT	NNNNNTGCTGCGCCGGTACAACATCCCGCA
		-19	1%	CTTTCGGATACCGAGCTGACC----	---------------ACATCCCGCACGGGC
		-7	1%	CTTTCGGATACCGAGCTGACCACCT	-------CCGGTACAACATCCCGCACGGGC
3	1F3	+1	25%	CTTTCGGATACCGAGCTGACCACCT	NTGCTGCGCCGGTACAACATCCCGCACGGG
		-10	21%	CTTTCGGATACCGAGCTGACCACC-	---------GGTACAACATCCCGCACGGGC
		-12	13%	CTTTCGGATACCGAGCTGACCACCT	------------ACAACATCCCGCACGGGC
		0	10%	CTTTCGGATACCGAGCTGACCACCT	TGCTGCGCCGGTACAACATCCCGCACGGGC
		-12	9%	CTTTCGGATACCGAGCTG-------	-----CGCCGGTACAACATCCCGCACGGGC
		-12	9%	CTTTCGGATACCGAGCTGA------	------GCCGGTACAACATCCCGCACGGGC
		-10	9%	CTTTCGGATACCGAGCTGACCACCT	----------GTACAACATCCCGCACGGGC
4	1D1	-12	99%	CTTTCGGATACCGAGCTG-------	-----CGCCGGTACAACATCCCGCACGGGC
5	1F4	-21	40%	CTTTCGGATACCGAGCTGA------	---------------ACATCCCGCACGGGC
		-17	26%	CTTTCGGATACCG-----------	-----CGCCGGTACAACATCCCGCACGGGC
		0	11%	CTTTCGGATACCGAGCTGACCACCT	TGCTGCGCCGGTACAACATCCCGCACGGGC
		+1	7%	CTTTCGGATACCGAGCTGACCACCT	NTGCTGCGCCGGTACAACATCCCGCACGGG
		-17	4%	CTTTCGGATACCGAGC---------	--------CGGTACAACATCCCGCACGGGC
		-17	4%	CTTTCGGATACCGAGCTGACCAC--	---------------ACATCCCGCACGGGC
		-17	3%	CTTTCGGATACCGAGCTGA------	----------TACAACATCCCGCACGGGC
6	2D2	+1	83%	CTTTCGGATACCGAGCTGACCACCT	NTGCTGCGCCGGTACAACATCCCGCACGGG
		-4	9%	CTTTCGGATACCGAGCTGACCACC-	---TGCGCCGGTACAACATCCCGCACGGG
		-4	3%	CTTTCGGATACCGAGCTGACCA---	-GCTGCGCCGGTACAACATCCCGCACGGG
		-21	2%	CTTTCGGA-----------------	----GCGCCGGTACAACATCCCGCACGGG
		-18	1%	CTTTCGGA----------------	-GCTGCGCCGGTACAACATCCCGCACGGG
7	2H2	-4	41%	CTTTCGGATACCGAGCTGACCAC--	--CTGCGCCGGTACAACATCCCGCACGGG
		-1	40%	CTTTCGGATACCGAGCTGACCACC-	TGCTGCGCCGGTACAACATCCCGCACGGG
		-6	14%	CTTTCGGATACCGAGCTGACCACCT	------GCCGGTACAACATCCCGCACGGG
		-23	2%	CTTTC-------------------	---TGCGCCGGTACAACATCCCGCACGGG
8	2D6	+1	90%	CTTTCGGATACCGAGCTGACCACCT	NTGCTGCGCCGGTACAACATCCCGCACGGG
		-1	6%	CTTTCGGATACCGAGCTGACCACCT	-GCTGCGCCGGTACAACATCCCGCACGGG
		-36	1%	CTTTCGGAT----------------	--------------------CCGCACGGGC
		-18	1%	CTTTCGGAT----------------	--CTGCGCCGGTACAACATCCCGCACGGG
9	2G4	+1	82%	CTTTCGGATACCGAGCTGACCACCT	NTGCTGCGCCGGTACAACATCCCGCACGGG
		-1	13%	CTTTCGGATACCGAGCTGACCACC-	TGCTGCGCCGGTACAACATCCCGCACGGG
		+16	1%	CTTTCGGATACCGAGCTGACCACCT	NNNNNNNNNNNNNNNNTGCTGCGCCGG
		-36	1%	CTTTCGGAT----------------	--------------------CCGCACGGGC
		0	1%	CTTTCGGATACCGAGCTGACCACCT	TGCTGCGCCGGTACAACATCCCGCACGGGC
10	2D3	+2	78%	CTTTCGGATACCGAGCTGACCACCT	NNTGCTGCGCCGGTACAACATCCCGCACG
		0	17%	CTTTCGGATACCGAGCTGACCACCT	TGCTGCGCCGGTACAACATCCCGCACGGGC
		-35	1%	CTTTCGG-----------------	----------------ATCCCGCACGGGC
11	2B2	0	74%	CTTTCGGATACCGAGCTGACCACCT	TGCTGCGCCGGTACAACATCCCGCACGGGC
		+1	24%	CTTTCGGATACCGAGCTGACCACCT	NTGCTGCGCCGGTACAACATCCCGCACGGG

Figure A-4. Sanger sequencing of EMD knockout clones isolated from transfected HEK293 cells. Detailed sequences of distribution in 6 mutants, resulting frame deletion (expanded from Figure 4-14), 5 clones-containing wild-type (as highlighted in grey boxes) in mixture were discarded from further analysis. The 20nt-matching sgRNA sequence (blue) and PAM region (Top line).

A.5   Transfection efficiency via CRISPRko approach

Table A-1. The determination of transfection efficiency of sgRNAs-coupling CRISPR/Cas9 in editing the human cell lines. Detection of %INDELs represented in this table as a result from In Silico 'ICE' analysis.

Cell lines	The percentage of INDELs		
	normal media	5ug/ml of Puro^R-media (2nd Trypsinisation)	5ug/ml of Puro^R-media (4th Trypsinisation)
BJ1-hTERT	5%	52-54%	65%
HEK293	22%	81%	n.t.
MCF-7*	25%	91%	n.t.

*The transfected cells were performed for comparison in the panel of human cell lines transfection efficiency with this approach and sgRNA tested.

n.t.; Not tested

LIST OF REFERENCES

Agah, A., Kyriakides, T. R., Lawler, J. and Bornstein, P. (2002) 'The lack of thrombospondin-1 (TSP1) dictates the course of wound healing in double-TSP1/TSP2-null mice', *Am J Pathol,* 161(3), pp. 831-9.

Ahmed, W. W., Wolfram, T., Goldyn, A. M., Bruellhoff, K., Rioja, B. A., Moller, M., Spatz, J. P., Saif, T. A., Groll, J. and Kemkemer, R. (2010) 'Myoblast morphology and organization on biochemically micro-patterned hydrogel coatings under cyclic mechanical strain', *Biomaterials,* 31(2), pp. 250-8.

Albanna, M., Binder, K. W., Murphy, S. V., Kim, J., Qasem, S. A., Zhao, W., Tan, J., El-Amin, I. B., Dice, D. D., Marco, J., Green, J., Xu, T., Skardal, A., Holmes, J. H., Jackson, J. D., Atala, A. and Yoo, J. J. (2019) 'In Situ Bioprinting of Autologous Skin Cells Accelerates Wound Healing of Extensive Excisional Full-Thickness Wounds', *Sci Rep,* 9(1), pp. 1856.

Alves, N. M., Pashkuleva, I., Reis, R. L. and Mano, J. F. (2010) 'Controlling cell behavior through the design of polymer surfaces', *Small,* 6(20), pp. 2208-20.

Amitai, G. and Sorek, R. (2016) 'CRISPR-Cas adaptation: insights into the mechanism of action', *Nat Rev Microbiol,* 14(2), pp. 67-76.

Anderson, J. M. (1988) 'Inflammatory response to implants', *ASAIO Trans,* 34(2), pp. 101-7.

Andorko, J. I. and Jewell, C. M. (2017) 'Designing biomaterials with immunomodulatory properties for tissue engineering and regenerative medicine', *Bioeng Transl Med,* 2(2), pp. 139-155.

Astejada, M. N., Goto, K., Nagano, A., Ura, S., Noguchi, S., Nonaka, I., Nishino, I. and Hayashi, Y. K. (2007) 'Emerinopathy and laminopathy clinical, pathological and molecular features of muscular dystrophy with nuclear envelopathy in Japan', *Acta Myol,* 26(3), pp. 159-64.

Aszodi, A., Legate, K. R., Nakchbandi, I. and Fassler, R. (2006) 'What mouse mutants teach us about extracellular matrix function', *Annu Rev Cell Dev Biol,* 22, pp. 591-621.

Atcha, H., Davis, C. T., Sullivan, N. R., Smith, T. D., Anis, S., Dahbour, W. Z., Robinson, Z. R., Grosberg, A. and Liu, W. F. (2018) 'A Low-Cost Mechanical Stretching Device for Uniaxial Strain of Cells: A Platform for Pedagogy in Mechanobiology', *J Biomech Eng,* 140(8), pp. 0810051-9.

Aumailley, M., Bruckner-Tuderman, L., Carter, W. G., Deutzmann, R., Edgar, D., Ekblom, P., Engel, J., Engvall, E., Hohenester, E., Jones, J. C., Kleinman, H. K., Marinkovich, M. P., Martin, G. R., Mayer, U., Meneguzzi, G., Miner, J. H., Miyazaki, K., Patarroyo, M., Paulsson, M., Quaranta, V., Sanes, J. R., Sasaki, T., Sekiguchi, K., Sorokin, L. M., Talts, J. F., Tryggvason, K., Uitto, J., Virtanen, I., von der Mark, K., Wewer, U. M., Yamada, Y. and Yurchenco, P. D. (2005) 'A simplified laminin nomenclature', *Matrix Biol,* 24(5), pp. 326-32.

Ball, J. R. and Ullman, K. S. (2005) 'Versatility at the nuclear pore complex: lessons learned from the nucleoporin Nup153', *Chromosoma,* 114(5), pp. 319-30.

Banerjee, D., Vitelli, V., Julicher, F. and Surowka, P. (2021) 'Active Viscoelasticity of Odd Materials', *Phys Rev Lett,* 126(13), pp. 138001.

Barrangou, R., Fremaux, C., Deveau, H., Richards, M., Boyaval, P., Moineau, S., Romero, D. A. and Horvath, P. (2007) 'CRISPR provides acquired resistance against viruses in prokaryotes', *Science,* 315(5819), pp. 1709-12.

Bazzoni, G. and Dejana, E. (2002) 'Keratinocyte junctions and the epidermal barrier: how to make a skin-tight dress', *J Cell Biol,* 156(6), pp. 947-9.

Bengtsson, L. and Wilson, K. L. (2004) 'Multiple and surprising new functions for emerin, a nuclear membrane protein', *Curr Opin Cell Biol,* 16(1), pp. 73-9.

Berezney, R. and Coffey, D. S. (1977) 'Nuclear matrix. Isolation and characterization of a framework structure from rat liver nuclei', *J Cell Biol,* 73(3), pp. 616-37.

Berk, J. M., Tifft, K. E. and Wilson, K. L. (2013) 'The nuclear envelope LEM-domain protein emerin', *Nucleus,* 4(4), pp. 298-314.

Bershadsky, A., Kozlov, M. and Geiger, B. (2006) 'Adhesion-mediated mechanosensitivity: a time to experiment, and a time to theorize', *Curr Opin Cell Biol,* 18(5), pp. 472-81.

Bhaskara, S., Knutson, S. K., Jiang, G., Chandrasekharan, M. B., Wilson, A. J., Zheng, S., Yenamandra, A., Locke, K., Yuan, J. L., Bonine-Summers, A. R., Wells, C. E., Kaiser, J. F., Washington, M. K., Zhao, Z., Wagner, F. F., Sun, Z. W., Xia, F., Holson, E. B., Khabele, D. and Hiebert, S. W. (2010) 'Hdac3 is essential for the maintenance of chromatin structure and genome stability', *Cancer Cell,* 18(5), pp. 436-47.

Bhattacharjee, O., Ayyangar, U., Kurbet, A. S., Ashok, D. and Raghavan, S. (2019) 'Unraveling the ECM-Immune Cell Crosstalk in Skin Diseases', *Front Cell Dev Biol,* 7, pp. 68.

Bissell, M. J., Hall, H. G. and Parry, G. (1982) 'How does the extracellular matrix direct gene expression?', *J Theor Biol,* 99(1), pp. 31-68.

Bolotin, A., Quinquis, B., Sorokin, A. and Ehrlich, S. D. (2005) 'Clustered regularly interspaced short palindrome repeats (CRISPRs) have spacers of extrachromosomal origin', *Microbiology (Reading),* 151(Pt 8), pp. 2551-2561.

Bonakdar, N., Gerum, R., Kuhn, M., Sporrer, M., Lippert, A., Schneider, W., Aifantis, K. E. and Fabry, B. (2016) 'Mechanical plasticity of cells', *Nat Mater,* 15(10), pp. 1090-4.

Bondy-Denomy, J. and Davidson, A. R. (2014) 'To acquire or resist: the complex biological effects of CRISPR-Cas systems', *Trends Microbiol,* 22(4), pp. 218-25.

Brachner, A. and Foisner, R. (2011) 'Evolvement of LEM proteins as chromatin tethers at the nuclear periphery', *Biochem Soc Trans,* 39(6), pp. 1735-41.

Bradley, C. M., Ronning, D. R., Ghirlando, R., Craigie, R. and Dyda, F. (2005) 'Structural basis for DNA bridging by barrier-to-autointegration factor', *Nat Struct Mol Biol,* 12(10), pp. 935-6.

Bradshaw, A. D., Reed, M. J. and Sage, E. H. (2002) 'SPARC-null mice exhibit accelerated cutaneous wound closure', *J Histochem Cytochem,* 50(1), pp. 1-10.

Bressel, E. and McNair, P. J. (2002) 'The effect of prolonged static and cyclic stretching on ankle joint stiffness, torque relaxation, and gait in people with stroke', *Phys Ther,* 82(9), pp. 880-7.

Brouns, S. J., Jore, M. M., Lundgren, M., Westra, E. R., Slijkhuis, R. J., Snijders, A. P., Dickman, M. J., Makarova, K. S., Koonin, E. V. and van der Oost, J. (2008) 'Small CRISPR RNAs guide antiviral defense in prokaryotes', *Science,* 321(5891), pp. 960-4.

Brown, T. M. and Krishnamurthy, K. (2020) 'Histology, Dermis', *StatPearls.* Treasure Island (FL).

Bryant, D. M. and Stow, J. L. (2005) 'Nuclear translocation of cell-surface receptors: lessons from fibroblast growth factor', *Traffic,* 6(10), pp. 947-54.

Buganza Tepole, A. and Kuhl, E. (2013) 'Systems-based approaches toward wound healing', *Pediatr Res,* 73(4 Pt 2), pp. 553-63.

Cai, M., Huang, Y., Suh, J. Y., Louis, J. M., Ghirlando, R., Craigie, R. and Clore, G. M. (2007) 'Solution NMR structure of the barrier-to-autointegration factor-Emerin complex', *J Biol Chem,* 282(19), pp. 14525-35.

Cai, Y. and Sheetz, M. P. (2009) 'Force propagation across cells: mechanical coherence of dynamic cytoskeletons', *Curr Opin Cell Biol,* 21(1), pp. 47-50.

Caputa, G., Castoldi, A. and Pearce, E. J. (2019) 'Metabolic adaptations of tissue-resident immune cells', *Nat Immunol,* 20(7), pp. 793-801.

Caputo, A. T., Eder, O. M., Bereznakova, H., Pothuis, H., Ardevol, A., Newman, J., Nuttall, S., Peat, T. S. and Adams, T. E. (2021) 'Structure-guided selection of puromycin N-acetyltransferase mutants with enhanced selection stringency for deriving mammalian cell lines expressing recombinant proteins', *Sci Rep,* 11(1), pp. 5247.

Carroll, D. (2014) 'Genome engineering with targetable nucleases', *Annu Rev Biochem,* 83, pp. 409-39.

Cenni, V., Squarzoni, S., Loi, M., Mattioli, E., Lattanzi, G. and Capanni, C. (2020) 'Emerin Phosphorylation during the Early Phase of the Oxidative Stress Response Influences Emerin-BAF Interaction and BAF Nuclear Localization', *Cells,* 9(6).

Chau, B. N. and Wang, J. Y. (2003) 'Coordinated regulation of life and death by RB', *Nat Rev Cancer,* 3(2), pp. 130-8.

Chaudhuri, O., Parekh, S. H. and Fletcher, D. A. (2007) 'Reversible stress softening of actin networks', *Nature,* 445(7125), pp. 295-8.

Chaumet, A., Wright, G. D., Seet, S. H., Tham, K. M., Gounko, N. V. and Bard, F. (2015) 'Nuclear envelope-associated endosomes deliver surface proteins to the nucleus', *Nat Commun,* 6, pp. 8218.

Chavez, M., Chen, X., Finn, P. B. and Qi, L. S. (2023) 'Advances in CRISPR therapeutics', *Nat Rev Nephrol,* 19(1), pp. 9-22.

Chen, F. M. and Liu, X. (2016) 'Advancing biomaterials of human origin for tissue engineering', *Prog Polym Sci,* 53, pp. 86-168.

Chen, K., Vigliotti, A., Bacca, M., McMeeking, R. M., Deshpande, V. S. and Holmes, J. W. (2018) 'Role of boundary conditions in determining cell alignment in response to stretch', *Proc Natl Acad Sci U S A,* 115(5), pp. 986-991.

Chen, W. Y. and Rogers, A. A. (2007) 'Recent insights into the causes of chronic leg ulceration in venous diseases and implications on other types of chronic wounds', *Wound Repair Regen,* 15(4), pp. 434-49.

Chiquet, M., Renedo, A. S., Huber, F. and Fluck, M. (2003) 'How do fibroblasts translate mechanical signals into changes in extracellular matrix production?', *Matrix Biol,* 22(1), pp. 73-80.

Chu, V. T., Weber, T., Wefers, B., Wurst, W., Sander, S., Rajewsky, K. and Kuhn, R. (2015) 'Increasing the efficiency of homology-directed repair for CRISPR-Cas9-induced precise gene editing in mammalian cells', *Nat Biotechnol,* 33(5), pp. 543-8.

Ciobanasu, C., Faivre, B. and Le Clainche, C. (2012) 'Actin dynamics associated with focal adhesions', *Int J Cell Biol,* 2012, pp. 941292.

Clark, R. A. (1990) 'Fibronectin matrix deposition and fibronectin receptor expression in healing and normal skin', *J Invest Dermatol,* 94(6 Suppl), pp. 128S-134S.

Cohen, M., Lee, K. K., Wilson, K. L. and Gruenbaum, Y. (2001) 'Transcriptional repression, apoptosis, human disease and the functional evolution of the nuclear lamina', *Trends Biochem Sci,* 26(1), pp. 41-7.

Collins, C. M., Ellis, J. A. and Holaska, J. M. (2017) 'MAPK signaling pathways and HDAC3 activity are disrupted during differentiation of emerin-null myogenic progenitor cells', *Dis Model Mech,* 10(4), pp. 385-397.

Cong, L., Ran, F. A., Cox, D., Lin, S., Barretto, R., Habib, N., Hsu, P. D., Wu, X., Jiang, W., Marraffini, L. A. and Zhang, F. (2013) 'Multiplex genome engineering using CRISPR/Cas systems', *Science,* 339(6121), pp. 819-23.

Connelly, J. T., Gautrot, J. E., Trappmann, B., Tan, D. W., Donati, G., Huck, W. T. and Watt, F. M. (2010) 'Actin and serum response factor transduce physical cues from the microenvironment to regulate epidermal stem cell fate decisions', *Nat Cell Biol,* 12(7), pp. 711-8.

Cortese, B., Gigli, G. and Riehle, M. (2009) 'Mechanical Gradient Cues for Guided Cell Motility and Control of Cell Behavior on Uniform Substrates. Adv. Funct. Mater', 19, pp. 2961–68. doi:10.1002/adfm.200900918

Crisp, M. and Burke, B. (2008) 'The nuclear envelope as an integrator of nuclear and cytoplasmic architecture', *FEBS Lett,* 582(14), pp. 2023-32.

Cristea, S., Freyvert, Y., Santiago, Y., Holmes, M. C., Urnov, F. D., Gregory, P. D. and Cost, G. J. (2013) 'In vivo cleavage of transgene donors promotes nuclease-mediated targeted integration', *Biotechnol Bioeng,* 110(3), pp. 871-80.

Cullot, G., Boutin, J., Toutain, J., Prat, F., Pennamen, P., Rooryck, C., Teichmann, M., Rousseau, E., Lamrissi-Garcia, I., Guyonnet-Duperat, V., Bibeyran, A., Lalanne, M., Prouzet-Mauleon, V., Turcq, B., Ged, C., Blouin, J. M., Richard, E., Dabernat, S., Moreau-Gaudry, F. and Bedel, A. (2019) 'CRISPR-Cas9 genome editing induces megabase-scale chromosomal truncations', *Nat Commun,* 10(1), pp. 1136.

Curtis, A. S. and Varde, M. (1964) 'Control of Cell Behavior: Topological Factors', *J Natl Cancer Inst,* 33, pp. 15-26.

Das, S., Ippolito, A., McGarry, P. and Deshpande, V. S. (2022) 'Cell reorientation on a cyclically strained substrate', *PNAS Nexus,* 1(5), pp. pgac199.

de Araujo, R., Lobo, M., Trindade, K., Silva, D. F. and Pereira, N. (2019) 'Fibroblast Growth Factors: A Controlling Mechanism of Skin Aging', *Skin Pharmacol Physiol,* 32(5), pp. 275-282.

Dechat, T., Pfleghaar, K., Sengupta, K., Shimi, T., Shumaker, D. K., Solimando, L. and Goldman, R. D. (2008) 'Nuclear lamins: major factors in the structural organization and function of the nucleus and chromatin', *Genes Dev,* 22(7), pp. 832-53.

Deltcheva, E., Chylinski, K., Sharma, C. M., Gonzales, K., Chao, Y., Pirzada, Z. A., Eckert, M. R., Vogel, J. and Charpentier, E. (2011) 'CRISPR RNA maturation by trans-encoded small RNA and host factor RNase III', *Nature,* 471(7340), pp. 602-7.

Demmerle, J., Koch, A. J. and Holaska, J. M. (2012) 'The nuclear envelope protein emerin binds directly to histone deacetylase 3 (HDAC3) and activates HDAC3 activity', *J Biol Chem,* 287(26), pp. 22080-8.

Deolal, P. and Mishra, K. (2021) 'Regulation of diverse nuclear shapes: pathways working independently, together', *Commun Integr Biol,* 14(1), pp. 158-175.

DiPietro, L. A., Polverini, P. J., Rahbe, S. M. and Kovacs, E. J. (1995) 'Modulation of JE/MCP-1 expression in dermal wound repair', *Am J Pathol,* 146(4), pp. 868-75.

Distler, J. H. W., Gyorfi, A. H., Ramanujam, M., Whitfield, M. L., Konigshoff, M. and Lafyatis, R. (2019) 'Shared and distinct mechanisms of fibrosis', *Nat Rev Rheumatol,* 15(12), pp. 705-730.

Diz-Munoz, A., Fletcher, D. A. and Weiner, O. D. (2013) 'Use the force: membrane tension as an organizer of cell shape and motility', *Trends Cell Biol,* 23(2), pp. 47-53.

Doudna, J. A. and Charpentier, E. (2014) 'Genome editing. The new frontier of genome engineering with CRISPR-Cas9', *Science,* 346(6213), pp. 1258096.

Driskell, R. R., Lichtenberger, B. M., Hoste, E., Kretzschmar, K., Simons, B. D., Charalambous, M., Ferron, S. R., Herault, Y., Pavlovic, G., Ferguson-Smith, A. C. and Watt, F. M. (2013) 'Distinct fibroblast lineages determine dermal architecture in skin development and repair', *Nature,* 504(7479), pp. 277-281.

Duan, J., Lu, G., Xie, Z., Lou, M., Luo, J., Guo, L. and Zhang, Y. (2014) 'Genome-wide identification of CRISPR/Cas9 off-targets in human genome', *Cell Res,* 24(8), pp. 1009-12.

Dubinska-Magiera, M., Koziol, K., Machowska, M., Piekarowicz, K., Filipczak, D. and Rzepecki, R. (2019) 'Emerin Is Required for Proper Nucleus Reassembly after Mitosis: Implications for New Pathogenetic Mechanisms for Laminopathies Detected in EDMD1 Patients', *Cells,* 8(3).

Ducret, C., Maira, S. M., Lutz, Y. and Wasylyk, B. (2000) 'The ternary complex factor Net contains two distinct elements that mediate different responses to MAP kinase signalling cascades', *Oncogene,* 19(44), pp. 5063-72.

Duval, K., Grover, H., Han, L. H., Mou, Y., Pegoraro, A. F., Fredberg, J. and Chen, Z. (2017) 'Modeling Physiological Events in 2D vs. 3D Cell Culture', *Physiology (Bethesda),* 32(4), pp. 266-277.

Earle, A. J., Kirby, T. J., Fedorchak, G. R., Isermann, P., Patel, J., Iruvanti, S., Moore, S. A., Bonne, G., Wallrath, L. L. and Lammerding, J. (2020) 'Mutant lamins cause nuclear envelope rupture and DNA damage in skeletal muscle cells', *Nat Mater,* 19(4), pp. 464-473.

Edwards, J. (2013) 'Burn wound chronicity – myth or reality?', *Wounds UK*, 9(3), pp. 4-5

Eldeeb, A. E., Salah, S. and Elkasabgy, N. A. (2022) 'Biomaterials for Tissue Engineering Applications and Current Updates in the Field: A Comprehensive Review', *AAPS PharmSciTech*, 23(7), pp. 267.

Esnault, C., Stewart, A., Gualdrini, F., East, P., Horswell, S., Matthews, N. and Treisman, R. (2014) 'Rho-actin signaling to the MRTF coactivators dominates the immediate transcriptional response to serum in fibroblasts', *Genes Dev*, 28(9), pp. 943-58.

Evers, B., Jastrzebski, K., Heijmans, J. P., Grernrum, W., Beijersbergen, R. L. and Bernards, R. (2016) 'CRISPR knockout screening outperforms shRNA and CRISPRi in identifying essential genes', *Nat Biotechnol*, 34(6), pp. 631-3.

Fabry, B., Maksym, G. N., Butler, J. P., Glogauer, M., Navajas, D. and Fredberg, J. J. (2001) 'Scaling the microrheology of living cells', *Phys Rev Lett*, 87(14), pp. 148102.

Fairley, E. A., Kendrick-Jones, J. and Ellis, J. A. (1999) 'The Emery-Dreifuss muscular dystrophy phenotype arises from aberrant targeting and binding of emerin at the inner nuclear membrane', *J Cell Sci*, 112 (Pt 15), pp. 2571-82.

Favreau, C., Delbarre, E., Courvalin, J. C. and Buendia, B. (2008) 'Differentiation of C2C12 myoblasts expressing lamin A mutated at a site responsible for Emery-Dreifuss muscular dystrophy is improved by inhibition of the MEK-ERK pathway and stimulation of the PI3-kinase pathway', *Exp Cell Res*, 314(6), pp. 1392-405.

Fernandez, A., Bautista, M., Wu, L. and Pinaud, F. (2022) 'Emerin self-assembly and nucleoskeletal coupling regulate nuclear envelope mechanics against stress', *J Cell Sci*, 135(6).

Fletcher, D. A. and Mullins, R. D. (2010) 'Cell mechanics and the cytoskeleton', *Nature*, 463(7280), pp. 485-92.

Foley, R. A., Sims, R. A., Duggan, E. C., Olmedo, J. K., Ma, R. and Jonas, S. J. (2022) 'Delivering the CRISPR/Cas9 system for engineering gene therapies: Recent cargo and delivery approaches for clinical translation', *Front Bioeng Biotechnol*, 10, pp. 973326.

Forbes, S. J. and Rosenthal, N. (2014) 'Preparing the ground for tissue regeneration: from mechanism to therapy', *Nat Med*, 20(8), pp. 857-69.

Fowler, T., Sen, R. and Roy, A. L. (2011) 'Regulation of primary response genes', *Mol Cell*, 44(3), pp. 348-60.

Frantz, C., Stewart, K. M. and Weaver, V. M. (2010) 'The extracellular matrix at a glance', *J Cell Sci*, 123(Pt 24), pp. 4195-200.

Funakoshi, M., Tsuchiya, Y. and Arahata, K. (1999) 'Emerin and cardiomyopathy in Emery-Dreifuss muscular dystrophy', *Neuromuscul Disord,* 9(2), pp. 108-14.

Furusawa, T., Rochman, M., Taher, L., Dimitriadis, E. K., Nagashima, K., Anderson, S. and Bustin, M. (2015) 'Chromatin decompaction by the nucleosomal binding protein HMGN5 impairs nuclear sturdiness', *Nat Commun,* 6, pp. 6138.

Fu, Y., Foden, J. A., Khayter, C., Maeder, M. L., Reyon, D., Joung, J. K. and Sander, J. D. (2013) 'High-frequency off-target mutagenesis induced by CRISPR-Cas nucleases in human cells', *Nat Biotechnol,* 31(9), pp. 822-6.

Gaj, T., Epstein, B. E. and Schaffer, D. V. (2016) 'Genome Engineering Using Adeno-associated Virus: Basic and Clinical Research Applications', *Mol Ther,* 24(3), pp. 458-64.

Garg, A., Lohmueller, J. J., Silver, P. A. and Armel, T. Z. (2012) 'Engineering synthetic TAL effectors with orthogonal target sites', *Nucleic Acids Res,* 40(15), pp. 7584-95.

Gau, D. and Roy, P. (2018) 'SRF'ing and SAP'ing - the role of MRTF proteins in cell migration', *J Cell Sci,* 131(19).

Gautel, M. (2011) 'Cytoskeletal protein kinases: titin and its relations in mechanosensing', *Pflugers Arch,* 462(1), pp. 119-34.

Geiger, B., Spatz, J. P. and Bershadsky, A. D. (2009) 'Environmental sensing through focal adhesions', *Nat Rev Mol Cell Biol,* 10(1), pp. 21-33.

Giannone, G. and Sheetz, M. P. (2006) 'Substrate rigidity and force define form through tyrosine phosphatase and kinase pathways', *Trends Cell Biol,* 16(4), pp. 213-23.

Gilbert, L. A., Larson, M. H., Morsut, L., Liu, Z., Brar, G. A., Torres, S. E., Stern-Ginossar, N., Brandman, O., Whitehead, E. H., Doudna, J. A., Lim, W. A., Weissman, J. S. and Qi, L. S. (2013) 'CRISPR-mediated modular RNA-guided regulation of transcription in eukaryotes', *Cell,* 154(2), pp. 442-51.

Gill, S. E., Pape, M. C., Khokha, R., Watson, A. J. and Leco, K. J. (2003) 'A null mutation for tissue inhibitor of metalloproteinases-3 (Timp-3) impairs murine bronchiole branching morphogenesis', *Dev Biol,* 261(2), pp. 313-23.

Gineitis, D. and Treisman, R. (2001) 'Differential usage of signal transduction pathways defines two types of serum response factor target gene', *J Biol Chem,* 276(27), pp. 24531-9.

Gnocchi, V. F., Scharner, J., Huang, Z., Brady, K., Lee, J. S., White, R. B., Morgan, J. E., Sun, Y. B., Ellis, J. A. and Zammit, P. S. (2011) 'Uncoordinated transcription and compromised muscle function in the lmna-null mouse model of Emery- Emery-Dreyfuss muscular dystrophy', *PLoS One,* 6(2), pp. e16651.

Goldyn, A. M., Rioja, B. A., Spatz, J. P., Ballestrem, C. and Kemkemer, R. (2009) 'Force-induced cell polarisation is linked to RhoA-driven microtubule-independent focal-adhesion sliding', *J Cell Sci,* 122(Pt 20), pp. 3644-51.

Gomez, T. M. and Letourneau, P. C. (2014) 'Actin dynamics in growth cone motility and navigation', *J Neurochem,* 129(2), pp. 221-34.

Goult, B. T., von Essen, M. and Hytonen, V. P. (2022) 'The mechanical cell - the role of force dependencies in synchronising protein interaction networks', *J Cell Sci,* 135(22).

Goult, B. T., Yan, J. and Schwartz, M. A. (2018) 'Talin as a mechanosensitive signaling hub', *J Cell Biol,* 217(11), pp. 3776-3784.

Griffis, E. R., Craige, B., Dimaano, C., Ullman, K. S. and Powers, M. A. (2004) 'Distinct functional domains within nucleoporins Nup153 and Nup98 mediate transcription-dependent mobility', *Mol Biol Cell,* 15(4), pp. 1991-2002.

Gruenbaum, Y., Lee, K. K., Liu, J., Cohen, M. and Wilson, K. L. (2002) 'The expression, lamin-dependent localization and RNAi depletion phenotype for emerin in C. elegans', *J Cell Sci,* 115(Pt 5), pp. 923-9.

Gualdrini, F., Esnault, C., Horswell, S., Stewart, A., Matthews, N. and Treisman, R. (2016) 'SRF Co-factors Control the Balance between Cell Proliferation and Contractility', *Mol Cell,* 64(6), pp. 1048-1061.

Guest, J. F., Ayoub, N., McIlwraith, T., Uchegbu, I., Gerrish, A., Weidlich, D., Vowden, K. and Vowden, P. (2015) 'Health economic burden that wounds impose on the National Health Service in the UK', *BMJ Open,* 5(12), pp. e009283.

Guest, J. F., Ayoub, N., McIlwraith, T., Uchegbu, I., Gerrish, A., Weidlich, D., Vowden, K. and Vowden, P. (2017) 'Health economic burden that different wound types impose on the UK's National Health Service', *Int Wound J,* 14(2), pp. 322-330.

Guest, J. F., Vowden, K. and Vowden, P. (2017) 'The health economic burden that acute and chronic wounds impose on an average clinical commissioning group/health board in the UK', *J Wound Care,* 26(6), pp. 292-303.

Guilluy, C., Osborne, L. D., Van Landeghem, L., Sharek, L., Superfine, R., Garcia-Mata, R. and Burridge, K. (2014) 'Isolated nuclei adapt to force and reveal a mechanotransduction pathway in the nucleus', *Nat Cell Biol,* 16(4), pp. 376-81.

Gurtner, G. C., Werner, S., Barrandon, Y. and Longaker, M. T. (2008) 'Wound repair and regeneration', *Nature,* 453(7193), pp. 314-21.

Haase, K. and Pelling, A. E. (2013) 'The role of the actin cortex in maintaining cell shape', *Commun Integr Biol,* 6(6), pp. e26714.

Haft, D. H., Selengut, J., Mongodin, E. F. and Nelson, K. E. (2005) 'A guild of 45 CRISPR-associated (Cas) protein families and multiple CRISPR/Cas subtypes exist in prokaryotic genomes', *PLoS Comput Biol,* 1(6), pp. e60.

Harada, T., Swift, J., Irianto, J., Shin, J. W., Spinler, K. R., Athirasala, A., Diegmiller, R., Dingal, P. C., Ivanovska, I. L. and Discher, D. E. (2014) 'Nuclear lamin stiffness is a barrier to 3D migration, but softness can limit survival', *J Cell Biol,* 204(5), pp. 669-82.

Harper, C. E., Zhang, W., Lee, J., Shin, J. H., Keller, M. R., van Wijngaarden, E., Chou, E., Wang, Z., Dorr, T., Chen, P. and Hernandez, C. J. (2023) 'Mechanical stimuli activate gene expression via a cell envelope stress sensing pathway', *Sci Rep,* 13(1), pp. 13979.

Harrison, R. G. (1912). 'The cultivation of tissues in extraneous media as a method of morphogenetic study', *The Anatomical Record*, 6(4), pp. 181–193.

Hayashi, H., Kubo, Y., Izumida, M. and Matsuyama, T. (2020) 'Efficient viral delivery of Cas9 into human safe harbor', *Sci Rep,* 10(1), pp. 21474.

Heino, J. (2007) 'The collagen family members as cell adhesion proteins', *Bioessays,* 29(10), pp. 1001-10.

Hochmuth, R. M. and Waugh, R. E. (1987) 'Erythrocyte membrane elasticity and viscosity', *Annu Rev Physiol,* 49, pp. 209-19.

Ho, C. Y., Jaalouk, D. E., Vartiainen, M. K. and Lammerding, J. (2013) 'Lamin A/C and emerin regulate MKL1-SRF activity by modulating actin dynamics', *Nature,* 497(7450), pp. 507-11.

Hoffman-Kim, D., Mitchel, J. A. and Bellamkonda, R. V. (2010) 'Topography, cell response, and nerve regeneration', *Annu Rev Biomed Eng,* 12, pp. 203-31.

Holaska, J. M., Kowalski, A. K. and Wilson, K. L. (2004) 'Emerin caps the pointed end of actin filaments: evidence for an actin cortical network at the nuclear inner membrane', *PLoS Biol,* 2(9), pp. E231.

Holaska, J. M. and Wilson, K. L. (2007) 'An emerin "proteome": purification of distinct emerin-containing complexes from HeLa cells suggests molecular basis for diverse roles including gene regulation, mRNA splicing, signaling, mechanosensing, and nuclear architecture', *Biochemistry,* 46(30), pp. 8897-908.

Hsu, P. D., Scott, D. A., Weinstein, J. A., Ran, F. A., Konermann, S., Agarwala, V., Li, Y., Fine, E. J., Wu, X., Shalem, O., Cradick, T. J., Marraffini, L. A., Bao, G. and Zhang, F. (2013) 'DNA targeting specificity of RNA-guided Cas9 nucleases', *Nat Biotechnol,* 31(9), pp. 827-32.

Ingber, D. E. (2008) 'Tensegrity-based mechanosensing from macro to micro', *Prog Biophys Mol Biol,* 97(2-3), pp. 163-79.

Ishino, Y., Shinagawa, H., Makino, K., Amemura, M. and Nakata, A. (1987) 'Nucleotide sequence of the iap gene, responsible for alkaline phosphatase isozyme conversion in Escherichia coli, and identification of the gene product', *J Bacteriol,* 169(12), pp. 5429-33.

Iwadate, Y., Okimura, C., Sato, K., Nakashima, Y., Tsujioka, M. and Minami, K. (2013) 'Myosin-II-mediated directional migration of Dictyostelium cells in response to cyclic stretching of substratum', *Biophys J,* 104(4), pp. 748-58.

Jaffe, A. B. and Hall, A. (2005) 'Rho GTPases: biochemistry and biology', *Annu Rev Cell Dev Biol,* 21, pp. 247-69.

Jakutis, G. and Stainier, D. Y. R. (2021) 'Genotype-Phenotype Relationships in the Context of Transcriptional Adaptation and Genetic Robustness', *Annu Rev Genet,* 55, pp. 71-91.

Janeway, C. A., Jr. and Medzhitov, R. (2002) 'Innate immune recognition', *Annu Rev Immunol,* 20, pp. 197-216.

Jang, M., Pete, E. S. and Bruheim, P. (2022) 'The impact of serum-free culture on HEK293 cells: From the establishment of suspension and adherent serum-free adaptation cultures to the investigation of growth and metabolic profiles', *Front Bioeng Biotechnol,* 10, pp. 964397.

Jansen, R., Embden, J. D., Gaastra, W. and Schouls, L. M. (2002) 'Identification of genes that are associated with DNA repeats in prokaryotes', *Mol Microbiol,* 43(6), pp. 1565-75.

Jiang, F. and Doudna, J. A. (2015) 'The structural biology of CRISPR-Cas systems', *Curr Opin Struct Biol,* 30, pp. 100-111.

Jo, C., Jang, B. G. and Jo, S. A. (2009) 'MEK1 plays contrary stage-specific roles in skeletal myogenic differentiation', *Cell Signal,* 21(12), pp. 1910-7.

Joyce, K., Fabra, G. T., Bozkurt, Y. and Pandit, A. (2021) 'Bioactive potential of natural biomaterials: identification, retention and assessment of biological properties', *Signal Transduct Target Ther,* 6(1), pp. 122.

Kalukula, Y., Stephens, A. D., Lammerding, J. and Gabriele, S. (2022) 'Mechanics and functional consequences of nuclear deformations', *Nat Rev Mol Cell Biol,* 23(9), pp. 583-602.

Kalverda, B., Pickersgill, H., Shloma, V. V. and Fornerod, M. (2010) 'Nucleoporins directly stimulate expression of developmental and cell-cycle genes inside the nucleoplasm', *Cell,* 140(3), pp. 360-71.

Kamble, H., Vadivelu, R., Barton, M., Boriachek, K., Munaz, A., Park, S., Shiddiky, M. J. A. and Nguyen, N. T. (2017) 'An Electromagnetically Actuated Double-Sided Cell-Stretching Device for Mechanobiology Research', *Micromachines (Basel),* 8(8).

Kanapathy, M., Hachach-Haram, N., Bystrzonowski, N., Harding, K., Mosahebi, A. and Richards, T. (2016) 'Epidermal grafting versus split-thickness skin grafting for wound healing (EPIGRAAFT): study protocol for a randomised controlled trial', *Trials,* 17(1), pp. 245

Kay, A. D., Husbands-Beasley, J. and Blazevich, A. J. (2015) 'Effects of Contract-Relax, Static Stretching, and Isometric Contractions on Muscle-Tendon Mechanics', *Med Sci Sports Exerc,* 47(10), pp. 2181-90.

Khatau, S. B., Hale, C. M., Stewart-Hutchinson, P. J., Patel, M. S., Stewart, C. L., Searson, P. C., Hodzic, D. and Wirtz, D. (2009) 'A perinuclear actin cap regulates nuclear shape', *Proc Natl Acad Sci U S A,* 106(45), pp. 19017-22.

Kielty, C. M., Sherratt, M. J. and Shuttleworth, C. A. (2002) 'Elastic fibres', *J Cell Sci,* 115(Pt 14), pp. 2817-28.

Kim, D. and Rossi, J. (2008) 'RNAi mechanisms and applications', *Biotechniques,* 44(5), pp. 613-6.

Kim, E. H., Oh, N., Jun, M., Ko, K. and Park, S. (2015) 'Effect of cyclic stretching on cell shape and division', *BioChip J* (9), pp. 306–312.

Kim, S. G., Akaike, T., Sasagaw, T., Atomi, Y. and Kurosawa, H. (2002) 'Gene expression of type I and type III collagen by mechanical stretch in anterior cruciate ligament cells', *Cell Struct Funct,* 27(3), pp. 139-44.

Kirby, T. J. and Lammerding, J. (2016) 'Cell mechanotransduction: Stretch to express', *Nat Mater,* 15(12), pp. 1227-1229.

Kirby, T. J. and Lammerding, J. (2018) 'Emerging views of the nucleus as a cellular mechanosensor', *Nat Cell Biol,* 20(4), pp. 373-381.

Knight, E. and Przyborski, S. (2015) 'Advances in 3D cell culture technologies enabling tissue-like structures to be created in vitro', *J Anat,* 227(6), pp. 746-56.

Knockenhauer, K. E. and Schwartz, T. U. (2016) 'The Nuclear Pore Complex as a Flexible and Dynamic Gate', *Cell,* 164(6), pp. 1162-1171.

Kobayashi, S., Saio, M., Fukuda, T., Kimura, K., Hirato, J. and Oyama, T. (2019) 'Image analysis of the nuclear characteristics of emerin protein and the correlation with nuclear grooves and intranuclear cytoplasmic inclusions in lung adenocarcinoma', *Oncol Rep,* 41(1), pp. 133-142.

Koch, A. J. and Holaska, J. M. (2012) 'Loss of emerin alters myogenic signaling and miRNA expression in mouse myogenic progenitors', *PLoS One,* 7(5), pp. e37262.

Koch, A. J. and Holaska, J. M. (2014) 'Emerin in health and disease', *Semin Cell Dev Biol,* 29, pp. 95-106.

Kolaczkowska, E. and Kubes, P. (2013) 'Neutrophil recruitment and function in health and inflammation', *Nat Rev Immunol,* 13(3), pp. 159-75.

Kolind, K., Leong, K. W., Besenbacher, F. and Foss, M. (2012) 'Guidance of stem cell fate on 2D patterned surfaces', *Biomaterials,* 33(28), pp. 6626-33.

Kollmannsberger, P., Mierke, C. T. and Fabry, B. (2011) 'Nonlinear viscoelasticity of adherent cells is controlled by cytoskeletal tension', *Soft Matter,* 7, pp. 3127-3132.

Kumar, S., Maxwell, I. Z., Heisterkamp, A., Polte, T. R., Lele, T. P., Salanga, M., Mazur, E. and Ingber, D. E. (2006) 'Viscoelastic retraction of single living stress fibers and its impact on cell shape, cytoskeletal organization, and extracellular matrix mechanics', *Biophys J,* 90(10), pp. 3762-73.

Kuscu, C., Arslan, S., Singh, R., Thorpe, J. and Adli, M. (2014) 'Genome-wide analysis reveals characteristics of off-target sites bound by the Cas9 endonuclease', *Nat Biotechnol,* 32(7), pp. 677-83.

Kushida, N., Yamaguchi, O., Kawashima, Y., Akaihata, H., Hata, J., Ishibashi, K., Aikawa, K. and Kojima, Y. (2016) 'Uni-axial stretch induces actin stress fiber reorganization and activates c-Jun NH2 terminal kinase via RhoA and Rho kinase in human bladder smooth muscle cells', *BMC Urol,* 16, pp. 9.

Kuznetsova, T. G., Starodubtseva, M. N., Yegorenkov, N. I., Chizhik, S. A. and Zhdanov, R. I. (2007) 'Atomic force microscopy probing of cell elasticity', *Micron,* 38(8), pp. 824-33.

Kyriakides, T. R. and Bornstein, P. (2003) 'Matricellular proteins as modulators of wound healing and the foreign body response', *Thromb Haemost,* 90(6), pp. 986-92.

Lammerding, J., Hsiao, J., Schulze, P. C., Kozlov, S., Stewart, C. L. and Lee, R. T. (2005) 'Abnormal nuclear shape and impaired mechanotransduction in emerin-deficient cells', *J Cell Biol,* 170(5), pp. 781-91.

Larson, M. H., Gilbert, L. A., Wang, X., Lim, W. A., Weissman, J. S. and Qi, L. S. (2013) 'CRISPR interference (CRISPRi) for sequence-specific control of gene expression', *Nat Protoc,* 8(11), pp. 2180-96.

Laskin, D. L., Sunil, V. R., Gardner, C. R. and Laskin, J. D. (2011) 'Macrophages and tissue injury: agents of defense or destruction?', *Annu Rev Pharmacol Toxicol,* 51, pp. 267-88.

Lavoie, H., Gagnon, J. and Therrien, M. (2020) 'ERK signalling: a master regulator of cell behaviour, life and fate', *Nat Rev Mol Cell Biol,* 21(10), pp. 607-632.

Le Dour, C., Chatzifrangkeskou, M., Macquart, C., Magiera, M. M., Peccate, C., Jouve, C., Virtanen, L., Helio, T., Aalto-Setala, K., Crasto, S., Cadot, B., Cardoso, D., Mougenot, N., Adesse, D., Di Pasquale, E., Hulot, J. S., Taimen, P., Janke, C. and Muchir, A. (2022) 'Actin-microtubule cytoskeletal interplay

mediated by MRTF-A/SRF signaling promotes dilated cardiomyopathy caused by LMNA mutations', *Nat Commun,* 13(1), pp. 7886.

Lee, J. S., Kallehauge, T. B., Pedersen, L. E. and Kildegaard, H. F. (2015) 'Site-specific integration in CHO cells mediated by CRISPR/Cas9 and homology-directed DNA repair pathway', *Sci Rep,* 5, pp. 8572.

Lele, T. P., Dickinson, R. B. and Gundersen, G. G. (2018) 'Mechanical principles of nuclear shaping and positioning', *J Cell Biol,* 217(10), pp. 3330-3342.

Lessey, E. C., Guilluy, C. and Burridge, K. (2012) 'From mechanical force to RhoA activation', *Biochemistry,* 51(38), pp. 7420-32.

Lewis, J. (2014) 'A systematic literature review of the relationship between stretching and athletic injury prevention', *Orthop Nurs,* 33(6), pp. 312-20; quiz 321-2.

Liddane, A. G., McNamara, C. A., Campbell, M. C., Mercier, I. and Holaska, J. M. (2021) 'Defects in Emerin-Nucleoskeleton Binding Disrupt Nuclear Structure and Promote Breast Cancer Cell Motility and Metastasis', *Mol Cancer Res,* 19(7), pp. 1196-1207.

Li, R., Xia, X., Wang, X., Sun, X., Dai, Z., Huo, D., Zheng, H., Xiong, H., He, A. and Wu, X. (2020) 'Generation and validation of versatile inducible CRISPRi embryonic stem cell and mouse model', *PLoS Biol,* 18(11), pp. e3000749.

Li, X., Li, C., Zhang, W., Wang, Y., Qian, P. and Huang, H. (2023) 'Inflammation and aging: signaling pathways and intervention therapies', *Signal Transduct Target Ther,* 8(1), pp. 239.

Li, Z., Yang, G., Khan, M., Stone, D., Woo, S. L. and Wang, J. H. (2004) 'Inflammatory response of human tendon fibroblasts to cyclic mechanical stretching', *Am J Sports Med,* 32(2), pp. 435-40.

Lin, S. Y., Makino, K., Xia, W., Matin, A., Wen, Y., Kwong, K. Y., Bourguignon, L. and Hung, M. C. (2001) 'Nuclear localization of EGF receptor and its potential new role as a transcription factor', *Nat Cell Biol,* 3(9), pp. 802-8.

Lindley, L. E., Stojadinovic, O., Pastar, I. and Tomic-Canic, M. (2016) 'Biology and Biomarkers for Wound Healing', *Plast Reconstr Surg,* 138(3 Suppl), pp. 18S-28S.

Liu, A. P., Appel, E. A., Ashby, P. D., Baker, B. M., Franco, E., Gu, L., Haynes, K., Joshi, N. S., Kloxin, A. M., Kouwer, P. H. J., Mittal, J., Morsut, L., Noireaux, V., Parekh, S., Schulman, R., Tang, S. K. Y., Valentine, M. T., Vega, S. L., Weber, W., Stephanopoulos, N. and Chaudhuri, O. (2022) 'The living interface between synthetic biology and biomaterial design', *Nat Mater,* 21(4), pp. 390-397.

Liu, W. F. (2012) 'Mechanical regulation of cellular phenotype: implications for vascular tissue regeneration', *Cardiovasc Res,* 95(2), pp. 215-22.

Lombardi, M. L., Jaalouk, D. E., Shanahan, C. M., Burke, B., Roux, K. J. and Lammerding, J. (2011) 'The interaction between nesprins and sun proteins at the nuclear envelope is critical for force transmission between the nucleus and cytoskeleton', *J Biol Chem,* 286(30), pp. 26743-53.

Lopez-Bergami, P., Lau, E. and Ronai, Z. (2010) 'Emerging roles of ATF2 and the dynamic AP1 network in cancer', *Nat Rev Cancer,* 10(1), pp. 65-76.

Luger, A. L., Sauer, B., Lorenz, N. I., Engel, A. L., Braun, Y., Voss, M., Harter, P. N., Steinbach, J. P. and Ronellenfitsch, M. W. (2018) 'Doxycycline Impairs Mitochondrial Function and Protects Human Glioma Cells from Hypoxia-Induced Cell Death: Implications of Using Tet-Inducible Systems', *Int J Mol Sci,* 19(5).

Luxton, G. W., Gomes, E. R., Folker, E. S., Vintinner, E. and Gundersen, G. G. (2010) 'Linear arrays of nuclear envelope proteins harness retrograde actin flow for nuclear movement', *Science,* 329(5994), pp. 956-9.

MacLeod, R. S., Cawley, K. M., Gubrij, I., Nookaew, I., Onal, M. and O'Brien, C. A. (2019) 'Effective CRISPR interference of an endogenous gene via a single transgene in mice', *Sci Rep,* 9(1), pp. 17312.

Maeda, N., Urabe, Y., Fujii, E., Moriyama, N., Iwata, S. and Sasadai, J. (2016) 'The effect of different stretching techniques on ankle joint range of motion and dynamic postural stability after landing', *J Sports Med Phys Fitness,* 56(6), pp. 692-8.

Maeda, N., Urabe, Y., Tsutsumi, S., Sakai, S., Fujishita, H., Kobayashi, T., Asaeda, M., Hirata, K., Mikami, Y. and Kimura, H. (2017) 'The Acute Effects of Static and Cyclic Stretching on Muscle Stiffness and Hardness of Medial Gastrocnemius Muscle', *J Sports Sci Med,* 16(4), pp. 514-520.

Mali, P., Aach, J., Stranges, P. B., Esvelt, K. M., Moosburner, M., Kosuri, S., Yang, L. and Church, G. M. (2013) 'CAS9 transcriptional activators for target specificity screening and paired nickases for cooperative genome engineering', *Nat Biotechnol,* 31(9), pp. 833-8.

Malm, M., Saghaleyni, R., Lundqvist, M., Giudici, M., Chotteau, V., Field, R., Varley, P. G., Hatton, D., Grassi, L., Svensson, T., Nielsen, J. and Rockberg, J. (2020) 'Evolution from adherent to suspension: systems biology of HEK293 cell line development', *Sci Rep,* 10(1), pp. 18996.

Malpica, A., Deavers, M. T., Lu, K., Bodurka, D. C., Atkinson, E. N., Gershenson, D. M. and Silva, E. G. (2004) 'Grading ovarian serous carcinoma using a two-tier system', *Am J Surg Pathol,* 28(4), pp. 496-504.

Manilal, S., Nguyen, T. M., Sewry, C. A. and Morris, G. E. (1996) 'The Emery-Dreifuss muscular dystrophy protein, emerin, is a nuclear membrane protein', *Hum Mol Genet,* 5(6), pp. 801-8.

Maniotis, A. J., Chen, C. S. and Ingber, D. E. (1997) 'Demonstration of mechanical connections between integrins, cytoskeletal filaments, and nucleoplasm that stabilize nuclear structure', *Proc Natl Acad Sci U S A,* 94(3), pp. 849-54.

Mans, B. J., Anantharaman, V., Aravind, L. and Koonin, E. V. (2004) 'Comparative genomics, evolution and origins of the nuclear envelope and nuclear pore complex', *Cell Cycle,* 3(12), pp. 1612-37.

Maraldi, N. M., Lattanzi, G., Capanni, C., Columbaro, M., Merlini, L., Mattioli, E., Sabatelli, P., Squarzoni, S. and Manzoli, F. A. (2006) 'Nuclear envelope proteins and chromatin arrangement: a pathogenic mechanism for laminopathies', *Eur J Histochem,* 50(1), pp. 1-8.

Marano, N. and Holaska, J. M. (2022) 'Emerin interacts with histone methyltransferases to regulate repressive chromatin at the nuclear periphery', *Front Cell Dev Biol,* 10, pp. 1007120.

Margadant, F., Chew, L. L., Hu, X., Yu, H., Bate, N., Zhang, X. and Sheetz, M. (2011) 'Mechanotransduction in vivo by repeated talin stretch-relaxation events depends upon vinculin', *PLoS Biol,* 9(12), pp. e1001223.

Marjoram, R. J., Lessey, E. C. and Burridge, K. (2014) 'Regulation of RhoA activity by adhesion molecules and mechanotransduction', *Curr Mol Med,* 14(2), pp. 199-208.

Martins, R. P., Finan, J. D., Guilak, F. and Lee, D. A. (2012) 'Mechanical regulation of nuclear structure and function', *Annu Rev Biomed Eng,* 14, pp. 431-55.

Maruthamuthu, V., Sabass, B., Schwarz, U. S. and Gardel, M. L. (2011) 'Cell-ECM traction force modulates endogenous tension at cell-cell contacts', *Proc Natl Acad Sci U S A,* 108(12), pp. 4708-13.

Matamoro-Vidal, A. and Levayer, R. (2019) 'Multiple Influences of Mechanical Forces on Cell Competition', *Curr Biol,* 29(15), pp. R762-R774.

Matzinger, P. (2002) 'The danger model: a renewed sense of self', *Science,* 296(5566), pp. 301-5.

Maver, T., Maver, U., Kleinschek, K. S., Rascan, I. M. and Smrke, D. M. (2015) 'Advanced therapies of skin injuries', *Wien Klin Wochenschr,* 127 Suppl 5, pp. S187-98.

McCain, M. L. and Parker, K. K. (2011) 'Mechanotransduction: the role of mechanical stress, myocyte shape, and cytoskeletal architecture on cardiac function', *Pflugers Arch,* 462(1), pp. 89-104.

McNair, P. J., Dombroski, E. W., Hewson, D. J. and Stanley, S. N. (2001) 'Stretching at the ankle joint: viscoelastic responses to holds and continuous passive motion', *Med Sci Sports Exerc,* 33(3), pp. 354-8.

Meier, I. and Brkljacic, J. (2009) 'Adding pieces to the puzzling plant nuclear envelope', *Curr Opin Plant Biol,* 12(6), pp. 752-9.

Mejat, A. and Misteli, T. (2010) 'LINC complexes in health and disease', *Nucleus,* 1(1), pp. 40-52.

Mellad, J. A., Warren, D. T. and Shanahan, C. M. (2011) 'Nesprins LINC the nucleus and cytoskeleton', *Curr Opin Cell Biol,* 23(1), pp. 47-54.

Mendoza, M. C., Vilela, M., Juarez, J. E., Blenis, J. and Danuser, G. (2015) 'ERK reinforces actin polymerization to power persistent edge protrusion during motility', *Sci Signal,* 8(377), pp. ra47.

Mika, S. and Rost, B. (2005) 'NMPdb: Database of Nuclear Matrix Proteins', *Nucleic Acids Res,* 33(Database issue), pp. D160-3.

Miralles, F., Posern, G., Zaromytidou, A. I. and Treisman, R. (2003) 'Actin dynamics control SRF activity by regulation of its coactivator MAL', *Cell,* 113(3), pp. 329-42.

Mirbagheri, M., Adibnia, V., Hughes, B. R., Waldman., S. D., Banquy, X. and Hwang, D. K. (2019) 'Advanced cell culture platforms: A growing quest for emulating natural tissues', Materials Horizons, 6, pp. 45-71.

Mitra, S. K., Hanson, D. A. and Schlaepfer, D. D. (2005) 'Focal adhesion kinase: in command and control of cell motility', *Nat Rev Mol Cell Biol,* 6(1), pp. 56-68.

Mitsunobu, H., Teramoto, J., Nishida, K. and Kondo, A. (2017) 'Beyond Native Cas9: Manipulating Genomic Information and Function', *Trends Biotechnol,* 35(10), pp. 983-996.

Mojica, F. J., Diez-Villasenor, C., Soria, E. and Juez, G. (2000) 'Biological significance of a family of regularly spaced repeats in the genomes of Archaea, Bacteria and mitochondria', *Mol Microbiol,* 36(1), pp. 244-6.

Monemian Esfahani, A., Rosenbohm, J., Reddy, K., Jin, X., Bouzid, T., Riehl, B., Kim, E., Lim, J. Y. and Yang, R. (2019) 'Tissue Regeneration from Mechanical Stretching of Cell-Cell Adhesion', *Tissue Eng Part C Methods,* 25(11), pp. 631-640.

Montel, L., Sotiropoulos, A. and Henon, S. (2019) 'The nature and intensity of mechanical stimulation drive different dynamics of MRTF-A nuclear redistribution after actin remodeling in myoblasts', *PLoS One,* 14(3), pp. e0214385.

Montes de Oca, R., Lee, K. K. and Wilson, K. L. (2005) 'Binding of barrier to autointegration factor (BAF) to histone H3 and selected linker histones including H1.1', *J Biol Chem,* 280(51), pp. 42252-62.

Moya, I. M. and Halder, G. (2019) 'Hippo-YAP/TAZ signalling in organ regeneration and regenerative medicine', *Nat Rev Mol Cell Biol,* 20(4), pp. 211-226.

Muchir, A., Pavlidis, P., Bonne, G., Hayashi, Y. K. and Worman, H. J. (2007) 'Activation of MAPK in hearts of EMD null mice: similarities between mouse models of X-linked and autosomal dominant Emery Dreifuss muscular dystrophy', *Hum Mol Genet,* 16(15), pp. 1884-95.

Muchir, A., Wu, W. and Worman, H. J. (2009) 'Reduced expression of A-type lamins and emerin activates extracellular signal-regulated kinase in cultured cells', *Biochim Biophys Acta,* 1792(1), pp. 75-81.

Muehlich, S., Wang, R., Lee, S. M., Lewis, T. C., Dai, C. and Prywes, R. (2008) 'Serum-induced phosphorylation of the serum response factor coactivator MKL1 by the extracellular signal-regulated kinase 1/2 pathway inhibits its nuclear localization', *Mol Cell Biol,* 28(20), pp. 6302-13.

Muro, A. F., Chauhan, A. K., Gajovic, S., Iaconcig, A., Porro, F., Stanta, G. and Baralle, F. E. (2003) 'Regulated splicing of the fibronectin EDA exon is essential for proper skin wound healing and normal lifespan', *J Cell Biol,* 162(1), pp. 149-60.

Murray, R. Z., West, Z. E., Cowin, A. J. and Farrugia, B. L. (2019) 'Development and use of biomaterials as wound healing therapies', *Burns Trauma,* 7, pp. 2.

Myllyharju, J. and Kivirikko, K. I. (2004) 'Collagens, modifying enzymes and their mutations in humans, flies and worms', *Trends Genet,* 20(1), pp. 33-43.

Nakamura, M., Gao, Y., Dominguez, A. A. and Qi, L. S. (2021) 'CRISPR technologies for precise epigenome editing', *Nat Cell Biol,* 23(1), pp. 11-22.

Nestle, F. O., Di Meglio, P., Qin, J. Z. and Nickoloff, B. J. (2009) 'Skin immune sentinels in health and disease', *Nat Rev Immunol,* 9(10), pp. 679-91.

Niethammer, P., Grabher, C., Look, A. T. and Mitchison, T. J. (2009) 'A tissue-scale gradient of hydrogen peroxide mediates rapid wound detection in zebrafish', *Nature,* 459(7249), pp. 996-9.

Nishimasu, H., Ran, F. A., Hsu, P. D., Konermann, S., Shehata, S. I., Dohmae, N., Ishitani, R., Zhang, F. and Nureki, O. (2014) 'Crystal structure of Cas9 in complex with guide RNA and target DNA', *Cell,* 156(5), pp. 935-49.

O'Geen, H., Henry, I. M., Bhakta, M. S., Meckler, J. F. and Segal, D. J. (2015) 'A genome-wide analysis of Cas9 binding specificity using ChIP-seq and targeted sequence capture', *Nucleic Acids Res,* 43(6), pp. 3389-404.

Olsnes, S., Klingenberg, O. and Wiedlocha, A. (2003) 'Transport of exogenous growth factors and cytokines to the cytosol and to the nucleus', *Physiol Rev,* 83(1), pp. 163-82.

Olson, E. N. and Nordheim, A. (2010) 'Linking actin dynamics and gene transcription to drive cellular motile functions', *Nat Rev Mol Cell Biol,* 11(5), pp. 353-65.

Osmanagic-Myers, S., Dechat, T. and Foisner, R. (2015) 'Lamins at the crossroads of mechanosignaling', *Genes Dev,* 29(3), pp. 225-37.

Ozawa, R., Hayashi, Y. K., Ogawa, M., Kurokawa, R., Matsumoto, H., Noguchi, S., Nonaka, I. and Nishino, I. (2006) 'Emerin-lacking mice show minimal motor and cardiac dysfunctions with nuclear-associated vacuoles', *Am J Pathol,* 168(3), pp. 907-17.

Paluch, E. K. and Discher, D. E. (2015) 'Cell motion and mechanobiology', *Mol Biol Cell,* 26(6), pp. 1011.

Panayiotou, R., Miralles, F., Pawlowski, R., Diring, J., Flynn, H. R., Skehel, M. and Treisman, R. (2016) 'Phosphorylation acts positively and negatively to regulate MRTF-A subcellular localisation and activity', *Elife,* 5.

Papapetrou, E. P. and Schambach, A. (2016) 'Gene Insertion Into Genomic Safe Harbors for Human Gene Therapy', *Mol Ther,* 24(4), pp. 678-84.

Park, C. H., Ryu, H. G., Kim, S. H., Lee, D., Song, H. and Kim, K. T. (2015) 'Presumed pseudokinase VRK3 functions as a BAF kinase', *Biochim Biophys Acta,* 1853(7), pp. 1738-48.

Parnas, O., Jovanovic, M., Eisenhaure, T. M., Herbst, R. H., Dixit, A., Ye, C. J., Przybylski, D., Platt, R. J., Tirosh, I., Sanjana, N. E., Shalem, O., Satija, R., Raychowdhury, R., Mertins, P., Carr, S. A., Zhang, F., Hacohen, N. and Regev, A. (2015) 'A Genome-wide CRISPR Screen in Primary Immune Cells to Dissect Regulatory Networks', *Cell,* 162(3), pp. 675-86.

Parsons, J. T., Horwitz, A. R. and Schwartz, M. A. (2010) 'Cell adhesion: integrating cytoskeletal dynamics and cellular tension', *Nat Rev Mol Cell Biol,* 11(9), pp. 633-43.

Parsons, J. T., Martin, K. H., Slack, J. K., Taylor, J. M. and Weed, S. A. (2000) 'Focal adhesion kinase: a regulator of focal adhesion dynamics and cell movement', *Oncogene,* 19(49), pp. 5606-13.

Pattanayak, V., Lin, S., Guilinger, J. P., Ma, E., Doudna, J. A. and Liu, D. R. (2013) 'High-throughput profiling of off-target DNA cleavage reveals RNA-programmed Cas9 nuclease specificity', *Nat Biotechnol,* 31(9), pp. 839-43.

Place, E. S., Evans, N. D. and Stevens, M. M. (2009) 'Complexity in biomaterials for tissue engineering', *Nat Mater,* 8(6), pp. 457-70.

Polstein, L. R., Perez-Pinera, P., Kocak, D. D., Vockley, C. M., Bledsoe, P., Song, L., Safi, A., Crawford, G. E., Reddy, T. E. and Gersbach, C. A. (2015) 'Genome-wide specificity of DNA binding, gene regulation, and chromatin remodeling by TALE- and CRISPR/Cas9-based transcriptional activators', *Genome Res,* 25(8), pp. 1158-69.

Price, R. L., Chintanowonges, C., Shiraishi, I., Borg, T. K. and Terracio, L. (1996) 'Local and regional variations in myofibrillar patterns in looping rat hearts', *Anat Rec,* 245(1), pp. 83-93.

Qi, L. S., Larson, M. H., Gilbert, L. A., Doudna, J. A., Weissman, J. S., Arkin, A. P. and Lim, W. A. (2013) 'Repurposing CRISPR as an RNA-guided platform for sequence-specific control of gene expression', *Cell,* 152(5), pp. 1173-83.

Qi, Y. X., Yao, Q. P., Huang, K., Shi, Q., Zhang, P., Wang, G. L., Han, Y., Bao, H., Wang, L., Li, H. P., Shen, B. R., Wang, Y., Chien, S. and Jiang, Z. L. (2016) 'Nuclear envelope proteins modulate proliferation of vascular smooth muscle cells during cyclic stretch application', *Proc Natl Acad Sci U S A,* 113(19), pp. 5293-8.

Raharjo, W. H., Enarson, P., Sullivan, T., Stewart, C. L. and Burke, B. (2001) 'Nuclear envelope defects associated with LMNA mutations cause dilated cardiomyopathy and Emery-Dreifuss muscular dystrophy', *J Cell Sci,* 114(Pt 24), pp. 4447-57.

Raices, M. and D'Angelo, M. A. (2012) 'Nuclear pore complex composition: a new regulator of tissue-specific and developmental functions', *Nat Rev Mol Cell Biol,* 13(11), pp. 687-99.

Rajagopalan, P., Kasif, S. and Murali, T. M. (2013) 'Systems biology characterization of engineered tissues', *Annu Rev Biomed Eng,* 15, pp. 55-70.

Ramakrishna, S., Cho, S. W., Kim, S., Song, M., Gopalappa, R., Kim, J. S. and Kim, H. (2014) 'Surrogate reporter-based enrichment of cells containing RNA-guided Cas9 nuclease-induced mutations', *Nat Commun,* 5, pp. 3378.

Ramalingam, P. (2016) 'Morphologic, Immunophenotypic, and Molecular Features of Epithelial Ovarian Cancer', *Oncology (Williston Park),* 30(2), pp. 166-76.

Ramdas, N. M. and Shivashankar, G. V. (2015) 'Cytoskeletal control of nuclear morphology and chromatin organization', *J Mol Biol,* 427(3), pp. 695-706.

Ran, F. A., Cong, L., Yan, W. X., Scott, D. A., Gootenberg, J. S., Kriz, A. J., Zetsche, B., Shalem, O., Wu, X., Makarova, K. S., Koonin, E. V., Sharp, P. A. and Zhang, F. (2015) 'In vivo genome editing using Staphylococcus aureus Cas9', *Nature,* 520(7546), pp. 186-91.

Randolph, L. N., Bao, X., Zhou, C. and Lian, X. (2017) 'An all-in-one, Tet-On 3G inducible PiggyBac system for human pluripotent stem cells and derivatives', *Sci Rep,* 7(1), pp. 1549.

Ranjbar, M., Amiri, F., Nourigorji, M., Torabizadeh, F., Dara, M. and Dianatpour, M. (2022) 'B2M gene knockout in HEK293T cells by non-viral delivery of CRISPR-Cas9 system for the generation of universal cells', *Egypt J Med Hum Genet*, 23(62).

Ratner, B. D. (2019) 'Biomaterials: Been There, Done That, and Evolving into the Future', *Annu Rev Biomed Eng,* 21, pp. 171-191.

Raut, H. K., Das, R., Liu, Z., Liu, X. and Ramakrishna, S. (2020) 'Biocompatibility of Biomaterials for Tissue Regeneration or Replacement', *Biotechnol J,* 15(12), pp. e2000160.

Raveling, A. R., Theodossiou, S. K. and Schiele, N. R. (2018) 'A 3D printed mechanical bioreactor for investigating mechanobiology and soft tissue mechanics', *MethodsX,* 5, pp. 924-932.

Ray, A., Lee, O., Win, Z., Edwards, R. M., Alford, P. W., Kim, D. H. and Provenzano, P. P. (2017) 'Anisotropic forces from spatially constrained focal adhesions mediate contact guidance directed cell migration', *Nat Commun,* 8, pp. 14923.

Riveline, D., Zamir, E., Balaban, N. Q., Schwarz, U. S., Ishizaki, T., Narumiya, S., Kam, Z., Geiger, B. and Bershadsky, A. D. (2001) 'Focal contacts as mechanosensors: externally applied local mechanical force induces growth of focal contacts by an mDia1-dependent and ROCK-independent mechanism', *J Cell Biol,* 153(6), pp. 1175-86.

Reis-Sobreiro, M., Chen, J. F., Novitskaya, T., You, S., Morley, S., Steadman, K., Gill, N. K., Eskaros, A., Rotinen, M., Chu, C. Y., Chung, L. W. K., Tanaka, H., Yang, W., Knudsen, B. S., Tseng, H. R., Rowat, A. C., Posadas, E. M., Zijlstra, A., Di Vizio, D. and Freeman, M. R. (2018) 'Emerin Deregulation Links Nuclear Shape Instability to Metastatic Potential', *Cancer Res,* 78(21), pp. 6086-6097.

Roberts, P. J. and Der, C. J. (2007) 'Targeting the Raf-MEK-ERK mitogen-activated protein kinase cascade for the treatment of cancer', *Oncogene,* 26(22), pp. 3291-310.

Robinson, C. J. and Stringer, S. E. (2001) 'The splice variants of vascular endothelial growth factor (VEGF) and their receptors', *J Cell Sci,* 114(Pt 5), pp. 853-65.

Rodrigues, M. and Gurtner, G. (2017) 'Black, White, and Gray: Macrophages in Skin Repair and Disease', *Curr Pathobiol Rep,* 5(4), pp. 333-342.

Rodrigues, M., Kosaric, N., Bonham, C. A. and Gurtner, G. C. (2019) 'Wound Healing: A Cellular Perspective', *Physiol Rev,* 99(1), pp. 665-706.

Rowat, A. C., Jaalouk, D. E., Zwerger, M., Ung, W. L., Eydelnant, I. A., Olins, D. E., Olins, A. L., Herrmann, H., Weitz, D. A. and Lammerding, J. (2013) 'Nuclear envelope composition determines the ability of neutrophil-type cells to passage through micron-scale constrictions', *J Biol Chem,* 288(12), pp. 8610-8618.

Salminen, A. (2023) 'The plasticity of fibroblasts: A forgotten player in the aging process', *Ageing Res Rev,* 89, pp. 101995.

Salpingidou, G., Smertenko, A., Hausmanowa-Petrucewicz, I., Hussey, P. J. and Hutchison, C. J. (2007) 'A novel role for the nuclear membrane protein emerin in association of the centrosome to the outer nuclear membrane', *J Cell Biol,* 178(6), pp. 897-904.

Salvany, L., Muller, J., Guccione, E. and Rorth, P. (2014) 'The core and conserved role of MAL is homeostatic regulation of actin levels', *Genes Dev,* 28(10), pp. 1048-53.

Samson, C., Petitalot, A., Celli, F., Herrada, I., Ropars, V., Le Du, M. H., Nhiri, N., Jacquet, E., Arteni, A. A., Buendia, B. and Zinn-Justin, S. (2018) 'Structural analysis of the ternary complex between lamin A/C, BAF and emerin identifies an interface disrupted in autosomal recessive progeroid diseases', *Nucleic Acids Res,* 46(19), pp. 10460-10473.

Samulski, R. J., Zhu, X., Xiao, X., Brook, J. D., Housman, D. E., Epstein, N. and Hunter, L. A. (1991) 'Targeted integration of adeno-associated virus (AAV) into human chromosome 19', *EMBO J,* 10(12), pp. 3941-50.

Sanjana, N. E., Cong, L., Zhou, Y., Cunniff, M. M., Feng, G. and Zhang, F. (2012) 'A transcription activator-like effector toolbox for genome engineering', *Nat Protoc,* 7(1), pp. 171-92.

Sastry, S. K. and Burridge, K. (2000) 'Focal adhesions: a nexus for intracellular signaling and cytoskeletal dynamics', *Exp Cell Res,* 261(1), pp. 25-36.

Scaffidi, P. and Misteli, T. (2006) 'Good news in the nuclear envelope: loss of lamin A might be a gain', *J Clin Invest,* 116(3), pp. 632-4.

Schlessinger, J., Plotnikov, A. N., Ibrahimi, O. A., Eliseenkova, A. V., Yeh, B. K., Yayon, A., Linhardt, R. J. and Mohammadi, M. (2000) 'Crystal structure of a ternary FGF-FGFR-heparin complex reveals a dual role for heparin in FGFR binding and dimerization', *Mol Cell,* 6(3), pp. 743-50.

Schreiner, S. M., Koo, P. K., Zhao, Y., Mochrie, S. G. and King, M. C. (2015) 'The tethering of chromatin to the nuclear envelope supports nuclear mechanics', *Nat Commun,* 6, pp. 7159.

Schuster, A., Erasimus, H., Fritah, S., Nazarov, P. V., van Dyck, E., Niclou, S. P. and Golebiewska, A. (2019) 'RNAi/CRISPR Screens: from a Pool to a Valid Hit', *Trends Biotechnol,* 37(1), pp. 38-55.

Schwarz, U. S. and Gardel, M. L. (2012) 'United we stand: integrating the actin cytoskeleton and cell-matrix adhesions in cellular mechanotransduction', *J Cell Sci,* 125(Pt 13), pp. 3051-60.

Sedlmayer, F., Aubel, D. and Fussenegger, M. (2018) 'Synthetic gene circuits for the detection, elimination and prevention of disease', *Nat Biomed Eng,* 2(6), pp. 399-415.

Sen, C. K. and Roy, S. (2019) 'Sociogenomic Approach to Wound Care: A New Patient-Centered Paradigm', *Adv Wound Care (New Rochelle),* 8(11), pp. 523-526.

Shao, Y., Tan, X., Novitski, R., Muqaddam, M., List, P., Williamson, L., Fu, J. and Liu, A. P. (2013) 'Uniaxial cell stretching device for live-cell imaging of mechanosensitive cellular functions', *Rev Sci Instrum,* 84(11), pp. 114304.

Sharrocks, A. D., Brown, A. L., Ling, Y. and Yates, P. R. (1997) 'The ETS-domain transcription factor family', *Int J Biochem Cell Biol,* 29(12), pp. 1371-87.

Sheikholeslam, M., Wright, M. E. E., Jeschke, M. G. and Amini-Nik, S. (2018) 'Biomaterials for Skin Substitutes', *Adv Healthc Mater,* 7(5).

Shi, J., Wang, E., Milazzo, J. P., Wang, Z., Kinney, J. B. and Vakoc, C. R. (2015) 'Discovery of cancer drug targets by CRISPR-Cas9 screening of protein domains', *Nat Biotechnol,* 33(6), pp. 661-7.

Shimi, T., Pfleghaar, K., Kojima, S., Pack, C. G., Solovei, I., Goldman, A. E., Adam, S. A., Shumaker, D. K., Kinjo, M., Cremer, T. and Goldman, R. D. (2008) 'The A- and B-type nuclear lamin networks: microdomains involved in chromatin organization and transcription', *Genes Dev,* 22(24), pp. 3409-21.

Sidorenko, E. and Vartiainen, M. K. (2019) 'Nucleoskeletal regulation of transcription: Actin on MRTF', *Exp Biol Med (Maywood),* 244(15), pp. 1372-1381.

Simpson, D. G., Majeski, M., Borg, T. K. and Terracio, L. (1999) 'Regulation of cardiac myocyte protein turnover and myofibrillar structure in vitro by specific directions of stretch', *Circ Res,* 85(10), pp. e59-69.

Singer, A. J. and Boyce, S. T. (2017) 'Burn Wound Healing and Tissue Engineering', *J Burn Care Res,* 38(3), pp. e605-e613.

Skaper, S. D., Facci, L. and Giusti, P. (2014) 'Mast cells, glia and neuroinflammation: partners in crime?', *Immunology,* 141(3), pp. 314-27.

Smeets, B., Cuvelier, M., Pesek, J. and Ramon, H. (2019) 'The Effect of Cortical Elasticity and Active Tension on Cell Adhesion Mechanics', *Biophys J,* 116(5), pp. 930-937.

Smith, E. R., Meng, Y., Moore, R., Tse, J. D., Xu, A. G. and Xu, X. X. (2017) 'Nuclear envelope structural proteins facilitate nuclear shape changes accompanying embryonic differentiation and fidelity of gene expression', *BMC Cell Biol,* 18(1), pp. 8.

Snyers, L., Lohnert, R., Weipoltshammer, K. and Schofer, C. (2022) 'Emerin prevents BAF-mediated aggregation of lamin A on chromosomes in telophase to allow nuclear membrane expansion and nuclear lamina formation', *Mol Biol Cell,* 33(14), pp. ar137.

Song, R., Murphy, M., Li, C., Ting, K., Soo, C. and Zheng, Z. (2018) 'Current development of biodegradable polymeric materials for biomedical applications', *Drug Des Devel Ther,* 12, pp. 3117-3145.

Sosa, B. A., Kutay, U. and Schwartz, T. U. (2013) 'Structural insights into LINC complexes', *Curr Opin Struct Biol,* 23(2), pp. 285-91.

Speight, P., Kofler, M., Szaszi, K. and Kapus, A. (2016) 'Context-dependent switch in chemo/mechanotransduction via multilevel crosstalk among cytoskeleton-regulated MRTF and TAZ and TGFbeta-regulated Smad3', *Nat Commun,* 7, pp. 11642.

Starr, D. A. and Fridolfsson, H. N. (2010) 'Interactions between nuclei and the cytoskeleton are mediated by SUN-KASH nuclear-envelope bridges', *Annu Rev Cell Dev Biol,* 26, pp. 421-44.

Steinberg, M. S. (1963) 'Reconstruction of tissues by dissociated cells. Some morphogenetic tissue movements and the sorting out of embryonic cells may have a common explanation', *Science,* 141(3579), pp. 401-8.

Stroud, M. J. (2018) 'Linker of nucleoskeleton and cytoskeleton complex proteins in cardiomyopathy', *Biophys Rev,* 10(4), pp. 1033-1051.

Sullivan, T., Escalante-Alcalde, D., Bhatt, H., Anver, M., Bhat, N., Nagashima, K., Stewart, C. L. and Burke, B. (1999) 'Loss of A-type lamin expression compromises nuclear envelope integrity leading to muscular dystrophy', *J Cell Biol,* 147(5), pp. 913-20.

Sun, D., Evans, L., Perrone, F., Sokleva, V., Lim, K., Rezakhani, S., Lutolf, M., Zilbauer, M. and Rawlins, E. L. (2021) 'A functional genetic toolbox for human tissue-derived organoids', *Elife,* 10.

Szabowski, A., Maas-Szabowski, N., Andrecht, S., Kolbus, A., Schorpp-Kistner, M., Fusenig, N. E. and Angel, P. (2000) 'c-Jun and JunB antagonistically control cytokine-regulated mesenchymal-epidermal interaction in skin', *Cell,* 103(5), pp. 745-55.

Taber, L. A., Lin, I. E. and Clark, E. B. (1995) 'Mechanics of cardiac looping', *Dev Dyn,* 203(1), pp. 42-50.

Tabdanov, E. D., Puram, V., Zhovmer, A. and Provenzano, P. P. (2018) 'Microtubule-Actomyosin Mechanical Cooperation during Contact Guidance Sensing', *Cell Rep,* 25(2), pp. 328-338 e5.

Tajik, A., Zhang, Y., Wei, F., Sun, J., Jia, Q., Zhou, W., Singh, R., Khanna, N., Belmont, A. S. and Wang, N. (2016) 'Transcription upregulation via force-induced direct stretching of chromatin', *Nat Mater,* 15(12), pp. 1287-1296.

Tan, D., Yang, H., Yuan, Y., Bonnemann, C., Chang, X., Wang, S., Wu, Y., Wu, X. and Xiong, H. (2015) 'Phenotype-Genotype Analysis of Chinese Patients with

Early-Onset LMNA-Related Muscular Dystrophy', *PLoS One,* 10(6), pp. e0129699.

Tata, A., Chow, R. D. and Tata, P. R. (2021) 'Epithelial cell plasticity: breaking boundaries and changing landscapes', *EMBO Rep,* 22(7), pp. e51921.

Telgenhoff, D. and Shroot, B. (2005) 'Cellular senescence mechanisms in chronic wound healing', *Cell Death Differ,* 12(7), pp. 695-8.

Tews, D. S. (1999) 'Emerin', *Int J Biochem Cell Biol,* 31(9), pp. 891-4.

Tiffin, N., Adi, S., Stokoe, D., Wu, N. Y. and Rosenthal, S. M. (2004) 'Akt phosphorylation is not sufficient for insulin-like growth factor-stimulated myogenin expression but must be accompanied by down-regulation of mitogen-activated protein kinase/extracellular signal-regulated kinase phosphorylation', *Endocrinology,* 145(11), pp. 4991-6.

Tiwari, V. K. (2012) 'Burn wound: How it differs from other wounds?', *Indian J Plast Surg,* 45(2), pp. 364-73.

Truong, D. J., Kuhner, K., Kuhn, R., Werfel, S., Engelhardt, S., Wurst, W. and Ortiz, O. (2015) 'Development of an intein-mediated split-Cas9 system for gene therapy', *Nucleic Acids Res,* 43(13), pp. 6450-8.

Unal, M., Alapan, Y., Jia, H., Varga, A. G., Angelino, K., Aslan, M., Sayin, I., Han, C., Jiang, Y., Zhang, Z. and Gurkan, U. A. (2014) 'Micro and Nano-Scale Technologies for Cell Mechanics', *Nanobiomedicine (Rij),* 1, pp. 5.

Ungricht, R. and Kutay, U. (2017) 'Mechanisms and functions of nuclear envelope remodelling', *Nat Rev Mol Cell Biol,* 18(4), pp. 229-245.

Ursekar, C. P., Teo, S. K., Hirata, H., Harada, I., Chiam, K. H. and Sawada, Y. (2014) 'Design and construction of an equibiaxial cell stretching system that is improved for biochemical analysis', *PLoS One,* 9(3), pp. e90665.

Uzer, G., Rubin, C. T. and Rubin, J. (2016) 'Cell Mechanosensitivity is Enabled by the LINC Nuclear Complex', *Curr Mol Biol Rep,* 2(1), pp. 36-47.

van der Oost, J., Westra, E. R., Jackson, R. N. and Wiedenheft, B. (2014) 'Unravelling the structural and mechanistic basis of CRISPR-Cas systems', *Nat Rev Microbiol,* 12(7), pp. 479-92.

Vang, R., Shih Ie, M. and Kurman, R. J. (2009) 'Ovarian low-grade and high-grade serous carcinoma: pathogenesis, clinicopathologic and molecular biologic features, and diagnostic problems', *Adv Anat Pathol,* 16(5), pp. 267-82.

Vig, K., Chaudhari, A., Tripathi, S., Dixit, S., Sahu, R., Pillai, S., Dennis, V. A. and Singh, S. R. (2017) 'Advances in Skin Regeneration Using Tissue Engineering', *Int J Mol Sci,* 18(4).

Vining, K. H. and Mooney, D. J. (2017) 'Mechanical forces direct stem cell behaviour in development and regeneration', Nat Rev Mol Cell Biol, 18(12), pp. 728-742.

Vitor, A. C., Huertas, P., Legube, G. and de Almeida, S. F. (2020) 'Studying DNA Double-Strand Break Repair: An Ever-Growing Toolbox', *Front Mol Biosci*, 7, pp. 24.

Vogel, V. and Sheetz, M. (2006) 'Local force and geometry sensing regulate cell functions', *Nat Rev Mol Cell Biol*, 7(4), pp. 265-75.

Walboomers, X. F., Croes, H. J., Ginsel, L. A. and Jansen, J. A. (1998) 'Growth behavior of fibroblasts on microgrooved polystyrene', *Biomaterials*, 19(20), pp. 1861-8.

Walma, D. A. C. and Yamada, K. M. (2020) 'The extracellular matrix in development', *Development*, 147(10).

Wang, H., La Russa, M. and Qi, L. S. (2016) 'CRISPR/Cas9 in Genome Editing and Beyond', *Annu Rev Biochem*, 85, pp. 227-64.

Wang, H. X., Song, Z., Lao, Y. H., Xu, X., Gong, J., Cheng, D., Chakraborty, S., Park, J. S., Li, M., Huang, D., Yin, L., Cheng, J. and Leong, K. W. (2018) 'Nonviral gene editing via CRISPR/Cas9 delivery by membrane-disruptive and endosomolytic helical polypeptide', *Proc Natl Acad Sci U S A*, 115(19), pp. 4903-4908.

Wang, J. H. and Li, B. (2010) 'Mechanics rules cell biology', *Sports Med Arthrosc Rehabil Ther Technol*, 2, pp. 16.

Wang, N., Tytell, J. D. and Ingber, D. E. (2009) 'Mechanotransduction at a distance: mechanically coupling the extracellular matrix with the nucleus', *Nat Rev Mol Cell Biol*, 10(1), pp. 75-82.

Wang, X., Xu, S., Rivolta, C., Li, L. Y., Peng, G. H., Swain, P. K., Sung, C. H., Swaroop, A., Berson, E. L., Dryja, T. P. and Chen, S. (2002) 'Barrier to autointegration factor interacts with the cone-rod homeobox and represses its transactivation function', *J Biol Chem*, 277(45), pp. 43288-300.

Wasylyk, B., Hagman, J. and Gutierrez-Hartmann, A. (1998) 'Ets transcription factors: nuclear effectors of the Ras-MAP-kinase signaling pathway', *Trends Biochem Sci*, 23(6), pp. 213-6.

Watabe, S., Kobayashi, S., Hatori, M., Nishijima, Y., Inoue, N., Ikota, H., Iwase, A., Yokoo, H. and Saio, M. (2022) 'Role of Lamin A and emerin in maintaining nuclear morphology in different subtypes of ovarian epithelial cancer', *Oncol Lett*, 23(1), pp. 9.

Watanabe, N. and Mitchison, T. J. (2002) 'Single-molecule speckle analysis of actin filament turnover in lamellipodia', *Science*, 295(5557), pp. 1083-6.

Watt, F. M. and Fujiwara, H. (2011) 'Cell-extracellular matrix interactions in normal and diseased skin', *Cold Spring Harb Perspect Biol,* 3(4).

Webster, K. D., Ng, W. P. and Fletcher, D. A. (2014) 'Tensional homeostasis in single fibroblasts', *Biophys J,* 107(1), pp. 146-55.

Weissbach, J., Schikora, F., Weber, A., Kessels, M. and Posern, G. (2016) 'Myocardin-Related Transcription Factor A Activation by Competition with WH2 Domain Proteins for Actin Binding', *Mol Cell Biol,* 36(10), pp. 1526-39.

Weiss, P. (1945) 'Experiments on cell and axon orientation in vitro; the role of colloidal exudates in tissue organization', *J Exp Zool,* 100, pp. 353-86.

Wells, R. G. (2013) 'Tissue mechanics and fibrosis', *Biochim Biophys Acta,* 1832(7), pp. 884-90.

Werner, S. and Grose, R. (2003) 'Regulation of wound healing by growth factors and cytokines', *Physiol Rev,* 83(3), pp. 835-70.

Willer, M. K. and Carroll, C. W. (2017) 'Substrate stiffness-dependent regulation of the SRF-Mkl1 co-activator complex requires the inner nuclear membrane protein Emerin', *J Cell Sci,* 130(13), pp. 2111-2118.

Woodall, B. P., Nystrom, A., Iozzo, R. A., Eble, J. A., Niland, S., Krieg, T., Eckes, B., Pozzi, A. and Iozzo, R. V. (2008) 'Integrin alpha2beta1 is the required receptor for endorepellin angiostatic activity', *J Biol Chem,* 283(4), pp. 2335-43.

Wozniak, M. A. and Chen, C. S. (2009) 'Mechanotransduction in development: a growing role for contractility', *Nat Rev Mol Cell Biol,* 10(1), pp. 34-43.

Wright, A. V., Sternberg, S. H., Taylor, D. W., Staahl, B. T., Bardales, J. A., Kornfeld, J. E. and Doudna, J. A. (2015) 'Rational design of a split-Cas9 enzyme complex', *Proc Natl Acad Sci U S A,* 112(10), pp. 2984-9.

Wu, X., Scott, D. A., Kriz, A. J., Chiu, A. C., Hsu, P. D., Dadon, D. B., Cheng, A. W., Trevino, A. E., Konermann, S., Chen, S., Jaenisch, R., Zhang, F. and Sharp, P. A. (2014) 'Genome-wide binding of the CRISPR endonuclease Cas9 in mammalian cells', *Nat Biotechnol,* 32(7), pp. 670-6.

Xia, X., Ayala, M., Thiede, B. R. and Zhang, S. C. (2008) 'In vitro- and in vivo-induced transgene expression in human embryonic stem cells and derivatives', *Stem Cells,* 26(2), pp. 525-33.

Xie, L. (2014) 'MKL1/2 and ELK4 co-regulate distinct serum response factor (SRF) transcription programs in macrophages', *BMC Genomics,* 15, pp. 301.

Xu, X., Gao, D., Wang, P., Chen, J., Ruan, J., Xu, J. and Xia, X. (2018) 'Efficient homology-directed gene editing by CRISPR/Cas9 in human stem and primary cells using tube electroporation', *Sci Rep,* 8(1), pp. 11649.

Yang, Y., Wang, L., Bell, P., McMenamin, D., He, Z., White, J., Yu, H., Xu, C., Morizono, H., Musunuru, K., Batshaw, M. L. and Wilson, J. M. (2016) 'A dual AAV system enables the Cas9-mediated correction of a metabolic liver disease in newborn mice', *Nat Biotechnol,* 34(3), pp. 334-8.

Yokoyama, T., Takano, K., Yoshida, A., Katada, F., Sun, P., Takenawa, T., Andoh, T. and Endo, T. (2007) 'DA-Raf1, a competent intrinsic dominant-negative antagonist of the Ras-ERK pathway, is required for myogenic differentiation', *J Cell Biol,* 177(5), pp. 781-93.

Yuan, J. and Xue, B. (2015) 'Role of structural flexibility in the evolution of emerin', *J Theor Biol,* 385, pp. 102-11.

Yusko, E. C. and Asbury, C. L. (2014) 'Force is a signal that cells cannot ignore', *Mol Biol Cell,* 25(23), pp. 3717-25.

Zakaria, A. A., Kiningham, R. B. and Sen, A. (2015) 'Effects of Static and Dynamic Stretching on Injury Prevention in High School Soccer Athletes: A Randomized Trial', *J Sport Rehabil,* 24(3), pp. 229-35.

Zaytsev, S. M., Amouroux, M., Khairallah, G., Bashkatov, A. N., Tuchin, V. V., Blondel, W. and Genina, E. A. (2022) 'Impact of optical clearing on ex vivo human skin optical properties characterized by spatially resolved multimodal spectroscopy', *J Biophotonics,* 15(1), pp. e202100202.

Zetsche, B., Volz, S. E. and Zhang, F. (2015) 'A split-Cas9 architecture for inducible genome editing and transcription modulation', *Nat Biotechnol,* 33(2), pp. 139-42.

Zhang, Y. and Habibovic, P. (2022) 'Delivering Mechanical Stimulation to Cells: State of the Art in Materials and Devices Design', *Adv Mater,* 34(32), pp. e2110267.

Zheng, Q., Choi, J., Rouleau, L., Leask, R. L., Richardson, J. A., Davis, E. C. and Yanagisawa, H. (2006) 'Normal wound healing in mice deficient for fibulin-5, an elastin binding protein essential for dermal elastic fiber assembly', *J Invest Dermatol,* 126(12), pp. 2707-14.

Zhu, M., Li, W., Dong, X., Yuan, X., Midgley, A. C., Chang, H., Wang, Y., Wang, H., Wang, K., Ma, P. X., Wang, H. and Kong, D. (2019) 'In vivo engineered extracellular matrix scaffolds with instructive niches for oriented tissue regeneration', *Nat Commun,* 10(1), pp. 4620.

Zielinski, A., Linnartz, C., Pleschka, C., Dreissen, G., Springer, R., Merkel, R. and Hoffmann, B. (2018) 'Reorientation dynamics and structural interdependencies of actin, microtubules and intermediate filaments upon cyclic stretch application', *Cytoskeleton (Hoboken),* 75(9), pp. 385-394.

Zohn, I. M., Campbell, S. L., Khosravi-Far, R., Rossman, K. L. and Der, C. J. (1998) 'Rho family proteins and Ras transformation: the RHOad less traveled gets congested', *Oncogene,* 17(11 Reviews), pp. 1415-38.

Zuris, J. A., Thompson, D. B., Shu, Y., Guilinger, J. P., Bessen, J. L., Hu, J. H., Maeder, M. L., Joung, J. K., Chen, Z. Y. and Liu, D. R. (2015) 'Cationic lipid-mediated delivery of proteins enables efficient protein-based genome editing in vitro and in vivo', *Nat Biotechnol,* 33(1), pp. 73-80.